

# **Design and Operation of Low Frequency AC (LFAC) Transmission System for Connecting Offshore Wind Farms**

**Spyridon Karamitsos**

A Thesis presented in fulfilment of the requirements for the degree of  
Doctor of Philosophy

Department of Electronic and Electrical Engineering  
University of Strathclyde, Glasgow, UK

March 2020

This thesis is the result of the author's original research. It has been composed by the author and has not been previously submitted for examination which has led to the award of a degree.

The copyright of this thesis belongs to the author under the terms of the United Kingdom Copyright Acts as qualified by University of Strathclyde Regulation 3.50. Due acknowledgement must always be made of the use of any material contained in, or derived from, this thesis.

Signed:

Date:

*Dedicated to Alexia and my Family*

## Acknowledgements

I would like to express my sincerest gratitude to my supervisor, Prof. Lie Xu, for his guidance and assistance. His technical expertise, research ideas and helpful feedback have guided this study. My special thanks also go to my mentor, Andre Canelhas, for his invaluable technical advice and HVDC-TECH that provided the required financial backing for this Industrial PhD project. Without their help, it would not have been possible to conduct this research.

Last but not least, a gracious acknowledgement is made to my family for their love and continuous encouragement during my study and my life in general. I am extremely grateful to Dora, Kostas, Eleftheria, Maria and Alexia for their valuable support, understanding and patience all these years. You are always there for me!



## Abstract

The offshore power transmission market continuously grows as government incentives for Renewable Energy, and technological advancements lead to the exploitation of offshore wind for electricity generation due to its high capacity factors and the abundant offshore space. Currently, the High Voltage AC (HVAC) and High Voltage DC (HVDC) transmission systems (TS) are the commercial options for integrating the wind power to the onshore grid. The technical and economic efficiency of each approach is evaluated on a case-by-case basis and is mainly dependent on the Offshore Wind Power Plant (OWPP) capacity and its distance from shore, with HVAC TS being the most common solution for distances lower than 100km.

The Low Frequency AC (LFAC) technology can provide an attractive transmission solution for exporting power from vast and remote OWPPs within a distance range of 80-300km. The basic idea of the LFAC system is to use lower AC frequency to reduce the effective electrical length of the equivalent HVAC subsea cable, so that its transmission capacity is increased, and also to eliminate the need for bulk offshore HVDC platforms, so that the installation, operation and maintenance costs are decreased. Despite the theoretical advantages of LFAC, the related research and its previous application in the rail and oil industries, there is no prior operational experience in similar type and scale networks, increasing the uncertainty for investors regarding the LFAC compliance capability and technology readiness level for offshore transmission purposes.

The aim of this industrial PhD Thesis is to result in robust and feasible LFAC TS options that can be realised by common industry practices and comply with typical Transmission System Operator's (TSO) grid code requirements. The LFAC TS is designed as a combined offshore HVAC system utilising an onshore Back-to-Back Modular Multilevel Converter (BtB MMC) scheme for frequency conversion. Point-to-Point (PtP) and Multi-Terminal (MT) LFAC topologies are examined for various cable lengths to export the nominal capacity of the OWPPs or interconnect different OWFs and different grids through single-cable connections to minimise costs. The technical feasibility of the LFAC TS is assessed through comprehensive steady-state, frequency and time-domain studies to optimise the system performance, its transmission capability and identify probable limitations.

Initially, the main transmission equipment specifications are appropriately adapted and rated for LFAC operation. Frequency scan studies are performed to investigate the low-order resonances of the LFAC TS, and suitable C-Type harmonic filter combinations are introduced

to avoid potential harmonic stability issues. Power-flow cases are studied to calibrate the operating conditions of the system (e.g. reactive power compensation, control strategies, etc.) and optimise the schemes in terms of power losses and shunt cable compensation, placed only at the onshore side. It is yielded that by utilising the AC voltage control strategy of the OWPP inverters together with the reactive power capability of the BtB MMCs can maximise the power transfer through the cables.

Finally, detailed EMT models of the optimised PtP and MT-LFAC TS are simulated to evaluate its dynamic performance, stability and FRT capability against faults in the offshore LFAC and AC sides. It is concluded that if the LFAC grid-forming MMC employs a typical islanded control scheme without Inner Current Controllers (ICCs), it should always use harmonic filtering to avoid low order harmonic stability issues caused by the system resonance. Even then, its FRT response against an LFAC side fault would be unacceptable, due to its unconstrained LFAC fault current. However, by implementing high-bandwidth ICCs with appropriate current saturation and integrator anti-windup mechanisms to the islanded-control system, the LFAC TS rides through faults successfully and complies with the respective typical TSO limits. Also, depending on the system rating, DBRs may need to be applied in the DC sides of the OWTGs and the onshore BtB frequency converters.

# Table of Contents

<b>Acknowledgements .....</b>	<b><i>i</i></b>
<b>Abstract.....</b>	<b><i>ii</i></b>
<b>Table of Contents.....</b>	<b><i>iv</i></b>
<b>List of Figures .....</b>	<b><i>ix</i></b>
<b>List of Tables.....</b>	<b><i>xiii</i></b>
<b>Abbreviations .....</b>	<b><i>xv</i></b>
<b>Chapter 1: Introduction .....</b>	<b><i>1</i></b>
<b>1.1 Transmission Systems for OWP Exploitation.....</b>	<b><i>1</i></b>
1.1.1 HVAC.....	<i>2</i>
1.1.2 HVDC .....	<i>3</i>
<b>1.2 LFAC Transmission System .....</b>	<b><i>5</i></b>
1.2.1 LFAC TS Concepts in the Literature .....	<i>6</i>
1.2.2 WF Collection Systems in LFAC TS Concepts .....	<i>9</i>
1.2.3 Frequency Selection .....	<i>10</i>
1.2.4 Frequency Conversion .....	<i>11</i>
1.2.5 LFAC TS Benefits .....	<i>14</i>
1.2.6 LFAC TS Issues.....	<i>16</i>
<b>1.3 Scope of the Thesis.....</b>	<b><i>18</i></b>
1.3.1 Research Motivation .....	<i>18</i>
1.3.2 Thesis Objectives .....	<i>20</i>
<b>1.4 Thesis Contributions.....</b>	<b><i>21</i></b>
<b>1.5 Author's Publications .....</b>	<b><i>22</i></b>
<b>1.6 Thesis Outline .....</b>	<b><i>23</i></b>
<b>Chapter 2: LFAC TS Equipment Overview .....</b>	<b><i>24</i></b>
<b>2.1 Introduction .....</b>	<b><i>24</i></b>
<b>2.2 Submarine Export Cables and Reactors .....</b>	<b><i>25</i></b>
2.2.1 Technical Benefits of LFAC for Cables .....	<i>25</i>

2.2.2	Submarine LFAC Export Cable Designs .....	28
2.2.3	Cable Impact to the LFAC TS Design .....	31
<b>2.3</b>	<b>Switchgears and Circuit Breakers .....</b>	<b>32</b>
2.3.1	Switchgears .....	32
2.3.2	Circuit Breakers .....	33
<b>2.4</b>	<b>Power Transformers .....</b>	<b>33</b>
2.4.1	LFAC Power Transformer Design Features .....	36
2.4.2	Impedance Effects on Transformer Weight .....	39
2.4.3	Impedance Effects on Transformer Losses.....	39
2.4.4	Comparison of 16.7Hz and 50Hz Transformer Designs .....	40
<b>2.5</b>	<b>Harmonic Filtering - Capacitors .....</b>	<b>41</b>
<b>2.6</b>	<b>Wind Turbine Generators .....</b>	<b>41</b>
<b>2.7</b>	<b>Frequency Converters.....</b>	<b>43</b>
<b>2.8</b>	<b>Summary and Conclusions .....</b>	<b>44</b>
<b>Chapter 3:</b>	<b><i>Offshore LFAC TS Electrical Design and Specifications.....</i></b>	<b>46</b>
<b>3.1</b>	<b>Introduction .....</b>	<b>46</b>
<b>3.2</b>	<b>Offshore Wind Power Plant System Layout .....</b>	<b>47</b>
3.2.1	OWTG / OWF System Configuration .....	50
3.2.2	Medium Voltage Collector System Layout .....	59
<b>3.3</b>	<b>Offshore LFAC Transmission System Layout.....</b>	<b>61</b>
3.3.1	LFAC Transformer .....	62
3.3.2	LFAC Export Cable .....	63
3.3.3	Reactive Power Compensation .....	67
3.3.4	System Impedance Damping .....	68
<b>3.4</b>	<b>Onshore BtB Frequency Converter .....</b>	<b>69</b>
3.4.1	MMC Control Arrangements .....	69
3.4.2	MMC System Configuration .....	71
3.4.3	Two-Level MMC and Half-Bridge Sub-Module (HBSM).....	72
3.4.4	PWM Technique .....	73
3.4.5	Number of HBSMs – DC Voltage .....	73
3.4.6	HBSM Capacitance .....	74
3.4.7	Arm Inductors.....	75

3.4.8	Interface MMC Transformers .....	77
<b>3.5</b>	<b>Summary and Conclusions .....</b>	<b>77</b>
<b>Chapter 4:</b>	<b><i>Frequency Domain Assessment</i>.....</b>	<b>79</b>
<b>4.1</b>	<b>Introduction .....</b>	<b>79</b>
4.1.1	Frequency Analysis Objectives for LFAC TS .....	79
<b>4.2</b>	<b>System Frequency Domain Modelling .....</b>	<b>80</b>
4.2.1	Modelling of the LFAC Subsea Cable .....	81
4.2.2	Cable Reactive Compensation Equipment .....	86
4.2.3	LFAC Transformers .....	86
4.2.4	Offshore Collector System (OCS) Representation .....	88
4.2.5	OWTGs and Onshore Frequency MMC Representation.....	89
<b>4.3</b>	<b>Export (PtP) LFAC TS Schemes without Filtering.....</b>	<b>90</b>
<b>4.4</b>	<b>Harmonic Mitigation Measures.....</b>	<b>92</b>
4.4.1	Passive Harmonic Filtering .....	93
4.4.2	C-Type Filter Design.....	94
<b>4.5</b>	<b>Export (PtP) LFAC TS Schemes with Filtering.....</b>	<b>99</b>
<b>4.6</b>	<b>Meshed (MT) LFAC TS Schemes without and with Filtering .....</b>	<b>101</b>
4.6.1	MT-LFAC TS with 200km-50km-200km Cables.....	101
4.6.2	MT-LFAC TS with 200km-50km-300km Cables.....	102
<b>4.7</b>	<b>System Impedance and Operating Frequency .....</b>	<b>103</b>
<b>4.8</b>	<b>Summary and Conclusions .....</b>	<b>105</b>
<b>Chapter 5:</b>	<b><i>Steady-State Analysis</i>.....</b>	<b>106</b>
<b>5.1</b>	<b>Introduction .....</b>	<b>106</b>
5.1.1	Steady-State Assessment Objectives for the LFAC TS .....	106
5.1.2	Offshore LFAC TS Grid Integration Requirements.....	107
<b>5.2</b>	<b>System Steady State Modelling.....</b>	<b>109</b>
5.2.1	AC Grid Representation .....	109
5.2.2	LFAC Transmission System Representation .....	109
5.2.3	Onshore BtB Frequency MMC-HVDC System.....	111
5.2.4	OWTGs Representation.....	112

<b>5.3</b>	<b>Power-Flow Studies for LFAC TS Schemes.....</b>	<b>113</b>
5.3.1	Set-Up of LFAC Export Power Flow Cases .....	114
5.3.2	Power Flow Cases Evaluation Principles.....	115
<b>5.4</b>	<b>Point-to-Point LFAC TS Schemes for OWF Integration .....</b>	<b>117</b>
5.4.1	Overall Results Evaluation .....	118
5.4.2	Feasible Point-to-Point Cases Examination .....	121
<b>5.5</b>	<b>Multi-Terminal (Meshed) Offshore LFAC TS Schemes.....</b>	<b>123</b>
5.5.1	Set-Up of Meshed LFAC TS Power Flow Cases .....	124
5.5.2	Full Power Export of the Two OWFs – (PF5e).....	126
5.5.3	Partly OWFs Export & Grid Interconnection Power Exchange (PF5d).....	126
<b>5.6</b>	<b>Summary and Conclusions .....</b>	<b>129</b>
<b>Chapter 6: System EMT Modelling and Controller Design.....</b>		<b>130</b>
<b>6.1</b>	<b>Introduction .....</b>	<b>130</b>
<b>6.2</b>	<b>System EMT Modelling .....</b>	<b>131</b>
6.2.1	AC Grid Representation .....	131
6.2.2	Cable EMT Model and Energisation .....	132
6.2.3	Onshore BtB MMC EMT Model .....	134
6.2.4	OWPP EMT Model.....	136
<b>6.3</b>	<b>VSC Control System Structure and Design.....</b>	<b>137</b>
6.3.1	VSC Models Control Hierarchy .....	137
6.3.2	VSC Synchronisation .....	138
6.3.3	Generic VSC Control System.....	139
6.3.4	Non-Island Control for Grid-Following Converters.....	141
6.3.5	Island Control of the Grid-Forming Converter .....	153
6.3.6	Circulating Current Suppression Control (CCSC) in MMC Systems.....	156
<b>6.4</b>	<b>Converter Control System Analysis.....</b>	<b>156</b>
6.4.1	Transfer Function Analysis .....	157
6.4.2	OWF Module EMT Implementation .....	164
<b>6.5</b>	<b>Summary and Conclusions .....</b>	<b>165</b>
<b>Chapter 7: Dynamic Performance Time Domain Evaluation.....</b>		<b>166</b>
<b>7.1</b>	<b>Introduction .....</b>	<b>166</b>
7.1.1	LFAC TS Scheme Model for EMT Simulation Studies.....	167

7.1.2	Offshore LFAC TS Energisation .....	168
7.1.3	Offshore LFAC TS LVRT/FRT Requirements .....	169
<b>7.2</b>	<b>EMT Studies Set-Up and Scenario Cases for LFAC TS Schemes .....</b>	<b>171</b>
<b>7.3</b>	<b>Point-to-Point LFAC TS Schemes for OWF Integration .....</b>	<b>172</b>
7.3.1	EMT1: Island Control without ICC on the LFAC Side MMC-T1.....	172
7.3.2	EMT2: Island Control with ICC on the LFAC Side MMC-T1 .....	186
7.3.3	Evaluation of the Point-to-Point LFAC TS Schemes .....	191
<b>7.4</b>	<b>Multi-Terminal (Meshed) Offshore LFAC TS Scheme .....</b>	<b>195</b>
7.4.1	EMT3: Island Control with ICC on the LFAC Side MMC1-T1 .....	196
7.4.2	Performance Evaluation of the Feasible LFAC TS Cases .....	208
<b>7.5</b>	<b>Summary and Conclusions .....</b>	<b>210</b>
<b>Chapter 8: Conclusion and Future Work.....</b>		<b>212</b>
<b>8.1</b>	<b>Summary and Discussion .....</b>	<b>212</b>
<b>8.2</b>	<b>Conclusions and Recommendations .....</b>	<b>213</b>
<b>8.3</b>	<b>Thesis Contributing Points .....</b>	<b>217</b>
<b>8.4</b>	<b>Limitations and Future Work .....</b>	<b>219</b>
<b>References.....</b>		<b>221</b>
<b>APPENDIX A.....</b>		<b><i>i</i></b>
<b>APPENDIX B.....</b>		<b><i>iii</i></b>
<b>APPENDIX C.....</b>		<b><i>xiii</i></b>
<b>APPENDIX D.....</b>		<b><i>xvi</i></b>

## List of Figures

Figure 1.1: Typical HVAC vs HVDC Cost Break-Even Distance for Power Transmission.....	1
Figure 1.2: Typical Layout of HVAC TS for Multiple OWF Integration to the Grid.....	2
Figure 1.3: Typical layout of a PtP HVDC TS Integrating two Interconnected OWFs to the grid, ABB. ....	3
Figure 1.4: Typical Schematic of a PtP HVDC TS for OWPP Integration to the AC Grid.....	4
Figure 1.5: First Structure of FFTS with a Magnetic Frequency Tripler. ....	6
Figure 1.6: Configuration of the LFAC TS utilising a Cyclo-Converter.....	7
Figure 1.7: Hypothetical North Sea Grid LFAC 220kV at 16.7Hz, route length in km. ....	8
Figure 1.8: Typical Diagram of a DC to Three-Phase AC MMC using Half-Bridge Sub-Modules. ....	9
Figure 1.9: Type 4 OWTG collection system arrangement for LFAC System. ....	10
Figure 1.10: Levelized Cost of Energy vs. a) Frequency for OWPP and b) Distance from Shore for OWP.....	11
Figure 1.11: Single Line Diagram of a Converter Station (IGCT) for Rail Application. ....	12
Figure 1.12: Energy Transmission Systems for OWFs: a) HVDC, b) LFAC: 16.7Hz. ....	15
Figure 2.1: HVAC AI Export Cable Losses at 50Hz, 16.7Hz and DC for: a) 230kV-1900mm <sup>2</sup> , b) 345kV-1400mm <sup>2</sup> . .	26
Figure 2.2: LFAC Cable System and Potential Compensation Scheme.....	27
Figure 2.3: Export Cable Transmission Capacity, for various reactive compensation schemes: a) 230 kV at 50Hz and 16.7Hz (left) and b) 345kV at 16.7Hz (Right). ....	27
Figure 2.4: Export Cable Alternatives - 1) XLPE - 345 kV 3x1x1400 mm <sup>2</sup> Al, 2) XLPE - 230 kV 3x1x1200 mm <sup>2</sup> Cu. .	28
Figure 2.5: Voltage and Current Profile over length for 200km - a) 230kV, 1600mm <sup>2</sup> Cu, b) 345kV, 1400mm <sup>2</sup> Al.30	
Figure 2.6: Arrangement of the components in the modular container concept by Alstom, for Railway application (all components are designed for the transportation via rail and standard road haulage), ALSTOM. ....	34
Figure 2.7: Theoretical design of a 50Hz transformer for comparison with the corresponding 16.66Hz, Theoretical design of a 16.7Hz transformer: a) Wide design, b) Tall design.....	35
Figure 2.8: LFAC Transformer Design Schematic. ....	36
Figure 2.9: Weight vs Impedance for a Single-Phase 141MVA 66/345kV Transformer at a) 16.7Hz, b) 50Hz.....	39
Figure 2.10: Losses vs Impedance for a Single-Phase 141MVA 66/345kV Transformer at a) 16.7Hz, b) 50Hz. ....	39
Figure 2.11: Comparison between 50 Hz (1p.u.) and 16.7 Hz Transformer designs.....	40
Figure 2.12: Capacitive Impedance and Q-Supply of a 10 $\mu$ F capacitor as a function of frequency. ....	41
Figure 2.13: Full Converter, Type-4 WTG configuration, ABB. ....	42
Figure 3.1: Meshed Offshore LFAC Transmission System for Offshore Wind integration. ....	46
Figure 3.2: Connection Point Terminology. ....	49
Figure 3.3: Type-4, Full Converter WTG Schematic. ....	50
Figure 3.4: Generic Vector Control Arrangement for the Equivalent WTG VSI Topology.....	52
Figure 3.5: Basic VSC Circuit Topologies for Type-4 WTGs: a) Two-Level, b) Three-Level VSC. ....	53
Figure 3.6: DBR in the DC-Link Side of the Type 4 WTG and its Typical Operation Characteristic.....	55
Figure 3.7: VSI LCL-Filter Schematic. ....	56
Figure 3.8: Frequency Response of the LCL Filter Design: Impedance Magnitude (Red) and Phase (Blue). ....	58
Figure 3.9: Schematic Representation of the 66kV Offshore WPP Layout, incl. Detail of a Single Array. ....	60
Figure 3.10: Simplified Representation of a PtP Scheme Integrating a 704MW OWPP Block to the Grid. ....	61
Figure 3.11: Offshore MT-LFAC System Integrating 1408MW OWF and Interconnecting different Grids. ....	62



Figure 3.12: Two-port, ABCD Network Equivalent for LFAC Cable. ....	65
Figure 3.13: Two-Port Oriented to a Cable $\Pi$ -Circuit System in the Phasor Domain. ....	66
Figure 3.14: LFAC Cable Total Current and Power Losses vs Cable Length. ....	67
Figure 3.15: Approximate Reactive Compensation of LFAC Cable and Shunt Reactor Size vs Cable Length. ....	68
Figure 3.16: Export Cable Impedance vs Cable Length, for Various Operating Frequencies. ....	69
Figure 3.17: Onshore Frequency MMCs in BtB Configuration and Potential Control Arrangements. ....	70
Figure 3.18: MMC Structure and Configuration. ....	71
Figure 3.19: MMC - HBSM Operation Modes. ....	72
Figure 3.20: PWM Patterns for Two-Level MMC using HBSM: a) PD-PWM and b) PSC-PWM. ....	73
Figure 4.1: Models for Cable Representation. ....	82
Figure 4.2: Frequency-Dependent Phase Cable Model Equivalent Circuit. ....	83
Figure 4.3: Graphic Representation of the Three-Phase XLPE cable in PSCAD. ....	84
Figure 4.4: Impedance Profile Difference of FDPM vs. $\Pi$ -Circuit Model of the XLPE-1400mm <sup>2</sup> -Al LFAC Cable. ....	85
Figure 4.5: a) Impedance vs. Frequency and b) Resonance vs. Harmonic Order Plots for various Cable Lengths. ....	85
Figure 4.6: Frequency Scans of the 200km Cable Alone and Connected to LFAC Transformers with Different $X_L$ . ....	87
Figure 4.7: Harmonic Order Impedance vs. Distance of LFAC Cable-Transformer pair for $X_L$ : a) 7% and b) 15%. ....	88
Figure 4.8: Array of 8 x OWTGs for Frequency Scan Studies. ....	88
Figure 4.9: VSC Model for Frequency Scans. ....	89
Figure 4.10: Impedance vs. Frequency Variation of the PtP LFAC TS with 200km cable, for various VSC states. ....	90
Figure 4.11: Simplified PtP LFAC TS Schematic with the Impedance Measurement Points. ....	91
Figure 4.12: PtP LFAC TS Impedance Profiles vs. Frequency for various Cable Lengths. Measurements at 345kV Onshore and Offshore and at 66kV OCS. ....	91
Figure 4.13: Harmonic Filters: a) Single-Tuned, b) Single-Damped, c) C-type, d) Double-Damped. ....	94
Figure 4.14: Combination of C-Type Filters rated 200MVAR at 43Hz and 100MVAR at 64Hz with $Q=2$ . ....	96
Figure 4.15: Filters Response Characteristics: Left-Impedance vs. Frequency Response, Right-Power Losses. ....	96
Figure 4.16: Effect of Harmonic Filter Implementation on the PtP LFAC TS Resonance for 200km Cable. ....	97
Figure 4.17: PtP LFAC TS Impedance Magnitude and Angle Profile vs. Frequency, after the Implementation of the Harmonic Filter for 200km Export Cable Length. ....	97
Figure 4.18: Impedance vs. Frequency Profiles of the C-Type Filters to the PtP LFAC TS. ....	98
Figure 4.19: Simplified PtP LFAC TS Schematic with Harmonic Filters and the Impedance Measurement Points. ....	99
Figure 4.20: Impedance vs. Frequency Profiles of the PtP LFAC TS with Harmonic Filters. ....	99
Figure 4.21: PtP LFAC TS Resonances for various Cable Lengths without (Left) and with (Right) H-Filters. ....	100
Figure 4.22: Simplified MT-LFAC TS Schematic with its Impedance Measurement Points. ....	101
Figure 4.23: Impedance vs. Frequency Profile (Onshore/Offshore) of PtP and MT-LFAC TS for 200km Cables. ....	101
Figure 4.24: Impedance vs. Frequency Profile (Onshore/Offshore) of PtP and MT-LFAC TS with Harmonic Filters for 200km Export Cables. ....	102
Figure 4.25: Impedance vs. Frequency Profile (Onshore/Offshore) of PtP and MT-LFAC TS before (Left) and after (Right) the Implementation of the Harmonic Filters, for 200km and 300km Export Cables. ....	102
Figure 4.26: System Frequency Scan approximations for various Operating Frequencies. ....	104
Figure 4.27: System Impedance Resonance (blue) and Resonant Harmonic Order range (orange) approximation for various Operating Frequencies. ....	104
Figure 5.1: a) Typical P/Q Variants required by TSOs on the PCC and b) WTG PQ Capability Curve. ....	108

Figure 5.2: Typical V-Q/Pmax Envelopes of OWPP at the PCC over 110kV, as TSO requirements. ....	108
Figure 5.3: Equivalent Cable $\Pi$ -Circuit Representation. ....	109
Figure 5.4: P/Q Capability Curves of the Grid-Following MMC Terminals.....	111
Figure 5.5: Power Capability Curves for OWTGs: a) Voltage-Dependent and b) P/Q Curves (WEA). ....	112
Figure 5.6: P-Q Capability Profile of the OWPP for 352 MW/440 MVA part of the 704MW OWF.....	112
Figure 5.7:SLD of the PtP LFAC TS Configuration. ....	113
Figure 5.8: Top Graphs: Total Power Losses and Voltage Regulation, Bottom Graphs: Total and Passive Reactive Compensation, for the PtP LFAC TS Cases.....	118
Figure 5.9: Top Graphs: Cable Total and Compensated Currents Loading, Bottom Graphs: OWF and MMC-T1 Loading, for the PtP LFAC TS Cases. ....	119
Figure 5.10: Power Losses, Voltage Regulation and Reactive Power Compensation, in each Main Busbar, for the Optimised PtP LFAC TS Cases.....	121
Figure 5.11: Current and Voltage Distribution in the Cable, for the Optimised PtP LFAC TS Cases.....	122
Figure 5.12: LFAC Cable Current Profile and Operating Points of the Frequency MMC against their Real and Reactive Counterparts, for the Optimised PtP LFAC TS Cases. ....	122
Figure 5.13:SLD of the MT-LFAC TS Configuration. ....	123
Figure 5.14: Power Losses, Voltage Regulation and Reactive Compensation in each Main Busbar of the MT-LFAC TS, for Cases PF5d and PF5dh. ....	127
Figure 5.15: LFAC Cable Current Loading and Operation of the MMCs against their Real and Reactive Counterparts, for the MT-LFAC TS Cases PF5d and PF5dh.....	128
Figure 6.1: Equivalent Circuit for AC Grid Representation. ....	131
Figure 6.2: Equivalent Circuit for LFAC Cable Energisation Study. ....	132
Figure 6.3: Cable Energisation Graphs as they appear from Top to Bottom: $V_{sa}$ , $V_{ra}$ , $I_{sa}$ , $I_{ra}$ and the Three-Phase Breaker Current, for a 200km (Left) and a 300km (Right) LFAC Subsea Cables. ....	133
Figure 6.4: HBSM Switching Circuit (Left) to Thevenin Equivalent Circuit (Right) for MMC Cell Modelling. ....	134
Figure 6.5: Layout of the Equivalent OWPP EMT Model.....	136
Figure 6.6: Control Hierarchy of the Dynamic VSC Models. ....	137
Figure 6.7: General Phase Lock Loop (PLL) and Voltage Controlled Oscillator (VCO) Structures. ....	138
Figure 6.8: Equivalent PWM VSC Time-Delay Block Diagram. ....	141
Figure 6.9: General VSC Outer Controller and Current Saturation Structure. ....	141
Figure 6.10: Generic Droop Characteristics for the DC and LFAC Voltage Controller References. ....	143
Figure 6.11: General ICC Block Diagram Implementation into a Grid Following VSC/MMC System.....	144
Figure 6.12: General ICC Closed-Loop Block Diagram.....	146
Figure 6.13: General DCVC Closed-Loop Block Diagram. ....	149
Figure 6.14: Locus demonstrating the Location of the Roots in the Complex Plane for Varying ' $\alpha$ '. ....	150
Figure 6.15: Generic ACVC Closed-Loop Block Diagram for the Equivalent OWF VSI.....	151
Figure 6.16: Generic ACVC Closed-Loop Block Diagram for the Grid-Following MMC facing the LFAC Side. ....	151
Figure 6.17: Generic APC and RPC Closed-Loop Block Diagrams. ....	152
Figure 6.18: General Islanded Control Block Diagram Implementation into the Grid-Forming MMC System. ....	154
Figure 6.19: Enhanced Islanded Control with ICC Block Diagram Implementation into the Grid-Forming MMC. ....	155
Figure 6.20: General CCSC Block Diagram Implementation into an MMC System.....	156
Figure 6.21: ICC (Left) and DCVC (Right) Pole-Zero Maps of CLTFs and Root Loci of OLTFs for the OWF VSI.....	159
Figure 6.22: DCVC-ICC (Top) and LFACV-ICC (Bottom) Bode Diagrams and Step Responses for the OWF VSI. ....	160

Figure 6.23: ICC (Left) and ACVC (Right) Pole-Zero Maps of CLTFs and RL of OLTFs for the MMC-T1 with ICC....	162
Figure 6.24: LFACVC – ICC Bode Diagram and Step Response for the MMC-T1 with ICC.....	162
Figure 6.25: ICC (Left) and DCVC (Right) Pole-Zero Maps of CLTFs and Root Loci of OLTFs for the MMC-T2.....	163
Figure 6.26:: DCVC – ICC Bode Diagram and Step Response for the MMC-T2 with ICC. ....	163
Figure 6.27: EMT Dynamic Response of the APC of OWF-VSC Rectifier and DCVC and ICC of OWF-VSI. ....	164
Figure 6.28: EMT Response of the OWF, showing the LFAC Voltage, Current, Active and Reactive Power. ....	164
Figure 7.1: ENTSO-E RfG - Voltage Against Time Profile for PPM connected at or above 110kV.....	170
Figure 7.2: Schematic of the EMT model for OWPP Integration using the PtP LFAC Export System.....	172
Figure 7.3: EMT1ai) Study Result Graphs at the Offshore (Left) and Onshore (Right) LFAC Cable Sides.....	174
Figure 7.4: EMT1ai) Onshore 345kV-Top: THDv and THDi [%], Bottom: Voltage Harmonics [kV-V <sub>lpeak</sub> ] (1 <sup>st</sup> out).175	175
Figure 7.5: LFAC DQ-Voltage of the Islanded Controller in the MMC-T1 for EMT1ai), (d-green, q-purple).....	176
Figure 7.6: EMT1ai) Study Result Graphs at the PCC with the AC Grid. ....	177
Figure 7.7: EMT1aii) Study Results at the Offshore (Left) and Onshore (Right) LFAC Cable Sides.....	178
Figure 7.8:EMT1aii) Onshore 345kV-Top: THDv and THDi [%], Bottom: Voltage Harmonics [kV-V <sub>lpeak</sub> ] (1 <sup>st</sup> out).178	178
Figure 7.9: LFAC DQ-Voltage of the Islanded Controller in MMC-T1 for EMT1aii), (d-green, q-purple).....	179
Figure 7.10: EMT1ai) Study Result Graphs at the PCC with the AC Grid. ....	179
Figure 7.11: EMT1b Study Results at the Onshore LFAC Cable Side (Left) and the PCC with the AC Grid (Right). 180	180
Figure 7.12: LFAC-DQ Voltage of the Islanded Controller in MMC-T1 for EMT1b, (d-green, q-purple).....	181
Figure 7.13: DC-Pole Voltages (Two-Top Graphs) and DC-Pole Currents (Two-Bottom Graphs), in MMC-T1 and MMC-T2 of the BtB Frequency MMC, Respectively, for EMT1b.....	181
Figure 7.14: EMT1ci) Results at the Onshore LFAC Cable Side (Left) and the PCC with the AC Grid (Right).....	182
Figure 7.15: Left: DC-Voltage (Top), and DQ-Voltage (Bottom), Right: DQ-ICCs in the MMC-T1 for EMT1ci). ....	183
Figure 7.16: EMT1cii) Study Result Graphs at the Offshore (Left) and Onshore (Right) LFAC Cable Sides. ....	184
Figure 7.17: Equivalent DC-Voltage (Top), and DC-Current (Bottom) of the BtB VSCs in the OWF for EMT1cii)..	184
Figure 7.18: EMT1cii) Study Result Graphs at the PCC with the AC Grid.....	185
Figure 7.19: EMT2b) DQ-Voltage (Top), and DQ-ICCs (Bottom) of the Enhanced Islanded Control in MMC-T1. .	187
Figure 7.20: EMT2c Study Result at: Top - PCC at AC Grid, Bottom - OCS (Left) and Onshore (Right) LFAC Sides.188	188
Figure 7.21: DC-Voltage (Top), and LFAC DQ-Voltage (Bottom) of the BtB Frequency MMCs for EMT2c. ....	189
Figure 7.22: EMT2c) Total and Saturated Current (Top), and DQ-ICCs (Bottom) of the BtB Frequency MMCs....	190
Figure 7.23: Schematic of the EMT model for OWPP Integration and Interconnection using the MT-LFAC TS....	195
Figure 7.24: EMT3a Study Results at: → Top - PCC with the AC Grid, (MMC1-T2 and MMC2-T2).....	198
Figure 7.25: Onshore 345kV Left: MMC1-T1, Right: MMC2-T1 - THD (Top) and Voltage Harmonics (Bottom)...	199
Figure 7.26: EMT3b Study Results at: → Top - PCC with the AC Grid, (MMC1-T2 and MMC2-T2).....	201
Figure 7.27: DC-Pole Voltages (Two-Top Graphs) and DC-Pole Currents (Two-Bottom Graphs), in MMC1 (Left) and MMC2 (Right) BtB Frequency Converters, Respectively, for EMT3b. ....	202
Figure 7.28: EMT3b) DQ-Voltage (Top), and DQ-ICCs (Bottom) of the Enhanced Island Controller in MMC1-T1.202	202
Figure 7.29: EMT3c Study Results at: → Top - PCC with the AC Grid, (MMC1-T2 and MMC2-T2).....	204
Figure 7.30: Onshore LFAC 345kV Left: MMC1-T1, Right: MMC2-T1 - EMT3c Results in the order they appear: DC-Voltage (Top), LFAC DQ-Voltage (Left) and ACVC (Right), Total and Saturated Currents, DQ-ICCs (Bottom). ....	205
Figure 7.31: Limits for RMS Value of TOVs for 400kV and 275 kV in GB Network. ....	207

## List of Tables

<i>Table 2-1: LFAC Export Cable Electrical Parameters for 230kV and 345kV - NEXANS.</i>	29
<i>Table 2-2: Offshore LFAC Transmission System Design Parameters &amp; Ambient Conditions - Seabed.</i>	29
<i>Table 2-3: System values for 200km - 230kV, 1600mm<sup>2</sup> Cu and 345kV, 1400mm<sup>2</sup> Al.</i>	30
<i>Table 2-4: Parameter Assumptions for Transformer Design Calculations.</i>	36
<i>Table 2-5: Transformer Standard Design Equations.</i>	37
<i>Table 2-6: International Projects using MMC Technology in Similar Scale ~700MW.</i>	44
<i>Table 3-1: Electrical Data of the OWF Integration System.</i>	47
<i>Table 3-2: Full-Converter WTG Electrical Rating.</i>	48
<i>Table 3-3: Investigated LFAC Power Export Arrangements.</i>	48
<i>Table 3-4: Aggregate WTG VSI Electrical Parameter Data.</i>	51
<i>Table 3-5: DC Side Parameters of the Equivalent BtB VSC Scheme.</i>	53
<i>Table 3-6: DC Capacitor Parameters</i>	54
<i>Table 3-7: Dynamic Braking Resistor Parameters.</i>	55
<i>Table 3-8: VSI LCL-Filter Parameters.</i>	58
<i>Table 3-9: LFAC OWF-Inverter Transformer Parameters.</i>	59
<i>Table 3-10: The 72.5kV Class Switchgear System Configuration (GIS)</i>	59
<i>Table 3-11: Inter-Array String Cable Parameters.</i>	60
<i>Table 3-12: Array 800mm<sup>2</sup>, Cu-XLPE Cable Utilization.</i>	60
<i>Table 3-13: Medium Voltage - 66kV - Array and Sub-Array Submarine XLPE Cables (ABB).</i>	61
<i>Table 3-14: LFAC Step-Up Transformer Electrical Parameters</i>	62
<i>Table 3-15: 345kV Submarine LFAC – XLPE Export Cable Electrical Parameters (NEXANS).</i>	63
<i>Table 3-16: 200km LFAC – XLPE Export Cable Characteristic Parameters.</i>	64
<i>Table 3-17: LFAC Export Cable <math>\Pi</math>-Circuit Impedance and Admittance for 200km.</i>	66
<i>Table 3-18: LFAC Export Cable <math>\Pi</math>-Circuit Parameters for Various Lengths.</i>	66
<i>Table 3-19: LFAC Export Cable Electrical Performance based on <math>\Pi</math>-Circuit Analysis, for Various Lengths.</i>	67
<i>Table 3-20: Indicative Reactive Power Compensation of the LFAC Export Cable for Various Lengths.</i>	68
<i>Table 3-21: Back to Back MMCs AC System Electrical Data.</i>	70
<i>Table 3-22: Number of HBSM and Voltage Levels in the MMC</i>	74
<i>Table 3-23: HBSM Capacitance for the BtB MMC Terminals.</i>	75
<i>Table 3-24: MMC Transformer Specifications at both MMC Terminals.</i>	77
<i>Table 4-1: 300MVar C-Type, Single and Double-Damped Filter Parameters for LFAC TS with 200km Cable.</i>	96
<i>Table 4-2: C-Type Filter Parameters for PtP LFAC TS with various Cable Lengths.</i>	98
<i>Table 4-3: Voltage Distortion Limits for General Transmission Systems.</i>	100
<i>Table 4-4: Current Distortion Limits for General Transmission Systems &gt;161kV.</i>	100
<i>Table 5-1: List of the Power-Flow Cases for the PtP LFAC TS.</i>	114
<i>Table 5-2: Evaluation Criteria for the PtP LFAC TS Cases (Dark Colouring for Higher Values).</i>	118
<i>Table 5-3: List of the Power-Flow Cases for the MT-LFAC TS.</i>	124
<i>Table 6-1: Equivalent AC Grid Parameters.</i>	131
<i>Table 6-2: Base Parameters of the LFAC TS for p.u. Representation</i>	140

<b>Table 6-3: Tuning Parameters of the Equivalent OWF VSI Modules. ....</b>	<b>158</b>
<b>Table 6-4: Control System Response Characteristics of the Equivalent OWF VSI TFs. ....</b>	<b>159</b>
<b>Table 6-5: Tuning Parameters of the Equivalent BtB MMC Modules ....</b>	<b>161</b>
<b>Table 6-6: Control System Response Characteristics of the Equivalent MMCs TFs. ....</b>	<b>161</b>
<b>Table 7-1: List of EMT Studies and Cases for PtP LFAC TS. ....</b>	<b>171</b>
<b>Table 7-2: List of EMT Studies and Cases for MT-LFAC TS. ....</b>	<b>171</b>
<b>Table 7-3: List of Cases for EMT1 Study.....</b>	<b>172</b>
<b>Table 7-4: Simulation Sequence for Case EMT1a.....</b>	<b>173</b>
<b>Table 7-5: Simulation Sequence for Case EMT1b.....</b>	<b>180</b>
<b>Table 7-6: Simulation Sequence for Case EMT1c, i) and ii). ....</b>	<b>182</b>
<b>Table 7-7: List of Cases for EMT2 Study.....</b>	<b>186</b>
<b>Table 7-8: Simulation Sequence for Case EMT2c.....</b>	<b>188</b>
<b>Table 7-9: Summary and Evaluation Table for the PtP LFAC TS EMT Cases. ....</b>	<b>191</b>
<b>Table 7-10: List of Cases for EMT3 Study.....</b>	<b>196</b>
<b>Table 7-11: Simulation Sequence for Case EMT3a.....</b>	<b>196</b>
<b>Table 7-12: Simulation Sequence for Case EMT3b.....</b>	<b>200</b>
<b>Table 7-13: Simulation Sequence for Case EMT3c. ....</b>	<b>203</b>

## Abbreviations

AC	-	Alternating Current
ACVC	-	AC Voltage Controller
APC/RPC	-	Active/Reactive Power Controller
APOD	-	Alternate Phase Opposition Disposition
BtB	-	Back-to-Back
CAPEX	-	Capital Expenditure
CB	-	Circuit Breaker
CC	-	Cascaded
CCSC	-	Circulating Current Suppression Controller
CLTF	-	Closed Loop Transfer Function
DBR	-	Dynamic Braking Resistor
DC	-	Direct Current
DCVC	-	DC Voltage Controller
DFIG	-	Doubly-Fed Induction Generator
EMT	-	Electro-Magnetic Transient
FBSM	-	Full Bridge Submodule
FDPM	-	Frequency Dependent Phase Model
FFTS	-	Fractional Frequency Transmission System
FS	-	Frequency Scan
HBSM	-	Half Bridge Submodule
HBSM	-	Half Bridge Sub-Module
HF	-	Harmonic Filter
HVAC	-	High Voltage AC
HVDC	-	High Voltage DC
IC	-	Islanded Control
ICC	-	Inner Current Controller
IGBT	-	Insulated-Gate Bipolar Transistor
ITAE	-	Integral Time Absolute Error
LCC	-	Line Commutated Converter
LFAC	-	Low Frequency AC
LPF	-	Low-Pass Filter
LTF	-	Laplace Transform
MATLAB	-	Matrix Laboratory
MCPWM	-	Multi Carrier PWM
MMC	-	Modular Multi-Level Converter
MO	-	Modulus Optimum
MT	-	Multi-Terminal
NPC	-	Neutral Point Clamped
O&M	-	Operation and Maintenance
OCS	-	Offshore Collector System

OECD	-	Organisation for Economic Cooperation and Development
OHTL	-	Over-Head Transmission Line
OLTF	-	Open Loop Transfer Function
OPEX	-	Operational Expenditure
OWE	-	Offshore Wind Energy
OWF	-	Offshore Wind Farm
OWP	-	Offshore Wind Power
OWPP	-	Offshore Wind Power Plant
OWTG	-	Offshore Wind Turbine Generator
PD	-	Phase Disposition
PF	-	Power Flow
PI	-	Proportional Integral
PLL	-	Phase Locked Loop
POD	-	Phase Opposition Disposition
PSCAD	-	Power Systems Cad
PSPWM	-	Phase Shifted PWM
PtP	-	Point-to-Point
PWM	-	Pulse Width Modulation
RES	-	Renewable Energy Sources
RL	-	Root Locus
RMS	-	Root Mean Square
SCC	-	Short Circuit Capacity
SFC	-	Static Frequency Converter
SG	-	Synchronous Generator
SiSo	-	Single Input-Single Output
SM	-	Sub-Module
SO	-	Symmetrical Optimum
T&D	-	Transmission and Distribution
T1,2	-	Terminal 1,2
TD	-	Time-Domain
TF	-	Transfer Function
THD	-	Total Harmonic Distortion
TOV	-	Temporary Over-Voltage
TS	-	Transmission System
VAR	-	Voltage Ampere Rating
VCC	-	Vector Current Control
VCO	-	Voltage Controlled Oscillator
VSC	-	Voltage Source Converter
VSI	-	Voltage Source Inverter
WTG	-	Wind Turbine Generator
XLPE	-	Cross-linked polyethylene

# Chapter 1: Introduction

## 1.1 Transmission Systems for OWP Exploitation

Over the past decades, the markets for the electric power industry and by proximity, for the Transmission and Distribution (T&D) equipment and grid solutions, have undergone profound transformations as a consequence of the pace of Renewable Energy Sources (RES) penetration to the grid, the concurrent retirement of carbon-emitting sources, and the fluctuation oil and gas prices. The amount of investment worldwide in the T&D sector is estimated at \$6.9 trillion per year in the next 15 years. Nearly two-thirds of this investment takes place in emerging economies, with the focus for investment moving beyond China to other parts of Asia, Africa and Latin America; but ageing infrastructure and climate policies create large requirements also across the OECD member countries [98].

Recently, the exploitation of Offshore Wind Energy (OWE) for electricity generation has been expanding rapidly due to technological advancements, the abundant offshore space, the increased capacity factors of this wind resource and government incentives. However, there are certain drawbacks associated with remote OWE systems which may increase the cost of electric power generation. The intermittent wind power supply may lead to lower capacity credits, while the transmission of bulk amount of power over long distances generally increases the power losses as well as operational and maintenance (O&M) costs. Thus, the choice of a technically efficient and economical approach for exporting the wind power to the AC grid is mainly determined by the Offshore Wind Power Plant (OWPP) capacity and its distance from shore and can be the principal expenditure affecting the economics of the system. Currently, the HVAC and HVDC TS are the commercial options for integrating OWPPs to the grid and a typical break-even distance curve is shown in Figure 1.1 [101].

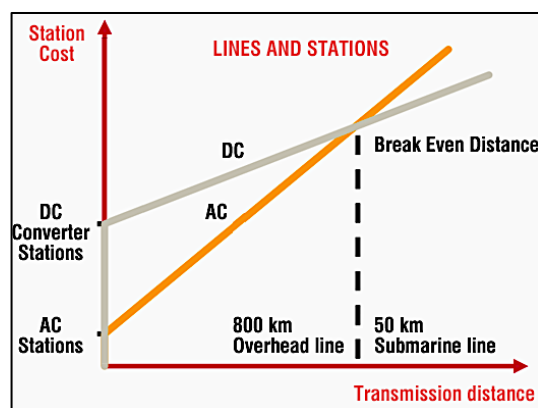


Figure 1.1: Typical HVAC vs HVDC Cost Break-Even Distance for Power Transmission.



### 1.1.1 HVAC

Currently, the HVAC transmission system with subsea cables is the most common scheme for integrating OWPPs to the grids [93]. The major advantage of this technology is its simple and robust system design and protection that results in relatively low Capital and Operational Expenses (CAPEX & OPEX) if adopted for relatively short offshore transmission distances (e.g. less than 50km, Figure 1.1 [101]).

In typical OWPP arrangements, the OWTGs can be connected to the Offshore Collector System (OCS) point at Medium Voltage level, as is depicted in Figure 1.2 [102]. In the offshore substation of an HVAC TS, the transformers steps-up the AC voltage to higher levels for power transmission purposes. Thus, wind power is transferred through HVAC subsea cables to an onshore substation where it is interfaced to the grid by power transformers that adjust the voltage level using tap changers. Depending on project-specific characteristics of an HVAC TS, offshore and/or onshore shunt reactive power compensation is employed in the form of switched reactors, STATCOMs or SVCs to limit voltage rise and improve efficiency [113].

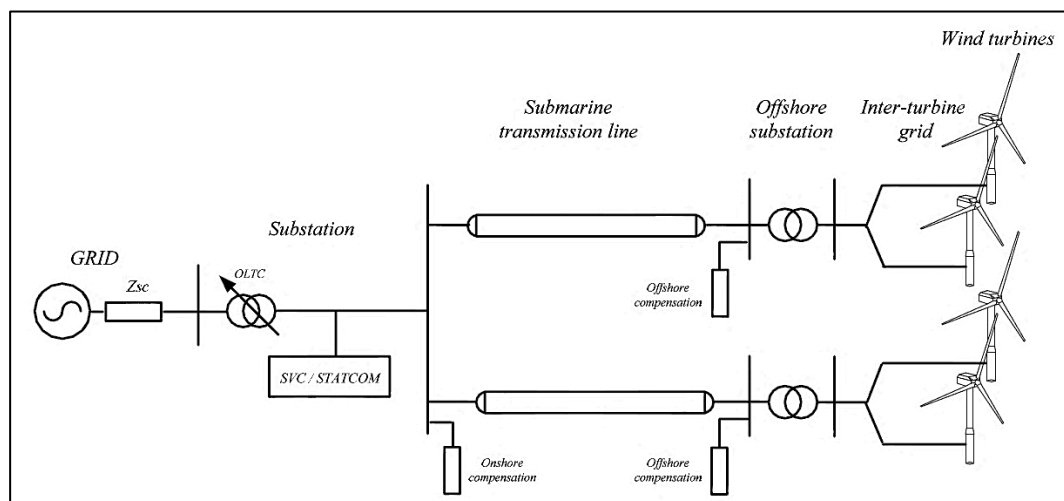


Figure 1.2: Typical Layout of HVAC TS for Multiple OWF Integration to the Grid.

However, the offshore HVAC TS is mainly limited by the charging current due to the high capacitance of the submarine cables. Thus, for relatively longer distances (i.e. >50km), there is a reduction in transmission capacity and an increase in transmission losses. Besides, over a certain distance, the increased capacitance of the HVAC cables may result in very low-order harmonic resonances [111]. Therefore, additional equipment may need to be implemented in order to enhance the stability and/or retain the overall system synchronisation under the same frequency, since the HVAC TS and the onshore grid are synchronously coupled, and faults or disturbances on one side of the network can directly affect the other.

### 1.1.2 HVDC

The HVDC may be preferred over the HVAC transmission for integrating distant (e.g. >100km) offshore renewable energy generation to the grid, mainly because it is not limited by the vast capacitive reactive power and the charging currents in submarine cables [132]. Although the thyristor-based LCC-HVDC is a reliable, proven transmission system, there are notable drawbacks associated with its use for OWP exploitation such as reactive power consumption and low-order harmonic distortion, which requires auxiliary equipment (static synchronous compensators, AC filters, capacitor banks, etc.) [20].

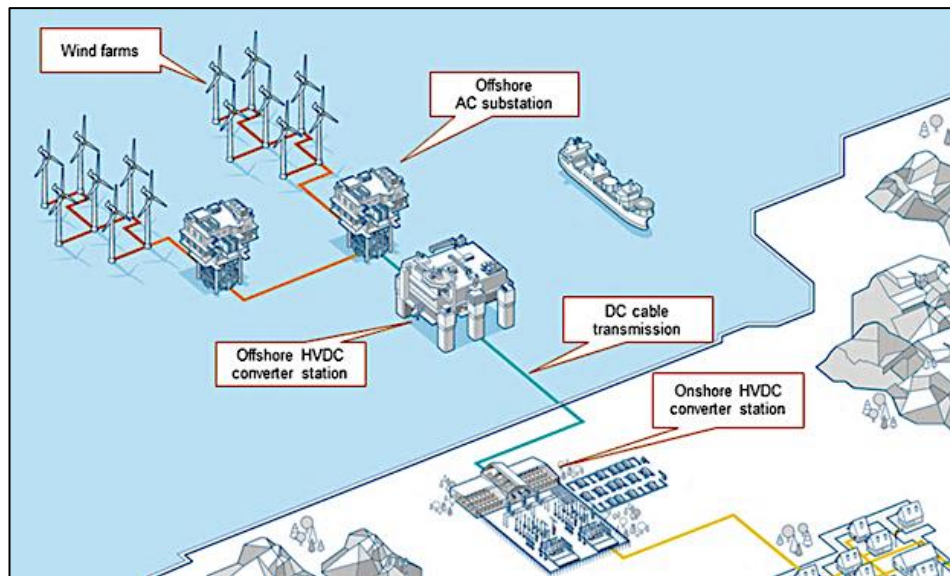


Figure 1.3: Typical layout of a PtP HVDC TS Integrating two Interconnected OWFs to the grid, ABB.

Technological advances in the current and voltage ratings of semiconductor switches (e.g. IGBTs) and improvements in converter control systems made it possible to independently regulate active and reactive power exchange between the onshore grid and the offshore AC collection point. The VSCs have been made reliable and economical for integrating remote OWFs to the grids through HVDC links, increasing wind power penetration and leading many T&D equipment manufacturers to introduce commercially available and practically regulated VSC-HVDC systems [125]. Also, developments in the converter valve technology allow higher DC voltage levels using the Modular Multilevel Converters (MMCs) can reduce the transmission losses of the system and enable radial, ring or even MT-HVDC schemes.

In principle, MMCs involve several series-connected half-bridge sub-modules, based on IGBTs that can turn on and off in a controlled manner at high switching frequency using a PWM technique for each module. These converters can provide independent control of active and reactive power, black-start and FRT capability. Depending on the number of modules utilised,

they can produce a nearly sinusoidal voltage, and as a result, the filter size is reduced or even eliminated. The switching frequency for each switch can be around 3 to 5 times that of the AC line frequency, which leads to much lower switching losses.

However, for the development of a meshed MTDC grid, the flexible and safe operation of the system must be guaranteed by an effective protection scheme that can isolate only specific branches in cases of DC faults without interrupting the operation of the whole HVDC grid. Hence, current zero-crossing equivalent conditions must be created to force the interruption of current whenever a DC fault occurs. The formation of such conditions relies on the development of either a mature HVDC circuit breaker technology that can handle fault situations and withstand the high voltage and current response of the network or an efficient MMC fault clearing control strategy through the full-bridge submodules since they can provide negative voltage. Both potential solutions can be technically challenging and expensive, but the key contributor to the overall HVDC schemes expenditure are the offshore HVDC platform costs.

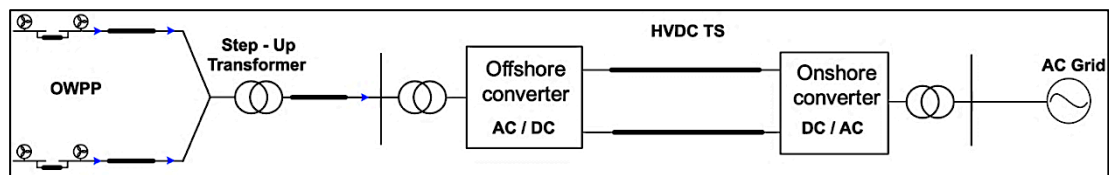


Figure 1.4: Typical Schematic of a PtP HVDC TS for OWPP Integration to the AC Grid.

Thus, the application of the HVDC TS for OWF integration to the grid, as shown in Figure 1.4, has the following conceptual and theoretical barriers and limitations:

- The need to place one VSC-HVDC converter, including the corresponding sensitive equipment on an offshore DC-platform increase the CAPEX and OPEX [130].
- HVDC Circuit Breakers (CBs) are complex components and costly to build [20].
- The space charge accumulation of the cable caused by the DC current during the construction period and corrosion are always serious concerns for HVDC systems.
- Realisation of multi-terminal DC (MTDC) systems is a principal challenge. Thus, wind farm parks commissioning must take place in stages; each one individually connected to the nearest onshore substation; point-to-point connections.
- It is not still possible to achieve a fully co-ordinated offshore DC grid. This happens mainly because DC circuit breakers (CB) are not yet commercially applicable and extra DC/DC converters should be used to interconnect DC links of different voltage levels since it is not possible to change voltage levels in DC networks by transformers.

## 1.2 LFAC Transmission System

The low frequency AC is an interesting technology which has been developed and used for several decades by the railway grid operated at frequencies of 50/3Hz, 16.7Hz, 20Hz, and 25Hz. The LFAC systems were introduced to solve a problem in finding an optimum universal motor for traction applications and reducing the adverse effects of the reactance at 50Hz. In recent years, though, this technology has become obsolete, thanks to advancements in the field of power electronics which enabled compact building blocks at low cost and high power, leading to mass production of power converters that could convert any AC frequency to DC or even transform single-phase to multiple-phases within the locomotive itself. Hence, some railways have been converted to standard grid frequencies, and only a few still follow the path of LFAC. A possible trend in this industry might be that by the end of asset life, the universal power supply on board of the locomotive that initially used LFAC, would be adjusted to operate also on the regular grid frequency.

The basic idea of the LFAC system is to use lower frequency to reduce the effective electrical length of the AC transmission cable, thus increasing its transmission capacity. The principle of LFAC can be viewed from the perspective of its electrical length. Considering the electricity transmission velocity equal to the speed of light, (300000 km/s), then the AC wavelength is  $\sim 1/3$  of the corresponding LFAC wavelength. Thus, for the same range, the electrical length shrinks three times, increasing the transmission capacity improving system performance. By establishing an offshore transmission system at approximately one-third of the grid frequency, the charging current reduces accordingly for the same cable lengths [1][5][8][10]. Therefore, theoretically either the reach of the cable could be approximately three times longer, or the capacity of the LFAC system can be as much as three times that of 50/60Hz system [30-45] [49-53].

LFAC technology can provide an attractive solution not only for exporting power from large and remote OWPPs but also for a potential offshore network development that could enable the exchange of power among different grids. It could be realised as a combined offshore HVAC system with onshore frequency conversion schemes, and thus removing the need of the bulk offshore HVDC platforms. Then, sea and land HVAC cables could be operated at lower frequencies, eliminating capacitive currents, reactive compensation and losses compared to HVAC and overcoming the technical and operating constraints of HVDC for the formation of offshore grids [7].

## 1.2.1 LFAC TS Concepts in the Literature

### 1.2.1.1 LFAC for Power Transmission

LFAC was proposed as a potential power system transmission technology in 1994 by Xifan and Xiuli Wang [54]. The authors presented a Fractional Frequency Transmission System (FFTS) that could reduce the AC reactance by operating at  $50/3\text{Hz}$ , increasing the power transfer capability of the AC system and improving the operating performance of the network. Computer simulation results in papers [47] and [40], illustrated that the FFTS could be a promising transmission technology, despite the low efficiency of the magnetic frequency changer shown in Figure 1.5 which has become obsolete, mainly replaced by PE converters.

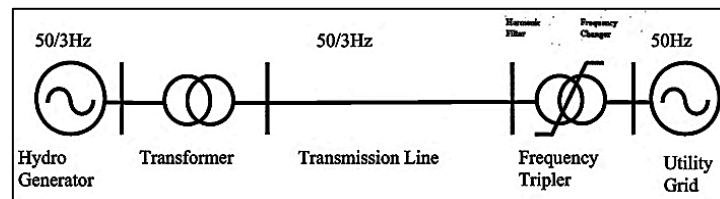


Figure 1.5: First Structure of FFTS with a Magnetic Frequency Tripler.

In 2000 T. Funaki and K. Matsuura studied the feasibility of LFAC for interconnecting grids that operate at different frequencies and voltage levels using conventional AC XLPE cables to avoid the high charging currents of HVAC or the space charge accumulation issue related to HVDC [53]. Simulation results showed high performance of power flow control for the LFAC system. Based on this work, in 2002, the writers, together with R. Nakagawa, assessed the possibility of employing cycloconverters for frequency conversion by introducing a novel control system [52]. However, large filters would be necessary at both ends to suppress low-order harmonics and adjust reactive power while the need for improvement of its transmission efficiency is mentioned in [46][49][50].

### 1.2.1.2 LFAC for Wind Power Integration

In 2009, the authors of [45] and [41] suggested the use of LFAC TS for connecting OWFs to the grid. The different transmission technologies were compared Equivalent layouts of, and LFAC system demonstrated considerable advantages. It improved transmission capability and reduced losses compared to HVAC, while it decreased Capex and maintenance costs over HVDC for a range of 30-150km, extending the lifespan of subsea cables and eliminating the need for WTG converters and offshore platforms. In addition, Xifan Wang et al. in [44] and [33] introduced a novel approach for integrating remote onshore WFs into the grid via a FFTS using the thyristor-based cycloconverter technology, as shown Figure 1.6, which has also been addressed for OWP applications in many scientific papers [18][23][34][35][36][36][51].

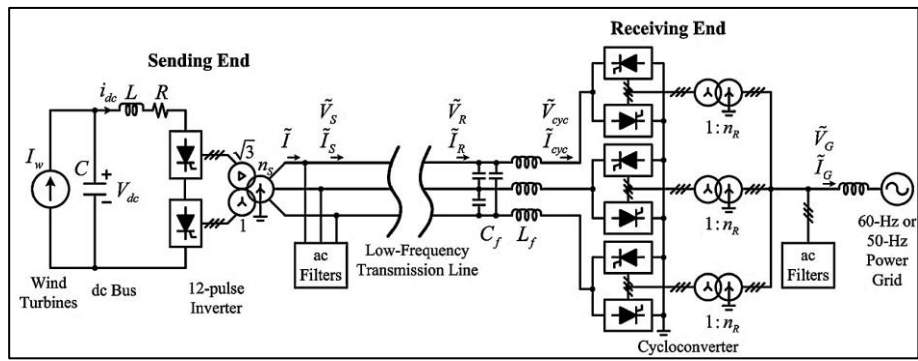


Figure 1.6: Configuration of the LFAC TS utilising a Cyclo-Converter.

The majority of the related research suggests various LFAC system arrangements which are connected at substations via cycloconverters, providing economic connection and synchronisation with the main grid [6][10][12]. Cost reduction enabled with cycloconverters can be substantial in comparison to HVDC options, but with many technical constraints such as the fixed frequency reduction at 50/3Hz or 60/3Hz [24]. For offshore power transmission at low frequency, subsea cables rated for 50 or 60Hz operation are employed and commercial transformer designs for 50Hz or 60Hz are adopted in systems that utilise low operating frequency, typically 16.7Hz or 20Hz, to minimise further the system cost [11][13][14][18].

### 1.2.1.3 LFAC for Offshore Grid Formation

In 2012, W. Fischer et al. suggested the potential use of LFAC TS for the development of an offshore grid with OWTGs generating power straight at 16.7Hz and AC/AC cycloconverters placed onshore for frequency conversion [30]. Simulation studies in which the cable was modelled as 100 pi-sections showed that the transmission distance at 16.7Hz could reach 300 to 400km. For the same application, in 2015 I. Erlich et al., mentioned that lower installation and operational costs could be achieved with LFAC transmission of 600MW up to a distance of 400km by using a 245kV XPLE submarine cable [3]. Moreover, by upgrading the AC circuit breaker technology, the required (n-1) reliability could be met for the offshore LFAC grid formation. However, they implied that the onshore BtB converter configuration would need further investigation (full or half-bridge MMC, Matrix Converter, Cyclo-converter, etc.), while the transformers and shunt reactors operated at low frequency would be larger and heavier. Based on these studies, U. Behmann and T. Schütte proposed LFAC to export wind power generation in the North Sea as depicted in Figure 1.7 [123], for schemes with long transmission distances in which the 50Hz AC system would not be technically viable. More specifically, the offshore LFAC TS can be created by an onshore frequency converter, converting the grid frequency to a low frequency, eliminating the need for offshore converter

platform which is a crucial contributor to HVDC schemes expenditure, and introducing a competitive offshore transmission system up to a particular cable length [2][4][7].

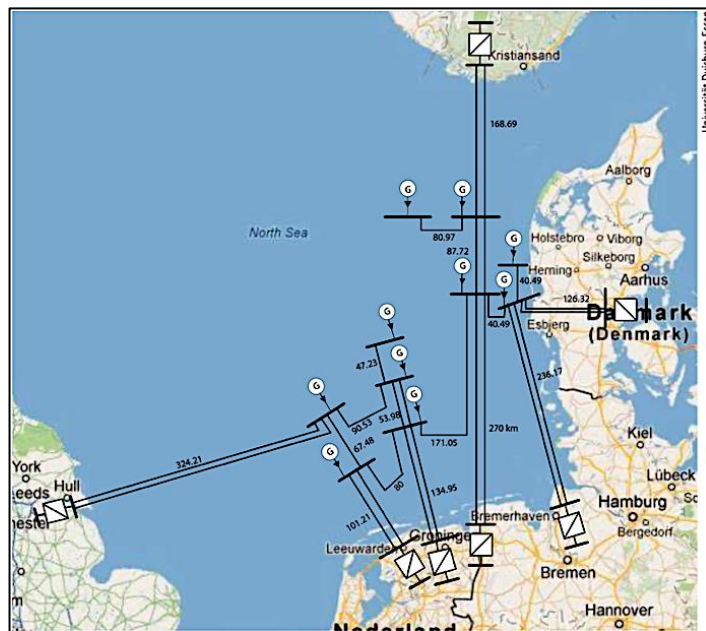


Figure 1.7: Hypothetical North Sea Grid LFAC 220kV at 16.7Hz, route length in km.

Based on these studies, U. Behmann and T. Schütte proposed LFAC to export wind power generation in the North Sea as depicted in Figure 1.7 [123], for schemes with long transmission distances in which the 50Hz AC system would not be technically viable. More specifically, the offshore LFAC TS can be created by an onshore frequency converter, converting the grid frequency to a low frequency, eliminating the need for offshore converter platform which is a crucial contributor to HVDC schemes expenditure, and introducing a competitive offshore transmission system up to a particular cable length [2][4][7].

#### 1.2.1.4 Advancements in Frequency Conversion and LFAC Equipment

Latest advancements in the field of power electronics have also made the Voltage Source Converter (VSC) and Modular Multilevel Converter (MMC, Figure 1.8 [107]) technology more reliable and economical. Back-to-back (BtB) VSC or MMC arrangements located onshore could be feasible for offshore wind farm (OWF) integration to the main grid using LFAC transmission system (LFAC TS) [2]. LFAC submarine cables that are designed and optimised for operation at low frequency and rated at 16.7Hz become available by the manufacturers for subsea power transmission over long distances [2][7]. Moreover, theoretical designs of three-phase power transformers are proposed in the literature, that are intended for operation at low frequency [5], while plenty of lower-rated single-phase-unit LFAC transformers are commercially available by various manufacturers for rail applications.



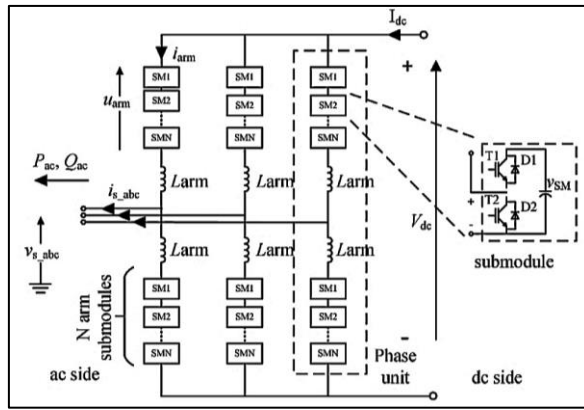


Figure 1.8: Typical Diagram of a DC to Three-Phase AC MMC using Half-Bridge Sub-Modules.

Thus, the LFAC technology could be applied for OWP export over a specific distance range of approximately 100-400km [3], leading to efficient power transmission and interconnection between the OWFs and the grids. It could suggest an alternative pathway for cases that the HVAC TS is not technically and economically feasible and aims at achieving a more straightforward technical solution than HVDC, without deploying a fully-fledged offshore HVDC converter station that leads to large platform topsides.

### 1.2.2 WF Collection Systems in LFAC TS Concepts

Many alternative medium-voltage collection system technologies are proposed in the literature for the integration of wind power through the LFAC TS. The DC collection systems are proposed for onshore and offshore WF configurations in [6][8][11][12][13][27]. The main reason for a DC collection system with LFAC transmission is that the WTs towers would not need larger, heavier, and costlier magnetic components (e.g. step-up transformers) to output their LFAC power. Hence, series and parallel DC WF connections are examined which are integrated through either radial or meshed LFAC network arrangements [39].

In addition, a fractional frequency system (FFWPS) concept was introduced in [38] and later on investigated through simulation studies in [34]. This system eliminates the need of the full-power converter in each WTG and can be beneficial for OWFs, due to the relatively small wind velocity difference. The FFWPS operates at a variable frequency (VF) that is defined by adjusting the cycloconverter's output in real-time, according to the wind velocity, so that more OWP could be captured. The frequency ranges from 12Hz to 19Hz in different research papers depending on the application, while in [1] a constant frequency (CF) operation is also introduced at 50/3Hz, that simplifies the cycloconverter control. Of course, power losses are caused by the removal of the full converter, but the OWP can be exported with relatively high efficiency, resulting in a potential future development that needs further research.



However, in several research works consider that the maturity level of the offshore wind equipment could be quite satisfactory for the application of LFAC technology [2][3][7][9]. Thus, individual OWTGs are interconnected to a medium voltage LFAC power collection system in a typical HVAC fashion e.g. at 66kV, as in Figure 1.9 [3] and their power is collected at the OCS where the voltage is increased to the transmission level by a step-up transformer. The power is then transferred to the grid utilising the LFAC transmission system.

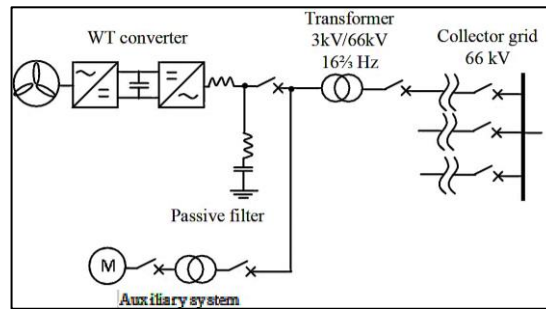


Figure 1.9: Type 4 OWTG collection system arrangement for LFAC System.

### 1.2.3 Frequency Selection

The selection of a specific low frequency level is a matter of immense importance for the overall system design and operation. Most feasibility studies on LFAC transmission for offshore wind power systems result in the utilisation of 16.7Hz or 50/3Hz, mainly because of the field-proven equipment that is developed by manufacturers for the rail industry. In addition, five European countries, namely, Austria, Germany, Switzerland, Sweden and Norway, standardised on 15kV and 50/3Hz single-phase AC. On 16 October 1995, Austria, Switzerland and Germany changed from 50/3Hz to 16.7Hz which is no longer precisely 1/3 of the AC grid frequency. Apparently, this has solved overheating problems of the rotary converters used to supply some of this power from the grid [123].

A frequency sensitivity study based on a Levelized Cost of Energy (LCOE) concerning efficiency, weight and cost for all vital wind farm components has been carried out by DNV-GL under the title of "Power Frequency Optimisation study for Offshore Wind Farms" [120]. The study focuses on the CAPEX, OPEX variations as a function of frequency to determine the optimal that minimises the lifetime costs of the WFs. The outcomes of this study suggest that:

- A change in frequency has a substantial impact on the LCOE of OWE, Figure 1.10a).
- LFAC of 10Hz-20Hz provides an economically advantageous alternative to 50Hz AC and HVDC solutions for medium/long-range export distances, as shown in Figure 1.10b).

Considering all frequency sensitivities, an optimal frequency with respect to cost is calculated at ~14Hz. As this frequency is marginally close to the standardised power frequency of 16.7Hz

with an established industrial base for electric power apparatuses, a choice of operating at 16.7Hz can be the most fit-for-purpose to reduce development and qualification costs.

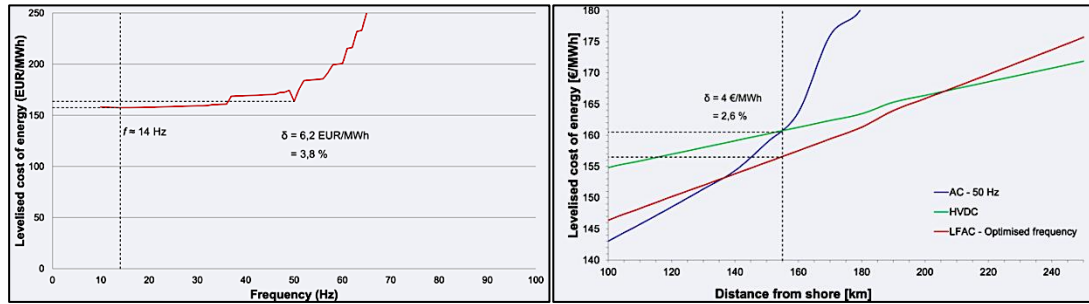


Figure 1.10: Levelized Cost of Energy vs. a) Frequency for OWPP and b) Distance from Shore for OWP.

Consequently, to determine a suitable low-frequency range for offshore power systems operation, some additional technical and operating aspects may need to be considered such as the power quality, technology readiness, stability aspects, power losses, etc. [2]. For optimal frequency selection, further adjustments and limitations may be imposed by other significant factors, e.g. structural, such as the equipment weight and size, in order to attain the most economically and technically feasible solution.

#### 1.2.4 Frequency Conversion

Initial studies mentioned the magnetic frequency changer as the key frequency conversion component in the FFTS [40][42][54]. The frequency changer stepped up the frequency from 50/3Hz to 50Hz and fed power into the grid, as shown in Figure 1.5. At the time, it presented some advantages over the cycloconverters regarding its simpler structure, lower cost, and more reliable operation, although its lower efficiency and lack of flexibility made this technology obsolete by technological advancements in power electronic devices.

The cycloconverter is the most common system mentioned in the literature for LFAC conversion. It converts three sets of three-phase AC voltages to three sets of single-phase LFAC voltages through Line Commutated Converters (LCCs) that work collaboratively to generate the three-phase LFAC outputs, either using the six-pulse or the more promising in terms of harmonic response twelve-pulse cycloconverter configuration [17][38]. Its structure is similar to a BtB thyristor-based LCC-HVDC system [42][43][44][45], with the only difference being the varying DC bus voltage, according to a given LFAC sinusoidal reference [12][34].

The cycloconverter can regulate its voltage level and phase angle at the output side by adjusting its control references. However, the reactive power at its input side cannot be controlled and is automatically adjusted according to the modulation index and the

displacement factor of the output side [18][22][23]. Moreover, its output over input frequency ratio affects the power quality of the produced voltage waveform, which may jeopardise the operation of an offshore export system that comprises long cables and low-order resonances [7]. Since the input side is the offshore system at 16.7Hz, increased size equipment or FACTS devices could be required to mitigate these effects, even in the case of a twelve-pulse converter [6]. Studies of a robust model for the six pulse cycloconverter for OWF integration, together with an advanced time-domain simulation method, were presented in [35][36]. The situation can improve if Thyristors are replaced by GTOs or IGCTs for higher power ratings instead, as shown in Figure 1.11 [70], but the compromise between efficiency, power quality, sophisticated control and the overall cost should be investigated.

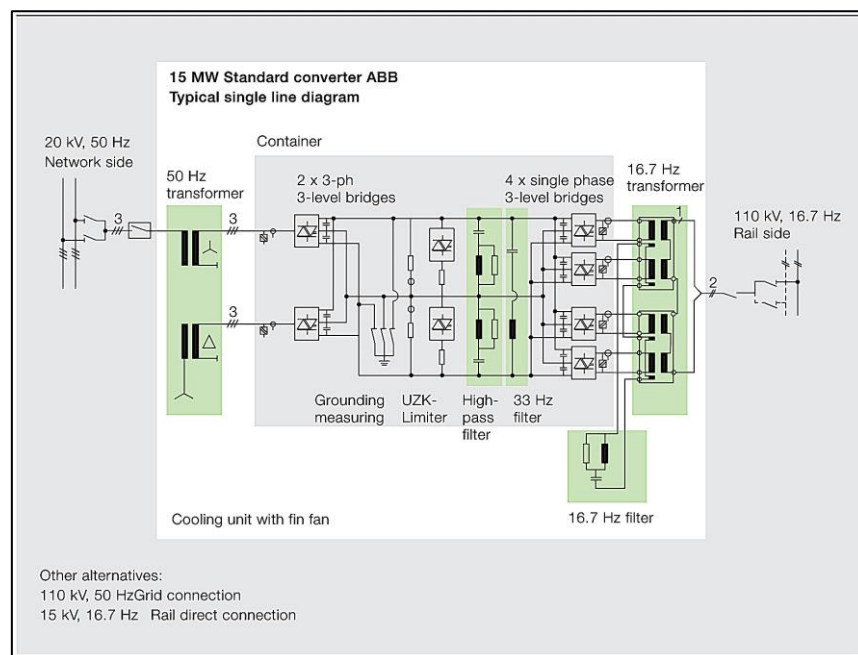


Figure 1.11: Single Line Diagram of a Converter Station (IGCT) for Rail Application.

Nowadays, such advanced frequency cycloconverters transfer electricity between national and railway grids. Several 15MW frequency converters, as shown in Figure 1.11, have been employed to supply power to the Swiss Lötschberg tunnel railway system, while larger power classes are considered in the future, with the most prominent plan being a 413MW IGCT based cycloconverter station for E.ON in Germany. As stated in the ABB's "Review" document [70], by using these static frequency converters, the interconnection of a single-phase and a three-phase grid can be more demanding than interconnecting two three-phase grids, which is the case in offshore transmission systems. A principal reason is that the power is basically constant in a three-phase system, whereas in the single-phase railway grid it oscillates at twice the operating frequency, with the oscillations being damped by tuned filters.

Furthermore, this static converter is able to resynchronise effectively with the rest of the railway system following a grid disturbance, which could resemble the clearance of a grid-side event during the energisation procedure of the offshore LFAC TS.

Another innovative cycloconverter-based technology is the Modular-Multi-Level Matrix Converter (MMMxC) [25][26] that employs H-bridge submodules to overcome the voltage and frequency constraints. It can be a compact solution in terms of size and weight, but the large number of submodules required for high power function introduces complex control strategies. The fact that it can regulate active and reactive power separately and improve the system's power quality is significant, though, the lack of DC side aggravates its LVRT and protection capability, exposing both the AC and the LFAC sides to disturbances occurring in either of them.

The Hexverters are hexagonal AC/AC MMCs utilising H-bridge submodules, which can be used for high-power and high-voltage ratings. In [56], the hexverter is utilised for subsea power transmission through 16Hz LFAC network comprising a 20MW OWF at 132kV, a 5MW induction motor that drives pumps and compressors for oil extraction and 5MW general purpose load. The converter achieves power regulation and minimises the zero-sequence circulating currents using a novel optimisation technique; though, further investigation of this concept is needed against system disturbances and for higher power order applications.

Back-to-back (BtB) VSC or MMC arrangements located onshore can be feasible for integrating OWPPs to the main grid by LFAC TS, providing independent active and reactive power control [2][7]. These arrangements can still decouple the input and output side voltages due to its DC-link and at the same time eliminate the chance of a DC bus short circuit fault, but even if a fault like this occurs, both the AC and LFAC side circuit breakers can isolate the faulted terminal. For such a case in a multi-terminal meshed arrangement, other healthy terminals would be able to transfer power from the interconnected wind farms to the onshore grid [4].

Finally, several frequency conversion devices are noted in the literature, which have been used in other industries but their operation may not be suitable for an LFAC TS, such as the rotary converters and transformers [74][97]. The rotary converter is a motor-generator couple that converts 16.7Hz to 50Hz to feed a load and has been used for power transfer to railways and subsea systems in the oil industry, while the rotary transformer can allow power exchange among non-synchronous grids by adjusting the frequency and angle [31][32].

### 1.2.5 LFAC TS Benefits

Potential cost benefits of using the LFAC technology for OWP exploitation are mentioned in the literature where it is estimated that the LFAC TS could bridge the gap between short offshore transmission distances where the 50Hz HVAC is more feasible and much longer distances where HVDC is the most cost-effective solution [1-4, 7]. This point is also made by economic feasibility studies, comparing CAPEX and OPEX among HVAC, LFAC and HVDC technologies for point-to-point, radial connections of OWFs to the grid [126]. However, the potentials of LFAC technology regarding reliability and power transfer flexibility can be significant if meshed network arrangements and interconnections among offshore projects and onshore grids are considered, where at the moment HVAC is not practical, and MTDC technology is not mature, due to complexity and lack of reliable and field-proven related protection equipment such as HVDC circuit breakers [77].

Below, some important points are presented that constitute LFAC a potential candidate for future power transmission in offshore wind applications over the competitive HVAC and HVDC technologies:

- In an OWPP HVAC export system, the capital and operating costs significantly upsurge over a certain distance range, as the charging currents of the cable rise. The CAPEX is affected as the reactive compensation requirements increase, unlike in an equivalent LFAC TS where these needs can be lower due to the lower cable charging currents and due to the capability of the onshore frequency converters, depending on the type of the adopted frequency converter technology. OPEX is affected mainly by the transmission losses in subsea cables, where a considerable part of these are due to reactive currents [126]. By using LFAC, the reactive power production in the transmission mediums is lower, and the losses caused by the skin effect are minimised, allowing more active power transfer through the same cables.
- In an OWPP HVDC export system, a significant part of its CAPEX is related to the offshore HVDC platform which in [140] is assumed five times pricier than an HVAC equivalent. Such a platform is absent in the LFAC TS since the frequency converters are placed at the same onshore location, without being exposed to environmental stresses and providing easy access for O&M. Thus, the corresponding OPEX is also reduced, which may be further improved by future technological advancements in AC/AC multilevel converters [3].
- Cost benefits for OWP industry may also arise if offshore projects are seen from a more holistic perspective, instead of the typical PtP OWPP connections to the grid. Obtainability

of high-power LFAC CBs and proven protection systems can allow fast detection and clearance of faults and guarantee the security of the supply. As a consequence, flexibility and reliability can be an advantage for LFAC technology if larger scale, interconnected offshore wind projects are considered, where MTDC might limit the potentials and be more challenging to apply [30]. Thus, the cost and technology readiness level may be sufficiently in favour of the LFAC technology for large OWP projects with multiple connections. Generally, a meshed MT-LFAC offshore grid, in comparison with a corresponding MTDC grid, could be a less challenging and more realistic solution, that can be mostly realised by employing currently available equipment [29].

Therefore, the OWPPs initially planned and installed as separate projects, could be interconnected to offshore multi-terminal, meshed arrangements, as shown in Figure 1.12b), similar to the onshore AC grids. LFAC submarine cables can be connected with one or more offshore LFAC platforms where the OCS medium voltage is transformed to a suitable voltage level for long-distance transmission [3][30]. Also, vast OWFs could be split into smaller blocks allowing their construction in sequences and offering high power transfer flexibility compared to a single HVDC platform, as in Figure 1.12a), where a potential single point of failure in an HVDC-link could make the whole wind farm unavailable [4].

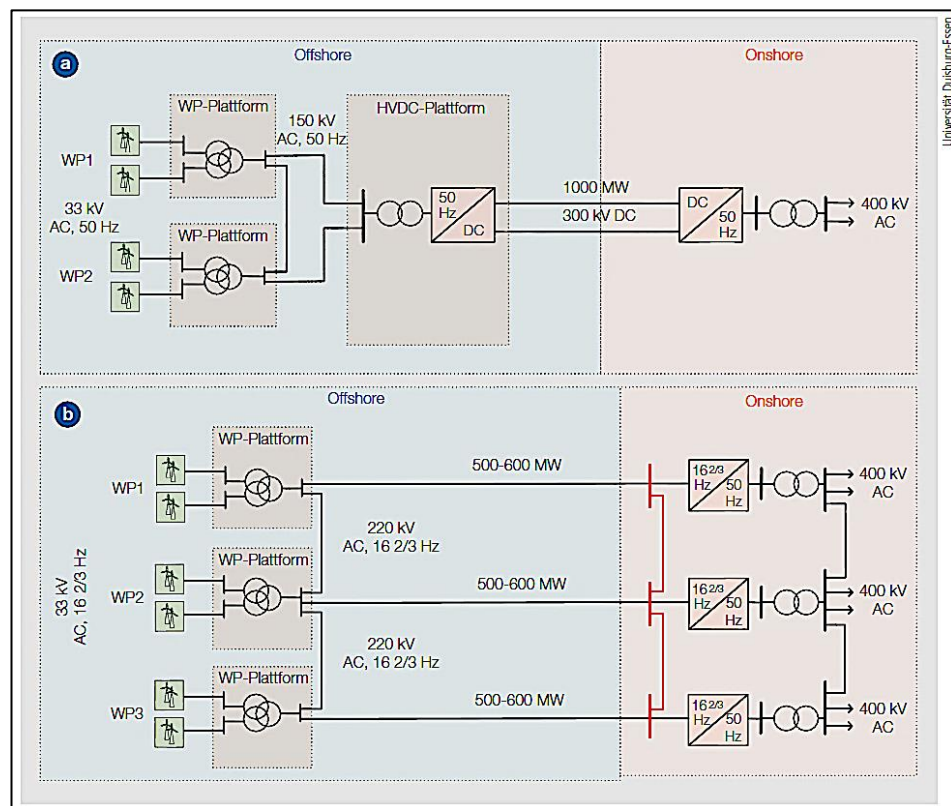


Figure 1.12: Energy Transmission Systems for OWFs: a) HVDC, b) LFAC: 16.7Hz.

However, most economic analysis studies that have been performed in the literature regarding the feasibility of the offshore transmission systems do not consider the potentials of networks broader than the typical radial connections for OWP export. As a result, the LFAC TS is evaluated in a comparison field for PtP topologies that has been developed for its commercially available competitive technologies and in which HVAC has limited but well-established range, while HVDC excels in the higher range for the corresponding applications.

#### 1.2.6 LFAC TS Issues

There are still some challenges associated with the operation of LFAC TS within the offshore distance range of its probable application. The most obvious are the increased size and weight of specific system components, e.g. transformers, inductors, etc., the THD due to converter switching operation or the harmonic stability issues due to the resonances of the system, and they basically depend on the topology of the system, the equipment rating and the adopted converter technology [2][3][4][37].

As the core cross-section area of the power transformers and shunt reactors, or their windings should be increased to achieve the same flux density in LFAC as in classic AC operation, they shall get bigger in volume and mass [5]. Additionally, DFIG based wind turbines would need a considerably larger and heavier induction generator [16][28][30], while the adaptation of the existing fully rated converter WTGs (Type 4) would need adjustments only for the related inverter components which involve DC capacitors, converter reactors and low-pass filters. The interface transformers would need to be redesigned for either of these WTG technologies [120]. Regarding the auxiliary systems, they could be designed for lower frequency operation, or the same 50Hz components might be used if power could be supplied through an extra 16.7/50Hz converter according to [3].

In addition, the overall system performance and its dynamic behaviour can be severely affected by the dynamic impedance of the system [7]. A low resonant frequency may introduce the necessity of very lossy damping harmonic filters, to avoid low-order harmonic stability issues [2]. Such issues may arise in an LFAC TS depending on its design, the implemented converter technologies, the control arrangements and tuning, as well as the effectiveness of any harmonic mitigation measures. System disturbances could also cause control interactions with low-order resonances, excite harmonics and jeopardise the harmonic and dynamic stability of the system, resulting in damaging the converter valves or disconnecting from the grid.



Findings from the research conducted in [60-64] provide insights for the impedance-based stability of PtP LFAC TS arrangements employing a grid-forming two-level VSCs. These studies have identified that by analysing the LFAC TS impedance measurements, potential high-order harmonic instabilities can be predicted, and results of certain cases have been verified through scaled hardware experimentation. In these cases, the system impedance is mainly dominated by the grid-forming converter control system for lower frequencies and by its LCL filter for higher frequencies. These results indicate that there is a relationship between the system impedance characteristics and the designated converter technology, the type of the applied grid-forming control system, as well as the converter filter design. However, other arrangements may result in different system impedance profile that would embrace particular mitigation measures. A natural progression of this work would be to conduct a more detailed EMT analysis for the offshore LFAC TS and investigate its dynamic response, FRT ability and stability characteristics under various system operating configurations.

Since the main goal of most studies in the literature was to determine the techno-economic feasibility of the LFAC TS and the operating characteristics of the frequency converter arrangements, very little research has been conducted regarding the stability aspects of the LFAC TS. In [57], a six-bus LFAC TS with Over-Head Transmission Lines (OHTLs) connected to a cycloconverter has been assessed, and its eigenvalue analysis showed that the lower reactance of the OHTLs due to the lower operating frequency, the better the system voltage regulation, improving the system's stability and power transfer capability. On the contrary, an offshore FFTS assessment using a subsea export cable connected to a cycloconverter showed that the lower resistive-damping of the cable due to low frequency reduces stability [58]. Finally, [59] performs a fault analysis in an LFAC system that results in high fault currents as the frequency converter and the OWF are represented by ideal voltage sources acting as swing buses, while the dynamic limitations of the system are not considered.

Considering all this evidence, it seems that several questions remain to be answered regarding the technical feasibility, operation and compliance of practical PtP or MT-LFAC TS configurations with the required operating and connection standards of modern power systems. There are many relatively unspecified aspects about the implementation of appropriate control strategies, the necessary control and protection coordination, the dynamic performance and stability of the system, the related active/reactive power, LVRT and FRT capability of the schemes, as well as the unique potential formation of an islanded offshore LFAC network, functioning totally among power converters.



## 1.3 Scope of the Thesis

### 1.3.1 Research Motivation

The offshore market continuously grows with forecasts indicating that the global OWP capacity could reach between 154GW and 193GW by 2030 [55]. A greater initiative that could expand the market availability for the LFAC technology and bring significant benefits for the OWP industry shall come by the prospective meshed offshore network developments that would enable the exchange of power among offshore projects and different grids. The concept of offshore grids could serve the purpose of integrating distant OWPPs and interconnecting AC grids, for balancing the power flow, enabling alternative power routes, international trade etc. Still offshore projects shall be seen from a more holistic viewpoint, than the radial OWF connections to the grid. Either if it is trade-driven or trade unconstrained, the various technical challenges associated with the formation of offshore transmission systems should be addressed and solved. In such a context, the offshore LFAC TS technology can be considered as a serious candidate. A primary task might be to adopt an approach of building networks that would either evolve from currently existing systems or organically grow with time from a single initial stage to fully functional integrated networks with minimum modifications from the perspective of both control and infrastructure.

In reviewing the literature, LFAC technology could be assumed as an attractive transmission solution Having a theoretical competitive edge over the HVAC and HVDC TS for exporting power from large and remote OWPPs within a specific distance range of, e.g. 80-250km. Plenty of academic effort has been devoted to investigating the design of alternative and inexpensive frequency conversion equipment and developing offshore LFAC TS schemes that would introduce a more economical solution with reduced footprint. Up to this point, the only real-time applications of LFAC system involve the supply of passive LFAC load networks in the Rail and Oil & Gas industries. Besides the promptings regarding the efficiency of the LFAC TS for medium distance range integration of OWPPs, no offshore power transmission application has been commissioned or planned to utilise the LFAC technology.

Thus, there has been no prior operational experience of LFAC in other applications that would correspond to a similar-scale of power exchange between the LFAC and AC systems or fulfil analogous requirements to an offshore TS. The field-proven HVAC and HVDC TS solutions are the preferred paths for the T&D vendors, the OWP industry and the investors for the whole offshore distance range and the different network types (e.g. radial or meshed), mainly due

to their high industrial readiness level. From the manufacturers' perspective, the LFAC technology for offshore transmission could be considered as "new", because there is a shortage in testing standards and prior LFAC equipment manufacturing experience of the expected size and ratings, even for key system components such as the power transformers, inductors, CBs, etc.

Among the various project investors and stakeholders, uncertainty can be precipitated regarding the LFAC technology readiness level for transmission purposes. Even if an economic feasibility evaluation of the LFAC TS scheme assures its efficiency in theory, it may be argued that certain implications could emerge upon operation that would render its practical implementation difficult. Hence, this ambiguity that the LFAC TS may encounter some unforeseen pitfalls jeopardising its technical feasibility and compliance with the demanding modern grid codes shall be tackled through research and development.

Furthermore, the continuous grid transformation with increasing RES penetration and the concurrent displacement of Synchronous Generation (SG), decreases the available inertia, the Short Circuit Capacity (SCC) and thus the strength of the AC systems. This leads several TSOs to employ stricter integration rules for the power converter interfaced generation that can even challenge the compliance capability of OWP projects using the established HVAC or HVDC technology. Also, some offshore installations have already encountered difficulties with, e.g. resonance issues [138][139], lack of suitable condition monitoring systems in the market for HVDC cable links [137], even OWP outages due to grid faults [136], that may render such systems vulnerable and challenge investment confidence in the OWP industry.

From the above, it is inferred that any envisaged "new" grid integration and transmission technology shall demonstrate not only technical and economic feasibility but also ensure safe and efficient power transfer in compliance with the modern grid integration rules. Despite the identified theoretical edge of a potential offshore LFAC TS for power transfer over specific distance ranges and for various configurations, the technical benefits of this technology shall be effectively communicated through further investigation and analysis in the present or future power systems frame. Practical solutions shall be achieved that will be based on realistic configurations with equipment designs and operating approaches closer to the established industry practice. Thus, interaction with the industry has been continuous during the course of this research for acquiring information regarding some key LFAC components, such as the submarine LFAC cables and transformers.

### 1.3.2 Thesis Objectives

This industrial PhD Thesis aims to result in realistic and feasible LFAC schemes for PtP and MT offshore power transmission networks, by identifying and resolving specific technical and operating challenges that emerge and by evaluating their performance, so that they could be materialised by the industry in a quite ordinary fashion and comply with typical TSO grid code requirements. The base to pursue an economical offshore transmission solution as well, competitive to the HVAC and HVDC for a certain distance range (100-400km) has been:

- To export the full power output of each OWPP through a single High Voltage LFAC cable supplied by a manufacturer (Nexans). Thus, the minimum number of cables are employed, and power is transmitted by maximising the power transfer through them.
- To implement any necessary passive mitigation and compensating equipment in the onshore frequency converter substations and avoid if technically possible the installation of additional components on the offshore LFAC platforms which would further increase their size, weight, cost and total footprint.

Thus, for the LFAC TS arrangements, all the main equipment parameters are suitably adapted for High-Voltage LFAC operation based on industry practices and the literature. Practical and straightforward offshore LFAC TS configurations are produced and accordingly rated to effectively export the nominal capacity of the OWPPs to the grid through PtP arrangements or interconnect different OWFs among them and to different grids in multi-terminal, meshed configurations. The operating performance of the designated schemes is assessed to identify any probable challenges that may emerge through this process and implement practical solutions towards the exploitation of this innovative offshore transmission technology.

More specifically, the technical feasibility of the different LFAC TS arrangements for various cable lengths is assessed through comprehensive engineering studies to optimise the system performance characteristics, its transmission capability and identify probable limitations. Detailed LFAC TS models are developed in DigSilent PowerFactory and PSCAD-EMTDC, with an accurate representation of the subsea export cables, the LFAC transformers, the power converter modules of the OWPP equivalent systems and the onshore frequency converters with their control systems designed and explicitly tuned according to specified requirements for the corresponding offshore transmission application. The conducted studies comprise steady-state, frequency and time-domain simulations for various operating conditions and different transient and fault events in the AC and LFAC sides. The system's dynamic voltage and low order harmonic stability are evaluated against typical performance requirements.

## 1.4 Thesis Contributions

The findings of this Industrial PhD Thesis make several contributions to the state-of-the-art and provide a basis for industrial exploitation of the offshore LFAC TS technology. Its novelty has been to introduce:

- ❖ The formation of realistic and feasible offshore LFAC TS schemes, rated for exporting the nominal capacity of OWPPs and equipped with components explicitly adapted for LFAC operation, based on standard industry practices. The key LFAC TS equipment comprises:
  - 1) The LFAC submarine cables, with parameters obtained by a cable manufacturer.
  - 2) The LFAC power transformers for which certain design estimates were investigated considering practical aspects like transport (size and weight) restrictions and impedance levels, following standard industry methods and assumptions, and introducing a trade-off among weight and losses.
  - 3) The BtB frequency MMCs with HBSM capacitors sizing and WTG VSCs rating for LFAC.
- ❖ The LFAC TS resonance investigation in the frequency domain, by utilising the most accurate FDPM subsea cable representation to evaluate the impact of its length to the total isolated LFAC TS. Also, the effect that the added branches of MT schemes have on the dynamic impedance of the LFAC TS has not been addressed before. Based on this analysis, passive harmonic-filtering combinations with minimal losses are designed to mitigate low-order resonances.
- ❖ Optimised offshore PtP and MT-LFAC TS layouts for minimum active power losses (maximising the power transfer through the cable), and minimum shunt compensation placed only at the onshore side. This is achieved through a detailed Steady-State analysis of cases with different cable lengths that may employ passive harmonic filtering, or not. Thus, the advocated fundamental conditions to accomplish the Thesis' objectives are established. This process also results in implementing suitable converter control strategies that improve stability and increase the power transfer efficiency of the scheme, such as the ACVC/DCVC mode for the OWTG inverters, and the APC/ACVC mode for the onshore LFAC side grid-following MMC that is added in MT arrangements. Studies assure compliance with the equipment loading limits and the network operating standards in steady-state conditions. The feasibility of the LFAC TS, as well as its competitive edge over the HVAC and HVDC technologies for establishing certain offshore networks, is clarified through an availability assessment shown in APPENDIX B.

- ❖ Effective coordination of the designated control strategies, together with practical mitigation measures and system enhancements for a PtP and even an MT-LFAC TS, so that compliance with typical grid code requirements and equipment capability limits is demonstrated. Compliance is accomplished by:
  - 1) Eliminating the impact of the resonance on the THD and the low-order harmonic stability of the system. It is shown that its impact is primarily affected by the type of islanded control mode applied on the onshore grid forming MMC terminal and its tuning. It can be mitigated by enhancing the islanded controller with a high bandwidth ICC or by applying passive damping filtering equipment, or a combination of both.
  - 2) Improving the fault handling ability of the system to contain the fault currents within limits, support voltage recovery and ensure appropriate system response in the LFAC, the DC and AC sides. The FRT capability of the feasible LFAC TS schemes is examined against faults in the offshore LFAC and the AC grids, while appropriate enhancements are adopted, and potential risks are addressed in case of uncoordinated control and protection operation.

## 1.5 Author's Publications

- ➔ A. Canelhas, S. Karamitsos, U. Axelsson and E. Olsen, "**A low frequency power collector alternative system for long cable offshore wind generation,**" 11th IET International Conference on AC and DC Power Transmission, Birmingham, 2015, pp. 1-6.

*Abstract: This paper aims at presenting further results of engineering studies undertaken to access relevant aspects to design and implement Low Frequency AC Power Transmission systems (LFAC) associated with large-scale, above 1,000 MW, offshore wind power generation distant 200 km or more from the shoreline. This technology was proposed in 2010, to evacuate wind power generation in the North Sea, for schemes with long transmission distances, for which 50 Hz AC systems are not technically viable. In addition, the application of this technology aims at achieving a simpler technical solution than deploying fully-fledged offshore HVDC converter stations proven to lead to large platform topsides. The use of simpler AC hubs is also proposed comprising a limited number of array cables connected to them such that the AC LFAC cables can concentrate the power from these AC hubs and export it to the shore at low frequency.*

→ A. Canelhas, S. Karamitsos, U. Axelsson and E. Olsen, "Low Frequency AC Transmission on Large Scale Offshore Wind Power Plants - Achieving the Best from Two Worlds?," in *13th Wind Integration Workshop*, Berlin, pp. 1-7, Nov. 2014.

*Abstract: Today the majority of large scale and remote OWF's (800– 1200 MW and more than 100km from the onshore connection point) are planned with HVDC solutions in mind. This paper gives a presentation of the opportunity to use LFAC systems for these large-scale OWFs.*

## 1.6 Thesis Outline

The Industrial PhD Thesis is organised as follows:

- In **Chapter 2**, the main equipment adopted for the offshore LFAC TS is described, and the necessary adaptations for operating in LFAC systems are discussed, while the impact of LFAC on the components' design and performance characteristics is also reviewed.
- In **Chapter 3**, the envisaged PtP and meshed MT-LFAC TS topologies are designated, the related equipment rating is established, and its parameters are specified in detail.
- In **Chapter 4**, the system is assessed in frequency-domain for harmonic impedance issues. Frequency scan studies are performed for various cable lengths to assess the harmonic impedance and potential low-order resonances that could negatively affect stability of the system, cause converter control interactions or damage the equipment. Passive mitigation measures are proposed to cease the adverse harmonic impact on the system.
- In **Chapter 5**, the LFAC TS arrangements for several cable lengths are modelled in steady-state. Power-flow cases are studied to calibrate the operating conditions of the system (e.g. reactive power compensation, control strategies, etc.) and define acceptable steady-state operation for each scenario. The availability of the produced LFAC TS cases is assessed and compared with the other offshore TS technologies in APPENDIX B.
- In **Chapter 6**, the LFAC TS components are explicitly modelled in time-domain, the requirements for the various converters control systems are defined, and the respective regulators are tuned through general optimisation algorithms and evaluated through Transfer Function analysis in time and frequency domain.
- In **Chapter 7**, detailed EMT simulation studies are conducted to evaluate the LFAC TS dynamic performance for characteristic cases. Adverse performance issues are alleviated by employing mitigation measures as addressed in the previous chapters or by control and protection coordination strategies. The stability and FRT capability of the system are demonstrated against dynamic events and faults in the LFAC as well as in the AC side.
- In **Chapter 8**, conclusions and contributions are discussed, and further-work is suggested.

## Chapter 2: LFAC TS Equipment Overview

### 2.1 Introduction

In this chapter, some assumptions and constraints for the design and selection of LFAC transmission equipment are described, based on theoretical background and industrial practice. The related equipment should be employed with the aim to form a fully-fledged offshore LFAC grid solution, able to Interconnect different grid systems and transfer power from big and distant OWFs. Thus, the design considerations for the main system components and the impact of the selected equipment on the offshore LFAC TS feasibility are discussed.

Currently, there is no clear differentiation between the LFAC and regular AC (50Hz or 60Hz) equipment or system standards and the international electrical and mechanical standards applicable to electrical apparatus, might also cover the LFAC systems. Hence, bodies such as the IEC, ANSI/IEEE, ISO standards, etc. could constitute a reference even for the LFAC systems, while some CIGRE recommendations and guidelines could even be applicable.

In addition, most of the commercial LFAC equipment aims at the track and rail market in the transportation segment, with the vast amount of such applications located in Europe and North America, while few LFAC submarine power distribution systems can be found for extracting oil and gas from the seabed. However, there is a broad industrial base that ranges from T&D power equipment suppliers (e.g. ABB, Alstom, Bombardier, GE, Siemens, etc.) to small system components vendors and system integrators that have developed some LFAC products, including transformers, frequency converters and industrial drives.

The offshore LFAC TS in this Industrial PhD Thesis is envisaged as a subset of Power Transmission and Distribution (T&D) applications and the potential suppliers for providing the corresponding equipment would be the T&D manufacturers. Hence, interaction with the industry has been a continuous process throughout this research, resulting in specifying the key LFAC components design, such as the subsea LFAC cables and the power transformers. Design estimates of these components are produced according to general industry practices, while other main system elements such as the WTGs the frequency converters, switchgears, damping filter capacitors, circuit breakers, etc. are reviewed. The approach has been to adopt robust, feasible and straight-forward solutions for a nominal operating system frequency of 16.7Hz based on techno-economic feasibility assessments [120][126] and prior industrial experience [70].

## 2.2 Submarine Export Cables and Reactors

### 2.2.1 Technical Benefits of LFAC for Cables

The main objective in conceiving the LFAC system is to utilise cables at lower frequencies and overcome the excessive requirement of HVAC for reactive power compensation in case of offshore long-distance transmission. The lower operating frequency contributes to a low charging current that does not compromise cable thermal ratings up to a certain degree and could make LFAC systems feasible for offshore long-distance and bulk power transmission.

Thus, the subsea export cable is the key component for the feasibility of LFAC technology as an offshore power transmission system and its power transfer capability is also the principal factor to determine the transmission voltage level of the LFAC TS. Moving to higher offshore transmission AC voltage levels gives the advantage of higher power transfer per conductor cross-section and enables manufacturers to assemble longer cables with reduced cost. However, a rise in either the operating voltage or the length of a cable increases the charging current creating a need for larger compensating reactors. The LFAC operation significantly reduces the capacitive reactive power effect of the cable system that can limit the voltage level selection, while compensating inductors can be sized lower in comparison with HVAC.

Assuming that the transmission voltage level can be optimal when it enables maximal power transfer capability through the cable, then the LFAC-XLPE submarine export cable system shall be rated in the region of the maximum allowable AC voltages for equipment on the offshore platform. However, cable dimensioning shall be in line to obtain LFAC cable design characteristics and electrical parameters by means of industrial cable technology, already used by the manufacturers.

Thus, the two different voltage levels of 230kV and 345kV have been considered as the technical basis for designing the HV LFAC export cable system used in this study. An effort has been made together with a cable manufacturer (NEXANS) to obtain the most suitable cable solutions, also taking into account results of recent research and development in this field. Three-core, submarine, XLPE cables are considered using either Aluminium (Al) or Copper (Cu) conductors of relatively moderate cross-section areas of 1200mm<sup>2</sup>-1600mm<sup>2</sup> adapted to 16.7Hz for offshore LFAC transmission purposes. Below the technical benefits of the LFAC technology in comparison with HVAC are discussed in terms of power losses, charging currents, reactive compensation and voltage levels, by examining a three-core, 1200mm<sup>2</sup> Cu export cable for 50Hz and 16.7Hz operating frequencies:



### 2.2.1.1. Cable Losses

In steady-state, the maximum loadability of a subsea cable is mostly limited by the maximum temperature of the insulating materials. Thus, the lower the losses in the cable, the higher its loading can be. Figure 2.1 shows the power losses in a 1900mm<sup>2</sup> export cable at 230kV and a 1400mm<sup>2</sup> Al cable at 345kV for 50Hz and 16.7Hz operating frequencies, as measured by NEXANS [7]. The higher operating voltage leads to lower cable losses, while the losses produced at LFAC are closer to the DC losses for the same cable type. This means that the same cable can be utilised for higher power transfer following a transition from 50 to 16.7Hz.

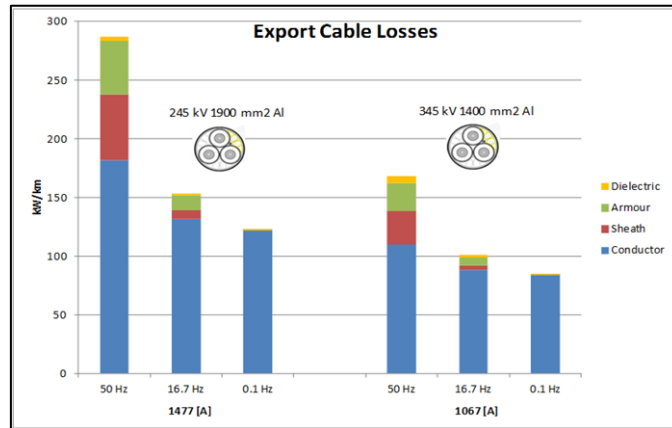


Figure 2.1: HVAC Al Export Cable Losses at 50Hz, 16.7Hz and DC for: a) 230kV-1900mm<sup>2</sup>, b) 345kV-1400mm<sup>2</sup>.

In Figure 2.1, frequency-dependent power losses can occur in various parts of the cable [2]:

- In the conductor:* Conductor losses depend on the electrical resistivity of the conductor that consists of the DC as well as the frequency-dependent resistivity due to the proximity and skin effect. This explains the reduction of conductor losses in LFAC.
- In the lead sheath and the armour:* Subsea cables are designed with screens and armours that are made of magnetic materials and can experience induction effects due to the alternating currents in the conductors. Thus, frequency-dependent circulating and eddy currents are induced in the lead-sheath and the screen of the cables, causing losses which are significantly reduced at 16.7Hz.
- In the insulation:* Dielectric losses are also related to frequency, although their contribution to the total cable losses is minimal.

Thus, by using LFAC at 16.7Hz, the total resistance is closer to the DC resistance, and the amount of transmitted power can increase, or lower cable cross-section could be adopted, reducing the cost. Another important outcome of the measurements performed on these submarine cables by the manufacturer (NEXANS) is that the cable resistance at 16.7Hz is nearly independent on current, in contrast with 50Hz where it slightly increases with current.

### 2.2.1.2 Reactive Current, Compensation and Loading

The main advantage of the LFAC power export technology compared with HVAC is the lower reactive power produced by the cable system at low frequencies, as the charging currents depend both on operating frequency and cable length. This way, cables that are rated and normally operated at conventional AC can further increase their capacity when operated at a lower frequency. Reactive power management is also essential for optimal utilization of the export cable transmission capability that is achieved when the current flowing through it is distributed as equally as possible. Theoretically, lower rated cable shunt reactors are needed at 16.7Hz. Though, to eliminate the impact of the reactor space on the cost of the LFAC offshore platform, dynamic MVAR from the OWTGs may be utilised if necessary, that in Figure 2.2 are drawn as a “fictitious” shunt reactor (dotted line).

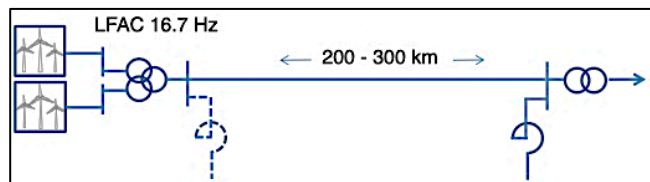


Figure 2.2: LFAC Cable System and Potential Compensation Scheme.

Figure 2.3a) shows a comparison in transmission capacity for the same three-core, Cu cable at 50Hz and 16.7Hz at 230kV according to the manufacturer (NEXANS). Since both the power losses and charging currents are lower in LFAC operation, the transmission lengths can be significantly extended at higher power ratings. In all cases, the reactive power becomes more dominant over a certain length and the power curves decay. Though, LFAC operation improves this figure drastically, while the mid-point compensation has smaller impact on the transmission length at 16.7Hz compared to 50Hz, which also suits offshore applications. In Figure 2.3b), the 345kV LFAC system can transfer 250MW more than the 230kV equivalent. Although losses are similar for 200km transmission ~7%, they almost double for 300km.

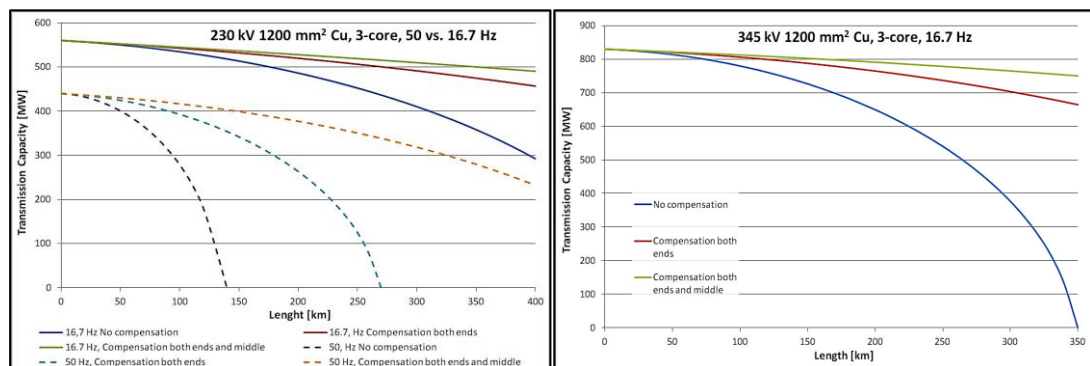


Figure 2.3: Export Cable Transmission Capacity, for various reactive compensation schemes: a) 230 kV at 50Hz and 16.7Hz (left) and b) 345kV at 16.7Hz (Right).

## 2.2.2 Submarine LFAC Export Cable Designs

There should be no significant difference in cable design, whether it is intended to be operated at 50Hz or 16.7Hz and therefore one of the most cost-driving components of this offshore transmission system can be based solely on well-known and field-proven technology. Subsea cables rated at 50Hz or 60Hz have been used for system studies in applications that utilise low operating frequency, typically 16.7Hz or 20Hz. However, more realistic outcomes can be produced for the feasibility of the LFAC TS if at least the main export cables of the investigated schemes are represented by frequency-optimised parameters. This work employs practical submarine LFAC cables for high-voltage offshore transmission applications that have been provided by the manufacturer. The two cable designs at 16.7Hz that have become available for this study are:

1. XLPE - 230kV 3x1x1600 mm<sup>2</sup> Cu
2. XLPE - 345kV 3x1x1400 mm<sup>2</sup> Al

As shown in Figure 2.4, both LFAC cables are built with multicore structures containing three-main phase conductors with a triple-extruded XLPE insulation system, metallic screen/water barrier, and protective polyethylene (PE) sheath. The cores are bundled with profiled extruded High Density (HD) fillers with one, two or three submarine Fibre Optical (FO) elements incorporated for power communication and temperature monitoring purposes.

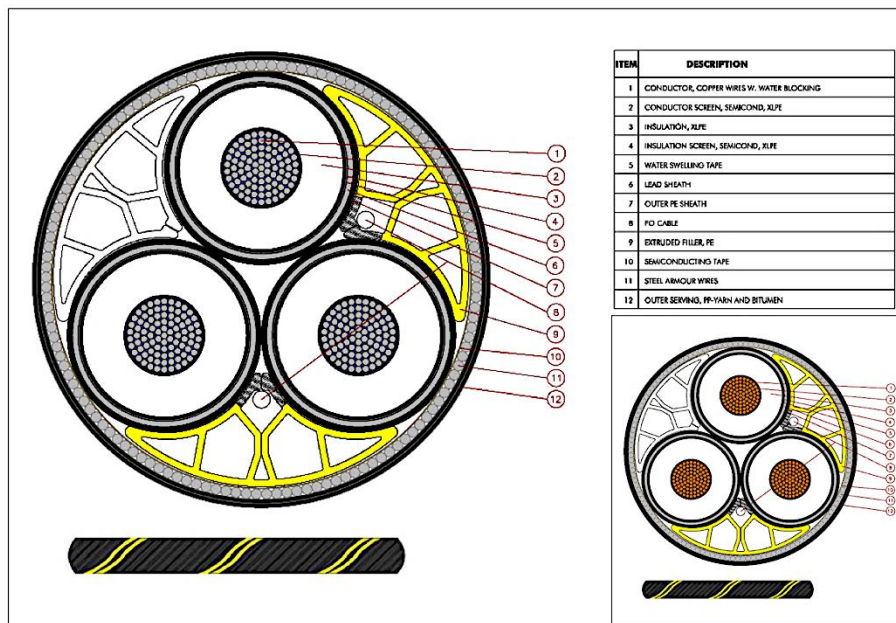


Figure 2.4: Export Cable Alternatives - 1) XLPE - 345 kV 3x1x1400 mm<sup>2</sup> Al, 2) XLPE - 230 kV 3x1x1200 mm<sup>2</sup> Cu.

The dimensioning of the LFAC cables that are used in this Thesis are based on intermittent loading, where the dynamic rating calculations are performed by the cable manufacturer.

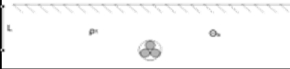
The dimensions and electrical parameters of the LFAC export cables are listed in Table 2-1.

*Table 2-1: LFAC Export Cable Electrical Parameters for 230kV and 345kV - NEXANS.*

LFAC Export Cable Electrical Parameters		230 kV 3x1x1600mm <sup>2</sup> Cu	345 kV 3x1x1400mm <sup>2</sup> Al
Rated Voltage	Rated/Nominal RMS Voltage (U <sub>n</sub> )	230 kV	345 kV
	Rated/Nominal RMS Voltage between conductor and screen (U <sub>0</sub> )	127 kV	190 kV
Highest Voltage	Highest continuous RMS system Voltage (U <sub>m</sub> )	245 kV	362 kV
Maximum Temperature	Maximum permissible conductor temperature	90 °C	90 °C
Frequency	Operational Frequency (f)	16.7 Hz	16.7 Hz
Basic Insulation Level (BIL)	Lightning Impulse Withstand Voltage (1.2/50 msec.)	1050 kV	1175 kV
Conductor Resistance	DC resistance at 20°C	0.0113 Ω/km	0.0212 Ω/km
	AC resistance at 90°C and 16.7 Hz	0.0155 Ω/km	0.0277 Ω/km
Capacitance	The capacitance between conductor and screen	0.218 mF/km	0.173 uF/km
Charging Current	Charging Current at 16.7 Hz	3.17 A/km	3.63 A/km
Impedance	Cable Impedance (Z <sub>1</sub> , Z <sub>2</sub> ) at 90°C	0.017+j0.037 Ω/km	0.0307+j0.044 Ω/km
	Zero Seq. Impedance (Z <sub>0</sub> ) at 90°C	0.145+j0.029 Ω/km	0.158+j0.032 Ω/km
Diameter	Cable outer Diameter (OD)	272 mm	267 mm
Weight	Cable Weight in air (approx.)	132 kg/m	98 kg/m

The cables that have been designed for the LFAC voltage levels of 230kV and 345kV are tested for maximum charging currents for different degrees of compensation. The systems are rated at approximately 700MW to achieve the maximum power transfer through the designed export cables, and their parameters are shown in Table 2-2.

*Table 2-2: Offshore LFAC Transmission System Design Parameters & Ambient Conditions - Seabed.*

System Parameter		230 kV	345 kV	Seabed	
System Voltage	System voltage at the onshore receiving end	230 kV	345 kV		
Sending Power	Total produced (installed) wind power	700 MW		Maximum seabed temperature (q <sub>a</sub> )	10 °C
Frequency	Operational frequency (f)	16.7 Hz		Thermal resistivity soil (ρ <sub>T</sub> )	0.8 K.m/W
Route Length	Export cable route length	200 km		Specific heat capacity of soil (c <sub>t</sub> )	4.2 e6 J/K.m <sup>3</sup>
				Soil diffusivity (d <sub>t</sub> )	2.98 e-7 m <sup>2</sup> /s
Reactive Compensation	Reactive compensation scheme	50/50 % (equal flow of current to each end)		Separation distance (s) (if more than one cable*)	> 20 m
End Currents (used 100% load)	The total current in each cable end with perfect compensation	1700 A	1200 A	Burial depth (L)	2.0 m

The voltage and current vary over the length of the cable as the contribution of reactive power changes. Here, the telegrapher's equations (distributed parameters), that describe the voltage and current of a cable over distance and time with respect to the voltage at its sending end ( $V_{send}$ ) are solved to maintain its rated current in both ends ( $I_{send}=I_{load}$ ) at 1700A or 1200A respectively. Subsequently, the transmitted active power in the cable ( $P_{send}$ ) with a characteristic impedance  $Z$  and length  $l$  can be yielded by Equations (2.1), (2.2).

$$U_{send} = U_{load} \cdot \cosh(\gamma \cdot l) + \sqrt{3} \cdot I_{load} \cdot Z \cdot \sinh(\gamma \cdot l) \quad (2.1)$$

Where:  $\gamma$  is the propagation constant of the cable:  $\gamma = \sqrt{(R + j \cdot \omega \cdot L) \cdot (G + j \cdot \omega \cdot C)}$

$$P_{send} = \sqrt{3} \cdot |I_{send}| \cdot |U_{send}| \cdot \cos(\phi_{send}) \quad (2.2)$$

Where:  $\phi_{send}$  is the angle between the sending end voltage ( $V_{send}$ ) and current ( $I_{send}$ ).

The voltage and current profiles of the 1600mm<sup>2</sup> Cu at 230kV and the 1400mm<sup>2</sup> Al at 345kV, for 200km export cables, are shown in Figure 2.5a) and b) respectively, and calculated in Table 2-3, for a compensation scheme that keeps the total current equal at both cable ends.

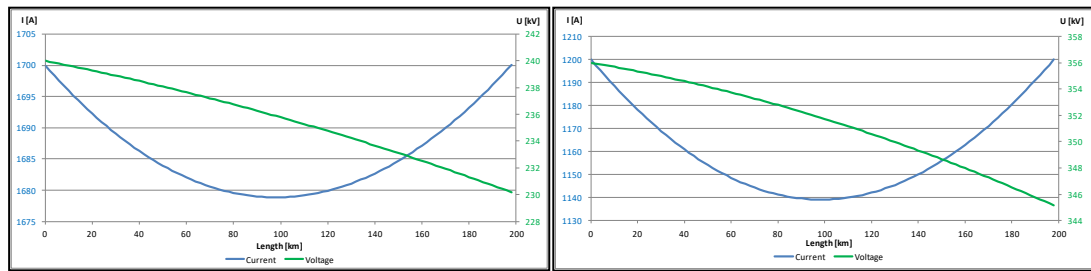


Figure 2.5: Voltage and Current Profile over length for 200km - a) 230kV, 1600mm<sup>2</sup> Cu, b) 345kV, 1400mm<sup>2</sup> Al.

The preliminary sizing of shunt reactors for 200km cable length provides a rating of 83MVAR at 230kV on both onshore and offshore sides of the export cables or 177MVAR installed only on the onshore side also at 230kV. For the 345kV system voltage, the ratings are 210MVAR and 425MVAR, respectively. The reactors, despite being much larger in rating, they do not increase in physical size by the same proportion, as they correspond to a higher voltage level.

Table 2-3: System values for 200km - 230kV, 1600mm<sup>2</sup> Cu and 345kV, 1400mm<sup>2</sup> Al.

Cable Performance	Sending end (offshore)		Load end (onshore)	
	230 kV	345 kV	230 kV	345 kV
Active Power [MW]	702	704.3	670.8	680.1
Reactive Power	98	233.3	-93.1	-227.2
Voltage [kV]	240.6 < 5.3°	356.9 < 2.5°	230.0 < 0°	345.0 < 0°
Current [A]	1700.5 < 13.2°	1200.4 < 20.8°	1700.0 < -7.9°	1200.0 < -18.5°
Power Factor, cos(φ)	0.99	0.95	0.99	0.95
Power Losses [MW]			31.16	24.13
Voltage Drop [%]			4.42%	3.32%

### 2.2.3 Cable Impact to the LFAC TS Design

The three-core XLPE subsea is one of the most significant main circuit elements of an offshore transmission system. It appears that the move to LFAC could imply in substantial advantages, many of which can be the foundations for the LFAC technology to become feasible and cost-competitive alternative for vast and remote OWFs. The 230kV and 345kV system voltages that have been selected in order to compare and quantify the impact that LFAC would have on their electrical response showed that both could be feasible and meet the requirements for such offshore LFAC TS. Though, further optimisation of cable system parameters could be dictated by project-specific details, its topology, the compensation degree, etc.

To attain the maximum power-transfer through a single subsea tri-core export cable, the LFAC transmission system capacity can be set approximately to 700MW. By operating the designed cables close to their transmission capacity limit for distances greater than the maximum range of a typical 50Hz HVAC export system (approx. 80-100km) and up to the point that the HVDC system can naturally become the most economical solution, the range of the offshore LFAC export system feasibility can be estimated. Moreover, the potentials of an offshore LFAC grid system formation can be unveiled, as well as the techno-economic benefits in comparison to a much more complex and technologically challenging offshore MTDC equivalent system.

In this Thesis, the Tri-Core, Cross-Linked Polyethylene (XLPE) LFAC cable design with conventional aluminium conductors (XLPE - 345 kV 3x1x1400 mm<sup>2</sup> Al) for a 345kV system is selected as the most cost-efficient alternative since the long length of the export cables, together with the number of cables to be laid underwater and the correlated installation costs form a significant part of the capital expenditure (CAPEX). This way, the offshore LFAC transmission system voltage level of 345kV is determined, and the corresponding aluminium conductor seems to be a more favourable solution in the sense of:

- Lower losses
- Less voltage variations
- Larger margin to critical conductor temperature at the given load cases; meaning that it can maintain higher periods of full load
- The much lower price due to the aluminium conductor
- Lighter weight
- The relatively compact physical size of shunt reactors

## 2.3 Switchgears and Circuit Breakers

### 2.3.1 Switchgears

Generally, the Gas-Insulated Switchgear (GIS) is preferred for offshore transmission systems either for OWPP or Oil and Gas applications. This occurs because the GIS features long maintenance intervals, having increased reliability under special conditions and environmentally challenging areas (e.g. salty, dusty, or polluted air, seismic active or offshore areas, very low or high temperatures, etc.). Also, it benefits fewer outages at offshore substations as well as cost savings by reducing the premium space needed in the offshore platforms due to its compactness.

In the industry, there is a long experience in supplying 16.7Hz GIS equipment for the rail industry. Hermetically sealed GISs with SF6 circuit breakers for 16.7Hz have already been in commercial operation for several years in the railway grids. Alstom Grid has also developed hybrid switchgear specially designed for the railway energy transmission networks in Germany, Austria and Switzerland, based on a rated frequency of 16.7Hz and a rated voltage up to 145kV. However, there can be some operational challenges in the 16.7Hz offshore networks, as their short circuit level in comparison with the single-phase railway networks may be lower, affecting the short-circuit interruption.

For the proposed offshore system configuration, GISs for the medium and high voltage levels are needed. Adopting 66kV array cables instead of 33kV can result in less electrical losses, increased potential connection distance and/or power transfer capacity for a specific conductor size and even in fewer offshore LFAC substations. Thus, for the medium voltage level of the OCS, the class of 72.5kV GIS is selected in order to connect the inter-array connection cables at 66kV. In addition, for the reasons analysed in 2.2.3, the 345kV (IEC 362kV class) is selected for the LFAC transmission system. More specifically, at the offshore connection decks:

- The 72.5kV class switchgear is chosen to form a 66kV GIS double LFAC busbar configuration at 16.7Hz which must have enough bays to connect all OWF array cables, two step-up transformer bays and one bus coupler.
- The 362kV class switchgear is chosen to form 345kV GIS double LFAC busbar configuration at 16.7Hz with one cable bay to connect to the submarine XLPE cable, also suitable to accommodate shunt reactor compensation if needed, two step-up power transformer bays and one bus coupler.



### 2.3.2 Circuit Breakers

Currently, there are existing models of circuit breakers (CBs) suitable for 16.7Hz transmission networks up to a voltage level of 145kV. Low frequency circuit breakers have been in use in Europe and are part of the railway supply system in Germany, Austria and a few other countries. For higher insulation voltages the development of the breakers should not pose any significant technological challenge as, in principle, should be able to operate under low frequency conditions according to the IEC-62271-100 Standard for High Voltage Alternating Current Circuit Breakers which gives the requirements for circuit breaker operation.

Nonetheless, the operation of circuit breakers at lower frequencies and higher voltage levels may raise some concerns due to the longer time between two successive current zero-crossings, and thus the longer duration of the arc that needs to be extinguished. It should be noted that in case of a short circuit fault in a system that operates at 16.7Hz LFAC (slower cycles), the current's zero crossings may be delayed up to three times more than in a typical 50Hz operation. Hence, certain adjustments shall be addressed in the existing 50Hz CB designs that could enable them to operate effectively at 16.7Hz.

Maintaining the generated arc for more time may be a challenge and could increase the probability of current chopping. In this phenomenon, the arc may extinguish before the current's natural zero crossing, which could cause equipment damage due to high di/dt as well as overvoltage at any inductive loads and the circuit breaker. To face this issue, some manufacturers cut the nozzle of the CB shorter to retain a slower flow of the insulation gas and thus to maintain the arc. An alternative might be to use CBs with higher interrupting capability and certify the standing voltage class in question, which for 362kV could result in the next IEC class and the 345kV and 16.7Hz system might be based on CBs for 400kV and 50Hz rating. Finally, there might also be a need for further verification of capacitive current switching limits at low frequency operation for specific offshore LFAC network applications.

## 2.4 Power Transformers

Power transformers are vital components for an offshore LFAC TS, as their weight and dimensions determine the weight and volume of the OCS topsides. In the offshore LFAC TS, the transformers are employed to step-up the OCS 33kV or 66 kV medium voltage level to the desired transmission voltage that optimises the cable design. As seen in 2.2.2, this voltage level can be in the IEC classes of 245kV or 362kV.



Most of the low frequency transformers designed for the rail industry to support the operation of frequency converters and adjust the voltage to the appropriate levels, as shown in Figure 2.6. They are single-phase type converter transformers, and they are energised at low frequency. They add up the partial voltages to a nearly sinusoidal single-phase 16.7Hz AC voltage and adapt it to the railway grid voltage at their high-voltage winding, with filters connected to tertiary windings. The rating of such units is less than 50MVA and therefore far from the intended application as power transformers. Though, the primary winding voltages can be in the range of, e.g. 132kV in the Swedish system.

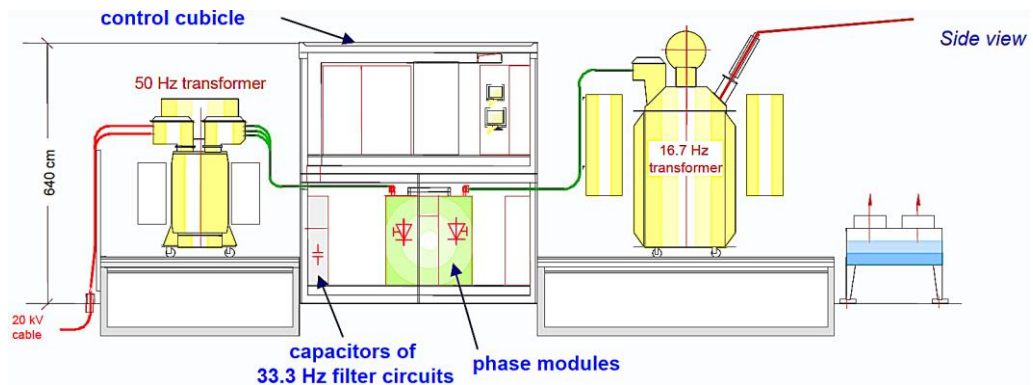


*Figure 2.6: Arrangement of the components in the modular container concept by Alstom, for Railway application (all components are designed for the transportation via rail and standard road haulage), ALSTOM.*

In the literature, there are many scientific papers and research projects for OWP exploitation using LFAC technology in which the power transformers that are employed to transform the voltage at the OCS substation to a transmission voltage level in a low frequency network, are originally designed for 50Hz or 60Hz operation [11, 13-15]. The idea behind these designs is that a higher frequency transformer could be utilised for operation at lower frequencies and maintain its rated magnetic flux in the iron core, if its nominal voltage rating is scaled down by an appropriate factor, according to the desired operating frequency of the scheme. In all cases, the same rated current must be kept. This way, it is claimed that the overall costs of power transformers for LFAC operation could be reduced by utilising some already existing assets where possible, whilst hysteresis and eddy current losses in the core could be eliminated, increasing transmission efficiency [18, 19, 20, 23, 30].

There are certain drawbacks associated with de-rating the transformer voltages for LFAC operation whilst sustaining the originally nominal current because the power rating is also reduced by the same factor. In addition, as discussed in 2.2.3, the offshore LFAC system can benefit from increasing the transmission voltage level due to the lower losses in the subsea cable. Thus, in a case that power transfer of 1GW is needed at e.g. 345kV, three equivalent

ultra-high-voltage (UHV) AC transformers rated at 1200kV, 1GW would need to be installed in an offshore platform, probably as nine single-phase units.

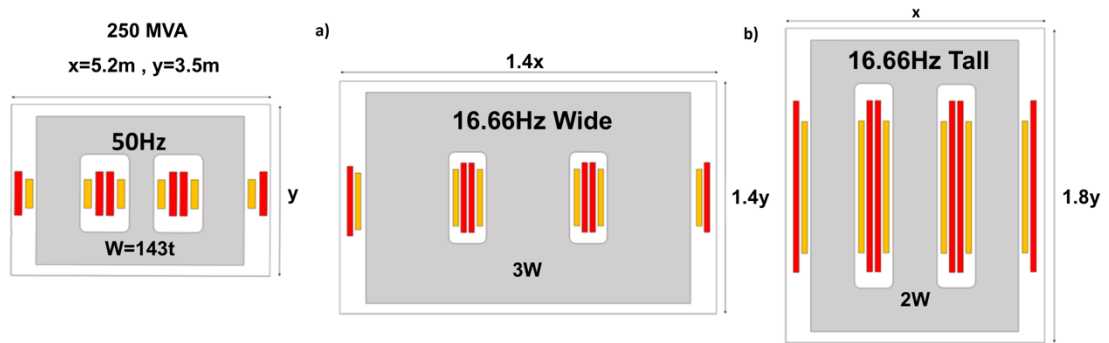


*Figure 2.7: Theoretical design of a 50Hz transformer for comparison with the corresponding 16.66Hz, Theoretical design of a 16.7Hz transformer: a) Wide design, b) Tall design*

In order to avoid such scenarios, theoretical designs of LFAC transformers are presented in the literature for both WTG and coupling transformers by changing either the core width (A) or the number of turns (N). Two extreme theoretical LFAC transformer designs were produced by P B Wyllie et al. [5] as shown in Figure 2.7, based on the fact that the magnetic flux density (B) remains technically the same with the variation of frequency (f), and according to the transformer Equation (2.3):

$$E = 4.44 \cdot f \cdot B \cdot N \cdot A \quad (2.3)$$

- a) The core thickness increased (A), and the number of winding turns (N) unchanged.
- b) The number of turns (N) increased to maintain the required voltage level.

It is evident that by keeping the core diameter constant and varying the number of turns gives a lighter design (approx. twice the weight of the 50Hz transformer - 2W), as the core is denser than the windings which means that the wide design is considerably more massive (approx. 3W). In all cases, the lower operating frequency implies an increase in the size, weight and footprint of the transformer with approximate 77% weight increase in WF transformer, and 107% weight increase WTG transformer according to [5][8][12].

The increase in the size of the transformer may also impact the design and cost of the offshore platform as well which can be expected to be bigger and more expensive than an HVAC equivalent [140], but still without requiring an additional, more massive and costlier HVDC converter platform. Lastly, the WT nacelle structure or tower design may be somewhat affected, as it might be challenging to fit an LFAC transformer unit in a WT tower rated for the full power, instead of a standard three-phase HVAC transformer.

### 2.4.1 LFAC Power Transformer Design Features

Power transformers rated for low frequency operation can be massive and may need project-specific design to account for weight, size, location and serviceability issues. LFAC transformer estimates in the literature indicate that lighter designs could be realised by increasing only the number of turns which could fit for purpose in offshore transmission applications. However, such lightweight designs severely increase the transformer’s height. Hence, in this industrial PhD Thesis, the U.K. transportation height limit of 4.875m, with an approximate shipping weight constraint of 300~350tonnes per transformer unit have been designated as key factors to define the level of compromise between its weight and height.

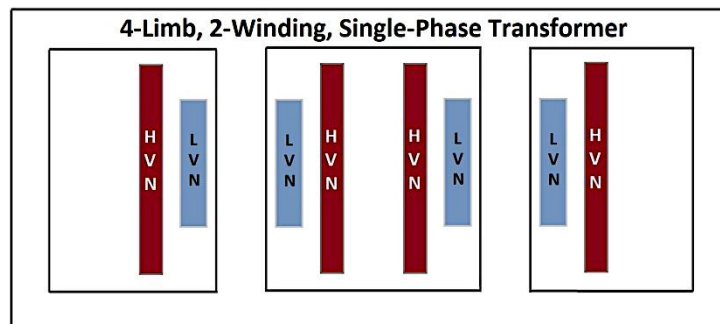


Figure 2.8: LFAC Transformer Design Schematic.

The increased weight and size of the 16.7Hz three-phase transformers lead to the selection of single-phase units, because the shipping weights of three-phase units exceeds transport limitations if design heights lower than 4.8m are considered. Furthermore, to allow for the tallest possible winding within the transport height limitation, the 4-limb core design could be applicable of which two limbs are fitted with windings as depicted in Figure 2.8. Such single-phase units could also serve as converter transformers, depending on converter type.

Table 2-4: Parameter Assumptions for Transformer Design Calculations.

Transformer Design Assumptions								
Electrical Parameters		Units	Geometrical Assumptions		Units	Tank Characteristics		Units
Frequency	16.7/50	[Hz]	Core Stacking Factor (SF)	0.91		Tank End Clearance	150	[mm]
Transformer Unit -Rating	141	[MVA]	Clearance Core/LV	40	[mm]	Side Clearances	800	[mm]
Primary Voltages	66	[kV]	Clearance LV/HV	94	[mm]	Top & Bottom Clearances	200	[mm]
Secondary Voltages	345	[kV]	LV or HV Winding SF	0.44		Total Base + Cover Thickness	80	[mm]
LV J or HV J	4	[A/mm <sup>2</sup> ]	Clearance HV to Outer Leg	150	[mm]	Mean Tank Wall Thickness	25	[mm]
			End Insulation	450	[mm]			

A series of design calculations have been performed for 66/345kV transformers rated at 141MVA, based on the of the assumptions in Table 2-4 and using the standard industrial design formulae of Table 2-5 according to [128] [141]-[143]. A range of impedances from 5% to 15% has been selected for analysis, while all transport heights have been assumed around ~4.8 metres, to produce “matching” designs for the different impedance values.

The design stage is crucial for the final volume, weight, and losses of the LFAC transformers. Weight and space are critical for the offshore platform design and transport arrangements while losses are important for the feasibility of the export system. Thus, the Site Weight of the transformer given in Equation (2.4) can also define the total loading of the platform.

$$\text{Site Weight [tonnes]} = \text{Total Shipping Weight [tonnes]} + \text{Oil Weight [tonnes]} \quad (2.4)$$

The Shipping Weight (or Dry Weight) is determined by the transport limitations that are translated to design specifications and is given by Equation (2.5).

$$\begin{aligned} \text{Total Shipping Weight [tonnes]} = & \text{Total Core Weight [tonnes]} + \text{Total Copper Weight [tonnes]} + \\ & + \text{Total Tank Weight [tonnes]} \end{aligned} \quad (2.5)$$

The necessary weight characteristics and dimensions of each transformer are calculated by the equations of Table 2-5 [141]-[143], assuming  $B=1.7T$  induction in the core, a steel density of  $7.65g/cm^2$ , and copper density of  $8.89 g/cm^2$  in the windings.

Table 2-5: Transformer Standard Design Equations.

Transformer Geometric and Weight Characteristic Equations	
1	<b>Total Core Weight [tonnes] = (Core Leg Weight [tonnes]+Yoke Weight [tonnes])</b>
1.1	<b>Core Leg Weight [tonnes] = 3*Core Section Main Leg [mm2]*Core Leg Length [mm]*7650/10<sup>12</sup>)</b>
CORE	1.1.1 Core Section Main Leg [mm2] = $V/N*10^6/4.44/\text{Frequency [Hz]}/B [T]$
	1.1.2 Core Leg Length [mm] = Winding Height [mm]+End Insulation [mm]
1.2	<b>Yoke Weight [tonnes] = Core Section Main Leg [mm2]*Yoke Length [mm]*7650/10<sup>12</sup>)</b>
YOKE	1.2.1 Yoke Length [mm] = Main Leg Centres [mm]+Outer Leg Centres [mm]+Core Dia. [mm]
	1.2.1.1 Main Leg Centres [mm] = HV OD [mm]+2*Clearance between Main Legs [mm]
	1.2.1.2 Outer Leg Centres [mm] = HV OD [mm]+2*Clearance HV to Outer Leg [mm]
	1.2.1.3 Core Dia. [mm] = $\text{SQRT}(\text{Core Section Main Leg [mm2]}*4/\text{Core SF}/\pi)$
	1.2.1.4 HV OD [mm] = HV ID [mm]+2*HV Radial [mm]
2	<b>Total Copper Weight [tonnes] = 2* (LV Winding Weight [tonnes/leg]+HV Winding Weight [tonnes/leg])</b>
2.1	<b>HV Winding Weight [tonnes/leg] = HV(N)*HV Section [mm2]*<math>\pi</math>*(HV ID [mm]+HV Radial [mm])*8890/10<sup>12</sup>)</b>
HV WINDING	2.1.1 HV(N) = Secondary Voltages [kV]/Primary Voltages [kV]*LV(N)
	2.1.2 HV Section [mm2] = HV Leg Current [A]/HV J [A/mm2] = Transformer Unit Rating [MVA]*10 <sup>3</sup> /Primary Voltages [kV]/2/HV J [A/mm2]
	2.1.3 HV ID [mm] = LV OD [mm]+2*Clearance LV/HV [mm] = LV ID [mm]+2*LV Radial [mm]+2*Clearance LV/HV [mm]
	2.1.4 HV Radial [mm] = HV Conductor Section [mm2]/HV Winding SF/Winding Height [mm] = HV(N)*HV Section [mm2]/HV Winding SF/Winding Height [mm]
2.2	<b>LV Winding Weight [tonnes/leg] = LV(N) *LV Section [mm2]*<math>\pi</math>*(LV ID [mm]+LV Radial [mm])*8890/10<sup>12</sup>)</b>
LV WINDING	2.2.1 LV Section [mm2] = LV Leg Current [A]/LV J [A/mm2]
	2.2.2 LV ID [mm] = Core OD [mm]+2*Clearance TV or Core/LV [mm]
	2.2.3 Core OD [mm] = $\text{SQRT}(\text{Core Section Main Leg [mm2]}*4/\text{Core SF}/\pi)$
	2.2.4 LV Radial [mm] = LV Conductor Section [mm2]/LV Winding SF/Winding Height [mm]
	2.2.4.1 LV Conductor Section [mm2] = LV(N) *LV Section [mm2] = Primary Voltages [kV]*10 <sup>3</sup> /Prelim V/N*LV Leg Current [A]/LV J [A/mm2]
3	<b>Total Tank Weight [tonnes] = Cover +Base Weight [tonnes]+Tank Wall Weight [tonnes]</b>
3.1	<b>Cover + Base Weight [tonnes] = Internal Tank Length [m]*Internal Tank Width [m]*Total Base + Cover Thickness [mm]*7650/10<sup>6</sup>)</b>
3.2	<b>Tank Wall Weight [tonnes] = 2*(Internal Tank Length [m]*Internal Tank Width [m])*Internal Tank Height [m]*Mean Tank Wall Thickness</b>
4	<b>Oil Weight [tonnes] = Oil Volume [litres]*0.88/10<sup>3</sup> = ((Internal Tank Length [m]*Internal Tank Width [m]*Internal Tank Height [m]*1.035)- (Total Core Weight [tonnes]/7.65)-(Total Copper Weight [tonnes]/8.89))*0.88</b>

By limiting the shipping height at 4.8 metres in every design, the inter-winding clearances are also adjusted according to the secondary voltage. This means that if there is an increase in the core diameter, a corresponding adjustment of the winding height is made without restriction up to a point over which the shipping height limitation forces it down. As the winding height decreases, its radial dimensions and core diameter increase to compensate.

In addition, the calculation of the core and winding weights according to the equations in Table 2-5 provides information for the approximate Total Losses of the transformer design

which are defined by its No-load or Core Losses and its Load Losses as follows:

$$Total\ Losses\ [kW] = No\ Load\ Losses\ [kW] + Load\ Losses\ [kW] \quad (2.6)$$

For a transformer design with specific shape and type of material (hysteresis) used in the core, No-load Losses are mainly affected by the core mass and the flux density which may vary in different parts of the core. Hence, they are a function of the magnitude, frequency, and waveform of the operating voltage, as these variables affect the magnetic flux waveform in the core. Assuming that the core losses are in the range of 1.1W/kg at 50Hz, or ~0.3W/kg at 16.7Hz for B=1.7T [142], it is:

$$No\ Load\ Losses\ [kW] = Total\ Core\ Weight\ [tonnes] \cdot k\ [kW/tonne] \quad (2.7)$$

Finally, the Load Losses are divided into two parts, the Resistive ( $I^2R$ ) and the Stray Losses, as in Equation (2.8).

$$Load\ Losses\ [kW] = (1 + Stray\ \&Eddy\ Factor) \cdot I^2R\ [kW] \quad (2.8)$$

The resistive or dc power losses ( $I^2R$ ) are given in Equation (2.9), and they represent the heat when the load current flows through the winding resistance. Thus, they do not depend on the operating frequency, but they are affected by the total copper mass, which is large in LFAC transformer designs.

$$I^2R\ [kW] = 2.36 \cdot (LVJ\ [A/mm^2])^2 \cdot Total\ Copper\ Weight\ [tonnes] \quad (2.9)$$

On the other hand, for transformer designs with the same core steel laminations and conductor strands, both the magnetic and electric or winding skin effects that are caused by the Stray and Eddy Current Losses increase with frequency and copper mass. Hence, in Equation (2.9) the effect of the operating frequency on these losses is assumed by empirical factors which are 0.09 for 16.7Hz and 0.12 for 50Hz designs.

Based on the power transformer design considerations above, single-phase, two winding (1ph2w) 16.7Hz and equivalent 50Hz designs are estimated that utilise the same core construction type shown in Figure 2.8. They are compared to each other and contrasted in terms of their Weight characteristics and Total Losses across a range of impedances (%), because of the wide variations in the conductor to core ratios. Nonetheless, the “natural” leakage reactance of a transformer solution that could be employed in the offshore LFAC transmission system, considering only the transport height restrictions, would lie in lower ohmic and per-unit value (in the range of 6 - 10%) than the impedance of a corresponding expected inductance at higher industrial frequencies, e.g. for a 50Hz or 60Hz systems.

## 2.4.2 Impedance Effects on Transformer Weight

As analysed above, the Shipping Weight is especially crucial in view of transport and hence design restrictions, while the Site Weight provides information for offshore platform design. Figure 2.9 shows a Site and Shipping Weight versus Impedance characteristic for an LFAC single-phase transformer rated at 141MVA and operating at 16.7Hz and 50Hz, respectively. These Weight figures can be used to identify the relative costs for each design.

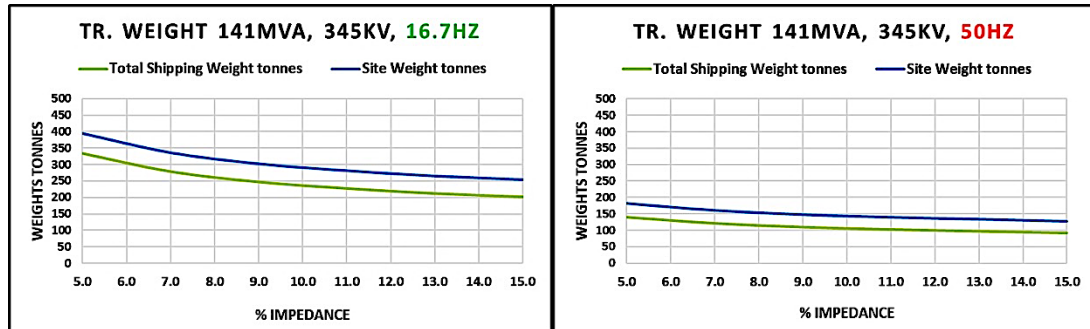


Figure 2.9: Weight vs Impedance for a Single-Phase 141MVA 66/345kV Transformer at a) 16.7Hz, b) 50Hz.

From Figure 2.9, it is evident that the Weight curves of the transformer designs become relatively “flat” after a certain impedance point which is in the order of 9% for 50Hz, and 11% for 16.7Hz designs, exhibiting a steep rise in transport weight for impedance levels lower than 7-8%. Though, even if a 5% impedance level is considered, the total Shipping Weight for the LFAC power transformers is in the order of 330 tonnes which is relatively heavy but can be acceptable for transport in the UK.

## 2.4.3 Impedance Effects on Transformer Losses

In Figure 2.10, the potential transformer power losses versus Impedance are plotted for the 141MVA designs, operating at 16.7Hz and 50Hz, respectively.

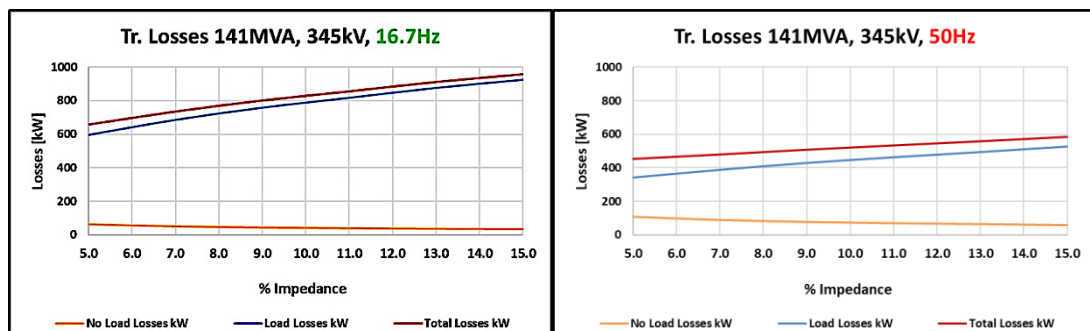


Figure 2.10: Losses vs Impedance for a Single-Phase 141MVA 66/345kV Transformer at a) 16.7Hz, b) 50Hz.

The above results show that the Total transformer Losses are primarily shaped by the Load Losses, which are mainly  $I^2R$  losses, with R representing the or the Total Copper Weight of

the transformer. Obviously, for the same A/mm<sup>2</sup> and despite the lower operating frequency of 16.7Hz compared to 50Hz designs, the increased number of windings of the LFAC transformer has a predominant impact on its Load Losses. As expected, the transformer load loss component also rises with increasing impedance in both designs.

On the contrary, the No-Load transformer losses are generally low, and although they are affected by the transformer core mass, the impact of the lower operating frequency dominates, leading the 16.7Hz designs to have lower such losses (almost half compared to 50Hz) that only slightly reduce in higher impedance levels. This means that their contribution to the LFAC transformer Total Losses is less significant than at 50Hz, due to the selected LFAC design process that increases the number of windings and thus, mainly the Load Losses, to achieve lighter transformers with acceptable height.

Further outcomes could be yielded from this analysis by applying a loss capitalisation formula to produce a net capitalised value curve for each impedance value.

#### 2.4.4 Comparison of 16.7Hz and 50Hz Transformer Designs

Figure 2.11 shows typical ratios of weights and losses between the 16.7Hz and 50Hz approximate transformer designs. The ratios of Shipping Weight and Site Weight fall slightly as the impedance rises and indications that they may start to rise again beyond 14% impedance. By contrast, the ratio of Total Losses rises with %Impedance.

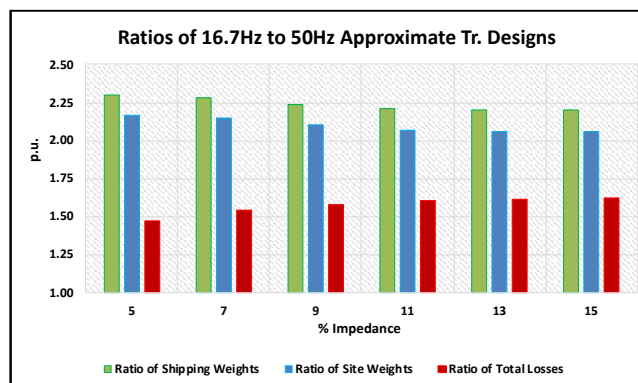


Figure 2.11: Comparison between 50 Hz (1p.u.) and 16.7 Hz Transformer designs.

It can be obvious that an acceptable LFAC transformer design can be 2 - 2.15 times heavier in terms of weight and consume 45% - 65% times more power than an equivalent 50Hz AC transformer of the same %Impedance. Hence, for a design based on a specific transformer impedance, there is a trade-off between transformer weight and losses. Though, in an offshore transmission system, both the losses and weight of the transformers shall be reduced as much as possible, to reduce operating costs and the footprint of the LFAC Topside.



## 2.5 Harmonic Filtering - Capacitors

Capacitor units and capacitor banks that may be used in passive damping filters do not impose any operational or performance issues for an LFAC system. Nonetheless, as shown in Figure 2.12, the capacitive reactive power drops as frequency decreases. In cases where capacitor banks would be required to accomplish tuned harmonic-filters at the low operating frequency, larger installations than usual might be necessary for the same MVA rating, although, operation at higher voltage levels could mitigate this effect.

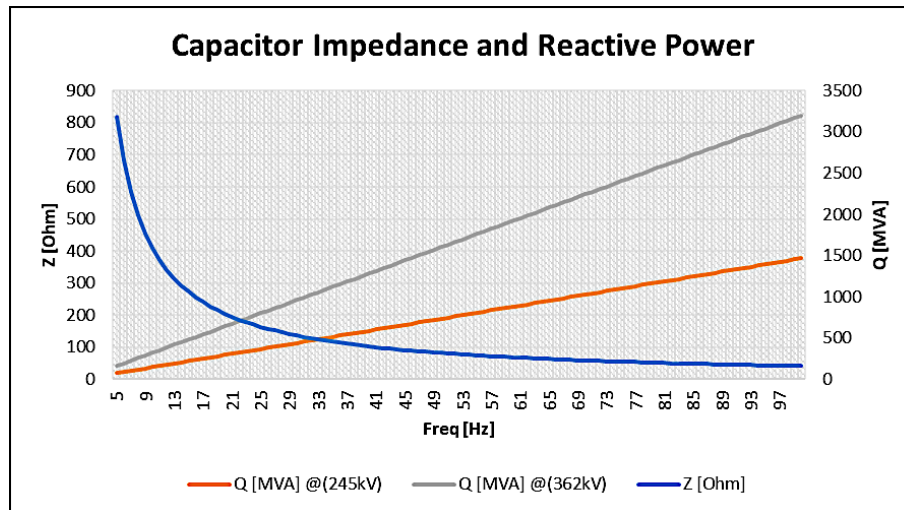


Figure 2.12: Capacitive Impedance and Q-Supply of a 10 $\mu$ F capacitor as a function of frequency.

Since the offshore LFAC TS can operate more efficiently at increased voltage levels ( explained in 2.2.1) in comparison with typical AC for long-length subsea cables (>100km), either the MVA production of similarly sized capacitors could be amplified, or smaller capacitor size increase might be required for similar harmonic mitigation needs. Regardless, any applicable filtering and shunt reactive compensation equipment, should be sited at the onshore LFAC sub-station from a reliability, maintenance and cost perspective, so that their increased size would not occupy the premium space on the topside of the offshore LFAC platforms.

## 2.6 Wind Turbine Generators

There are various WTG types with the doubly-fed induction generator (DFIG) - Type 3 WT and the Full Converter - Type 4 WT being the most dominant technologies [79]. The Type 3 WT, though, is not the preferred solution for offshore applications due to the increased maintenance requirements of its rotor slip rings and the common gearbox failures that can impose underlying challenges to the operation of OWFs, especially if located in a rough and



less-accessible marine environment [5][30]. Besides, connecting a DFIG to a 16.7Hz LFAC system instead of a typical 50Hz or 60Hz AC grid may necessitate further design revisions, affecting mainly the transformer, but also the alternator unit [3].

The Type-4 WTGs that are currently rated up to 12MW can be more suitable for operating in an offshore LFAC grid, as the WTG connects to the grid through a full-scale power converter that optimises its power output whilst it performs independent P/Q control on the grid side. The basic structure of a typical Type-4 WTG with its BtB VSC interface scheme is shown in Figure 2.13. It mainly consists of the WT arrangement with the generator, a BtB converter system, and an interface transformer providing electrical isolation at the AC side [20]. The most affected component within Type-4 WTGs by the lower operating frequency shall be inverter transformer. However, the rest of the equipment inside the WTG, such as rotor and drive train shall not be affected, while minor changes may be needed for the nacelle or tower.

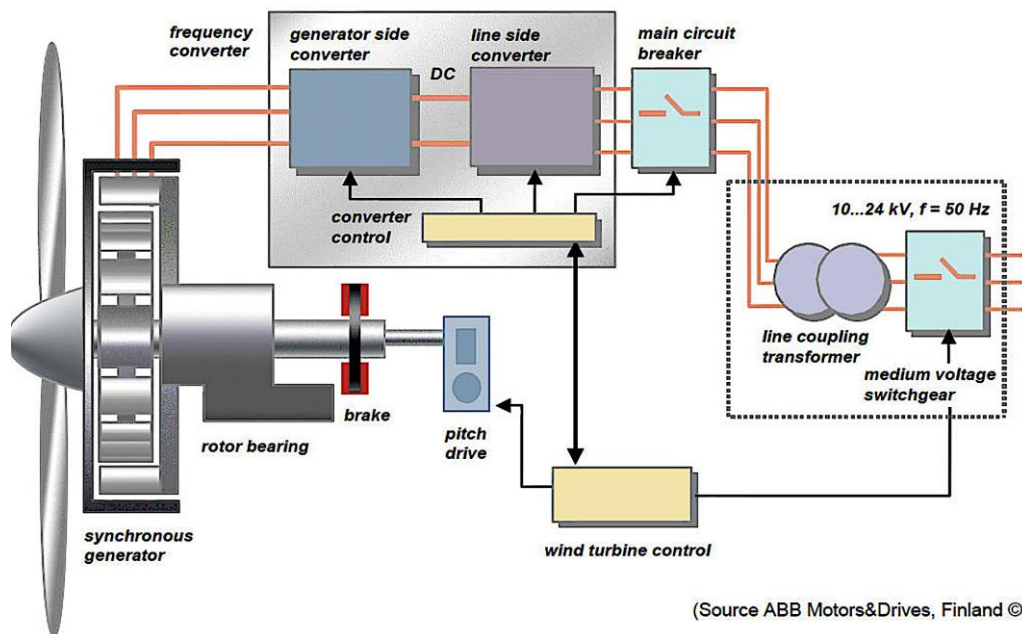


Figure 2.13: Full Converter, Type-4 WTG configuration, ABB.

For the purpose of this research, the Type-4 WTGs can be rated between 6 - 10MW with reference to the commercially available units that are employed in current OWP projects [144]. It is expected that the WTGs can adjust their reactive power settings either to unity power factor or “STATCOM” operating mode, controlling the voltage level at the offshore sending end of the XLPE cable for the entire load range. Such WTG control function could be essential if cases of meshed offshore systems with long LFAC export cables are appraised.

## 2.7 Frequency Converters

The power electronic converter technology that would be suitable for the integration of the offshore LFAC TS to the main grids shall be rated in a scale of several MWs, assure the LFAC network stable operation and comply with Transmission System Operators (TSOs) requirements at the Points of Common Coupling (PCC) with the modern AC grid systems. Hence, the power converter capability and control systems intended for power utility applications can be considered vital features. At the same time, the technology readiness level for this solution shall be high enough, in order to challenge the competitive and commercially available HVAC and HVDC transmission system solutions.

In principle, the Thyristor-based cycloconverters is a robust technology and might be able to transmit more power at a lower cost compared to BtB VSC-HVDC systems [6][12]. However, they do not engage all the required operating characteristics for integrating OWPPs, as they lack a robust black-start and LFAC grid forming capability [10], while it could be challenging to connect to relatively weak grids [89] or comply with modern OWPP integration rules [130]. The absence of a DC-link and probable commutation failures limit even further their fault-ride-through (FRT) capability, making them vulnerable to main power grid disturbances and necessitating a strong onshore interconnection grid. Since the cycloconverters also produce output voltage waveforms with high and complex harmonic content, their application would require the use of large filters at both LFAC and AC sides to suppress switching harmonics and handle reactive power. As a result, the cyclo-converters might only be applied in terminals with low-reliability and operating requirements and enough site space [4].

On the other hand, the BtB MMCs based on VSC technology can allow the formation of an LFAC voltage sine-wave with minimum harmonic content and adjust the magnitude and frequency (islanded operation mode), without a need for separate sources for black-start. Their four-quadrant operation on the PQ-plane enables the power reversal by altering the current direction and provides independent P/Q control. Thus, the MMCs could energise and stay connected to an offshore island LFAC network where no SGs would be present, but only inverter interfaced WTGs and support the system's voltage by regulating the reactive power at the connection point of the offshore LFAC network [65].

Such an LFAC system may not only integrate OWFs in radial, PtP arrangements but it may interconnect different grids or parts of the same grid, exchanging power among those points and forming a meshed offshore LFAC network. Besides, the BtB MMCs arrangements

eliminate the probability of DC short circuit faults, distressing the respective MTDC systems that currently lack a robust and feasible HVDC breaker technology. Hence, they may be able to integrate the LFAC TS to weak AC grids with relatively low Short Circuit Level (SCL) such as some modern inverter dominated grids and comply with the respective grid codes.

Finally, employing a high number of modules enables multiple discrete voltage steps that can reach up to the highest transmission voltages while operating at low switching-frequency per sub-module, reducing the related switching losses and eliminating the need for harmonic filters. Potential benefits may arise for an LFAC TS scheme if such filters are not present, as they can significantly affect its high-order harmonic stability [62][64].

For the reasons mentioned above, the BtB MMC technology has been employed for frequency conversion in this work. Table 2-6 shows the international experience of MMC HVDC technology applications with similar power ratings, e.g. ~700MW. As can be seen, MMCs are being used either for OWFs or Interconnector (IC) projects with commercial solutions supplied by the power industry.

*Table 2-6: International Projects using MMC Technology in Similar Scale ~700MW.*

Year	Project	Power	DC Voltage	AC Side 1 (Offshore)	AC Side 2 (Onshore)	Application	Manufacturer
		[MW]	[kV]	[kV]	[kV]		
2019	COBRA Cable	700	±320	400	400	IC	Siemens
2014	Skagerrak Pole4	700	±500	400	400	IC	ABB
2015	BorWin2	800	±300	155	380	OWF	Siemens
2019	BorWin3	900	±320	155	380	OWF	Siemens
2015	DolWin1	800	±320	155	380	OWF	ABB
2016	DolWin2	916	±320	155	380	OWF	ABB
2017	DolWin3	900	±320	155	380	OWF	GE-Alstom
2015	HelWin2	690	±320	155	400	OWF	Siemens
2015	SylWin1	864	±320	155	400	OWF	Siemens

## 2.8 Summary and Conclusions

This chapter presents an overview of the main equipment that is selected for the LFAC TS. The impact of low frequency on the equipment design, physical and operating features, as well as the potential effect of the components' electrical attributes to the LFAC TS operation, are discussed following research developments in the literature and industrial experience.

More specifically, technical benefits for three-phase subsea cables are presented in terms of losses, charging currents, reactive compensation and power transfer capability, based on cable parameters explicitly adapted for LFAC TS purposes by a cable manufacturer. Also, the LFAC TS voltage level is determined by evaluating the performance of different export cables at 230kV and 345kV. The power transfer capability significantly increases when operating at 345kV voltage level for distances greater than the maximum range of a typical 50Hz HVAC export system (approx. 80-100km) and up to the point that the HVDC system can naturally become the most economical solution. To attain the maximum power-transfer through a single subsea tri-core export cable, the capacity of the corresponding OWPP can be set approximately to the maximum power transfer capability of the subsea cable.

The effects of LFAC and different voltage levels on potential harmonic filter capacitors are also discussed. Based on the export cable selection, the 362kV class switchgear is chosen to form 345kV double LFAC busbar configuration at 16.7Hz, while for the medium voltage level of the OCS, the class of 72.5kV GIS is selected to connect the inter-array connection cables at 66kV. Certain adjustments are addressed to overcome the operating challenges of CBs at lower frequencies and avoid the probability of equipment damage or current chopping due to the longer time between two successive current zero-crossings, while further verification of capacitive current switching limits may be needed for an LFAC TS.

Furthermore, transformer design calculations are performed implementing practical constraints regarding their size and weight based on standard equations. The LFAC transformer designs are evaluated in terms of weight and losses for various impedance levels and compared with the respective AC. Results show that the estimated LFAC transformers could be 2-2.15 times bigger in terms of size and weight and consume 1.45-1.65 times more power than their 50Hz equivalents for the same p.u. impedance. Hence, for the appropriate transformer impedance selection, there is a trade-off between transformer weight and losses, although in an offshore transmission system application both the losses and weight of the transformers shall be reduced as much as possible.

Finally, it could be expected that the commercially available Type 4 WTGs in the range of 6-10MW and the recent BtB MMC technology that is selected for the formation of offshore LFAC network could be feasible solutions and comply with specific modern grid code standards. However, their rating and configuration should be appropriately adjusted for the needs of the LFAC TS, and their operation should be accordingly coordinated.

# Chapter 3: Offshore LFAC TS Electrical Design and Specifications

## 3.1 Introduction

Most of the OWP systems built so far are based on HVAC or HVDC radial connections, delivering power through a PtP scheme from an OCS to an onshore grid-connected substation. An improvement to this usual arrangement could be the introduction of a meshed, multi-terminal system design solution, e.g. by interconnecting multiple OCS. This way, in a case of scheduled or forced unavailability of individual elements which would have rendered a PtP system partially or totally non-operational, power could still be distributed through neighbouring routes. A truly integrated system could be formed by using LFAC TS technology, where the offshore system would be managed as a meshed grid and either alleviate congestion issues in the 50Hz AC grid or even interconnect different AC grids as depicted in Figure 3.1.

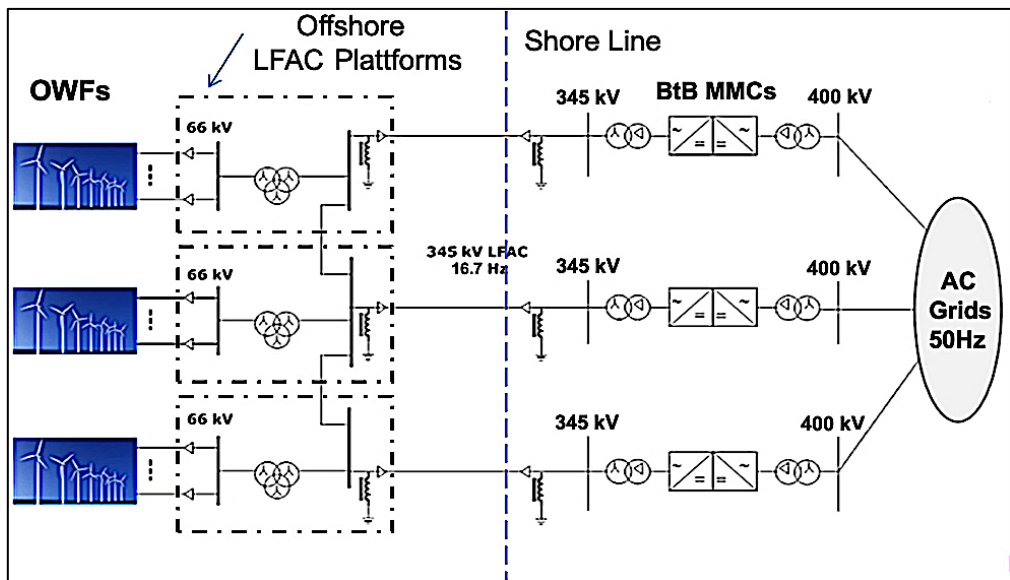


Figure 3.1: Meshed Offshore LFAC Transmission System for Offshore Wind integration.

The main LFAC transmission system (TS) configurations investigated in this Thesis consist of:

- 1 x 704MW Offshore Wind Farm being integrated to a 50Hz grid through a PtP LFAC transmission system for various cable lengths and
- 2 x 704MW Offshore Wind Farms that are interconnected to each other through an offshore LFAC interconnection cable and being integrated to two different grids or grid points via a meshed or MT-LFC transmission system for various cable lengths.

As shown in Figure 3.1, the LFAC TS design for exporting the power coming from remote offshore wind resources could be envisaged as multiple interconnected OWF blocks,

individually integrated to specific grid points in a typical PtP fashion. The electrical data that are used for representing each block in the LFAC TS EMT models are presented in Table 3-1.

*Table 3-1: Electrical Data of the OWF Integration System.*

WF INTEGRATION SYSTEM		
TOTAL SYSTEM ELECTRICAL DATA		
AC Grid Voltage	400	[kV]
AC Grid frequency	50	[Hz]
Total Capacity of the Project	704	[MW]
Transmission Type	HYBRID (e.g. LFAC)	
Collection Point Step-Up Transformers Total MVA	846	[MVA]
Nominal Voltage at the HV Trasmision Side (AC Collection Point)	345	[kV]
Nominal Voltage at the MV AC Collection Point Side	66	[kV]
Collection Grid / Transmission Frequency	16.7	[Hz]
No of HV AC Transmission Cables leaving the AC Collection Points	1	
Desired No of Equivalent WF Power Output Models (EMT)	1	
AC Node / Bus to be Controlled by the WF Model	345	[kV]
Offshore Interconnection Point between WF models either in 66[kV] or 345[kV]		
Wind Turbine Rated Power	8	[MW]
Full Scale WTG Converter Rated MVA	10	[MVA]

Careful consideration should be taken in the rating and design stage so that technical, as well as economic feasibility aspects of this innovative transmission system, are satisfied. The total LFAC transmission system arrangement for OWPP interconnection and integration consists of three main parts that are vital for the operation of the whole scheme and should be carefully designed and rated. These are the following:

- **Offshore Wind Power Plant System:** This system includes the WTGs and several strings of cables operating at 66kV and 16.7Hz forming the LFAC OCS network. This network terminates at 72.5kV class switchgear on the topside of the offshore LFAC platform.
- **Offshore LFAC TS Layout:** The LFAC TS includes the OWPP platforms, where the voltage is raised to the 345kV level by means of LFAC step-up transformers as well as the submarine LFAC cables for transferring the power to the onshore converter substation.
- **Onshore BtB Frequency Converter:** The onshore BtB-MMC station links the 16.7Hz LFAC TS with the 50Hz AC grid, and at the same time it separates their operation.

### 3.2 Offshore Wind Power Plant System Layout

The OWPPs are designed based on several radial strings of WTGs connected to an offshore substation. For larger schemes, the power plant can be divided into subsystems, structured in a modular fashion. In this work, full-converter WTGs are adopted, as described in Chapter 2, with a nominal power of 8MW, as presented in Table 3-2. Each WT is connected to a 66kV medium-voltage power collector system (OCS) that is explicitly described in section 3.2.2.

Table 3-2: Full-Converter WTG Electrical Rating.

WTG ELECTRICAL DATA		
Wind Turbine		
Rated power	8	[MW]
Full Scale WTG Converter		
Rated Apparent Power	10	[MVA]
Maximum Reactive Power Limit	0.6	[pu]
Max Reactive Power Output @ Full Power Operation	6	[MVar]
Min PF @ Full Power Operation	0.8	
WTG Inverter Transformer		
Transformer Total MVA	10	[MVA]
Base Operation Frequency	16.7	[Hz]
Nominal Voltage at the MV AC Collection Point Side	66	[kV]
Nominal Voltage at the VSC Side	8	[kV]

The 704MW OWF comprises 88 WTGs which can be considered here as one equivalent OWPP block. Each cluster can then supply a nominal power of ~700MW, for which one export LFAC cable is required at 345kV, as seen in Chapter 2. A maximum of two clusters has been studied here, with a capacity of approximately 1400MW. This has been assumed based on the current UK Grid Code standards (SQSS), where it is stated that the capacity for offshore power park modules should be limited to 1500MW.

The total installed capacity of 1408MW meshed offshore LFAC TS is split into two OWPP blocks of 704MW, per each point-to-point LFAC power export system. These blocks are interconnected offshore on the transmission voltage side of the step-up transformers, at 345kV level, to improve the security of supply and reliability of the scheme. Of course, this configuration might have been envisaged either on one or two offshore LFAC platforms. The corresponding arrangements are presented in Table 3-3.

Table 3-3: Investigated LFAC Power Export Arrangements.

Power Block (MW)	No. of Single Phase TRS	No. of Toppers	No. and Length of Cables (km)	Remarks
1 x 704	6	1	1 x 200	Radial PtP Connection to the Grid
			or	
			1 x 300...	
2 x 704	12	2	2 x 200 or	Two Independent, Inter-connected, Grids
			2 x 300 +	
			1 x 50	
			1 x 200 +	
1 x 300 +				
1 x 50				

If 1408MW installed capacity can be built on one topside in such a way that installation can be done through a single lift with ample availability of installation cranes, one superior OWPP block could be forming the system. Otherwise, a number of smaller “single cable” radial LFAC systems could be interconnected by means of cables and form an offshore meshed configuration that could be connected to the same or different grids or grid points, in a similar fashion as shown in Figure 3.1.

As there is no real LFAC system precedent for this application, no definition of such a system exists within the grid codes. However, this system could be seen as a hybrid combination of an OWF HVAC system integrated to the grid through an HVDC link. It is worth noting that for offshore projects the requirements differ between the offshore point of connection that Offshore Transmission Owners (OFTOs) call ‘Offshore Grid Entry Point’ and the onshore connection point termed the ‘Interface Point’ or Point of Common Coupling (PCC) shown in Figure 3.2. For the LFAC TS, the Interface Point would be on the onshore 50Hz side of the frequency converter while the Offshore Grid Entry Point could be offshore at 16.7Hz. Therefore, specific requirements would need to be met in two points of the LFAC TS.

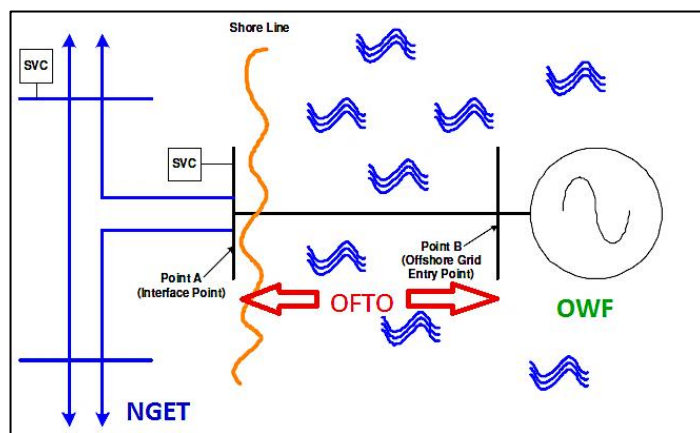


Figure 3.2: Connection Point Terminology.

This is particularly the case if the offshore LFAC TS is utilized to connect multiple offshore projects and integrate them into different grids, interconnecting AC grid systems as well. Either new OWPP projects or separate ventures could be interconnected to an offshore grid same as the commonly used practice in onshore grids. LFAC submarine cables can be connected to one or more offshore LFAC platforms where the internal grid voltage is transformed to a suitable voltage level for long-distance transmission. Thus, the LFAC TS should not only be considered as a simple OWPP integration medium, but it shall be intended as a potential solution to form meshed offshore networks, where specific requirements ought to be met by every LFAC grid-connected part.

In this Thesis, each 704MW OWPP block is intended to deliver its rated power output at the offshore 345kV - sending end of the corresponding subsea export cable. It can be operated either at unity power factor (i.e. zero reactive power exchange with the rest of the system) or as STATCOM regulating the 345kV LFAC transmission voltage level at the - 362kV class GIS that is placed in the offshore LFAC platform. As no tap-changers (OLTCs) have been assumed here for the LFAC step-up transformers, the function of each grid side WTG’s VSI is not only



to maintain the DC link voltage that varies due to the generated power being handled by the direct-drive rectifier but also to support the LFAC voltage by appropriately regulating the reactive power if required under certain operating conditions.

Since the offshore LFAC transmission system is formed and retained among converter terminals, it is strongly affected by the controllers' response at each 345kV point of connection. It can be assumed that the VSI control system of every WTG unit in a 704MW OWPP block is identically tuned to regulate the LFAC side voltage or reactive power at the offshore 345kV side of the step-up transformers. Hence, an equivalent OWPP module could be implicitly rated only for the relevant EMT studies to avoid the computational complexity and big simulation times of an EMT simulation software model. For the lumped design representation of each 704MW OWF cluster, the following parts have been considered:

- Two-Level BtB VSCs rated at 704MW with switching elements and control systems.
- An AC voltage source in the rectifier side and inverter transformers in the LFAC side.
- The equivalent 66kV topology with all the array and inter-array cable impedances and any other elements at the medium voltage level side.

### 3.2.1 OWTG / OWF System Configuration

In this Thesis, a BtB VSC configuration is assumed to connect the WTG to the LFAC TS, as shown in Figure 3.3. The VSCs are connected through a DC link. For both the rectifier and the inverter schemes, two-level VSCs are considered in a BtB arrangement. The rectifier acts as a direct drive adjusting the power output of the generator, while the DC-to-LFAC VSI independently controls the real and reactive power by adjusting the phase angle and magnitude of its output LFAC voltage ( $V_{c2}$ ). This independent control is a result of VSC's separate active and reactive power controllers [108]. The active control loop regulates the DC voltage, while the reactive control loop adjusts either the reactive power or the voltage level at the LFAC side. Since the generator is isolated from the LFAC system through the BTB VSCs, the WT drive-train side is not analysed here.

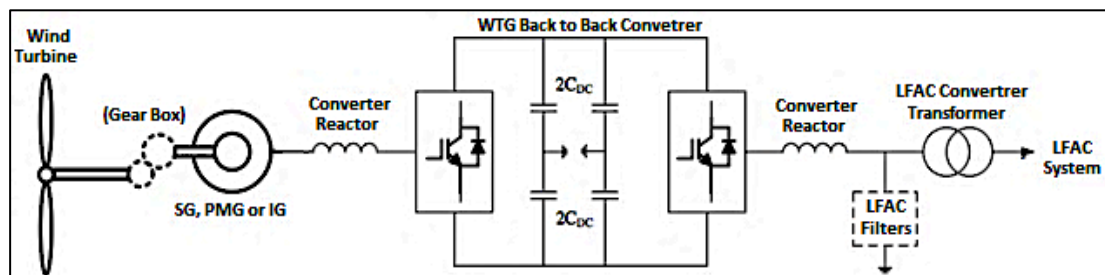


Figure 3.3: Type-4, Full Converter WTG Schematic.

Basically, VSCs could be considered as fast-controllable SGs, with a fundamental LFAC voltage output as follows:

$$V_{C2ph}(t) = \frac{1}{2} m_i \cdot V_{dc} \cdot \sin(\omega t + \delta_2) \quad (3.1)$$

Where:  $V_{C2ph}$  is the inverter output LFAC phase voltage,  $m_i$  is modulation index,  $V_{dc}$  is the rated DC link voltage,  $\omega$  is the angular frequency at 16.7Hz, and  $\delta_2$  is the phase shift of the inverter output voltage.

In this work, the total LFAC TS is represented in an EMT software environment, and an aggregate BtB VSC system rated at 704MW is modelled to represent the equivalent of the 88 WTGs. The BtB VSCs interface an AC voltage source instead of a permanent-magnet or synchronous alternator system in the rectifier side. Thus, the output of the whole BtB VSC scheme can be evaluated at 66kV, as the equivalent inverter control strategies of the Type-4 OWTGs are maintained, and the 66kV inter-array cable impedances and the related equipment is retained in the model. This simplification is assumed, as the framework of this Thesis is the offshore LFAC TS assessment and not the WTG interactions in an OWPP of the distinct electromechanical dynamics, which remain relatively unaffected, due to the full power electronic converter interface.

Hence, the DC-to-LFAC side VSI is the primary focus for rating the BtB system, while the rectifier VSC is designed accordingly. The electrical parameters of the LFAC grid interface inverter of the aggregate OWF are presented in Table 3-4, while an equivalent VSC of the adopted BtB system is shown in Figure 3.4. The converter rating has been set to 880MVA to enhance the converters reactive power capability. The comprehensive rating procedure, in conjunction with its low-pass LCL-type filter and LFAC interface transformer, is described in the following sections.

*Table 3-4: Aggregate WTG VSI Electrical Parameter Data.*

<b>Wind Farm Equivalent Model Data</b>		
<b>Full Scale WF Inverter</b>		
<b>Converter Name</b>	<b>WF - Inverter</b>	
<b>Control Strategy for d axis</b>	<b>Vdc</b>	
<b>Control Strategy for q axis</b>	<b>Q or Vac</b>	
<b>Apparent Power</b>	880	[MVA]
<b>Real power</b>	704	[MW]
<b>Nominal AC Voltage</b>	66	[kV]
<b>Maximum Reactive Power Limit</b>	0.6	[pu]
<b>Max Reactive Power @ Full Power Operation</b>	528	[MVar]
<b>PF</b>	0.8	
<b>AC Collection Point Side Frequency</b>	16.7	[Hz]

### 3.2.1.1 VSC Control System

Generally, the cascade vector-current control (VCC) shown in Figure 3.4 is the most common VSC control method. The equivalent VSI of the BtB system can apply both the DC Voltage and Reactive Power or LFAC Voltage control, while the rectifier regulates the Active Power.

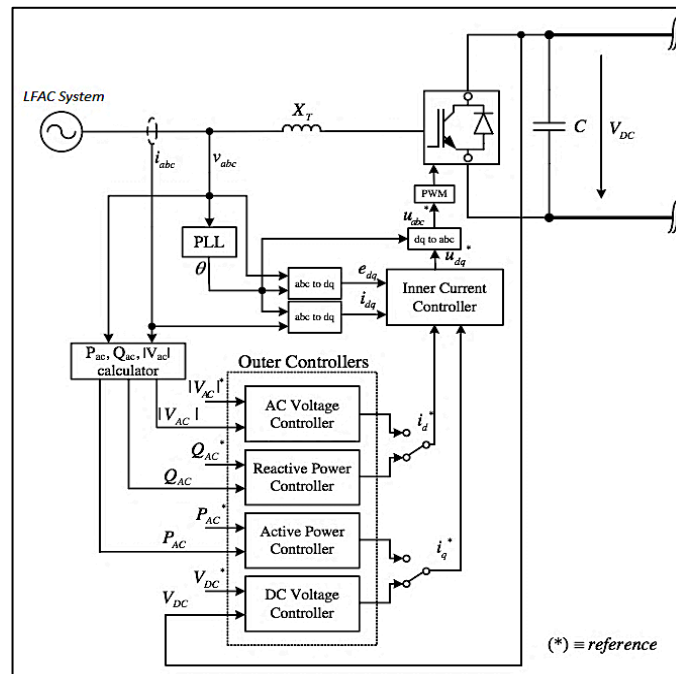


Figure 3.4: Generic Vector Control Arrangement for the Equivalent WTG VSI Topology.

The cascade VCC strategy is adopted in this Thesis due to its excellent dynamic characteristics and its inherent over-current limitation capabilities. It consists of faster inner current controllers (ICCs) and additional slower outer controllers which provide the reference values for the inner controllers. The outer controllers can be active power (APC) or DC voltage controllers (DCVC) as well as reactive power (RPC) or AC voltage controllers (ACVC) [108]. The implementation of a specific outer controller depends on the application and operating conditions of each VSC Terminal. This flexibility in terms of the controlled quantities provides two degrees of freedom at the inverter end, as the VCC scheme removes the coupling between the real and reactive power and ensures the independent control of each quantity, achieving robust and stable control as described in Chapter 6.

### 3.2.1.2 Two-Level Voltage Source Converter (VSC)

The VSCs are the core of the equivalent BtB converter system of the Type-4 WTGs. They are divided into several circuit topologies according to the converter output AC voltage levels. However, only two basic configurations of VSCs are mainly used on full-Converter WTGs; the two-level, and three-level forced commutated VSC bridges, which are shown in Figure 3.5 a)

and b), respectively. The three-level natural point clamp VSCs used to be favoured in the past due to the higher quality of output voltage waveform (e.g. lower THD), with fewer switching events, leading to lower switching losses. Low losses were achieved, though, at the expense of control system complexity and converter cost due to the increased number of valves (additional clamping diodes required) in the scheme compared to the two-level schemes.

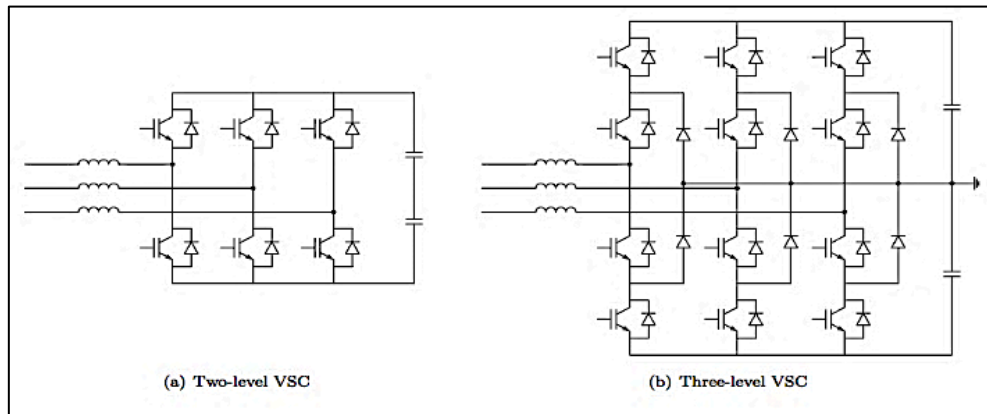


Figure 3.5: Basic VSC Circuit Topologies for Type-4 WTGs: a) Two-Level, b) Three-Level VSC.

Many full-converter WTGs have adopted the simpler and more compact two-level VSC, as the evolved PWM switching techniques have made it efficient and its switching losses have been considerably reduced. A square-wave output AC voltage with only two values is formed by controlling the switches and by filtering, a quasi-sinusoidal voltage waveform is obtained.

### 3.2.1.3 DC Voltage

For the equivalent WTGs BtB module, the value of 135kV has been selected, assuming the LFAC voltage level of 66kV in the converter output. Technically, the maximum operating DC voltage should be considered for the maximum steady-state acceptable AC - side voltage level of 105%, as seen on Table 3-5 and Equation (3.2), although this could be set even higher for this work's configuration, as the VSCs are arranged in a BtB pattern, and the offshore LFAC system could be regulated to operate up to 110% voltage level.

Table 3-5: DC Side Parameters of the Equivalent BtB VSC Scheme.

DC Side		
V <sub>dc</sub>	135	[kV]
I <sub>dc</sub>	5.23	[kA]
Before Filtering		
Converter AC Side Output		
Phase-to-DC Midpoint Pulse Voltage Magnitude	67.4	[kV]
Line Pulse Voltage Magnitude	135	[kV]

Accordingly, the minimum DC voltage level required to avoid converter saturation while using SPWM can be calculated from the corresponding limits shown in Equation (3.2), with

$m_i = 1$  and a minimum steady-state acceptable LFAC-voltage level of 95%, respectively.

$$95\% \cdot 2 \cdot \hat{V}_{Cph} \leq V_{dc} \leq 105\% \cdot 2 \cdot \frac{\hat{V}_{Cph}}{m_i} \quad (3.2)$$

Operating the BtB VSCs in DC voltage limits can increase the reactive power capability of the OWF system. Thus, by appropriately adjusting the LFAC voltage output, this feature could help towards handling reactive power at the cable sending end.

#### 3.2.1.4 DC-Link Capacitance

The DC link capacitance shall act to retain the DC voltage constant within limits, even if power oscillations occur in the DC-link during disturbances in the LFAC system side. Its size ( $C_{dc}$ ) is characterised by its time constant ( $\tau_{Cdc}$ ), defined as the ratio of its stored energy at the rated DC voltage ( $W_{Cdc}$ ) to the nominal apparent power of the VSC ( $S_{VSC}$ ), as in Equation (3.3) [90]:

$$\tau_{Cdc} = \frac{C_{dc} \cdot V_{dc}^2}{2 S_{VSC}} \quad (3.3)$$

The capacitor time constant ( $\tau_{Cdc}$ ) can be different depending on the converter application and is typically in the range of 10ms to 50ms according to [90], or it may correspond to 30 - 40kJ/MVA according to [94]. In addition, the amount of energy that needs to be stored in the DC side capacitors ( $W_{Cdc}$ ) is proportional to the power rating of the VSC system ( $S_{VSC}$ ) but inversely proportional to the DC voltage ripple ( $\Delta V_{dc}$ ) and the AC side operating frequency ( $\omega_e$ ); to cater for unbalances. Consequently, the size of the DC capacitance is then mainly defined also by the required DC voltage, according to the Equation (3.4) [90]:

$$C_{dc} = \frac{S_{VSC}}{2 \omega_e \cdot V_{dc} \cdot \Delta V_{dc} \cdot S_{VSC}} \quad (3.4)$$

As can be inferred by Equation (3.4), the value of an equivalent DC capacitance for the BtB VSC scheme that is connected to a 16.7Hz LFAC system can be up to three times higher than the corresponding 50Hz value. However, due to the BtB arrangement, the capacitor size may be compromised, considering a relatively higher DC voltage ripple tolerance.

Table 3-6: DC Capacitor Parameters

DC Capacitance		
DCV Ripple (p2p)	20	[%]
DC-Link Capacitors	0.001155	[F]
Energy Stored in the DC Capacitor	10.5	[MJ]
DC Capacitor Time Constant	0.0119	[sec]

In this study, a DC capacitance value of  $\sim 1.15\text{mF}$  is selected that corresponds to  $\sim 20\%$  voltage ripple and a  $\tau_{Cdc} \sim 12\text{ms}$ , as shown in Table 3-6.

### 3.2.1.5 DC-Link Dynamic Braking Resistor

The Dynamic Braking Resistor (DBR) is applied to protect the DC systems from over-voltages. Such over-voltages can be caused if the inverter system is not able to export the demanded amount of power that flows through the rectifier, e.g. during a fault in the LFAC system to which the inverter is connected [115]. Thus, by using DBRs in the WTG DC-Link, the excess energy is dissipated, offering the advantage of over-voltage protection against faults on the collector bus, and on the LFAC transmission system between them and onshore frequency converters. A typical DBR system with its operational characteristic is shown in Figure 3.6.

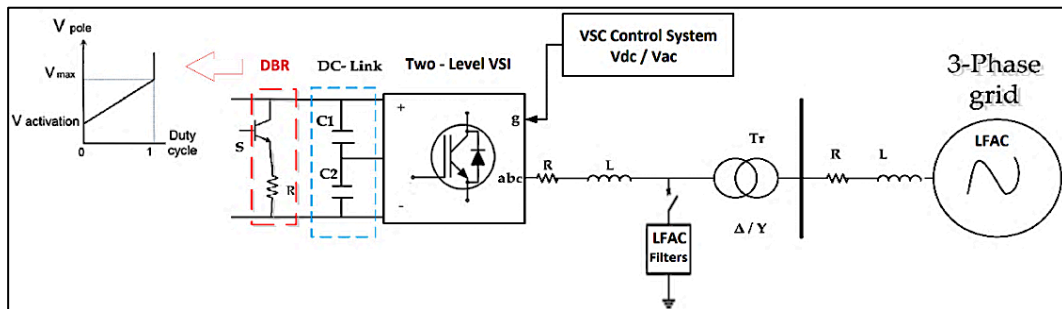


Figure 3.6: DBR in the DC-Link Side of the Type 4 WTG and its Typical Operation Characteristic.

The braking resistor for the equivalent 704MW aggregated EMT model should be rated to dissipate power equal to the whole OWF block. The DBR would be activated once the DC voltage exceeds 1.15p.u. while it would be turned off once the DC voltage has returned to its acceptable levels. These voltage thresholds prevent the braking resistor from interfering under normal operating conditions. The related DBR parameters are given in Table 3-7.

Table 3-7: Dynamic Braking Resistor Parameters.

DC Braking Resistor		
Activation DCV	1.15	[pu]
Max DCV	1.2	[pu]
DC braking resistor	46.6	[Ohm]

### 3.2.1.6 Converter Reactor

The phase reactors are mostly inductive elements with minimal resistance which are connected in series with the converter and the rest of the LFAC system. They are special types of reactors able to withstand high inter-turn voltage stress and need to be designed with a high degree of interwinding insulation. Their size depends on the converter saturation, its switching frequency, and the employed PWM strategy. They serve the following purposes:

- Fault-current reduction to the desired level within the rating of the converter. They protect the converter from the propagation of fast front voltage transients, occurring during faults and/or circuit breaker operations.

- Regulate the active and reactive power flow by adjusting the current through them. They affect the VSC control system tuning and the dynamic behaviour of the AC side.
- Decrease the high-frequency harmonic content of the AC current, caused by the switching operation of the VSC. As in this work, they can be parts of low-pass filters and reduce the Total Harmonic Distortion (THD), improving the power quality.

### 3.2.1.7 AC Filters

AC filters are used on the LFAC side of the two-level inverter to remove some of the VSC's output voltage harmonic components. The low pass filter prevents harmonics from entering into the transformer and the connected LFAC system, leading to smoother sinusoidal LFAC waveforms at the point of common coupling (PCC). The most common low pass AC filter design is the LCL filter, as presented in Figure 3.7.

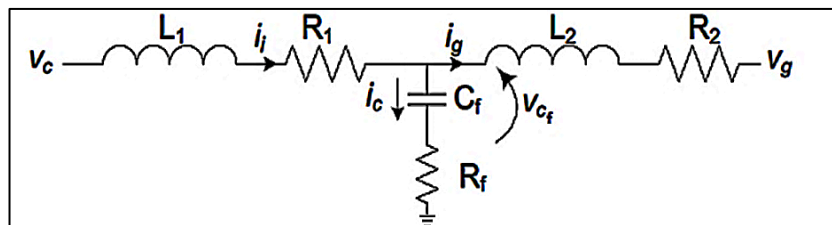


Figure 3.7: VSI LCL-Filter Schematic.

Configurations of LCL filters may vary for different applications depending on filter performance requirements. The equivalent VSI LCL-filter in the LFAC side comprises of two sets of inductors in the inverter ( $L_1$ ) and grid side ( $L_2$ ) respectively, and one set of shunt-connected capacitors ( $C_f$ ) with resistive damping ( $R_f$ ) which are placed between them. The capacitor of an LCL filter is essentially a high-pass filter, providing a low impedance path for high-frequency current components.

The parameters of this filter are carefully selected in order to avoid instability that could be caused if its resonant frequency is close to the switching frequency of the VSC and its odd harmonics. Given the fact that the size of the WTG-VSI transformer is quite bigger and heavier if rated for LFAC operation, its inductance is considered to form the ( $L_2$ ) part of the LCL-Filter. In order to limit PWM current ripple, the converter side inductors ( $L_1$ ) or phase reactors, must be much bigger  $L_1 \gg L_2$  for a practical LCL-filter. Additionally, many authors recommend that the converter output current ripple should be limited to less than 10% peak-to-peak of the rated fundamental current magnitude, in order to comply with standards and grid codes and avoid potential inductor saturation issues [71].

For the above reasons, the value of inductor L1 is independently selected to limit the ripple of the converter output current to less than 10% of the rated current amplitude, as a common practice, and its value together with the transformer leakage inductance L2 define the filter capacitance C<sub>f</sub> value. Equation (3.5) estimates the value of inductance for a given DC side voltage and PWM switching frequency f<sub>sw</sub> of the two-level PWM VSC [72].

$$L1 = \frac{V_{dc}}{8\Delta i_{max} \cdot f_{sw}} \quad (3.5)$$

$$\text{Where: } \Delta i_{max} = \lambda \cdot \hat{I}_{Cbase}, \quad \lambda \leq 10\%$$

The LCL-filter capacitor is typically rated to provide reactive power of less than 5% of the rated power of the converter. The larger the capacitance, the smaller the inverter side inductance which reduces the efficiency of the scheme, as more current is drawn from the converter. Equation (3.6) relates converter current and the harmonic current injected to grid at the switching frequency. By solving this equation for a total attenuation (k<sub>α</sub>) of 20%, L1 and L2, the value of C<sub>f</sub> can be determined [72].

$$k_{\alpha} = \left| \frac{I_{gsw}}{I_{Csw}} \right| = \frac{1}{|1 + L2/L1 - L2 \cdot C_f \cdot \omega_{sw}^2|} \quad (3.6)$$

In addition, since the resonant frequency f<sub>res</sub> is a function of the filter capacitance and grid impedance, it can vary under certain operating conditions. Hence, it should lie in a stable region where supplementary damping is not required, and the fundamental frequency converter current remains unaffected [111]. This region can be selected to be lower than half of the switching frequency f<sub>sw</sub> and higher than 10 times the grid electrical frequency f<sub>e</sub> to avoid resonance problems. This way, Proportional-Integral (PI) based current control can be achieved without active or passive damping if the resonance frequency f<sub>res</sub> is inside the interval [f<sub>cmin</sub>, f<sub>cmax</sub>], as defined by Equation (3.7) below:

$$f_{res} = \frac{1}{2\pi} \sqrt{\frac{L1+L2}{L1 \cdot L2 \cdot C_f}}, \quad \text{with } 10f_e \leq f_{res} \leq \frac{1}{2}f_{sw} \quad (3.7)$$

Other correlated oscillations around the resonant frequency can be suppressed by the resistor (R<sub>f</sub>) that is inserted in the capacitive branch as a simple form of damping, although it negatively affects the filter performance and causes fundamental frequency losses. The value of this resistance should be equal to one-third of the capacitive reactance at the resonant frequency and is given by the equation below:

$$R_f = \frac{1}{3\omega_{res} \cdot C_f} \quad (3.8)$$



The inverter side LCL-filter parameters for the equivalent 704MW system model are shown in Table 3-8, below. In this table, L1 can also be considered as the converter phase reactor, and L2 is the equivalent converter transformer leakage inductance.

Table 3-8: VSI LCL-Filter Parameters.

LCL - Filter		
Zbase at the VSC Side	4.95	[ohm]
Cbase at the VSC Side	0.0019253	[F]
Filter Capacitance, Cf	0.00000665	[F]
Reactive Power Supplied by the Filter Capacitor	3.04	[Mvar]
Converter Inductance L1	0.02252	[H]
Attenuation Factor ka	0.2	
Transformer Leakage Inductance L2	0.00627	[H]
$10 \cdot f_e < \text{Resonant/Cutting Frequency} < f_{sw}/2$	881.63	[Hz]
Damping Resistor Rf	9.051	[ohm]

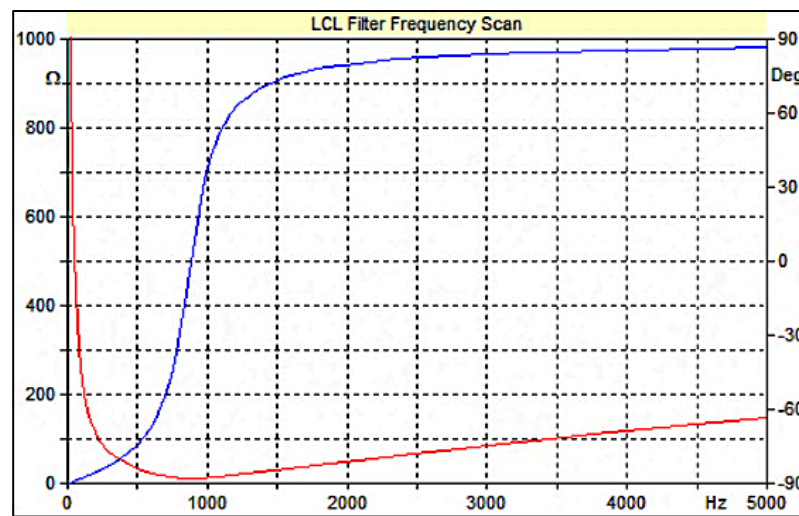


Figure 3.8: Frequency Response of the LCL Filter Design: Impedance Magnitude (Red) and Phase (Blue).

The impedance and phase against frequency plots show its cutting frequency being at 881Hz, providing a low-impedance route to ground for high-frequency current components, while for lower frequencies, its impact on the system impedance characteristics can be minimal.

### 3.2.1.8 Converter Transformer

The WTG-VSIs are connected to the LFAC system by means of converter transformers. Their primary function is to transform the Medium LFAC voltage to a suitable level for the VSCs to perform the AC-to-DC conversion. As mentioned in Chapter 2, these transformers may lead to WT nacelle or tower design modifications due to their increased size and weight. The electrical parameters for the equivalent inverter transformer models of the 704MW OWF modules used in this work are presented in Table 3-9, based on the LFAC transformer design characteristics estimated in section 2.4.

Table 3-9: LFAC OWF-Inverter Transformer Parameters.

Equivalent WTGs' Part of Total Converter Transformer		
Transformer Total MVA	880	[MVA]
Base Operation Frequency	16.7	[Hz]
Nominal Voltage at the MV AC Collection Point Side	66	[kV]
Nominal Voltage at the VSC Side	66	[kV]
Winding Type MV AC Collection Point Side	Y	
Winding Type VSC Side	D	
Transformer Positive Sequence Leakage Reactance	0.07	[pu]
No Load Losses	0.000156383	[pu]
Copper Losses	0.00233333	[pu]

### 3.2.2 Medium Voltage Collector System Layout

As suggested above, the power from the 88 WTG units of a ~700MW OWF is collected at the topside of a compact offshore LFAC platform and connected to 72.5kV class switchgear schemes by means of array connections at 66kV, as mentioned in section 2.3. The configuration of the 72.5kV class GIS system is described in Table 3-10. Besides the GISs, the platform houses the step-up transformers (bank of 3 x 141MVA, 16.7Hz single-phase units, as referred in Chapter 2, the 362kV class GIS, all auxiliaries, control and protection, if there is no offshore shunt compensation for the export cable.

Table 3-10: The 72.5kV Class Switchgear System Configuration (GIS)

COLLECTION POINT - SUBSTATION		
GIS SPECS WF - SIDE , @ kV 66		
GIS MAX Rated Voltage	72.5	[kV]
GIS Rated power frequency withstand voltage	140	[kV]
GIS Rated lightning impulse withstand voltage (BIL) [PEAK]	325	[kV]
Min Rated Current	1.25	[kA]
Max Rated Current	2.5	[kA]
<b>Total No of GISs of the WF - Side</b>	<b>4</b>	
Number of WTGs per GIS	22	
AC Current per GIS	1.925	[kA]
AC Current Magnitude per GIS	2.722	[kA]
<b>Loading is the Same to All GISs</b>		

The 704MW OWF requires a total number of 4 x 72.5kV GISs to be utilized, each connected to 22 WTGs. Thus, the total number of 88 WTGs is divided into twelve arrays, with eight strings of seven WTG units each and four strings of eight units each, respectively. Each seven or eight WTG array is shaped by two sub-array WTG-strings that are linked together and is connected to a 72.5kV class switchgear through one submarine Cu-XLPE, 800 mm<sup>2</sup> array-cable operating at 16.7Hz, according to Table 3-11.

Table 3-11: Inter-Array String Cable Parameters.

INTER-ARRAY-STRING CABLES	FOR GIS - MAX Loading	
Cable Placement (Air,(Under-)Ground, Submarine)	S	
Cable Isulation Material	XLPE	
Cable Cores [Single-Core, Three-Core]	T	
Cable Conductor Material	Cu	
Cable Operational Voltage	66	[kV]
Cable Rated Voltage Range	3C: 10 - 90	[kV]
Maximum Cable Cross Section to be utilised	800	[mm <sup>2</sup> ]
Cable Rated Current	0.775	[kA]
Cable Current (multiplied with 0.9 - Jtubes, etc.)	0.6975	[kA]

Therefore, in each 72.5kV GIS system, there will be 1 x 8 WTGs + 2 x 7 WTGs strings connected to it through the 800 mm<sup>2</sup> Cu-XLPE array cable. The medium 66kV voltage offshore system configuration schematic, as described, is shown in Figure 3.9. All the above-mentioned WTG units form one OWPP block, providing an installed capacity of 8 x 56MW + 4 x 64MW giving a total of 704MW at 66kV.

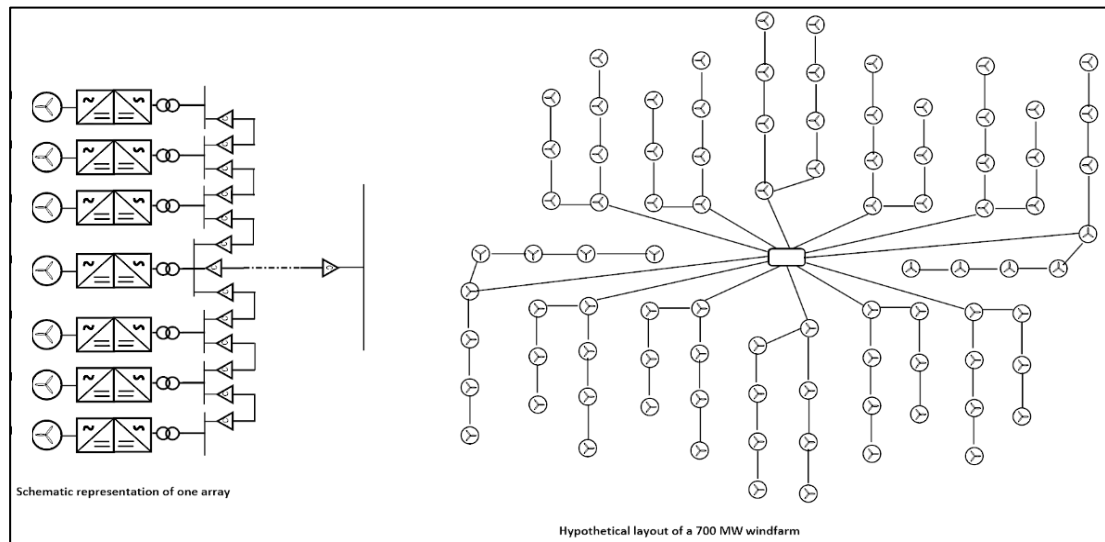


Figure 3.9: Schematic Representation of the 66kV Offshore WPP Layout, incl. Detail of a Single Array.

The utilization of the submarine array cable with reference to the number of WTGs per array is given in Table 3-12, where the cable rated current after the effect of J-tubes is considered. As can be seen for strings with 8 WTGs rated at 10MVA each, the utilization of the cable can reach up to 100%, while for strings with 7 WTGs its utilization can be as low as 88%.

Table 3-12: Array 800mm<sup>2</sup>, Cu-XLPE Cable Utilization.

WTGs TO EACH STRING / STRINGS TO EACH GIS	FOR GIS - MAX Loading	
Maximum No of WTGs per Cable	8	
No of these Cables per GIS / No of STRINGS per GIS	3	
Maximum No of WTGs per String	8	
Utilization of the Cable for Max No of WTGs per String	100	[%]
Minimum No of WTGs per String	7	
Utilization of the Cable for Min No of WTGs per String	88	[%]
Total No of Strings per GIS	3	Combined

In each array, the WTGs are connected with 400mm<sup>2</sup> Cu-XLPE sub-array cables. The length of each sub-array cable connecting the WTGs is assumed to be 1km, while each of the twelve 800mm<sup>2</sup> Cu-XLPE array cables is assumed to be 2km long. In Table 3-13, the cables' electrical parameters derived from the ABB's subsea XLPE cables catalogue for 66kV operation at 50Hz.

*Table 3-13: Medium Voltage - 66kV - Array and Sub-Array Submarine XLPE Cables (ABB).*

CABLE ELECTRICAL RESPONSE-ABB Submarine Power Cables				
		800 mm <sup>2</sup> Cu-XLPE	400 mm <sup>2</sup> Cu-XLPE	
Insulation Capacitance per km	Ccab	3.50E-07	2.60E-07	[F/km]
Meas.Cable Inductance per km	Lcab	3.20E-04	3.50E-04	[H/km]
Meas. Cable Resistance per km	Rcab	2.96E-02	5.14E-02	[ohm/km]

The total 704MW OWPP block is integrated to the grid through one 345kV XLPE-LFAC subsea export cable. Several cases with various export cable lengths have been studied for up to two of these blocks interconnected at their OCS through an LFAC cable, assuming a total installed capacity of approximately 1,400MW. Each OWF block acts as a separate unit facing the offshore LFAC TS side, although the 66kV medium voltage system is represented.

### 3.3 Offshore LFAC Transmission System Layout

In the OWPP platforms, mentioned above, the 66kV medium voltage level is raised to a suitable level for transmission by means of LFAC step-up transformers. The 345kV voltage level has been selected as the offshore LFAC transmission system voltage with the advantages of this choice explained in Chapter 2. The power is then transferred through the submarine LFAC cables to the onshore frequency converter station and subsequently converted for integration to the 50Hz AC grid.

Depending on the distance from shore, for 704MW power transmission, one submarine export cable can be sufficient as suggested in Chapter 2. Thus, one OCS with a single topside can be considered at the offshore platform for a radial, point-to-point transmission arrangement. In this study, the onshore frequency converter is assumed to be placed in one single substation site too, for every 704MW OWF power block as can be seen in Figure 3.10.

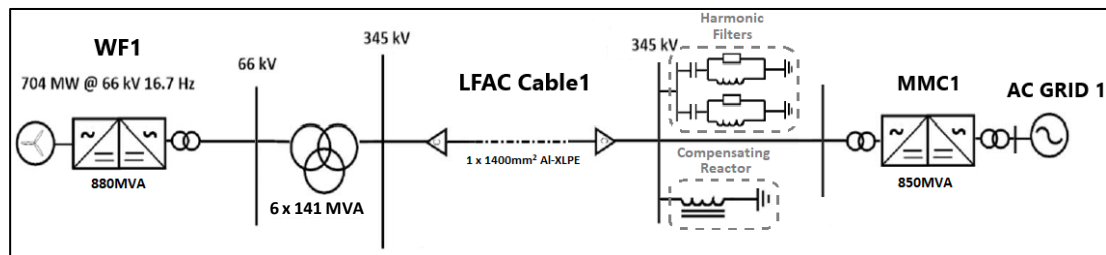


*Figure 3.10: Simplified Representation of a PtP Scheme Integrating a 704MW OWPP Block to the Grid.*

For the 1400MW meshed offshore LFAC system arrangement outlined in Figure 3.11, two of the above-mentioned Point-to-Point schemes can be interconnected in their offshore 345kV side through an additional, identical submarine cable. This cable, depending on its length, may carry the full capacity from an OWPP cluster or even power coming from one grid, transferring it to a different grid or grid point. This concept may be extended to include more offshore generation sources and more grids.

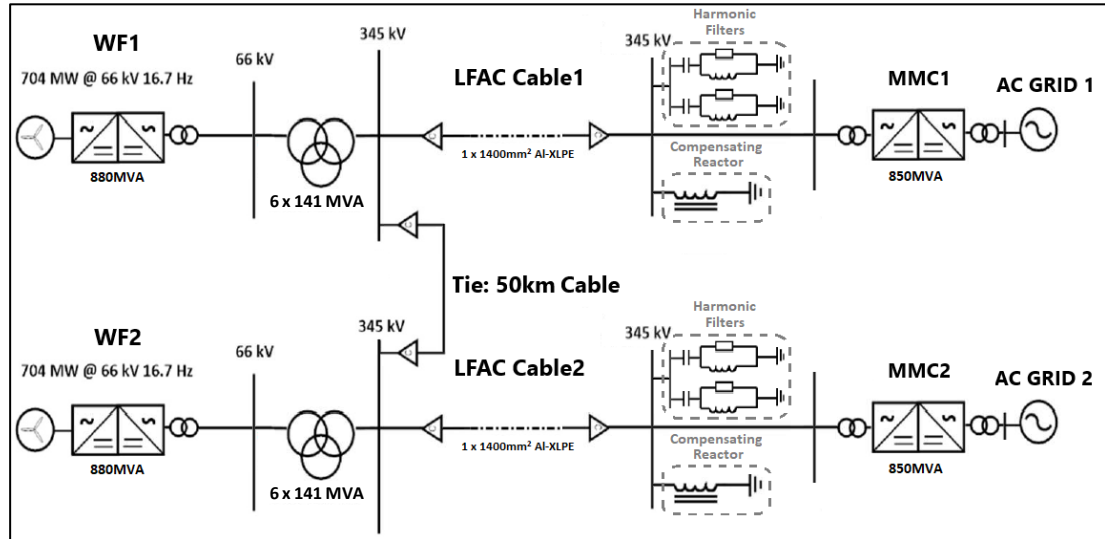


Figure 3.11: Offshore MT-LFAC System Integrating 1408MW OWF and Interconnecting different Grids.

### 3.3.1 LFAC Transformer

The LFAC transformer used in this analysis is based on the design calculations performed in Chapter 2, where a design with relatively increased core area and winding-number is estimated to compensate for the low frequency. The electrical parameters of the transformer are presented in Table 3-14.

Table 3-14: LFAC Step-Up Transformer Electrical Parameters

COLLECTION POINT - SUBSTATION		
Step-Up Transformers		
Transformer Total MVA	423	[MVA]
Total No of Step-Up Transformers in the Project	2	
Base Operation Frequency	16.7	[Hz]
Nominal Voltage at the HV AC Transmission Side	345	[kV]
Nominal Voltage at the MV AC Collection Point Side	66	[kV]
Transformer Type	3 Single Phase Tr	
No of Units per Transformer	141	[MVA]
Winding Type HV AC Transmission Side	Y	
Winding Type MV AC Collection Point Side	Y	
Delta Lags or Leads Y	-	
Transformer Positive Sequence Leakage Reactance	0.07	[pu]
No Load Losses	0.00016	[pu]
Copper Losses	0.00233	[pu]

It is worth noting that an absolute change in frequency does not result in three times bigger transformer size as various factors contribute to its overall dimensions. According to the conclusions presented in the LFAC transformer design section, if the height restrictions defined by transportation constraints are considered, the leakage reactance of an LFAC transformer design would lie in the range of 6-10%. Thus, the leakage reactance selected is 0.07p.u., which lies in lower p.u. value than the expected impedance at higher industrial frequencies, e.g. for a 50Hz or 60Hz.

### 3.3.2 LFAC Export Cable

The LFAC submarine power export cables adopted in this Thesis are based on the NEXANS design in coordination with HVDC TECH cable performance studies. All the transmission cables used for the specific LFAC transmission schemes are based on the 345kV-1400mm<sup>2</sup> Al cable which has been selected for the reasons explained in the ‘Submarine LFAC Export Cable Design’ section 2.2.2. The electrical parameters of this cable are given in Table 3-15.

*Table 3-15: 345kV Submarine LFAC – XLPE Export Cable Electrical Parameters (NEXANS).*

LFAC CABLE ELECTRICAL RESPONSE - NEXANS			
		1400mm <sup>2</sup> Al - XLPE	
Insulation Capacitance per km	Ccab	1.73E-07	[F/km]
Meas.Cable Inductance per km	Lcab	4.19E-04	[H/km]
Meas. Cable Resistance per km	Rcab	3.07E-02	[ohm/km]
<b>Total Current Limit</b>	<b>Imax</b>	<b>1.5</b>	<b>[kA]</b>

The level of detail in representing a cable’s electrical characteristics depends on the study requirements, as there is always a trade-off between cable parameter accuracy and simplicity of the model. Thus, models can be based on lumped or distributed parameters throughout the cable length and on constant or frequency-dependent parameters [110]. As this work aims at the detailed analysis of the LFAC TS, the explicit characteristics of the subsea cable are examined in Chapter 4, with distributed and frequency-dependent parameters representation for accurate investigation of its response in a broad frequency spectrum.

In this section, a simplified estimation of the submarine cable electrical parameters is intended throughout its length as well as the sizing of the corresponding compensating reactors. The equivalent  $\pi$ -circuit representation for various cable lengths is adopted, which can be used only for steady-state 16.7Hz assessment. A simple way to derive an equivalent  $\pi$ -circuit and consider the travelling voltage waves is by developing the cable system as a quadrupole or a two-ports network. The complete rating and appropriate planning of the required active and passive compensating measures can be defined after the detailed frequency, steady-state and time-domain assessments of Chapters 5,6,7, respectively.

Based on the 345kV submarine LFAC - XLPE export cable electrical parameters supplied by the manufacturer, the total impedance and admittance of the cable system can be yielded by the equations below [110]:

$$Z_{cab} = (R_{cab} + j\omega_e L_{cab}) \quad (3.9)$$

$$Y_{cab} = j\omega_e C_{cab} \quad (3.10)$$

Where:  $\omega_e=105.93$  rad/s is the operating angular frequency corresponding to  $f_e=16.7$ Hz.

The characteristic or "surge" impedance ( $Z_c$ ) is defined as:

$$Z_c = \sqrt{\frac{Z_{cab}}{Y_{cab}}} \quad (3.11)$$

The wave propagation constant ( $\gamma$ ) is given by Equation (3.12).

$$\gamma = \sqrt{Z_{cab} \cdot Y_{cab}} = \alpha + j\beta \quad (3.12)$$

Where:  $\alpha$  is the real part of the propagation constant, which represents the attenuation (Np/m) and  $\beta$  is its imaginary part which represents phase velocity (rad/m).

The Surge Impedance Loading (SIL) for the cable is:

$$SIL = \frac{V_{cab}^2}{|Z_c|} \quad (3.13)$$

The propagation speed ( $v_e$ ) for lossy cable can be calculated as:

$$v_e = \frac{1}{\sqrt{L_{cab} \cdot C_{cab}}} \quad (3.14)$$

Finally, the Travelling Wavelength ( $\lambda$ ) is:

$$\lambda = \frac{v_e}{f_e} \quad (3.15)$$

The above characteristic cable parameters are calculated and presented in Table 3-16. They are independent of the cable length, but they are affected by the operating frequency. For this reason, these results are only simplified estimates at the fundamental of 16.7Hz.

*Table 3-16: 200km LFAC – XLPE Export Cable Characteristic Parameters.*

<b>1400mm<sup>2</sup> Al - XLPE - LFAC Cable Characteristics</b>			
<b>z</b>	<b>Zcab</b>	0.0307+0.044i	<b>[ohm/km]</b>
<b>y</b>	<b>Ycab</b>	0.000018	<b>[Siemens/km]</b>
<b>Characteristic Impedance</b>	<b>Zc</b>	52-16.3i	<b>[Ohm]</b>
<b>Propagation Constant</b>	<b>γ</b>	0.000296+0.00094i	<b>[km<sup>-1</sup>]</b>
<b>Surge Impedance Loading</b>	<b>SIL</b>	2184	<b>[MW]</b>
<b>Propagation Speed</b>	<b>ve</b>	117408	<b>[km/s]</b>
<b>Traveling Wave Length</b>	<b>λ</b>	7030	<b>[km]</b>

From Equation (3.15), the travelling wavelength is inversely proportional to the operating frequency, and thus, for the low operating frequency of 16.7Hz, the wavelength is larger in comparison with 50Hz for the same cable length. This fact enables the initial estimation of the cable equivalent lumped parameters through the quadrupole representation as the travelling wave passes through it with less time delay in comparison with 50Hz operation. Since, the quadrupole modelling depends on the length of the transmission medium and the cables examined here can be relatively long (e.g. up to 400km) in comparison with the cable wavelength, the travelling time ( $\tau$ ) as given by Equation (3.16) of the electromagnetic waves shall not be neglected.

$$\tau = \frac{l}{v_e} \quad (3.16)$$

Therefore, the evolution of the travelling waves and the refraction at the cable ends should be taken into account. In order to obtain the equations of the power cable at 16.7Hz, the two-port (ABCD) network equivalent is adopted as presented in Figure 3.12.

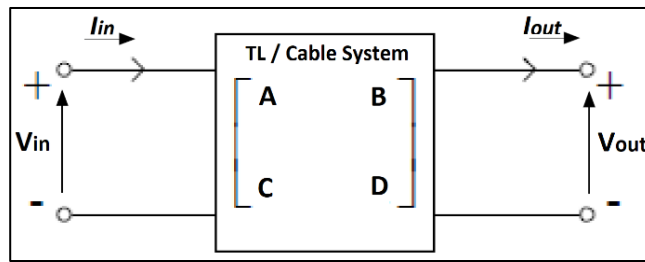


Figure 3.12: Two-port, ABCD Network Equivalent for LFAC Cable.

The ABCD are the parameters of the Transmission Matrix as given in Equation (3.17) [102].

$$\begin{bmatrix} V_{in} \\ V_{out} \end{bmatrix} = \begin{bmatrix} A & B \\ C & D \end{bmatrix} \cdot \begin{bmatrix} I_{in} \\ I_{out} \end{bmatrix} \quad (3.17)$$

Where A, B, C and D are defined by Equations (3.18-3.20), and each parameter represents:

- A) For open-circuit output: the voltage / ratio between the two ports.
- B) For short circuit output: the negative transference impedance.
- C) For open-circuit output: the transference admittance.
- D) For short circuit output: the negative current relation.

$$A = D = \cosh(\gamma \cdot l) \quad (3.18)$$

$$B = Z_C \cdot \sinh(\gamma \cdot l) \quad (3.19)$$

$$C = \frac{1}{Z_C} \cdot \sinh(\gamma \cdot l) \quad (3.20)$$



Three of the above terms are enough to model OTLs and cables with less than 500km, although the first two terms are usually enough in most cases. Consequently, the equivalent circuit for long cables is an equivalent "π" circuit as depicted in Figure 3.13, that its impedance ( $Z_{\pi}$ ) and admittance ( $Y_{\pi}$ ) can be expressed as follows:

$$Z_{\pi} = B \quad (3.21)$$

$$Y_{\pi} = 2 \cdot \frac{A-1}{B} \quad (3.22)$$

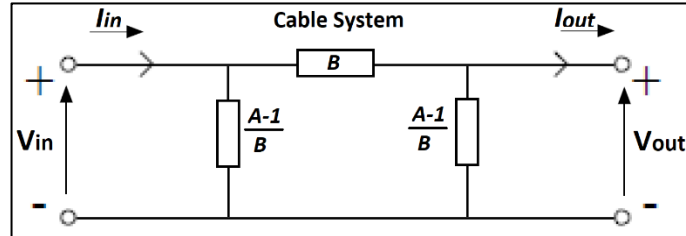


Figure 3.13: Two-Port Oriented to a Cable Π-Circuit System in the Phasor Domain.

The transmission impedance and admittance of the LFAC cable's π-circuit for a length of 200km are projected in Table 3-17, while Table 3-18 shows its calculated parameters for various cable lengths.

Table 3-17: LFAC Export Cable Π-Circuit Impedance and Admittance for 200km.

Transmission Parameters Cable Length 200km		
$Z_{\pi}$	6.074+8.776i	[ohm]
$Y_{\pi}$	3.4E-06+0.00182i	[Siemens]

Table 3-18: LFAC Export Cable Π-Circuit Parameters for Various Lengths.

LFAC Cable Π-Circuit @ Various Lengths		[km]	50	100	200	300	400
EQUIV. Insulation Capacitance	$C_{cab\_pi}$	[F]	8.65E-06	1.73E-05	3.47E-05	5.22E-05	6.99E-05
EQUIV. Cable Inductance	$L_{cab\_pi}$	[H]	2.10E-02	4.19E-02	8.36E-02	1.25E-01	1.66E-01
EQUIV. Cable Resistance	$R_{cab\_pi}$	[ohm]	1.53E+00	3.06E+00	6.07E+00	8.99E+00	1.18E+01
EQUIV. Cable ADMITANCE	$G_{cab\_pi}$	[ohm]	2.64E-08	2.11E-07	1.70E-06	5.77E-06	1.38E-05

The reactive power consumption ( $Q_L$ ) and generation ( $Q_C$ ) occurring in the LFAC cable is:

$$Q_L = \left(\frac{P_{cab}}{\sqrt{3}V_{cab}}\right)^2 \cdot X_{cab}, \quad Q_C = \frac{V_{cab}^2}{\frac{1}{B_{cab}}} \quad (3.23)$$

The charging current ( $I_{ch}$ ) is given by Equation (3.24), while the total ( $I_{tot}$ ) by Equation (3.25).

$$I_{ch} = \frac{V_{cab}}{\sqrt{3}} \omega_e \cdot C_{cab} \quad (3.24)$$

$$I_{tot} = \sqrt{\left(\frac{P_{cab}}{\sqrt{3}V_{cab}}\right)^2 + I_{ch}^2} \quad (3.25)$$

Thus, the total cable power losses ( $P_{Ltot}$ ) can be estimated by Equation (3.26), while Table 3-19 shows the corresponding LFAC cable electrical performance for various cable lengths.

$$P_{Ltot} = 3 \cdot I_{tot}^2 \cdot R_{cab} \quad (3.26)$$

Table 3-19: LFAC Export Cable Electrical Performance based on  $\Pi$ -Circuit Analysis, for Various Lengths.

LFAC Cable Electrical Performance		[km]	50	100	200	300	400
Cable Reactive Power Consumption	QL $\sim$	[MVA $\cdot$ r]	2.992	6.103	12.120	18.148	24.101
Cable Power Losses	Ploss $\sim$	[MW]	6.260	12.749	25.171	37.317	48.861
Cable Reactive Power Generation	QC $\sim$	[MVA $\cdot$ r]	105.888	216.207	431.101	649.887	871.286
EQUIV. Charging Current	Ich $\sim$	[kA]	0.181	0.362	0.725	1.091	1.462
EQUIV. Total Current	It $\sim$	[kA]	1.182	1.192	1.233	1.298	1.386
EQUIV. Total Cable Losses	Pltot $\sim$	[MW]	6.425	13.050	27.690	45.465	67.822
		[MW]/km	0.129	0.130	0.138	0.152	0.170

Figure 3.14, below shows the LFAC cable total current and losses for increasing cable length. It is evident that as cable length increases, the MW/km losses of the cable rise, as shown in Table 3-19, causing the total cable MW losses to upsurge in a non-linear manner.

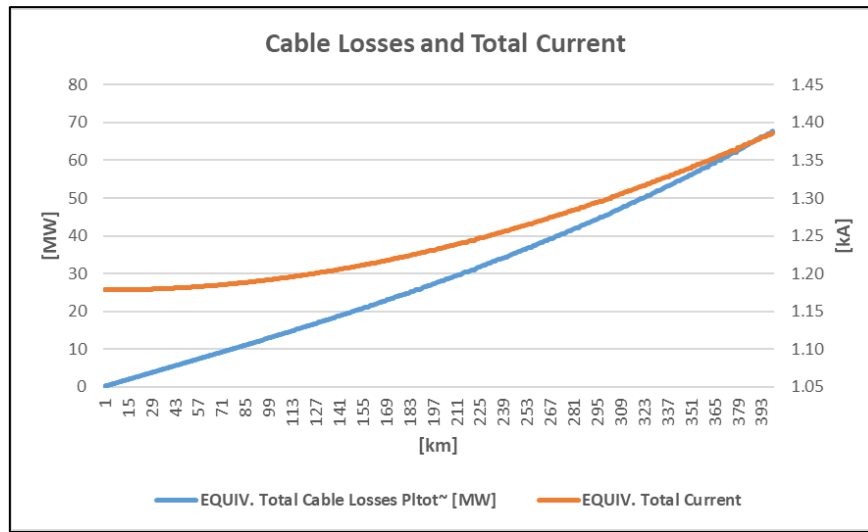


Figure 3.14: LFAC Cable Total Current and Power Losses vs Cable Length.

### 3.3.3 Reactive Power Compensation

Appropriate reactive power compensation should also be advocated wherever it is needed in the transmission scheme. This may be applied either in one or both the onshore and offshore sides of the cable. More specifically, active compensation could be applied in both sides if necessary, by utilizing the VSC-MMC control arrangements at the LFAC side of the onshore frequency converters and the reactive power capability of the corresponding OWPP blocks in order to achieve relatively even-loading in the export cables operating at 16.7Hz.

However, if additional active or passive compensation equipment (e.g. by means of STATCOM or shunt reactors) are considered essential, it would be more beneficial from an economic feasibility perspective to be installed only at the onshore side of the corresponding cables. In this work, the application of compensating reactors is considered only onshore for all the proposed topologies in an attempt to alleviate the weight and free up premium space on the offshore station topside.

From this simplified LFAC cable analysis, an approximation of the reactive power to be compensated and the corresponding inductance needed can be indicated by Equations (3.27-3.28). The values for various cable lengths are calculated in Table 3-20. In Chapter 5, detailed load-flow analysis specifies an accurate reactive power compensation for the scheme.

$$Q_{comp} = Q_C - Q_L \quad (3.27)$$

$$L_{comp} = \frac{V_{cab}^2}{\omega_e \cdot Q_{comp}} \quad (3.28)$$

*Table 3-20: Indicative Reactive Power Compensation of the LFAC Export Cable for Various Lengths.*

REACTIVE COMPENSATION		[km]	50	100	200	300	400
Reactive Power to Compensate	Q <sub>comp</sub> ~	[MVA <sub>r</sub> ]	105	210	419	634	849
Compensating Inductance	L <sub>comp</sub> ~	[H]	10.804	5.399	2.694	1.790	1.336

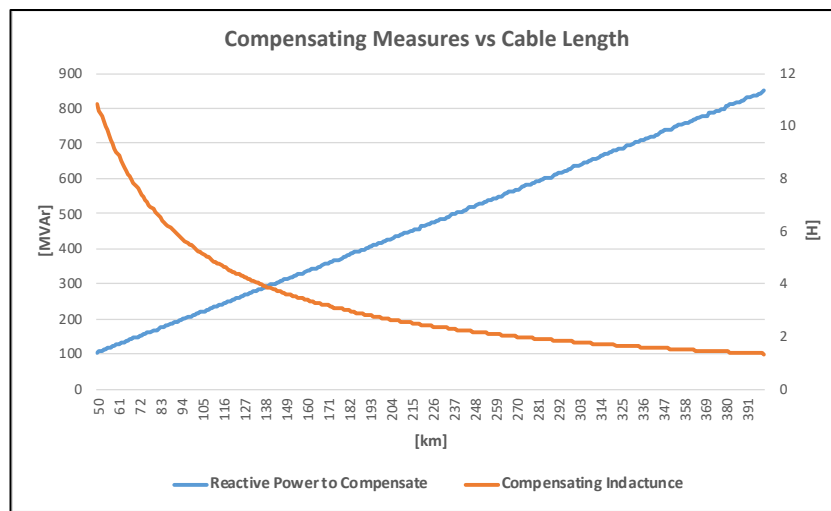


*Figure 3.15: Approximate Reactive Compensation of LFAC Cable and Shunt Reactor Size vs Cable Length.*

### 3.3.4 System Impedance Damping

System impedance damping measures may be needed in certain cases depending on both the loci of the low order harmonic frequencies on various spots of the respective LFAC topology and the control system configurations of the frequency converters. Figure 3.16 presents the export cable impedance for operation at the fundamental frequency (16.7Hz) up to the fifth harmonic order (83.5Hz), when the distance from shore increases. These impedance curves are estimated based on the simplified equivalent  $\pi$ -model for long cables as the cable length is much smaller than the travelling wavelength.

In Figure 3.16, it can be inferred that by increasing the cable length, the ohmic impedance always increases and even more sharply for higher operating frequencies. Thus, when operating at higher frequencies, the cable resonance point is much closer to the fundamental frequency or in much lower harmonic order level.

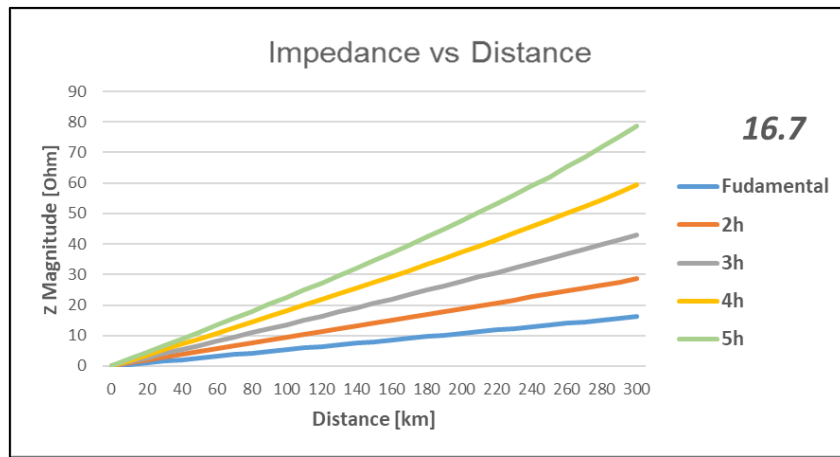


Figure 3.16: Export Cable Impedance vs Cable Length, for Various Operating Frequencies.

Although this can be another advantage of LFAC system operation, it shall be clarified that for the appropriate evaluation of such studies, the frequency-dependent parameter representation of these cables should be considered, as in Chapter 4.

### 3.4 Onshore BtB Frequency Converter

In this study, the onshore frequency converter station that links the 50Hz AC grid at 400kV with the offshore 16.7Hz LFAC TS at 345kV is based on MMC-HVDC technology, as mentioned in Chapter 2. The BtB configuration is implemented for the onshore substation, which allows the interconnection of two asynchronous networks with different frequencies. It has one MMC Terminal at each end, as shown in Figure 3.17. The DC rated voltage level of 640kV or of  $\pm 320kV$  is assumed in this work for the onshore frequency converter like many of the international projects that are rated at 700MW and use the MMC-HVDC technology, as presented in Chapter 2. Finally, if several steps are assumed for the MMC voltage, the AC side harmonic filters can be omitted, since the high number of modules allows almost sinusoidal output AC voltage waveforms.

#### 3.4.1 MMC Control Arrangements

Real power can be transferred either from the 16.7Hz LFAC system to the 50Hz AC system or vice versa subject to the application, e.g. OWF integration, interconnected grids through meshed offshore LFAC transmission system, etc. In addition, the LFAC side converter should be capable of grid forming and grid following operation, as presented in Figure 3.17 and explicitly described in Chapter 6.

In the islanded LFAC TS, the 345kV voltage level and the 16.7Hz frequency must be imposed. Thus, the LFAC side MMC shall include black-start capability and be able to form the voltage waveform for the LFAC TS (grid-forming function). The other converters then apply grid-following control and require a voltage reference to synchronize their real and reactive outputs [67]. On the other side, all the 50Hz grid facing MMCs shall establish the DC-Link voltage of the BtB schemes and fulfil the reactive power requirements at the PCCs.

### Back-to-Back Frequency MMCs

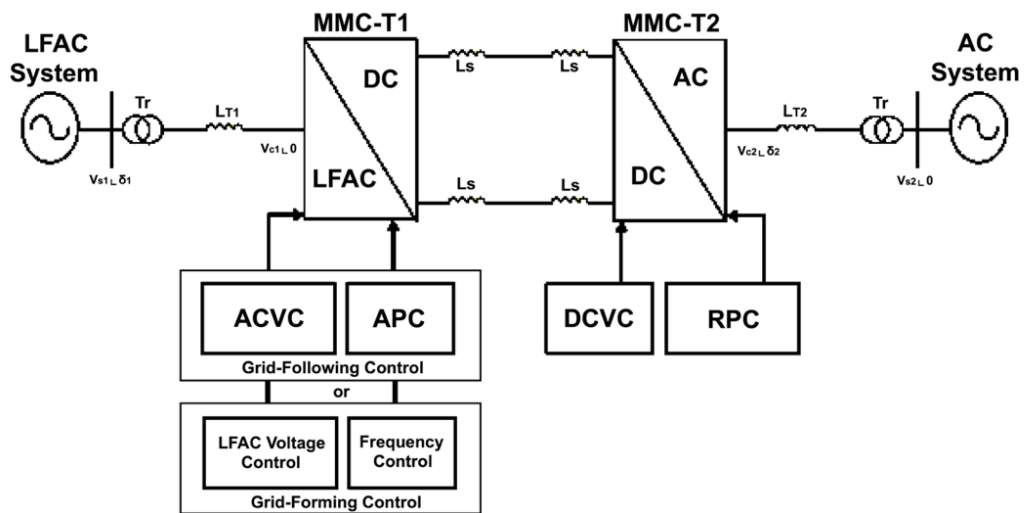


Figure 3.17: Onshore Frequency MMCs in BtB Configuration and Potential Control Arrangements.

The reactive power generation and consumption of the MMCs may also be used for compensating the connected LFAC network. Currently, there is no standardized requirement for an offshore LFAC network, and each MMC Terminal has been rated to be able to operate with a power factor of 0.83, even when it transfers the maximum output power of a Wind Farm block, as can be seen on Table 3-21, where all per-unit values are computed using the corresponding AC side rated apparent power.

Table 3-21: Back to Back MMCs AC System Electrical Data.

B2B MMC ELECTRICAL DATA			
MMC			
Converter Name	T1	T2	
Control Strategy for d axis	Islanded or P / Vac	Vdc	
Control Strategy for q axis		Vac	
Apparent Power	850	850	[MVA]
Real Power	704	704	[MW]
Maximum Reactive Power Limit	0.56	0.56	[pu]
Max Reactive Power @ Full Power Operation	476.0	476.0	[MVar]
Max Apparent Power @ Full Power Operation	850	850	[MVA]
PF	0.83	0.83	
AC Side Frequency	16.7	50	[Hz]

### 3.4.2 MMC System Configuration

In MMC systems, the DC and AC terminals are connected through the three converter phase legs, each one comprising two converter multivalves, a positive and a negative, called arms. Each arm includes a number ( $N$ ) of series or cascaded submodules (SMs) respectively and a corresponding arm reactor. The basic structure of a three-phase MMC is shown in Figure 3.18 [66]. In this configuration, each AC or LFAC phase is divided into positive and negative arms, while in each DC side terminal there is one positive and one negative voltage output that corresponds to positive and negative arms.

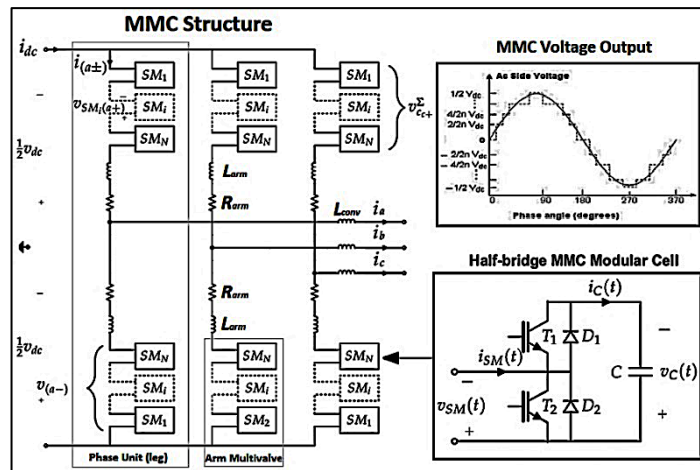


Figure 3.18: MMC Structure and Configuration.

By adjusting the converter arm-voltages-ratio in each phase module, the required sinusoidal voltage waveform at the AC or LFAC terminal can be attained, while the DC voltage is equal to the overall voltage of the two converter arms in one phase unit. This means that the MMC acts as a controllable AC voltage source that provides fundamental-frequency output voltage waveform, adjusted by the desired active and reactive power output. Moreover, the generation of harmonics is prevented due to the number of possible discrete voltage steps through the switching of individual cells.

The commercially available MMC modules can have either full or half-bridge cell arrangement. For HVDC transmission system with OTLs, the full-bridge configuration may be preferred due to its DC fault clearing capability to suppress the fault current. The half-bridge sub-modules (HBSMs), on the other hand, need the corresponding AC breaker opening, so they are used for submarine and underground transmission systems. Yet, HBSMs can be employed for BtB HVDC arrangements, due to the low probability of a DC fault. Also, an MMC with two-level full-bridge submodules requires twice the number of IGBTs of those with half-bridge submodules, which also lead to higher cost and losses.

Consequently, the two-level half-bridge MMC technology available from most vendors is selected for the purposes of the onshore BtB frequency conversion in this work. In the following sections, the operational principles of the HBSM will be described, the estimation of the necessary HBSM number and capacitance, as well as the total arm/limb reactance and resistance in both sides of the BtB MMC-HVDC frequency converter, will be discussed.

### 3.4.3 Two-Level MMC and Half-Bridge Sub-Module (HBSM)

The main components of each half-bridge sub-module are the two IGBTs with freewheeling diodes in antiparallel, forming a two-level half-bridge scheme that connects to a capacitor unit, as shown in Figure 3.18. It also contains a bypass-switch to isolate the module from the circuit in the event of an IGBT failure, a thyristor for overcurrent protection of the lower diode in case of DC fault, auxiliary components and electronics.

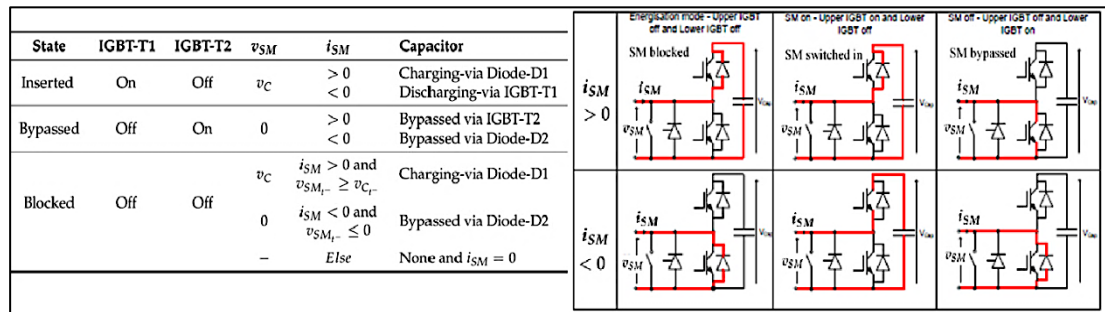


Figure 3.19: MMC - HBSM Operation Modes.

The table in Figure 3.19 above illustrates the potential conduction modes of operation for a half-bridge submodule [90]. The HBSMs are two-level devices that can be switched between an ON state with full module voltage (+V: effectively equal to the SM capacitor voltage) and an OFF state with no module voltage (0V) through gate signals to the two valves T1 and T2 respectively, for both current directions. Hence, if T1 is switched on, either the IGBT or the freewheeling diode of the corresponding valve conducts, depending on the direction of the current, which defines whether the capacitor is being charged or discharged [107].

Therefore, with this topology, each of the individual sub-modules can be distinctly controlled in a converter arm, and each MMC's arm can behave as a controllable voltage source, with the minimum voltage variation being equal to the HBSM capacitor voltage. Finally, in blocked state both switches are off and depending on their voltage and currents, only freewheeling diodes may conduct, restricting current flow in one of the two possible directions and making this converter unable to suppress DC side faults which necessitate the utilization of AC circuit breakers for the development of such a fault protection scheme.

### 3.4.4 PWM Technique

To date, the commonest MMCs' modulation methods are the Multi-Carrier PWM techniques, which are classified based on the spatial distribution of their carrier waves, comprising the Phase-Shifted-Carrier Modulation (PSC-PWM) and the Phase-Disposition or Level-Shifted-Carrier Modulation (PD-PWM) [73]. The carrier number and frequency depend on the amount of the MMC levels. For a high number of levels, the effective switching frequency increases and the THD can be very low (i.e. <2%), but the PWM method may result in being cumbersome due to a large number of submodules. Figure 3.20 shows PD (a) and PSC-PWM (b) triangular carrier waveforms being compared with a sinusoidal voltage reference.

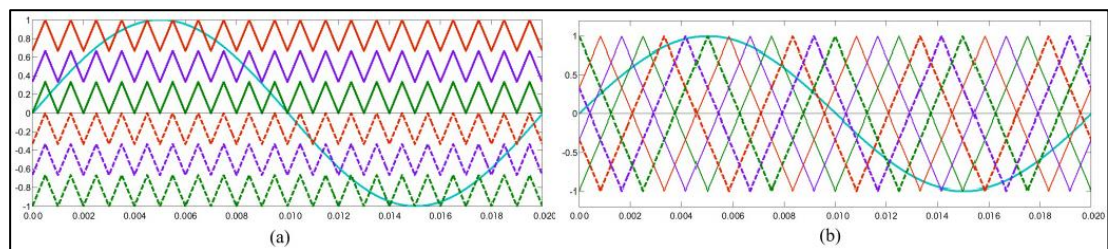


Figure 3.20: PWM Patterns for Two-Level MMC using HBSM: a) PD-PWM and b) PSC-PWM.

The PSC-PWM technique is adopted in this Thesis for the onshore BtB MMCs as it has some distinctive features on top of suppressing the low-order harmonics. In contrast to the PD-PWM, it can evenly distribute the power among the sub-modules and the semi-conductor stress, enabling better capacitor voltage balancing control. This point is critical as each sub-module has different individual characteristics, and its switching is performed by a specific triangular carrier waveform which can produce dynamic voltage balancing issues.

In PSC-PWM, the carrier frequency must not be integer multiple of the fundamental as it may cause the submodule capacitor voltages to diverge [73]. Thus, non-integer multiples of the fundamental frequencies are chosen here for both T1 and T2 MMC terminals. The HBSM switching frequency is set at 155Hz, converging the total count of switching per module to less than  $150\text{Hz} \pm 5\%$ , while an amplitude modulation index of  $M_i=0.945$  is selected.

### 3.4.5 Number of HBSMs – DC Voltage

In order to keep the phase-leg voltage amplitude of the MMC constant and equal to the DC Voltage, the sum of inserted sub-module cells in each phase leg should also be kept constant. So, by inserting one sub-module in one arm, one other should be bypassed in the other arm respectively, at the same time. Additionally, to eliminate any DC offset in the AC voltage output of each phase leg, the corresponding arm voltage amplitude may vary between zero to the DC voltage with an average value of half the DC voltage.



Thus, the HBSM capacitors of each arm can share the DC voltage according to the number of cells per arm (N) and should be rated as the IGBTs, considering that the necessary blocking voltage for each arm should be equal to the full DC voltage and twice the DC voltage for the total phase leg. Therefore, the capacitor voltage balancing is essential, as unequal DC voltages generated in any of the converter phase legs may cause circulating currents.

*Table 3-22: Number of HBSM and Voltage Levels in the MMC.*

MMC Side	@T1	@T2	
MMC - SM Rating			
SM Number			
SM Rated DC Voltage set	5	5	[kV]
IGBT Voltage rated	6.5	6.5	[kV]
N: Number of Operating MMC SMs per Arm	128	128	
Total Number of Operating MMC SMs	768	768	
SM Redundancy	10	10	[%]
Total Number of MMC SMs	846	846	
Total Voltage Levels (N+1)	129	129	

If an established 6.5kV IGBT module is employed for this application, the rated HBSM voltage can be set to 5kV, as can be seen in Table 3-22. A total number of 128 operating HBSMs is then needed to withstand the DC voltage of 640kV pole to pole accordingly, which is also the required number of HBSMs per arm, as can be inferred by:

$$N_{HBSM} = \frac{V_{DC}}{V_{HBSM}} \quad (3.29)$$

Supposing that a typical 10% policy for submodule redundancy is applied, then a total number of 846 HBSMs would be equipped, out of which only the 768 would be in use, and 384 would be operating at every instance in each MMC of the back to back arrangement.

### 3.4.6 HBSM Capacitance

Theoretically, since the BtB MMCs that link the offshore 16.7Hz system to the 50Hz grid are equally rated with the same number of HBSMs, the passive equipment components of the MMC interfacing the LFAC network should be three times bigger in size and rating than those of the 50Hz grid side MMC. Though, slight differences result out of practical calculations.

The choice of the HBSM capacitance value is always a trade-off between the capacitor size and its voltage ripple. A ripple in the range of  $\pm 5\%$  can be considered acceptable for MMCs, and the required capacitance value can be estimated by specifying the deviation in the energy of the converter arm, according to an analytical method suggested by Marquardt et al. [104]. Moreover, stored energy over 30kJ per MVA of a converter rating can be adequate to achieve a voltage ripple factor  $\epsilon \sim \pm 5\%$ , as suggested in [130]. The projected HBSM capacitance value shown in Table 3-23, is calculated by :

$$C_{SM} = \frac{2 \cdot W_{SM}}{V_{HBSM}^2} = \frac{\Delta W_{SM}}{2 \cdot \varepsilon \cdot V_{HBSM}^2} \quad (3.30)$$

Where:  $C_{SM}$  is the sub-module capacitance (no redundant submodules assumed)

$V_{HBSM}$ : the desired sub-module rated DC voltage

$W_{SM}$ : the stored energy in each submodule per MVA

$\Delta W_{SM}$ : Variation in SM stored energy  $\rightarrow \Delta W_{SM} = \frac{\Delta W_{arm}}{N_{HBSM}}$

Where:  $\Delta W_{arm}$ : Variation in the upper arm's stored energy

*Table 3-23: HBSM Capacitance for the BtB MMC Terminals.*

MMC Side	@T1	@T2	
MMC - SM Rating			
SM Capacitance			
$\Delta W_{arm}$ : Variation in the upper arm's stored energy	4.46	1.49	[MJ]
$\Delta W_{sm}$ : Variation in SM stored energy	0.035	0.012	[MJ]
$W_{sm}$	0.087	0.029	[MJ]
$C_{sm}$	7000	2350	[uF]

Hence, for a ripple voltage of 10%, the value for the HBSM capacitor of the LFAC side MMC is estimated near  $\sim 7000\mu\text{F}$  and for the HBSM capacitor of the 50Hz grid side near  $\sim 2350\mu\text{F}$ .

### 3.4.7 Arm Inductors

The arm inductors, also known as limb inductors, have two main functions:

- 1) They can limit the fault current rate of rise ( $di/dt$ ) through the converter to suitable levels, for faults happening either in or out of the converter.

The arm fault current should not exceed the value of  $20\text{A}/\mu\text{s}$  in any case [130]. This can be used as an initial criterion for a minimum value of arm reactor. According to SIEMENS, the "HVDC Plus" MMC system employs converter reactors that suppress the fault current to tens of amps per microsecond against the most onerous conditions, such as a DC pole-to-pole short-circuit fault. The value of limb reactance required to suppress the initial fault current rate-of-rise to less than  $20\text{A}/\mu\text{s}$  can be derived by the Equation (3.31), assuming that for the time period between a fault inauguration and the IGBTs turn-off, the DC voltage is kept fairly constant [90].

$$L_{arm} = \frac{V_{DC}}{2 \cdot (di_{flt}/dt)} \quad (3.31)$$

From Equation (3.31), the minimum arm inductor value is 16mH for the MMCs placed in both AC sides of the BtB scheme. It should be mentioned that the above limit can be considered for the LFAC side, only in the case that some minor modifications are considered in circuit breakers' design to operate at LFAC, for reasons stated in Chapter 2, e.g. to avoid the current chopping phenomenon.

2) They can limit the high-frequency arm current components such as the peak circulating currents.

In normal operation, the converter upper and lower total arm currents of each phase-leg comprise three current components as described by the Equation (3.32), below:

$$I_{arm} = \frac{I_{DC}}{3} \pm \frac{I_{ph}}{2} + I_{circ} \quad (3.32)$$

Where,  $I_{circ}$  is the circulating current caused by unequal DC voltages generated among the MMC phase legs or differences in the upper and lower arm voltages, e.g. due to different HBSM switching times. The  $I_{circ}$  is a negative-sequence current (a-c-b) at double the fundamental frequency, which distorts the arm currents and increases converter losses. They can be further suppressed through an additional Circulating Current Suppression Control (CCSC) mechanism.

However, the minimum limb inductor value of 16mH calculated above may still result in unnecessarily high circulating currents even with the CCSC. Hence, the limb reactance may be increased further as a compromise between the reactor size and the circulating current magnitude. A general rule is that the selected parameters should be outside a region of potential resonances that occur in the circulating currents [107]. For the selected HBSM capacitance, the corresponding region can be calculated by:

$$L_{arm} = \frac{N_{HBSM}}{C_{HBSM} \cdot \omega^2} \cdot \frac{2 \cdot (h^2 - 1) + m_i^2 \cdot h^2}{8 \cdot h^2 \cdot (h^2 - 1)} \quad (3.33)$$

Where,  $\omega$ : angular frequency in rad/s,  $h$ : harmonic orders, with  $h=2n$  ( $n=1,2,\dots,\infty$ )

According to [133] this harmful region has a lower limit defined by the 4<sup>th</sup> harmonic order and a modulation index of 0.1 ( $h = 4$  and  $m_i = 0.1$ ) as well as an upper limit defined by the highest resonant frequency which is obtained from Equation (3.33), above, for  $h = 2$  and  $m_i = 1$ . Hereafter, the converter should operate above the highest resonant frequency, so that the dependency on the arm resistance  $R_{arm}$  value eliminated, which should be as low as possible to avoid increasing losses. Hence, the following constraint is also imposed on the arm inductor and capacitor values:

$$L_{arm} \cdot C_{HBSM} > \frac{5 \cdot N_{HBSM}}{24 \cdot \omega^2} \quad (3.34)$$

According to Equation (3.34), the MMC arm inductance that corresponds to the highest resonant frequency should be 173mH on the LFAC side and 57.5mH on the 50 Hz AC side.

The arm reactors in an MMC system could also be assumed to have the functionality of Type-L filters and converter reactors in a two-level VSC system by enabling independent and continuous control of active and reactive power. Hence, the arm and converter reactors are finally rated at 0.2p.u. corresponding to 307mH of 16.7Hz LFAC side reactors and 102.5mH of 50Hz AC side reactors in order to avoid both the circulating current resonances and the fault current change rate limit, as they were also found to offer a satisfactory performance level when used in conjunction with the CCSC.

### 3.4.8 Interface MMC Transformers

The converter terminals are interfaced in both the AC and LFAC system sides through converter transformers. Their primary function is to transform the voltages of the 400kV AC and 345kV LFAC systems to a suitable level for the converters which is 370kV in both sides and to provide electrical isolation between AC and DC sides. The leakage impedance for the 50Hz AC system transformer is 0.15p.u. and 0.07p.u. for the 16.7Hz LFAC transformer based on their MVA rating and they are much bigger than their corresponding resistance which may even be neglected in some power calculations.

*Table 3-24: MMC Transformer Specifications at both MMC Terminals.*

MMC Side	@T1	@T2	
<b>MMC Transformer</b>			
<b>Transformer Total MVA</b>	850	850	<b>[MVA]</b>
<b>Base Operation Frequency</b>	16.7	50	<b>[Hz]</b>
<b>Nominal Voltage at the Grid Side</b>	345	400	<b>[kV]</b>
<b>Nominal Voltage at the MMC Side</b>	370	370	<b>[kV]</b>
<b>Winding Type Grid Side</b>	Y	Y	
<b>Winding Type MMC Side</b>	D	D	
<b>Delta Lags or Leads Y</b>	lags	lags	
<b>Transformer Positive Sequence Leakage Reactance</b>	0.07	0.15	<b>[pu]</b>

Table 3-24 shows the electrical parameters of the MMC transformers. Here, Delta connections are adopted to both AC and LFAC converter-side transformer windings in the case that MMCs apply a third harmonic injection technique which corresponds to zero sequence currents that can be blocked by a three-wire connection such as a delta transformer winding before entering the rest of the AC systems.

## 3.5 Summary and Conclusions

In this Chapter, offshore PtP and MT-LFC TS LFAC transmission schemes are designed, and their related equipment is specified and rated in detail. The PtP LFAC TS integrates a 704MW OWF to the grid through a long submarine export cable connected to frequency converters

located onshore, while the MT-LFAC TS configuration connects two distant but similar OWFs in a meshed arrangement that also interconnects two different grids. The layout of each 704MW OWPP system is explicitly defined by the 8MW Type-4 OWTGs, the 400mm<sup>2</sup> Cu-XLPE sub-array and the 800mm<sup>2</sup> Cu-XLPE array cables and the medium voltage collector system with 4 x 72.5kV GISs.

Moreover, the electrical parameters of the high voltage components of the offshore LFAC TS schemes are determined. The LFAC step-up transformers are specified based on the design estimation of Chapter 2, with a leakage reactance of 0.07p.u. as the “natural” leakage reactance of an LFAC transformer lies in lower p.u. value than the expected at 50Hz or 60Hz. The LFAC export cable parameters supplied by the manufacturer are utilised to assess a simplified equivalent  $\pi$ -circuit for various lengths and estimate the size of the corresponding compensating reactors. Results show that as cable length increases, the MW/km losses of the cable rise, causing the total cable losses to upsurge non-linearly. It is also indicated that when operating at higher frequencies, the cable resonance point could be much closer to the fundamental frequency or in much lower harmonic order level, introducing the need for potential mitigation measures for the dynamic impedance of the system.

Regarding the BtB VSC system of the equivalent OWTGs and the onshore BtB MMC-HVDC frequency converter system for integrating the LFAC TS to the grid, the following characteristics are specified:

- Potential control system principles
- Two-Level configurations
- DC voltage rating and PWM techniques
- The number of modules (in onshore MMCs)
- The suitable DC capacitance and DBR unit
- Converter reactors
- AC PWM Harmonic Filters (in the OWF VSI)
- Interface transformers

Since the MMCs are equally rated in the BtB arrangement linking a 50Hz grid with an offshore 16.7Hz system and having the same number of HBSMs, the passive equipment components of the MMC interfacing an LFAC network need to be rated almost three times higher than those of the MMC interfacing a 50Hz grid. This is obvious in the rating of the DC capacitors and arm or converter reactors, with slight differences in the result of the calculations.

## Chapter 4: Frequency Domain Assessment

### 4.1 Introduction

The frequency response assessment of a transmission system and the evaluation of the impact that some main components have upon it can help to avoid undesired resonances and harmonics. Harmonic resonances occur in frequencies where the impedance of a system that contains inductors and capacitors has a minimum or a maximum. Such resonances should be seriously considered to avoid harmonic distortion issues that can cause a range of instantaneous and long-term negative effects on a system's performance and equipment.

The resonance frequencies are of fundamental concern especially in offshore systems which comprise long submarine AC cables together with step-up transformers, shunt reactors, inter-array cables, wind collector system, etc. and their power sources are converter interfaced WTGs that demonstrate characteristic harmonic emission spectrums and power intermittency. The resonances in such systems can also be amplified when the offshore installations interact with a weak AC grid that has low short circuit capacity (SCC), making it difficult for the OWFs to comply with the grid code requirements at their PCCs [110].

The resonance interaction issue can be crucial in the case of islanded LFAC transmission system that is purely shaped among OWFs and HVDC converters without a straight connection to a strong grid [96]. There, the additional onshore back-to-back frequency converters may act as additional harmonic sources, apart from the fully converted WTGs [75].

#### 4.1.1 Frequency Analysis Objectives for LFAC TS

The knowledge of the frequency response for the offshore LFAC TS during the system design stage can help to avoid wider harmonic propagation problems. System impedance may resonate near a harmonic frequency produced by VSCs and exacerbate the harmonic voltage or current of the circuit. Typically, a parallel resonance can cause voltage THD amplification, and a series resonance can lead to high current THD at the resonant frequency. Except for the THD, a low-order resonance in the LFAC network could produce sustained overvoltages during transformer energisation or at fault-clearing which may damage the equipment.

Therefore, the frequency domain analysis of the system is performed to detect resonance conditions that could excite harmonic voltages and currents and create potential system performance or stability issues. The frequency scan studies indicate the impedance of the system in various frequencies. They can be useful for designing the appropriate mitigation

measures (e.g. harmonic filters, converter control systems, etc.) to damp the system resonances and prevent interference with other components [111]. In this Thesis, the frequency scan analysis of the LFAC TS evaluates the equivalent system impedance at the onshore and offshore 345kV busbars as well as at the 66kV collector bus of the WTGs. The study assesses the frequency response of the LFAC subsea cable and the transmission system at normal operation, by varying some of the design parameters such as the cable length and OWF power dispatch characteristics.

More specifically, static frequency scans are performed in the LFAC transmission system by applying the PSCAD's interface to harmonic impedance solution component from PSCAD master library at the standpoints of the power converters which are considered as potential harmonic sources. This frequency scanner tool is an impedance measurement module that is applied between the respective node and the ground. It generates the network's harmonic impedance matrix in the phase domain at the corresponding points, starting from 1Hz and up to the harmonic frequency of interest. In the produced frequency scan graphs, the resonant peaks or "parallel resonances" represent very high impedance points which can be excited by harmonic current sources such as the fully-converted WTGs and result in substantial harmonic voltages. On the other hand, the dips or valleys in the graphs are the "series resonances" and represent a low impedance path to the harmonic currents.

In the following sections, the modelling of the system is described in frequency domain, and its resonant frequencies are examined for different LFAC TS topologies and LFAC cable lengths. The impact of these resonances on the system is analysed, and passive filtering options are proposed to establish a degree of effective damping. Finally, useful observations are yielded regarding the projected offshore PtP and MT-LFAC TS designs.

## **4.2 System Frequency Domain Modelling**

There is a high number of system components that shape the offshore LFAC transmission scheme's frequency response. In particular, the export and inter-array cables capacitance can create significant parallel resonance interaction with the 66/345kV LFAC step-up transformers in the offshore platform and the various converter transformers as well as the onshore cable shunt compensating reactors, the LCL filters of the OWTGs VSIs, etc. In parallel operation of two or more OWPPs located within close electrical proximity, it is also necessary to avoid resonance conditions among these plants and the associated system equipment.

It should be noted that there is no specific value of system impedance magnitude that can cause harmonic issues in the LFAC TS unless a sufficient level of background harmonic currents and voltages near the resonant frequencies excite its resonances. However, an offshore LFAC scheme will generally have multiple such harmonic sources as it may only be established among various frequency converters. In addition, the impedance at individual harmonics can significantly change if contingencies occur such as cable and transformer outages, or operating conditions change under routine system variations, e.g. changes in the status of reactor banks or WTGs' disconnection, etc. In general, the LFAC TS impedance should not be considered as a single value for each harmonic order as it may vary over a range in the R-X plane due to the system loading condition. Hence, the extent to which the transmission system should be explicitly modelled depends on the harmonic orders of most interest and the required accuracy over the specified frequency range.

The measured harmonic impedance is characteristic of the specific system configuration and requires detailed modelling. Proper representation of the offshore LFAC TS impedance at all harmonic frequencies of interest is essential to quantify in detail all the probable harmonic issue. A complete harmonic analysis should be performed with manufacturer-provided data regarding the harmonic emission spectrum of the related equipment. The model of the offshore Multi-Terminal 16.7Hz part of the LFAC transmission system (MT-LFAC TS) developed in PSCAD-EMTDC for the passive frequency scan studies is realised as two OWF export LFAC systems that are interconnected at their offshore platforms, and it is shown in APPENDIX A. The system components in the frequency domain are explicitly described in the following sections.

#### 4.2.1 Modelling of the LFAC Subsea Cable

Comprehensive submarine cable modelling is crucial to analyse the offshore LFAC transmission system frequency response. The very essence of employing LFAC technology to form offshore transmission systems is the considerably longer transmission distances that could be achieved through the subsea cables in comparison with the AC systems. This means that the LFAC transmission cables are of major importance for these systems and their lengths will be significant. Modelling of such long cables as lumped circuits with constant parameters, as seen in Chapter 3, should not be used either for harmonic impedance studies or EMT dynamic simulations. Instead, distributed-parameter models based on travelling-wave theory should be adopted.



There are several different ways to model the electrical parameters of an LFAC cable and selecting the most suitable model depends on the simulation study objectives. The available options for modelling cables electrical parameter are shown in Figure 4.1, according to [102]. Cable models are classified into two main categories according to the way they estimate its electrical parameters, namely lumped and distributed. The latter can be more precise for longer cables and can be calculated either by constant parameters that are mainly suitable for steady-state fundamental frequency analysis or by frequency-dependent parameters. For sufficiently accurate harmonic impedance analysis and EMT dynamic simulations in a wider frequency spectrum, cable models with frequency-dependent parameters can be used, although more accurate cable data are needed in the modelling procedure and increased computational effort during the simulation studies.

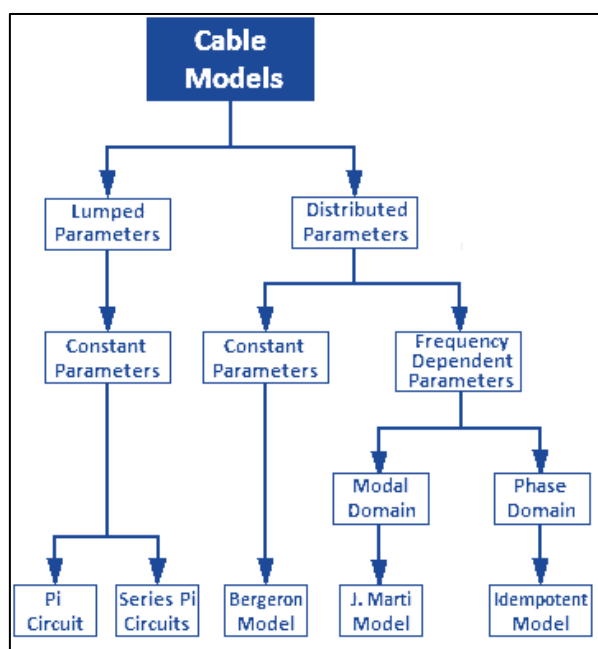


Figure 4.1: Models for Cable Representation.

As illustrated in Figure 4.1, frequency-dependent models can be represented either in the modal (J. Marti or Mode model) or phase domain (Idempotent or Phase model), and they have similar fundamentals such as their voltage-source based equivalent circuits, instead of current sources used by other models, e.g. Bergeron's. They are distributed travelling-wave models, and they can be valid for greater cable lengths and a wider range of frequencies compared to the constant parameter models. The fact that the resistance is distributed along with its reactance across the cable length and is not lumped at the endpoints allows modelling the distributed nature of the losses, while both the characteristic impedance ( $Z_0$ ) and the propagation constant ( $\gamma$ ) are dependent on the frequency.

However, the Frequency-Dependent Mode model may not be as accurate for short lines or at low frequencies, due to limitations in the time-domain system which assumes constant modal transformation and can only be accurate for modelling balanced systems [110]. On the other hand, the Phase model (FDPM) solves the problem of modal transformation matrixes by calculating the propagation wave in the phase domain. Thus, it allows accurate simulation of unbalanced AC/DC systems and provides a more accurate frequency-dependent representation for cables. In this Thesis, the frequency-dependent Phase model is selected for modelling the subsea LFAC transmission cables. Below, this method is evaluated, and its accuracy is discussed.

#### 4.2.1.1 The Distributed Parameters – Frequency-Dependent Phase Model

According to PSCAD EMTDC user guide, the frequency-dependent phase model provides the most accurate cable representation method. It is based on the Universal Line Model (ULM) theory and operates on the principle that the frequency dependence of a cable can be represented by fitting two separate matrix transfer functions, namely the characteristic admittance  $Y_C(s)$  and the propagation function  $H(s)$ . The equivalent circuit of this cable model (the idempotent model) is depicted in Figure 4.2

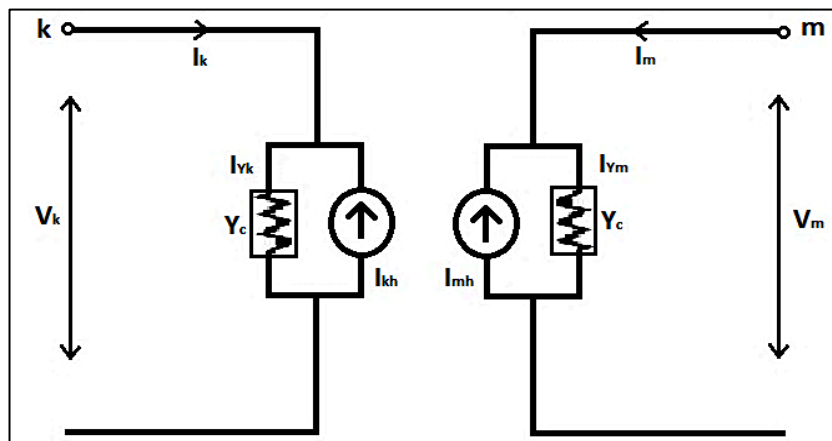


Figure 4.2: Frequency-Dependent Phase Cable Model Equivalent Circuit.

According to Figure 4.2, the following are derived from the “telegrapher’s equations”:

$$Y_C \cdot V_k - I_k = (Y_C \cdot V_m + I_m) \cdot H \quad (4.1)$$

$$Y_C \cdot V_m - I_m = (Y_C \cdot V_k + I_k) \cdot H \quad (4.2)$$

Where:  $H = e^{-\sqrt{\gamma}l}$ , is the propagation function matrix and  $\gamma$  is the propagation constant.  $Y_C$  is the characteristic admittance matrix.  $V_k$ ,  $I_k$  and  $V_m$ ,  $I_m$  are the node voltages and injected current vectors at k and m ends that also cause incident and reflected currents in the scheme.

$H(s)$  and  $Y_c(s)$  are calculated multiple times by PSCAD's Line Constants Program (LCP) at discrete points in the frequency domain, and the resulted representation is used for the harmonic impedance studies performed in this Chapter. Then, they are approximated using curve fitting methods and replaced by equivalent low-order rational functions, to allow time domain migration using computationally efficient recursive convolution techniques of PSCAD EMTDC. Hence, this cable model can also be used for the dynamic EMT simulation studies of the LFAC transmission system.

The subsea cable modelling procedure in PSCAD requires some basic physical and geometrical characteristics as inputs to estimate the equivalent electrical impedance and admittance matrixes and produce the cable Frequency-Dependent Phase Model. However, the input template provided by PSCAD comprises scalable concentric, circular and homogeneous conductor - insulation layers and its graphical representation is depicted in Figure 4.3. These may approximate but not accurately represent complex cable structures that may have different layer types (e.g. semiconductors) or other physical characteristics such as different fill between conductors, segmental or non-concentric strands, etc. Therefore, the calculated output FDPM parameters represent the input parameters but may not reflect the actual cable electrical characteristics.

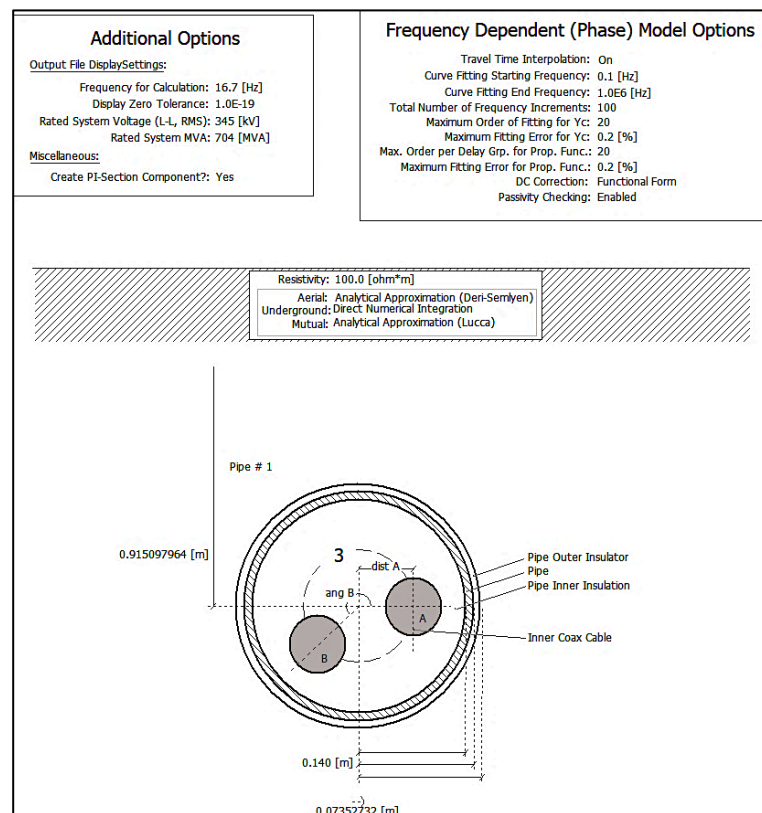


Figure 4.3: Graphic Representation of the Three-Phase XLPE cable in PSCAD.

For the reasons mentioned above, to explicitly represent a subsea cable in PSCAD, some input parameters of the default template need to be adjusted, as demonstrated in APPENDIX A [102]. The purpose of this correction is to match the cable electrical parameter values calculated by PSCAD with those measured by the cable manufacturer (NEXANS), as described in Chapter 2 and 3. Therefore, some parameters of the conductor, shield and insulation of the LFAC cable as well as the sea (burial) depth below the ground surface are adapted for PSCAD modelling.

#### 4.2.1.2 Frequency Response of the LFAC Subsea Cables

The analysis of the impact that each element has on the LFAC TS impedance profile is the first step to identify undesired system resonances and optimise its design. The frequency scan of the 345kV XLPE-1400mm<sup>2</sup>-Al LFAC cable is performed using the harmonic impedance solution component of PSCAD. Figure 4.4 shows the difference between the frequency response of the FDPM against a  $\pi$ -model equivalent of the same 200km cable as calculated by PSCAD EMTDC. Although the  $\pi$ -model provides the same impedance value at fundamental frequency, it does not accurately represent the cable properties at other frequencies.

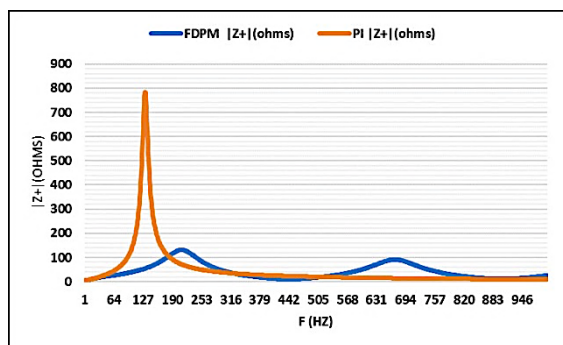


Figure 4.4: Impedance Profile Difference of FDPM vs.  $\pi$ -Circuit Model of the XLPE-1400mm<sup>2</sup>-Al LFAC Cable.

Figure 4.5a) and b) depicts the examined FDPM LFAC cable impedance and resonance points, respectively, against frequency for different cable lengths without any other system elements connected to it and shows how the impedance of the cable varies with its length.

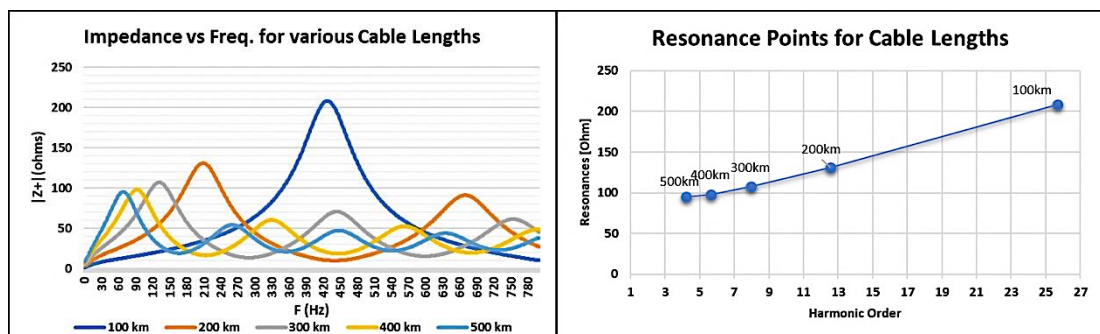


Figure 4.5: a) Impedance vs. Frequency and b) Resonance vs. Harmonic Order Plots for various Cable Lengths.

It can be observed that as the cable length increases, the shunt capacitance increases and the point of the natural resonance frequency of the LFAC cable moves to a lower value. However, cable resistance increases too, introducing more losses and damping that result in a lower resonant impedance of the cable. Thus, for longer cables the first resonance moves towards lower frequencies (every time the cable length doubles, the resonant harmonic order drops to almost half), having lower magnitude. At the same time, higher-order resonant peaks occur more frequently with lower impedance magnitude in all other resonant frequencies, due to the higher damping offered by the increasing total resistance.

As the capacitance of the export cable increases with its length, the problem of harmonic resonances becomes more prominent for long subsea cables, which dramatically affects the total system resonance, its operation and the other power system components. When the cable length is increased to 300km, its resonance occurs at 130Hz, and for 400km the cable resonant frequency appears at 94Hz which could be detrimental for typical HVAC operation of the system at 50Hz (i.e.~2nd order harmonic resonances) even without considering the rest of the system equipment that is inductive in nature or other phenomena related to the charging currents. Besides the cable itself, inductive transmission system components such as power transformers, shunt compensation and frequency converter reactors influence the resonant points as well, and they should also be included in the analysis.

#### 4.2.2 Cable Reactive Compensation Equipment

Since the study concentrates on low order harmonics of the passive LFAC system, the usage of reactive power compensation equipment and power factor correction devices should also be accounted as they alter the system impedance. Equipment, such as shunt reactors, Static VAR Compensators (SVCs), STATCOMs, etc. introduce shunt inductance in the LFAC network and can resonate with the capacitive elements of the system. Here, cable shunt reactors are assumed only at the onshore side of the cable for its reactive current compensation, and they are represented as lumped equivalent inductors in series with a resistor having an X/R of 300, having the values estimated in Chapter 3.

#### 4.2.3 LFAC Transformers

The above subsea cable assessment in frequency domain demonstrates the importance to evaluate the broader risk of potential system resonances for specific cable lengths. Since the LFAC step-up transformers are the main inductive components in the offshore LFAC transmission system, it is expected that inherent harmonic resonance issues could also be

related to the transformer leakage reactance, making it the main element for the transformer frequency-domain modelling. However, the transformer representation for harmonic analysis includes not only resistance and inductance connected in series but also accounts for its maximum X/R that occurs at a particular frequency.

As mentioned in Chapter 2, the per-unit leakage reactance of a 16.7Hz LFAC transformer can be naturally lower than this of a 50Hz equivalent with the same MVA rating, due to the dielectric gaps and core sizes. Figure 4.6 shows the impedance vs. frequency profiles of the 200km LFAC export cable alone and when connected only to the LFAC step-up transformers of the LFAC TS. Moreover, the impact of their leakage reactance ( $X_l$ ) is showcased for the values of 0.15p.u. and 0.07p.u.

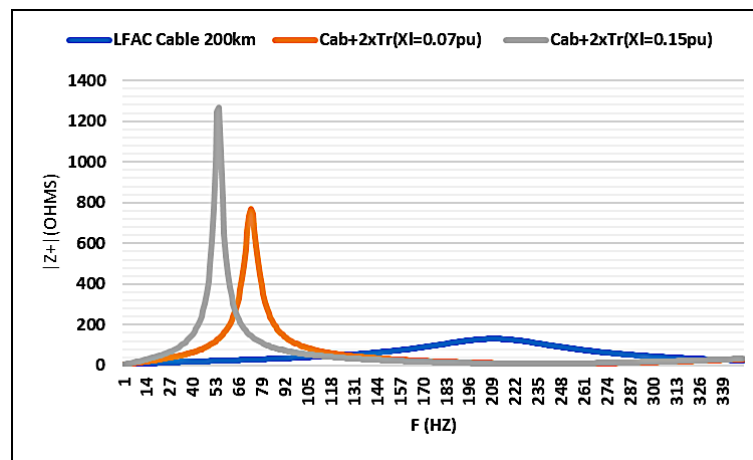


Figure 4.6: Frequency Scans of the 200km Cable Alone and Connected to LFAC Transformers with Different  $X_l$ .

It can be observed that the cable in conjunction with step-up transformers of the offshore platform can amplify low-frequency harmonics (inherently ~5th harmonic order for a 200km cable), without considering the converter transformers or the rest inductive and capacitive elements that are present in such an offshore power system. Furthermore, the lower the transformers relative leakage inductance in p.u., the higher the frequency of the system's first resonance and the lower its magnitude, whilst the fundamental 16.7Hz frequency impedance magnitude responsible for the system losses is also reduced. Notably, in Figure 4.6, for a transformer leakage reactance of 0.07p.u., the resonance is 770 Ohm and appears at 78Hz (harmonic order of ~4.7) while for 0.15p.u. the resonance reaches 1266 Ohm at 59Hz (harmonic order of ~3.5).

By examining Figure 4.7, the beneficial impact of the lower transformer reactance to the LFAC system impedance harmonics is obtained for various LFAC cable lengths.



#### 4.2.5 OWTGs and Onshore Frequency MMC Representation

As the LFAC TS is formed among power converters, its impedance profile is highly dependent on the converter types and their control system response and is not explicitly reflected in the passive frequency scan assessment of this Thesis, but its impact is evaluated through the EMT dynamic performance studies of Chapter 7 for different VSC control strategies. In this work, the static frequency scans of the LFAC TS indicate its impedance characteristics regardless of the implemented converter control systems, but they analyse the impact of the various passive components (e.g. Transformers, Cables, Filters, etc.) on the formation of the low-order resonances of the system and examine its behaviour for various configurations. Subsequently, any passive mitigation measures that are introduced to alleviate the dynamic impedance of the system is designated neglecting the VSC control system arrangements.

Thus, the Type 4 OWTGs being interfaced to the LFAC TS through their VSIs as well as the onshore LFAC side MMC Terminals can be considered to have low internal impedance at harmonic frequencies as viewed by the LFAC bus, and they are modelled as harmonic voltage sources with their equivalent converter impedance on the LFAC side without considering converter losses. This simplification is conservative as a voltage source is by definition a short circuit to ground in frequency scan studies while the actual converter harmonic impedance may exhibit a more damped resistive behaviour with low phase angle in steady-state operation and its losses contribute to system dynamic impedance damping as well [61]. Moreover, Type 4 WTGs are considered with their LCL harmonic filters, that are installed in the LFAC side of their VSIs. Henceforth, the LFAC system VSCs are modelled in the frequency domain, as shown in Figure 4.9 where the power output is represented as an impedance ( $Z_c$ ) in Ohms, which is an industry practice and has been used in related studies [92].

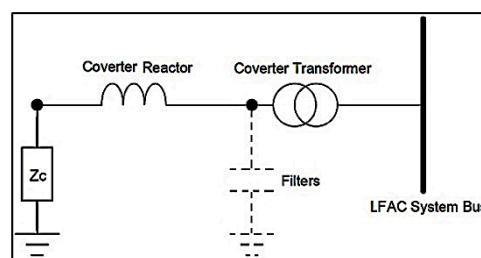


Figure 4.9: VSC Model for Frequency Scans.

Here, to estimate the influence that these power variations could potentially have, some resistive values of 0 to 100 Ohm can be assumed for the onshore MMC output impedance representation to account for probable steady-state conditions, while the OWF equivalent can be assumed to cover a range from 0 to 10 Ohm [92]. These impedance values could refer



to cases where either the number of WTGs in service or their output decrease. Figure 4.10, demonstrates PtP LFAC TS cases with 200km LFAC cable for which the harmonic resonances are plotted for various converter states.

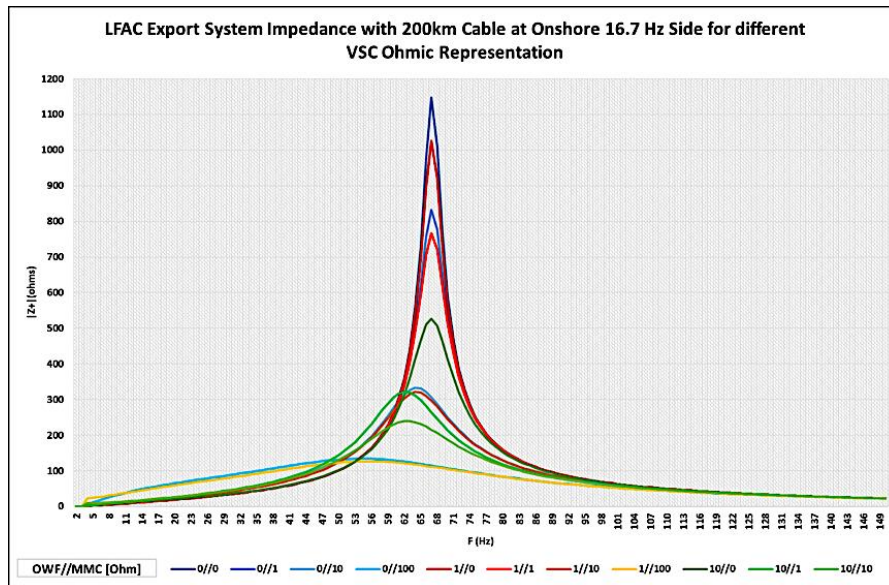


Figure 4.10: Impedance vs. Frequency Variation of the PtP LFAC TS with 200km cable, for various VSC states.

It is evident that if  $Z_c$  changes, it causes resonant points to change accordingly. More specifically, the increase of the equivalent OWF-VSI module resistance may somewhat reduce the system dynamic impedance magnitude, but also brings the resonance points to lower frequencies closer to 3<sup>rd</sup> harmonic order (~60Hz). Since the LFAC transmission system is formed exclusively among power electronic converters, it can be inferred that their dynamic operation can dominate the low-order frequency response of the LFAC TS by changing the frequency range and damping of its resonances. Conversely, as the operating state of the converters affects the dynamic impedance of the system, any probable non-passive, unstable response of the connected VSCs might even reduce the system damping and cause instability.

### 4.3 Export (PtP) LFAC TS Schemes without Filtering

Frequency scan studies are performed at various LFAC export system points and the MV collector bus to identify the points of potential harmonic issues and any need for installation of damping filters tuned around the problematic frequencies according to the loci of the low order harmonic frequencies. The passive LFAC system without any damping filter is connected to the cable and the impedance variations with frequency are noticed for different

cable lengths as seen from the offshore and onshore 345kV busbars as well as the 66kV OCS busbar at the 16.7Hz side. The export system under investigation with the impedance measurement points is depicted in Figure 4.11, without showing the inter-array cables for simplicity, while the obtained results for 100-500km cable lengths are presented in the graphs of Figure 4.12.

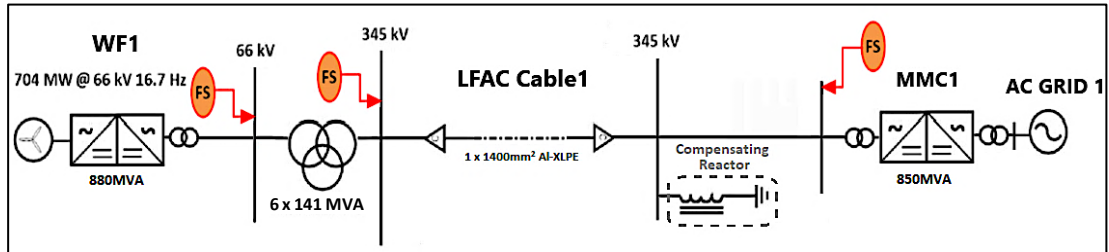


Figure 4.11: Simplified PtP LFAC TS Schematic with the Impedance Measurement Points.

From the impedance measurement points shown in Figure 4.11, the graphs of Figure 4.12 are obtained. It is evident that in the investigated LFAC export system, every resonance measured at the offshore 345kV busbar has relatively higher magnitude than at the onshore busbar, while the lowest resonance levels of all cases are noticed at the 66kV OWF, compared at a per-unit scale. Accordingly, as the cable length increases, the resonant frequencies move lower due to the increasing cable capacitance and inductance but with lower magnitudes as well, because of the increasing cable ohmic resistance that produces natural damping.

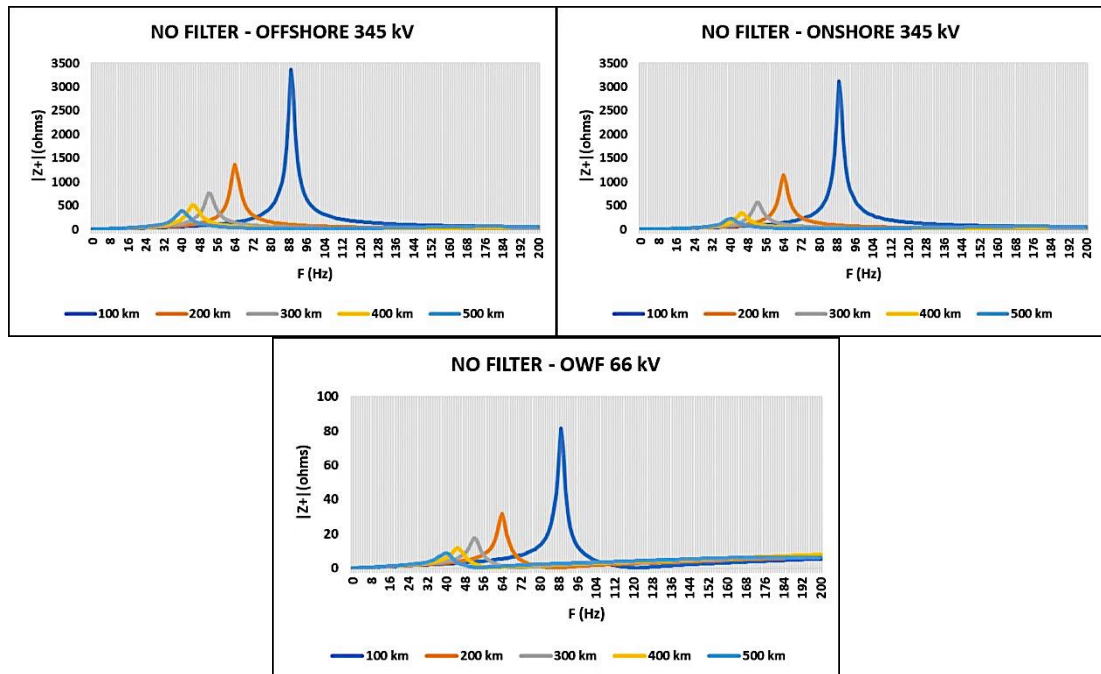


Figure 4.12: PtP LFAC TS Impedance Profiles vs. Frequency for various Cable Lengths. Measurements at 345kV Onshore and Offshore and at 66kV OCS.

It can be observed that the LFAC export system harmonics are inherently amplified at low frequencies from 41Hz for 500km cable length to 90Hz for 100km cable and up to the 3<sup>rd</sup> harmonic order for up to ~350km cables respectively. Another drawback of increasing the cable length is system power losses which could further rise if potential passive mitigation measures are adopted. Except for the harmonic filter losses that depend on its rating, type and quality factor (Q), additional shunt compensation may also be required, further increasing losses and jeopardising the system's overall life cycle cost.

The resonant frequency of the passive network for 100 to 300km cable length, lies between 53-90Hz, which would have jeopardised the viability of an OWF export system operating at 50 or 60Hz HVAC, while at 16.7Hz LFAC, this resonance lies still over its 3<sup>rd</sup> harmonic order. In the characteristic base-case comprising a 200km subsea cable that is also analysed in EMT simulations, the interaction of the cable's capacitive component with the inductive parts of the LFAC TS provokes a resonance at 65Hz with a magnitude of 1147 Ohm (or 1365 Ohm offshore). Depending on the operating mode of the system (e.g. energisation, full power, etc.), its resonance at that point may appear even lower than 60Hz, as seen in 4.2.5, rendering the frequencies around the 3<sup>rd</sup> and 4<sup>th</sup> harmonic order potentially problematic. Since the LFAC transmission system resonances can amplify the harmonic components of the OWPP and the onshore frequency converters, mitigation measures must be adopted.

#### **4.4 Harmonic Mitigation Measures**

In most OWPP applications with HVAC connections, the export cable lengths are generally not as long (i.e. <100km), and in the related HVDC configurations where the OWTG arrays feed into the HVDC platform, the AC cables that connect the OWPP collector stations (OCS) to the rectifiers together with the inter-array cables have relatively short lengths with resonances appearing in higher harmonic orders. Nevertheless, related harmonic amplification and propagation issues are reported in the literature for both offshore HVAC and HVDC transmission systems with the HVAC systems also being affected by the SCL of the system at the point of interconnection and the HVDC systems by the control settings of the offshore rectifier [134].

In HVAC systems, these issues are tackled by employing passive or active harmonic filters or even a combination of passive filtering with FACTS devices such as STATCOMs, SVCs, etc. at the onshore substation. In HVDC systems, passive or active harmonic filters can be installed

in the offshore platform or potential offshore converter control enhancements for high-frequency harmonics could be applied. In the island offshore LFAC export system configuration described in 4.3, the low-order harmonic resonances are mainly formed by the interaction between the impedance of the step-up transformers and the extensive high voltage cable system (i.e. >100 km). The resonant frequency of this system can range from 6<sup>th</sup> to 2.5 harmonic order for 100-500km cable lengths, respectively, while the LFAC system can also be affected by the control settings of the onshore MMC terminal. Hence, to mitigate the dynamic impedance of the system, the installation of passive or active harmonic filters or the islanded-control strategy of the grid-forming converter shall be considered [2].

In the following section, passive filtering solutions are analysed as a potential mitigation measure. They are the most common approach for alleviating the harmonics in OWPPs and preventing from undesirable harmonic propagation into the transmission systems. If certain system conditions are not known, or if the filtering equipment needs to be placed at the offshore platform, then the more compact active filtering solutions employing converters may be more suitable although more expensive, as they can be dynamically adjusted and continuously kept in tune to system variations [133].

Thus, the location of low-order passive resonant filters can be critical, as it can determine the impedance of the whole transmission system and affect the harmonic distortion and stability levels of the network. There are practical and techno-economic factors that affect the harmonic filter location. From an economic perspective, offshore, it is possible to directly connect the passive filters in the medium voltage of the OCS, in contrast to the onshore side where only high voltage is available, but the increased cost of the premium space in the offshore platforms, and the access difficulties for maintenance purposes can make it less feasible solution. From a practical perspective, if wider and meshed LFAC networks would be envisaged with LFAC inter-connected branches, then any extra filtering equipment that might be required would inherently necessitate bigger sized or even additional offshore LFAC platforms that could jeopardise the system flexibility and expandability.

#### 4.4.1 Passive Harmonic Filtering

Passive harmonic filters are connected in shunt configuration and suppress specific harmonic currents to their corresponding filter branches or by diverting them to ground. At these frequencies, the filter branches would present only the resistive part of their impedance. This way, they can prevent harmonic propagation from affecting the LFAC TS electric connection

infrastructure. Some of the most common passive harmonic filter designs in the industry are the single-tuned or notch filters, the single-damped, the c-type and the double-tuned damped filters [85], as shown in Figure 4.13.

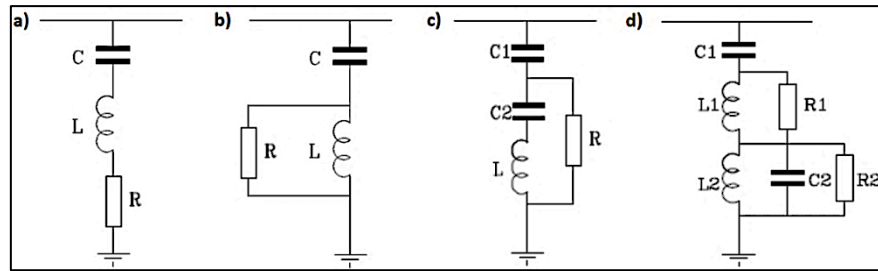


Figure 4.13: Harmonic Filters: a) Single-Tuned, b) Single-Damped, c) C-type, d) Double-Damped.

As the notch type filter offers small bandwidth, it can lead to sharp resonances at non-characteristic frequencies and produce undesirable resonant points that may be detrimental for a system with low order resonances. The single-damped and the c-type are second-order filters that are tuned to resonate at a single frequency, having similar impedance characteristics but offering better damping. In case there is a need for damping at two desired frequencies, then two of the above filters or the double-damped type filter may be used that has only one reactor subjected to full line voltage. In this study, the c-type filter is used as it can be designed to have minimum losses in fundamental-frequency operation and shunt to ground all frequencies above a specific harmonic.

#### 4.4.2 C-Type Filter Design

The primary parameters that define the impedance characteristics of the damping filters are:

- ❖ V: The system base voltage [kV].
- ❖ f or  $\omega$ : The system frequency [Hz] or angular frequency [rad/s].
- ❖ h: The harmonic order for filter tuning.
- ❖ Qc: Capacitive reactive power of the filter [MVar].
- ❖ Q: The quality factor of the filter ( $Q=X/R$ ) that defines its selectivity or tuning response.

From Figure 4.13c), neglecting the capacitors' dielectric power loss and the reactor's resistance, the c-type filter impedance can be expressed as [72]:

$$Z(\omega) = \frac{1}{\frac{1}{R} - j\frac{1}{\omega L} - \frac{1}{\omega C_2}} - j\frac{1}{\omega C_1} = \frac{R(\omega^2 LC_2 - 1)^2 + jR^2 \omega C_2 (\omega^2 LC_2 - 1)}{(R\omega C_2)^2 + (\omega^2 LC_2 - 1)^2} - j\frac{1}{\omega C_1} \quad (4.3)$$

The c-type filter is anticipated to provide damping of the system resonant impedance with a minimum amount of power dissipated across the damping resistor (R) at the fundamental frequency (f). For this reason, in Equation (4.3) the inductor (L) and the smaller capacitor (C2)

must be resonant or impedance matched at the fundamental frequency ( $\omega^2 LC_2 - 1 = 0$ ). This way, further system resonance damping is achieved over a wide frequency range and lower filter power losses during normal operation, as the filter impedance at the fundamental frequency is determined only by  $C_1$ , as follows:

$$Z(\omega) = j \frac{1}{\omega C_1} = -j \frac{V^2}{\omega Q_c} \quad (4.4)$$

Using the above fundamental filter characteristics ( $V, f, h, Q_c, Q$ ) as inputs, it is:

$$L = \frac{hV^2}{\omega Q_c (h^2 - 1)} \quad (4.5)$$

$$C_2 = \frac{1}{\omega^2 L} \quad (4.6)$$

Considering the total filter capacitance ( $C_{sd}$ ) as in a single-damped filter equivalent Figure 4.13b), and  $C_1, C_2$  of the c-type filter in a series connection, it is:

$$\frac{1}{C_1} = \frac{1}{C_{sd}} - \frac{1}{C_2} \quad (4.7)$$

Where:  $C_{sd} = \frac{(h-1)^2}{\omega h^2} \cdot \frac{Q_c}{V^2}$

By the quality factor ( $Q$ ) definition, the damping resistance value is yielded in Equation (4.8).

$$R = Q \frac{V^2}{h Q_c} \quad (4.8)$$

Except for these key filter specifications, an iterative design process is adopted to specify their suitable harmonic characteristics that includes EMT and frequency domain simulations for a range of system operating conditions. Since the power losses of this filter in steady-state are lower than of a single-damped equivalent,  $Q$  can be set to lower levels, resulting in better damping of the LFAC TS resonance. In addition, the tuning points ( $h$ ) of the filters are specified based on the "IEEE Guide for Application and Specification of Harmonic Filters" recommendation, that suggests the tuning of the harmonic filters up to 15% below the resonant frequency in order to achieve satisfactory harmonic performance across the whole frequency spectrum, even in a case of slight filter-detuning [85].

A combination of two c-type filters is utilised to mitigate the LFAC TS resonance of a base-case with 200km cable. The total size of the filtering branches is selected at 300MVar comprising of a 100MVar filter tuned at 64Hz and a 200MVar filter at 43Hz, while a  $Q=2$  is used. Initially, the 4<sup>th</sup> harmonic order filter is applied to mitigate the system's resonance, but it produces a new resonance with lower amplitude, closer to 3<sup>rd</sup> harmonic order which is



damped by an additional 3<sup>rd</sup> order harmonic filter. This combination of c-type filters is depicted in Figure 4.14.

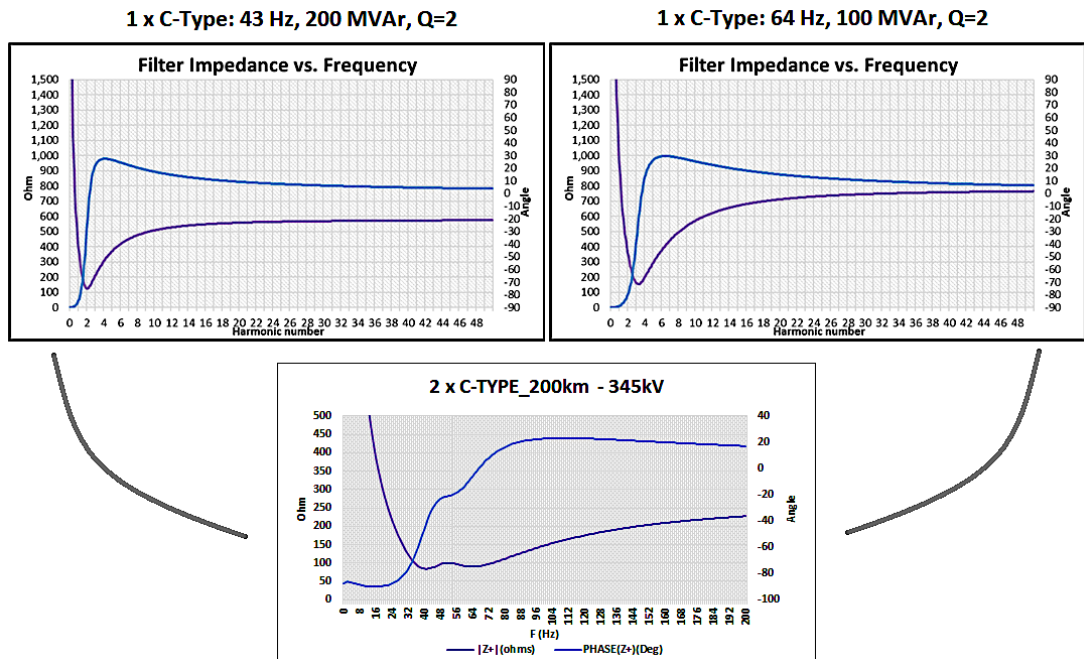


Figure 4.14: Combination of C-Type Filters rated 200MVAR at 43Hz and 100MVAR at 64Hz with Q=2.

Equivalent 300MVAR C-Type, Single and Double-Damped filters for the LFAC TS base-case with 200km cables are presented in Table 4-1, and their response characteristics are compared in Figure 4.15.

Table 4-1: 300MVAR C-Type, Single and Double-Damped Filter Parameters for LFAC TS with 200km Cable.

LFAC TS- H-FILTERS- 200km - 300MVAR/345kV								
H-Filter Type	h	f [Hz]	Qc [MVAR]	Q	C [μF]	L [mH]	R [Ohm]	C2 [μF]
Single-Damped	2.5	42	200	3	13.5	1.1	843.2	
Single-Damped	4.1	68	100	3	7.5	0.7	933.3	
C-Type	2.6	43	200	2	16.0	1.3	577.8	72.1
C-Type	3.8	64	100	2	8.0	1.0	776.5	87.7
Double-Damped	2.5	42	300	3	21	405	414	
	3.9	65		3	122	82	78	

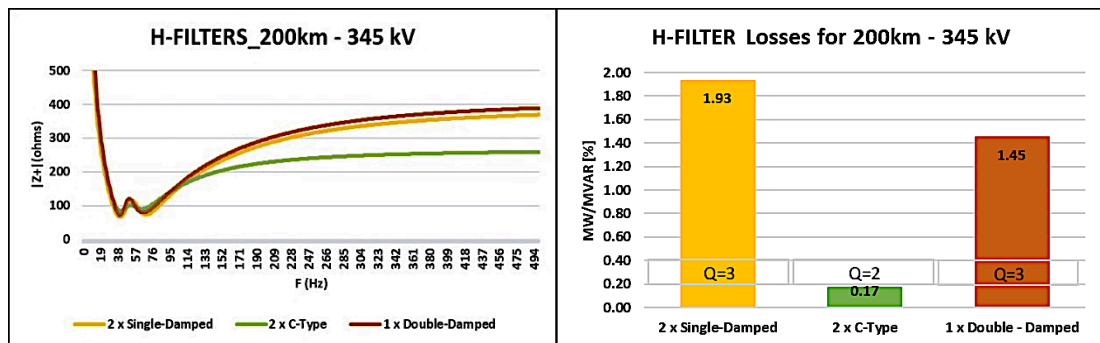


Figure 4.15: Filters Response Characteristics: Left-Impedance vs. Frequency Response, Right-Power Losses.

It is evident that for similar design characteristics, the c-type filters can offer better damping at the frequencies of interest with lower losses at the fundamental frequency.

In the above evaluation of the harmonic filter designs for the base case of 200km cable length, the c-type harmonic filters are the most practical solution in terms of the LFAC system impedance damping and power consumption. The implementation of such filters can improve the feasibility of the scheme compared to [2] where single-damped filters were employed, increasing the transmission system losses.

The damping effect of the applied 300MVAR c-type filters on the PtP LFAC TS resonance is obvious in Figure 4.16, while the export system impedance after the c-type filter implementation can be seen in Figure 4.17.

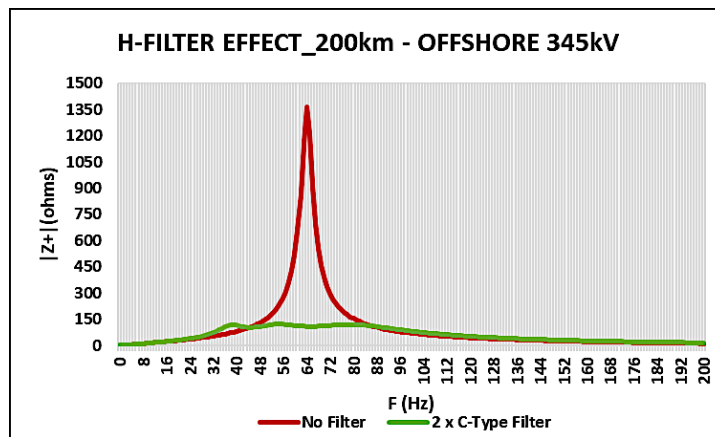


Figure 4.16: Effect of Harmonic Filter Implementation on the PtP LFAC TS Resonance for 200km Cable.

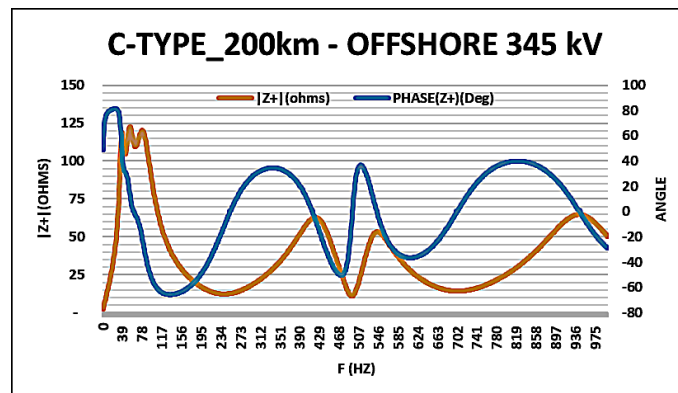


Figure 4.17: PtP LFAC TS Impedance Magnitude and Angle Profile vs. Frequency, after the Implementation of the Harmonic Filter for 200km Export Cable Length.

The phase angle in the above system impedance frequency scan diagram indicates the effect of damping on the resonances that appear. The undamped resonances of the system impedance can lead to undamped oscillatory behaviour of certain harmonic voltages and currents in the corresponding frequency range. This is why mitigation measures must be adopted, such as passive or active filters, or even damping through appropriate control



tuning or other resonance suppression control algorithms implemented in the MMC control system of the LFAC side terminal.

From the LFAC export system impedance graphs for various cable lengths seen in 4.3, the magnitude of the undamped system harmonic resonance decreases with increasing cable length while its frequency falls to lower than 3<sup>rd</sup> harmonic order for cables longer than 350km. Thus, for the 400km and 500km cable cases, the c-type filters should offer more damping in a single frequency to avoid tuning closer to 2<sup>nd</sup> harmonic order that could have been highly impractical. All the c-type filters tested are rated at 300MVar and Table 4-2 gives their parameter specifications for different cable lengths of the PtP LFAC TS schemes.

**Table 4-2: C-Type Filter Parameters for PtP LFAC TS with various Cable Lengths.**

Cable Length [km]	LFAC TS - C-TYPE FILTERS - 300MVar/345kV								Steady-State Losses
	h	f [Hz]	Qc [MVar]	Q	C [μF]	L [mH]	R [Ohm]	C2 [μF]	[% MW/MVar]
100	2.9	48	200	2	16.0	1.0	513.0	94.9	0.120
	5.1	85	100	2	8.0	0.6	583.5	160.2	
200	2.6	43	200	2	16.0	1.3	577.8	72.1	0.173
	3.8	64	100	2	8.0	1.0	776.5	87.7	
300	2.3	38	185	2.0	22.8	1.2	453.9	78.3	0.206
	3.1	52	115	2.0	9.2	1.4	834.7	63.4	
400	2.3	38	300	2.0	24.0	1.1	435.0	80.7	0.223
500	2.1	35	300	2.0	24.0	1.4	472.3	65.5	0.254

The impedance magnitude over frequency characteristics of the c-type filter designs for various cable lengths of the PtP LFAC TS are shown in Figure 4.18, below.

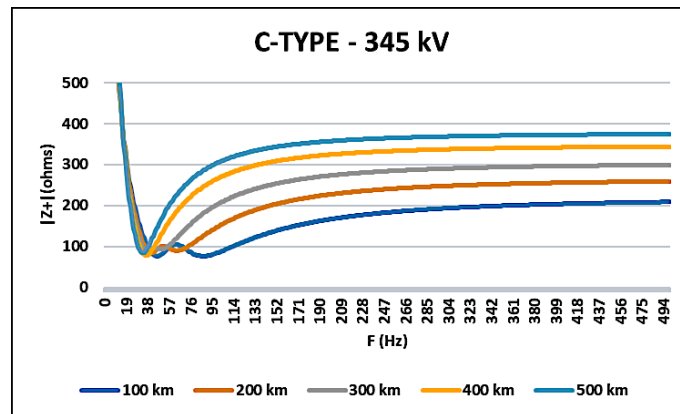


**Figure 4.18: Impedance vs. Frequency Profiles of the C-Type Filters to the PtP LFAC TS.**

In these plots, the lower the tuning frequency of the c-type filter, the less becomes the damping it can offer to higher frequencies for the same MVA rating and the higher its power consumption in the fundamental frequency can be, as presented in Table 4-2. However, as mentioned in 4.2.1.2, with increasing LFAC cable length, the resonant amplitude of the PtP LFAC TS becomes lower due to the increased cable resistance, offering natural damping to the system.

## 4.5 Export (PtP) LFAC TS Schemes with Filtering

The implementation of the c-type harmonic filters is shown in Figure 4.19, and their impact on the LFAC export system impedance for various cable lengths is shown in the impedance over frequency plots of Figure 4.20.

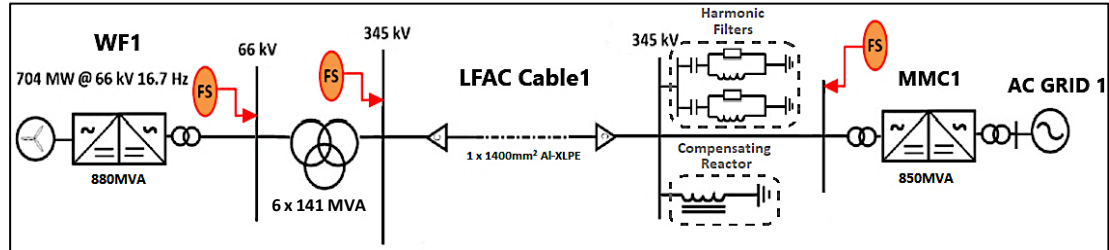


Figure 4.19: Simplified PtP LFAC TS Schematic with Harmonic Filters and the Impedance Measurement Points.

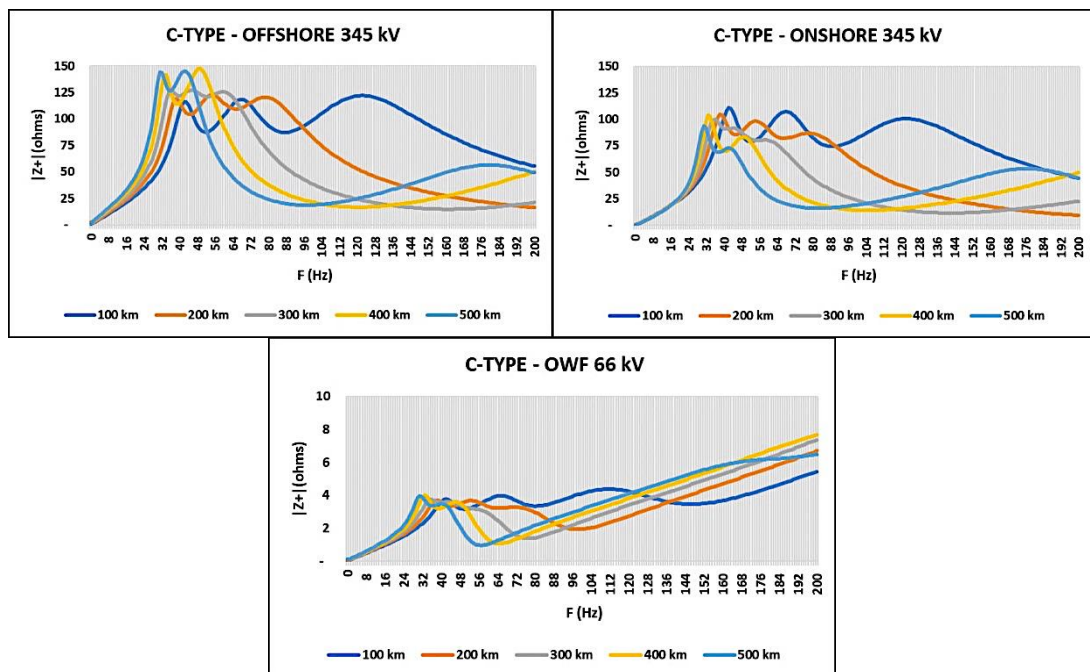


Figure 4.20: Impedance vs. Frequency Profiles of the PtP LFAC TS with Harmonic Filters.

The LFAC export system impedance profile has been drastically improved, eliminating the undamped resonances noticed in section 4.3. Although the highest amplitude impedance points have been shifted to lower harmonic orders, they are effectively damped without posing concerns for either the steady-state system operation or transient response. Nevertheless, higher system losses shall be expected not only because of the c-type filtering active power consumption but mainly in case larger shunt reactors are needed to compensate for the added reactive power generation of the filtering equipment to keep the LFAC side MMC operating within its capability range.

Figure 4.21 shows a side-by-side comparison of resonances in the LFAC export case examined for all cable lengths before and after the application of the harmonic filters. The illustrated peak positions are based on the impedance measurements at the offshore 345kV busbar.

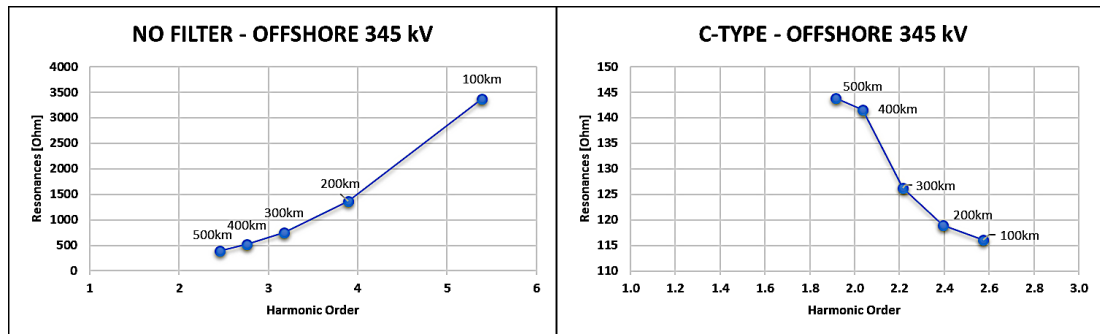


Figure 4.21: PtP LFAC TS Resonances for various Cable Lengths without (Left) and with (Right) H-Filters.

It can be observed that applying harmonic filters of the same size has a greater effect on damping the higher-order resonances that appear in cases with lower cable lengths (100km-300km) and slighter effect on the very low harmonic order resonances that appear in cases with 400km and 500km cable lengths. The 300MVar c-type filters designed for this assessment bring the voltage distortion levels to the range of 0.5% and current THD to ~1% for all cases, as can be noticed by the EMT simulations of Chapter 7. This approach is conservative according to the current and voltage distortion limits set by IEEE-519, 2014 as shown in Table 4-3 and Table 4-4, but it enables the understanding of the LFAC system response with and without the implementation of such filters for various cases. In a detailed and project-specific assessment, optimisation of filter sizes and characteristics should be performed for the explicit needs of the study.

Table 4-3: Voltage Distortion Limits for General Transmission Systems.

Bus voltage $V$ at PCC	Individual harmonic (%)	Total harmonic distortion THD (%)
$1 \text{ kV} < V \leq 69 \text{ kV}$	3.0	5.0
$69 \text{ kV} < V \leq 161 \text{ kV}$	1.5	2.5
$161 \text{ kV} < V$	1.0	1.5 <sup>a</sup>

Table 4-4: Current Distortion Limits for General Transmission Systems >161kV.

Maximum harmonic current distortion in percent of $I_L$						
Individual harmonic order (odd harmonics)						
$I_{sc}/I_L$	$3 \leq h < 11$	$11 \leq h < 17$	$17 \leq h < 23$	$23 \leq h < 35$	$35 \leq h \leq 50$	TDD
<25	1.0	0.5	0.38	0.15	0.1	1.5
25 < 50	2.0	1.0	0.75	0.3	0.15	2.5
$\geq 50$	3.0	1.5	1.15	0.45	0.22	3.75

Where  $I_{sc}$  is the maximum Short Circuit Current and  $I_L$  is the fundamental frequency component of the maximum load current at the PCC under normal operating conditions.

## 4.6 Meshed (MT) LFAC TS Schemes without and with Filtering

Meshed LFAC offshore systems are examined, in which the OWFs are either 200km or 300km away from the shore and connected to different grids while being interconnected to each other through a 50km submarine cable. This Multi-Terminal LFAC (MT-LFAC) system configuration, as well as the impedance measurement points, are presented in Figure 4.22.

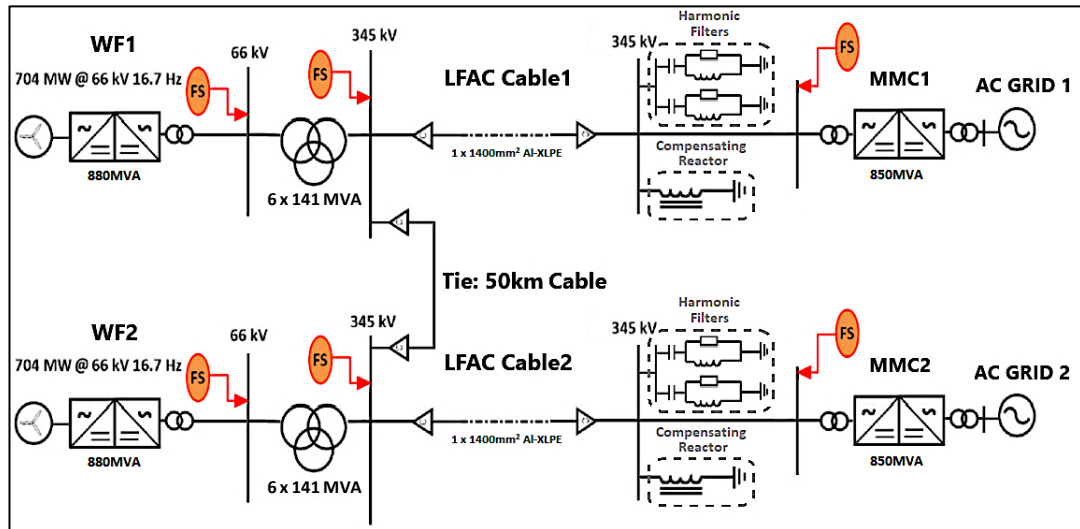


Figure 4.22: Simplified MT-LFAC TS Schematic with its Impedance Measurement Points.

### 4.6.1 MT-LFAC TS with 200km-50km-200km Cables

In Figure 4.23, the low-order resonance profile of the system without passive damping filters is assessed and compared with the respective 200km PtP base case examined in 4.3.

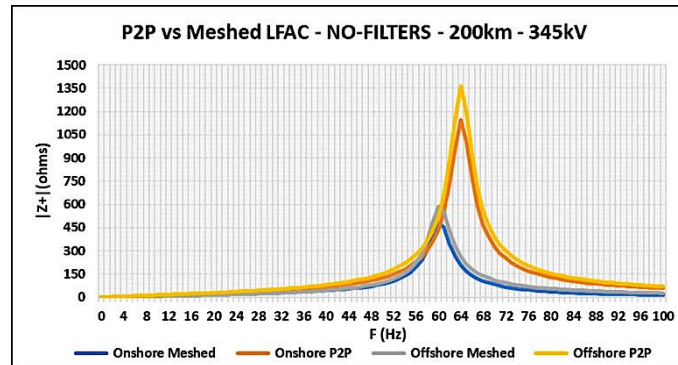


Figure 4.23: Impedance vs. Frequency Profile (Onshore/Offshore) of PtP and MT-LFAC TS for 200km Cables.

The impedance profile in the two offshore 345kV busbars of the MT-LFAC TS is identical as well as in the onshore 345kV busbars. The resonance in each 345kV cable side is greatly reduced compared to the 200km PtP base case, due to the natural damping introduced by the parallel cable paths and the addition of the 50km subsea interconnection cable. Even so, the resonant points lie at 60Hz instead of 65Hz, and damping may still be needed.

The same c-type harmonic filters designed in 4.4.2 for the LFAC export system with 200km cable are also applied in each onshore Terminal of the MT-LFAC system, and the meshed system impedance plot is shown in Figure 4.24 in conjunction with the respective PtP system.

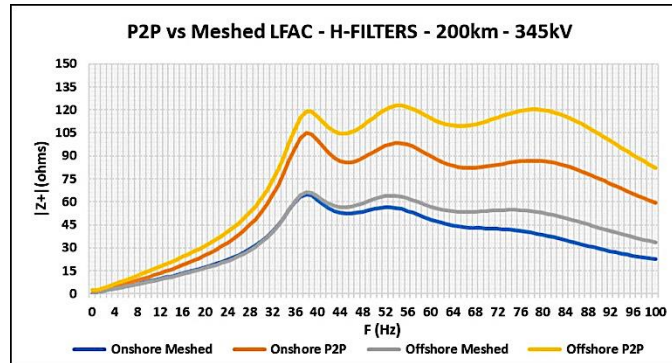


Figure 4.24: Impedance vs. Frequency Profile(Onshore/Offshore) of PtP and MT-LFAC TS with Harmonic Filters for 200km Export Cables.

Since the harmonic filters that are designed for the respective PtP LFAC TS configurations, are also effective for the MT-LFAC TS, they shall be installed in the scheme because they can guarantee, if necessary, the satisfactory standalone PtP system operation under certain conditions. However, for complying with the MT-LFAC TS requirements, some switching steps may be introduced to reduce their MVar and losses or avoid extra compensation needs.

#### 4.6.2 MT-LFAC TS with 200km-50km-300km Cables

In the above LFAC meshed system arrangement, one of the 200km cables together with its related compensating and potential harmonic filtering equipment is replaced by the equivalent 300km counterparts. The impedance profile of the resulted scheme without and with the implementation of passive damping filters is shown in Figure 4.25.

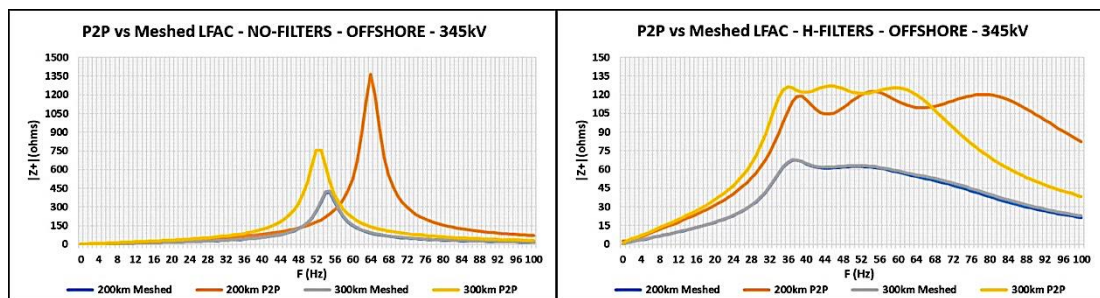


Figure 4.25: Impedance vs. Frequency Profile (Onshore/Offshore) of PtP and MT-LFAC TS before (Left) and after (Right) the Implementation of the Harmonic Filters, for 200km and 300km Export Cables.

The system resonance points seen from the offshore 345kV sides lie between the resonant frequencies of the corresponding individual PtP LFAC TS cases with 200km and 300km cables, but they are more damped. The filters also provide effective damping that greatly reduces the resonant impedance magnitude.

## 4.7 System Impedance and Operating Frequency

The selection of a specific low frequency level is a matter of immense importance for the overall system design and operation. Most feasibility studies on LFAC transmission for OWPP systems result in adopting 16.7Hz or 50/3Hz, mainly due to the field-proven assets developed by the manufacturers for the rail industry. As explained in this frequency domain analysis of the LFAC TS, the harmonic impedance profile may also affect the overall system technical performance and its dynamic behaviour. In general, this effect could be mitigated easier, and the system operation could be more efficient if the following occur in a specific scheme:

1. A relatively low impedance magnitude at the fundamental frequency,
2. The first resonance in the highest possible harmonic order,
3. The lowest possible impedance magnitude at the first resonant frequency,
4. The smallest number of harmonic resonances near the fundamental frequency or tuned to significant harmonics.

In this section, the correlation between the operating frequency and the dynamic impedance of an offshore system is discussed, through the investigation of simplified subsea cable-transformer pairs at 230kV level, using the corresponding cable parameters described in Chapter 2. Frequency scan studies are performed for various operating frequencies (i.e. 5, 10, 14, 16.7, 20, 25, 50, and 60Hz) utilising the same 200km cable in all cases and the same rated p.u. impedance values of the transformer. Thus, when changing the operating frequency, the percentage of transformer p.u. leakage reactance is kept constant, altering the total inductance of the system, while by using the same subsea cable, only the system's resistive response is affected, due to the skin effect.

Hence, the system's steady-state impedance and its resonances change for different operating frequencies. For higher operating frequencies, the resonance magnitude decreases due to the increased cable damping, and it occurs at higher resonant frequencies, although at lower harmonic orders, due to the lower transformer inductance. At the same time, the fundamental frequency impedance is larger, as both the resistive and reactive parts are higher. Figure 4.26 shows a correlation between the resonant points and the operating frequency of the system. Moreover, in Figure 4.27, the system resonances and their harmonic orders are plotted against various operating frequencies. It is evident that if the system operates at 16.7Hz the equivalent system resonant frequency lies within the range of the 4<sup>th</sup> harmonic order, which makes it a relatively better choice than 20Hz and beyond, while the resonance magnitude is relatively lower than the equivalent of 14Hz or 12Hz and below.



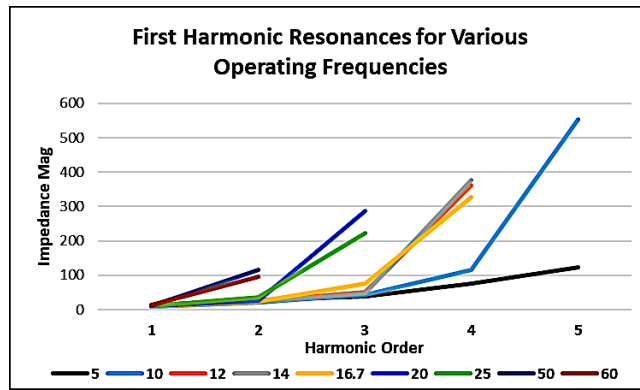


Figure 4.26: System Frequency Scan approximations for various Operating Frequencies.

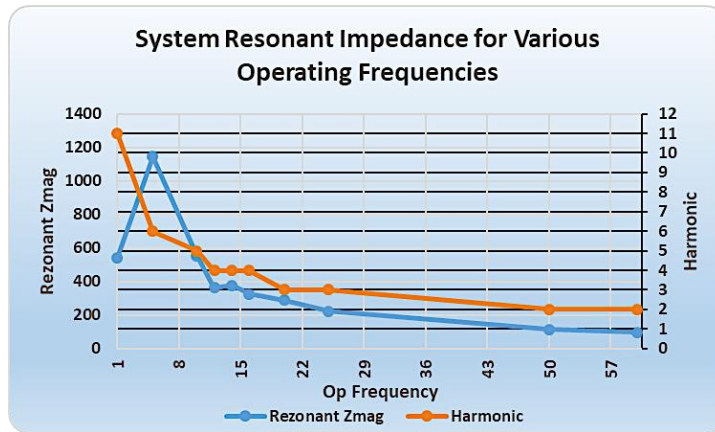


Figure 4.27: System Impedance Resonance (blue) and Resonant Harmonic Order range (orange) approximation for various Operating Frequencies.

From Figure 4.26 and Figure 4.27, it can also be inferred that an offshore system using such long cables operating at 50Hz may imply critical operating risks or pose severe harmonic stability issues. For this distance range, it would most certainly be into current amplification and undergo severe voltage distortion close to the second (2<sup>nd</sup>) harmonic. At any transient, or even a routine, credible system event such as switching a transformer or a cable could cause severe harmonic interactions, or even potential OWTGs PLL's synchronisation issues, that could lead to disconnections. In such cases, if the HVAC system design is conceded, it must be optimised with very efficient project-specific harmonic mitigation solutions.

As a consequence, in terms of the desired impedance profile characteristics and low-order resonance of an offshore system, the harmonic order of the resonant point and the resonance magnitude can be higher for lower operating frequencies. Other conditions though, might be more important for indicating the operating frequency of a specific configuration from a technical point of view, while further limitations imposed by other significant factors should be counted, such as technology readiness, equipment weight and size, etc. to attain the most technically and economically feasible solution.

## 4.8 Summary and Conclusions

In this chapter, the LFAC TS frequency response is evaluated through a frequency-scan assessment. The LFAC TS is modelled in frequency-domain, and the impact of each of the system's main components to its passive frequency response is assessed. The frequency response of the LFAC subsea cable (frequency-dependent phase model) with its shunt reactors, the LFAC step-up transformers, the OCS with its inter-array cables (pi-equivalent models), as well as the MMC and OWTG systems with their transformers and LCL filters are explicitly analysed. Potential mitigation measures are introduced in the form of passive filtering equipment for damping the harmonic resonance of the passive system. Various filter designs are compared in the frequency-domain for mitigating the LFAC TS resonance. The more efficient c-type filter combinations are adopted for multiple cable lengths that can also reduce the filtering losses compared to single or double damped filters.

More specifically, passive frequency-scan studies of the PtP and MT-LFAC TS schemes, as designed and rated in Chapter 3, are performed for various cable lengths. Their resonance response with regards to the length of the cables, and the effect of the implemented mitigation measures, are evaluated. The LFAC TS resonance has been found to have a relatively higher magnitude at the offshore side busbar, while the lowest resonance magnitudes in per-unit appear at the medium voltage OCS. In addition, as the submarine cable length increases, the resonant frequencies decrease due to the higher cable capacitance and inductance, although, lower resonance magnitudes are noted due to the increasing cable ohmic resistance, which produces natural damping. Furthermore, the lower the transformers relative leakage inductance in p.u., the higher the frequency of the system resonance and the lower its magnitude, whilst the fundamental 16.7Hz frequency impedance magnitude affecting the system losses is reduced.

Additionally, in the MT-LFAC TS schemes, the resonance magnitude and frequency are reduced compared with the corresponding PtP base cases, mainly due to the natural damping introduced by the parallel cable paths and the added cables. Thus, harmonic filters designed for the PtP schemes can be effective for MT systems as well. Finally, the correlation between the operating frequency and the dynamic impedance of an offshore system is discussed, through the investigation of a subsea cable-transformer pair that typically dominates the system's resonance characteristics. It is estimated that for PtP offshore schemes, both the resonance harmonic order and magnitude can be higher for lower operating frequencies.



## Chapter 5: Steady-State Analysis

### 5.1 Introduction

The load-flow assessment of a transmission system evaluates the steady-state system response under credible sets of operating conditions, only for the fundamental frequency. Essential information can be obtained from the load-flow analysis of the LFAC system by assessing its voltage profile and the flow of active and reactive power through it. The studies determine if the system voltages are within limits and currents do not cause equipment overloading under the specified conditions. This way, suitable reactive power compensation plans are defined to bring the voltage at the corresponding system busses at an acceptable level or relieve components overloading, decreasing the risk of equipment damage and unplanned system outages. Such plans include additional passive equipment installation or coordination between the converters and the passive elements of the system.

Moreover, other critical operating aspects of the LFAC TS are addressed by solving its nodal equations in steady-state. Since the shunt capacitance of the LFAC cable generates charging current that increases with cable length, then for a relatively high OWF power dispatch, the total load current may exceed the rated current of the cable. The overloading of the LFAC cable together with the voltage increase along the cable can lead to excessively high voltage at the respective onshore bus, a phenomenon known as the Ferranti effect [110].

Lastly, the availability of the resulted feasible offshore LFAC TS radial and meshed arrangements is estimated, followed by the energy availability comparison among the LFAC, the HVAC and HVDC offshore export technologies for matching configurations (APPENDIX B).

#### 5.1.1 Steady-State Assessment Objectives for the LFAC TS

In this Thesis, power-flow studies are performed using DigSilent PowerFactory to determine the steady-state operation of the LFAC TS. More specifically, the Newton-Raphson algorithm is employed to solve the network's non-linear nodal equations using an iterative method that constitutes the inner calculations loop. Once these iterations converge to a solution within a defined tolerance, an outer calculations loop is applied to reach the requested target values, by imposing limitations according to the system input data which involve minimum or maximum P or Q limits, converter capability curves, voltage or power-dispatch response dependency, etc. Solving the inner and outer loops involves computational effort until convergence is reached that depends on the network size, complexity and set conditions.

The load-flow studies of the offshore LFAC TS aim to attain practical bus voltage profiles, minimize the system power losses and estimate the real and reactive power flow under various conditions for PtP and meshed network configuration. The voltage level at each bus, the voltage-drop on each feeder and the power flow in all branches and feeder circuits of the system are monitored. In this work, the steady-state assessment of the LFAC TS focuses on:

- Converter control strategies for reactive power compensation and efficient operation of the transmission system under various conditions, such as different subsea cable lengths, PtP OWF export systems and multi-terminal/meshed network development.
- Onshore passive shunt compensation requirements to achieve a desired steady-state operation, comply with the equipment limitations and increase the power transfer capability of LFAC cables, mitigating the charging currents and the Ferranti effect.
- Reactive power management combining the system's resources (e.g. passive reactors and VSCs capability) for cases without or with low-order passive harmonic filters.
- Compliance with system operator (SO) requirements at the PCC.

### 5.1.2 Offshore LFAC TS Grid Integration Requirements

Currently, as there is no real LFAC system precedent for offshore transmission network application, no "Grid Code" equivalent has been developed to define the principles and procedures for connecting generation or demand to such a system. Though, the system closely resembles an OWF that connects to the main grid via an HVDC transmission link. While there is no specific HVDC code either, converter stations are defined and included amongst the general requirements [120]. Here it is assumed that the onshore LFAC converter station should conform to requirements set out for HVDC converter.

Although the requirements for OWFs depend on the characteristics of each specific transmission system, the structural harmonization study for the grid codes is meant to establish a general scheme with fixed specifications in a generic layout agreed by TSOs, developers of WPP, and WT manufacturers [130]. According to this approach and regardless of any specific grid codes, WPPs should meet some common requirements that comprise:

- a. Control of active power,
- b. Control of reactive power and voltage,
- c. Operating ranges of frequency and voltage,
- d. Fault Ride-Through (FRT) capability.

Grid codes indicate active and reactive power requirements by P/Q and V/Q curves, as in

Figure 5.1a) and b), while the system's FRT capability is evaluated through EMT studies [78].

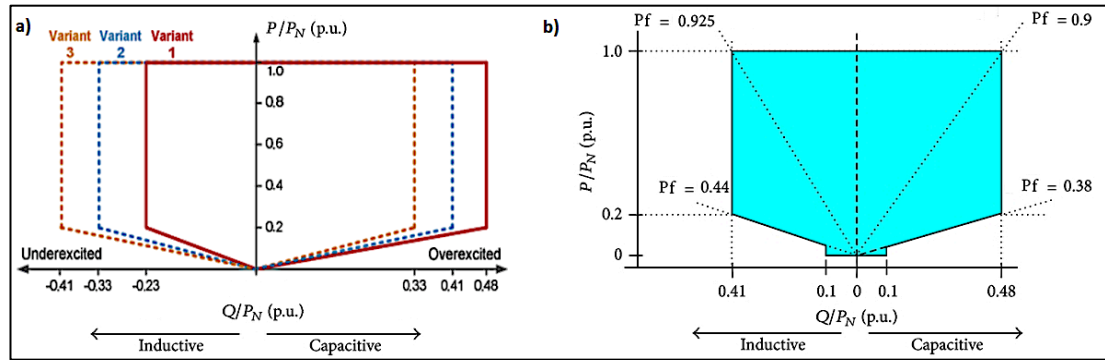


Figure 5.1: a) Typical P/Q Variants required by TSOs on the PCC and b) WTG PQ Capability Curve.

In steady-state operation, the OWTGs and onshore MMCs participate in the grid power regulation by either balancing or limiting their active power output. All the related generating units should be able to support active and reactive power at their LFAC grid entry point. In Figure 5.1a), the reactive power regulation depends on the real power export at the PCC, and also on the grid properties at this point, such as its SCC, X/R ratio, etc. Thus, the converter outputs at their PCCs should be adjusted according to the references advocated by the system operators (SOs), in response to voltage variations [82].

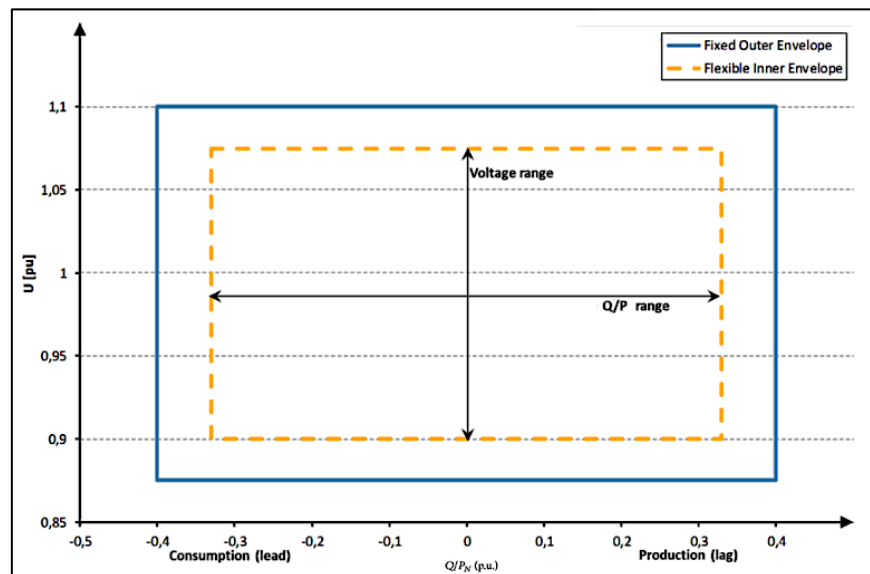


Figure 5.2: Typical V-Q/Pmax Envelopes of OWPP at the PCC over 110kV, as TSO requirements.

TSOs require the HVDC stations to follow certain U-Q/Pmax profile envelopes at the connection point, as presented in Figure 5.2 [122]. The converters need to maintain the required reactive power exchange with the grid at maximum active power output within the specified boundaries for the designated voltage range. Generally, their reactive power output shall be fully available within a voltage range of  $\pm 5\%$  in steady-state operation.

## 5.2 System Steady State Modelling

### 5.2.1 AC Grid Representation

For the load flow studies, the onshore 50Hz grid is represented as a Slack Bus type, imposing 1 p.u. voltage at the 400kV busbar that is also the PCC of the MMC terminal with the grid. A relatively strong AC system with a Short-Circuit Capacity (SCC) of 3400MVA corresponding to an SCR of 4 is assumed for the examined point-to-point cases, while the second AC grid of the multi-terminal (MT) LFAC arrangement has an SCC of 2550 (SCR of 3). An X/R value of 20 is selected for both AC systems.

### 5.2.2 LFAC Transmission System Representation

The LFAC step-up power transformers, as well as the delta/star converter transformers in the model, are represented in fundamental-frequency studies as series-connected inductance and resistance. As in Chapter 3, the transformer leakage reactance is set to 0.07p.u. and the copper losses to 0.0023p.u., while no tap-changers are employed on the transformer windings to assist with voltage regulation.

#### 5.2.2.1 LFAC Subsea Cable

For the load flow studies, the Bergeron cable model is adopted that represents the inductance and capacitance of the  $\pi$ -section analysed in Chapter 3 in a distributed manner with lumped resistance that is split between the middle and both ends of each cable segment. Thus, the voltage rises due to the Ferranti Effect that is prominent in subsea cable circuits can be assessed in the studies. This effect is more apparent when energising an unloaded or lightly loaded cable, as its charging current becomes higher than its active current and increases the voltage along the cable. Below, Figure 5.3 shows an equivalent cable  $\pi$ -circuit based on which Equation (5.1) describes its receiving end voltage.

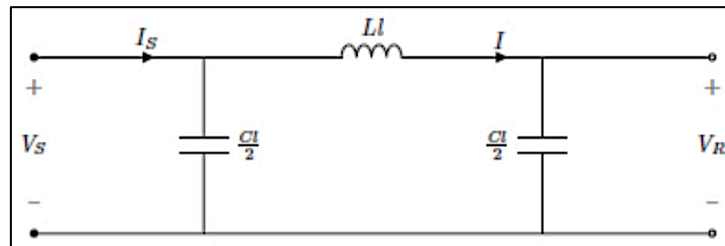


Figure 5.3: Equivalent Cable  $\pi$ -Circuit Representation.

$$V_s - V_r = j\omega L \cdot l \cdot I = -V_r \frac{\omega^2 LC \cdot l^2}{2} \Rightarrow V_r = \frac{1}{1 - \frac{\omega^2 LC \cdot l^2}{2}} V_s \quad (5.1)$$

Since the receiving end voltage ( $V_r$ ) rises with increasing frequency ( $\omega$ ), inductance ( $L$ ), capacitance ( $C$ ) and cable length ( $l$ ), the Ferranti Effect is less noticeable in LFAC cables than in HVAC for the same cable length. Though, for significant cable lengths, inductive compensation is also applied.

#### *5.2.2.2 Reactive Compensation Management*

The main objective of reactive power management is to enable optimum utilisation of the LFAC export cable and minimize its current by compensating the reactive current flowing through the cable. The reactive power generated by the subsea cables varies with cable length and the amount of transmitted active power. Thus, studies for a range of transmitted active power are performed as well as for the cases that the full OWF power is transferred, and the total active current flows through the cable. If the charging current is optimised and reduced for such cases, the total cable current can be reduced. For this purpose, cable reactive power compensation is needed, especially for long distances. In principle, MVAR compensation in both sides of a cable is preferred for long-distance power transmission and can be attained by employing passive or dynamic compensation or a combination of both.

As discussed in Chapter 3, the amount and location of shunt compensation affects the voltage profile along the cable, but it would be beneficial for the LFAC TS costs to place the necessary amount of shunt reactors at the onshore side of the cable only. To achieve this, the OWTGs' capability can be exploited to control the reactive power flow at the OCS or regulate the voltage level in the power entry point of the export LFAC cable, while the frequency MMCs capability is utilised by imposing the voltage level at the onshore 345kV LFAC busbar. Besides, the degree of shunt compensation required for the export cables is defined for many LFAC TS configurations, by means of shunt reactors.

During the system energisation or no-load condition, the voltage rise due to the Ferranti Effect at the receiving offshore cable end that is kept open should be lower than the maximum continuous operative voltage (MCOV) or temporary overvoltage (TOV) capacity of surge arresters and other system components. At the same time, the no-load current on the onshore side of the cable must not exceed the rated capacitive switching current capability of the circuit breakers. In the latter case, it is vital to reduce the cable charging current only by the implementation of passive shunt reactors at the onshore cable end as the MMC islanded and LFAC voltage controllers act to maintain the voltage level and not necessarily to reduce the capacitive current at this point where the CBs are placed. It should be noted,

though, that shunt reactors are only likely to be in service during relatively light-load conditions to limit excessively high system voltages, limiting the duration for which shunt reactor losses would be present on the system.

The shunt reactors employed are modelled here as inductors connected in series with resistors and in shunt with the LFAC cable system having a typical X/R ratio of 250-300 as small but constant losses in these devices are unavoidable. The system studies performed in this chapter, identify compensation schemes that can maintain acceptable voltage profiles and still be economically feasible.

### 5.2.3 Onshore BtB Frequency MMC-HVDC System

The implementation of a control strategy for the MMC terminals of the BtB frequency converters depends on the application and the operating conditions of the system. The particular control adopted by each MMC of the LFAC TS defines its bus-type representation in the power flow assessment. Typically, grid codes for WF integration demand unity power factor operation at their PCC with the grid to prevent conduction losses [120]. In the case of an LFAC TS, this requirement can be met if the AC grid side MMCs apply RPC at their PCC with the grid. Thus, they can be represented as Vdc/Q buses, ensuring zero reactive power exchange at their PCCs. For the LFAC side MMC Terminals, the control modes depend on the LFAC TS arrangement. In a PtP application, it must operate on islanded control, adjusting the LFAC Voltage while imposing the 16.7Hz frequency and it can be modelled as Vac/ $\phi$  bus. In MT-LFAC TS, only one MMC Terminal operates at this mode while the rest operate in P/Vac modes. Figure 5.4 shows the desired capability curves of the grid-following MMCs, where the blue circle corresponds to their rating and the red square defines their operating limits.

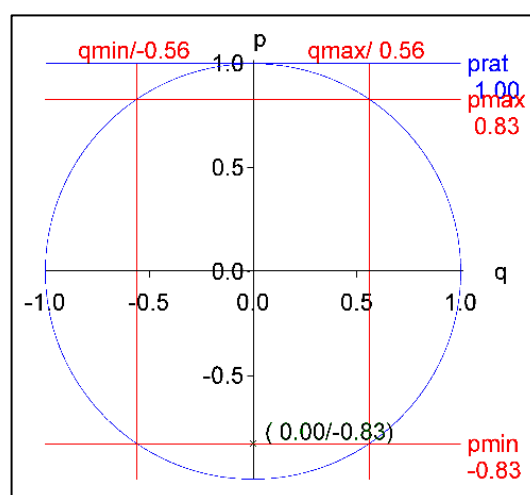


Figure 5.4: P/Q Capability Curves of the Grid-Following MMC Terminals.

### 5.2.4 OWTGs Representation

Although the analysis mainly focuses on the LFAC transmission system in steady-state, each OWTG is also modelled as a controlled PQ or PV source interfaced by an 8/66kV LFAC inverter transformer and utilising the reactive power capability curves shown in Figure 5.5

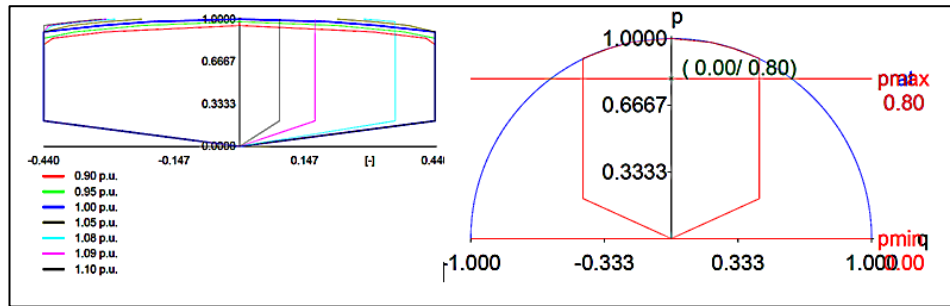


Figure 5.5: Power Capability Curves for OWTGs: a) Voltage-Dependent and b) P/Q Curves (WEA).

The modelled OWTGs are added in a Station Control arrangement that regulates either the reactive power at the sending end of the LFAC cable or the voltage level at the offshore 345kV busbar. In Figure 5.6, the diagram represents P-Q profile boundaries at the LFAC connection point, expressed by the maximum capacity ( $P_{max}$ ) in per unit, against the reactive power (Q).

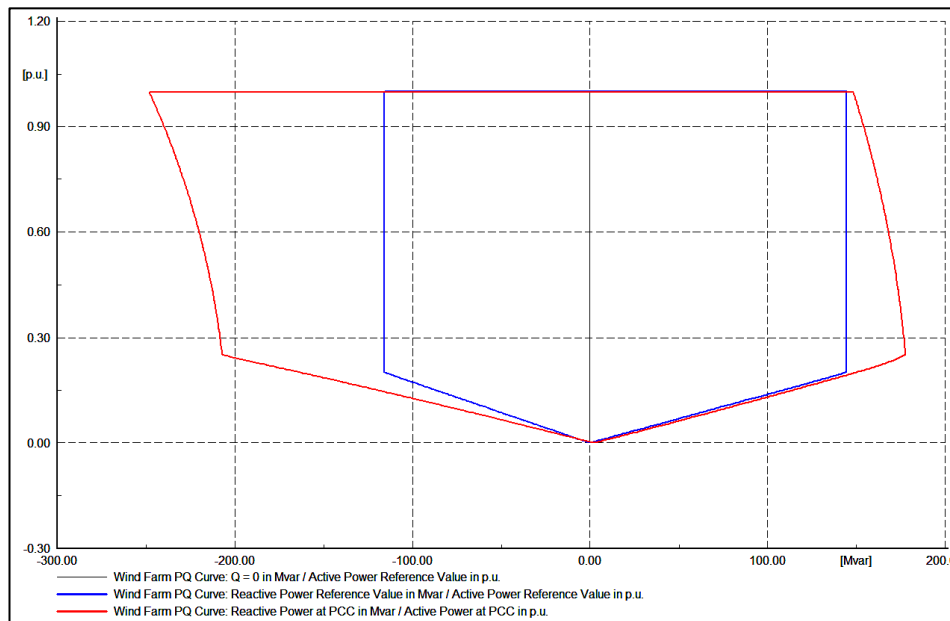


Figure 5.6: P-Q Capability Profile of the OWPP for 352 MW/440 MVA part of the 704MW OWF.

The blue line denotes typical (EWEA-EPIA) requirements for connecting WPPs to the grid, defining the P-Q - profile of a WF for under and over-excited operation. The red line shows the calculated capability curve for the 352MW part (half) of the OWF at the 345kV LFAC busbar for 100 different power-flow dispatch-cases, which affirms compliance with these requirements.

### 5.3 Power-Flow Studies for LFAC TS Schemes

In Figure 5.7, the single line diagram (SLD) of the 704MW offshore PtP LFAC TS is presented. For this scheme, a single submarine cable is utilised, and there are two transformer sets of three single-phase units each, on a single offshore LFAC platform. This schematic is vital for the power-flow studies evaluation and for estimating the LFAC TS availability (APPENDIX B).

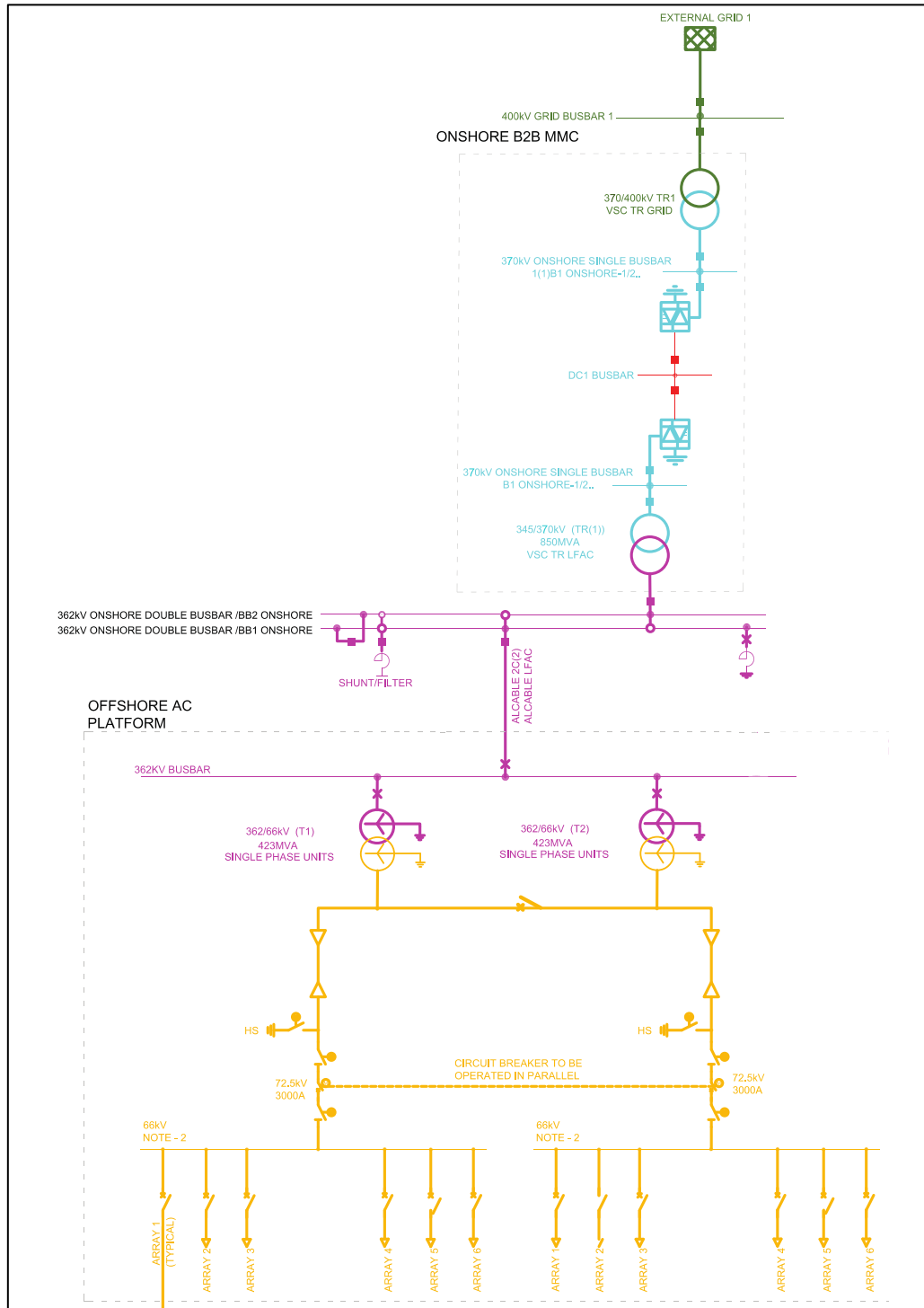


Figure 5.7: SLD of the PtP LFAC TS Configuration.



### 5.3.1 Set-Up of LFAC Export Power Flow Cases

The scenario-cases that are investigated in the power flow assessment engage potential point-to-point or export and multi-terminal or meshed offshore LFAC transmission system topologies, for various cable lengths, under different control arrangements and reactive power management strategies as well as harmonic filtering considerations. Initially, point-to-point cases are examined for 100km to 400km cable lengths (PF1-PF4) in which the OWTGs capability is utilised to either establish a unity power factor/zero reactive power exchange operation at the subsea cable offshore end (a-cases, RPC) or support the voltage level at the offshore 345kV busbar (b-cases, ACVC). The point-to-point export cases that are further analysed and compared are shown in Table 5-1, below.

*Table 5-1: List of the Power-Flow Cases for the PtP LFAC TS.*

List of PtP Power Flow Cases							
Power Transfer	Case	OWF CONTROL @ 345 kV OFFS	H-FILTERS @ 345k ONS	Shunt Reactor [MVAR] for different Cable Lengths			
				PF1 (1x100km)	PF2 (1x200km)	PF3 (1x300km)	PF4 (1x400km)
No Load	PF	-	-	15	230	460	705
Full Load	a	RPC - Q=0	a) NO HF	0	230	460	-
			ah) HF	0	230	460	-
	b	ACVC	b) NO HF	0	0	0	0
			bh) HF	0	0	0	150

Since the steady-state studies are conducted at the fundamental frequency, any probable employment of harmonic filters may only be evaluated using frequency and time-domain simulations, while in these studies only the reactive power generation and MW losses footprint of their potential application can be utilised to seize the appropriate reactive compensation equipment. Hence, the above cases are studied either for implementing the 300MVAR Harmonic-Filter solutions (h-cases) as obtained by the frequency-domain calculations with their estimated losses at the 16.7Hz fundamental frequency or for applying no passive filters at all, assuming potential active control system arrangements.

No-Load and Full-Load power flow studies have been performed for each case, as referred in Table 5-1, with the aim to determine the appropriate reactive power compensation for each scheme to comply with the operating criteria that are described in section 5.3.2. The Full-Load cases require the maximum power output of each 8MW OWTG, generating a total OWF output of 704MW at the 66kV busbars of the offshore LFAC platform. In No-Load studies, the offshore-end circuit-breaker is opened to simulate a perilous case of the system energisation procedure that could lead to restrike at the onshore-end CB in case it tries to isolate the LFAC cable system. Finally, the amount of passive shunt reactors installation has been selected after thoroughly assessing each case for the conditions defined in the following section.

## 5.3.2 Power Flow Cases Evaluation Principles

### 5.3.2.1 System Operating Criteria for Individual Cases

In order to attain only operational and efficient LFAC transmission system designs with the appropriate converter control system strategies and reactive compensation management comprising the converter's capability in conjunction with the selection of the fitting shunt reactors, as mentioned in Table 5-1, each PtP load flow case has been systematically assessed to meet the following criteria:

- a. The voltage regulation for each busbar as well as the voltage drop between two interconnected points of the system should not exceed +/-10%. The formula used for obtaining the percentage of voltage regulation in each busbar (i) is:

$$VR_i = 100 \cdot \frac{V_{base} - V_i}{V_{base}} [\%] \quad (5.2)$$

Where:  $V_{base}$  is the base voltage as defined by the respective transformer voltage ratio.

- b. System equipment such as transformers and subsea cables should not be overloaded, and converters should operate within their desired capability limitations.
- c. According to the IEC, the preferred value for the cable charging-breaking current (No-Load operation) should be less than 0.355 kA, (i.e. AC CB current limit standard).
- d. Passive reactive power compensation and harmonic filtering equipment, if needed, should be preferably placed at the onshore 345kV substation while power losses due to compensating reactors and harmonic filters should be kept as low as possible.
- e. The voltages and currents should be as equally distributed as possible along the cable.

Apart from the cable charging breaking current limitation, all the other criteria mentioned above are determined by the Full-Load cases, including the offshore end voltage rise and cable active power reduction due to cable charging current. Besides, the capability of the LFAC side converters at full-load conditions can define the extra cable shunt reactors to be installed at the onshore 345kV bus, in case the MMCs cannot provide the required reactive power to retain the target bus voltage to 1p.u.

No-Load cases provide information about the shunt reactors required in each scheme during the system energisation process. They represent scenarios in which the onshore-end CBs are closed to energise the subsea cable that is left open in its offshore side. Then, the Ferranti effect causes a voltage-rise from the sending end towards the remote end. This effect can get more pronounced for longer cables and higher voltages. If only the charging current flows

in the 345kV cable, there is an inherent risk of CB malfunction causing arcing 'restrike' because of severe voltage stress after interruption which is unlikely to occur in normal operation that the load-current dominates. Restrike can cause overvoltages like capacitor switching, that may damage circuit components depending on the network topology.

These concerns are reflected in the relevant IEC standard (IEC60056) under consideration. The IEC suggests a cable-charging breaking current limit value of 0.355kA as the maximum current that the CB can break at a rated voltage of 345kV. In a special arrangement, such as the LFAC system that comprises long cables to supply embedded generation like OWTGs, this condition can occur during the system energisation procedure as well as in case of a disconnection following a fault event at the offshore collector system (OCS) or another interconnected system if the breaker at the other end is called upon by an operator command or by a trip order to interrupt the cable's charging current.

In this work, the cable voltage and loading profiles are analysed across its length, assuming an open CB at the offshore end for each No-Load case. The compensation that needs to be placed between the cable and the onshore end CB is implemented in the form of shunt reactors to reduce the charging current into the limits and help the MMCs regulate the onshore bus voltage to 1p.u. The rating of the shunt reactors to be installed may be smaller than the total reactive power needed for adequate compensation during regular system operation, as supplementary compensating means can be available at the 345kV busbar for different loading conditions, e.g. utilising converter reactive power capability. Then, the continuous operation of the reactor and its default active power losses may be avoided.

#### *5.3.2.2 Evaluation Criteria for Comparing All Cases*

The various LFAC TS radial cases are assessed from the OWTGs 8kV buses at the 16.7Hz system to the onshore 50Hz grid at the 400kV level. The operating characteristics of each scheme are compared to each other and result in optimised PtP LFAC TS arrangements for each cable length. The cases in section 5.4 are used as a base to introduce the meshed offshore LFAC network structures, and the study cases are further evaluated in the dynamic, time-domain simulations of Chapter 7. The conditions that set the evaluation base for the PtP schemes are reviewed, and the corresponding cases are compared according to the following overall system percentage quantities defined for each case separately:

- A quantitative Total Voltage Regulation index for the overall topology with N=7 main busbars can be assumed for comparing the total voltage deviation of the scheme under different operating conditions. The lower percentage indicates a more stable system

voltage and the total voltage regulation in each case can be calculated as follows:

$$TVR = \sum_{i=1}^N |VR_i| \text{ [%]} \quad (5.3)$$

- The Total Power Losses over the generated power in each case.
- The Total Reactive Power Compensation degree for normal system operation.
- The Maximum Loading of the LFAC cables, transformers and converters of the scheme.
- The Total Passive Compensating Reactors that need to be installed in the scheme either for normal system operation or for energisation and low demand operation.

#### 5.4 Point-to-Point LFAC TS Schemes for OWF Integration

This section discusses the design considerations and results for the PtP power-flow cases as listed in Table 5-1, with one LFAC cable and possible shunt reactors only at the onshore end.

In No-Load cases, the minimum shunt compensation to keep the cable charging breaking current lower than 0.355kA for each case is: 15MVAR for PF1-100km, 230MVAR for PF2-200km, 460MVAR for PF3-300km and 705MVAR for PF4-400km transmission. This amount of shunt compensation, together with the MMC capacity, keep the onshore 345kV busbar voltage to 1p.u. in No-Load conditions. Though, these shunt reactors may be full in service only during light-load conditions to prevent the high voltages of the Ferranti Effect or the high breaking currents and may be switched off or partially used in other loading conditions.

In Full-Load cases the frequency converter reactive power contribution can be up to 0.56p.u. or 476MVAR per MMC according to 5.2.2.2, while converter transformers absorb 45MVAR.

##### *a) OWF RPC with $Q_{ref}=0$ at 345kV Offshore Cable Sending End.*

Since the full cable inductive compensation needed for PF1 is 210MVAR as calculated in Chapter 3, no shunt compensation would be necessary for either case PF1- without or PF1ah- with 300MVAR of damping harmonic filters, as the 16.7Hz side MMC Terminal (T1) is able to operate at both of these states and maintain onshore 345kV busbar voltage at 1p.u.

In PF2, the full cable compensation is 420MVAR which is within the LFAC side MMC-T1 capability, and thus no shunt compensation is needed for case PF2a. However, case PF2ah should utilise the 230MVAR shunt reactors installed due to the No-Load PF2 case, in conjunction with the MMC capability.

In PF3, since the full cable compensation is 635MVAR, both PF3a and PF3ah cases should utilise the 460MVAR shunt reactors installed for the No-Load PF3 case, in conjunction with the MMC capability to avoid voltage drop at the 345kV busbar.

Theoretically, 850MVAR of inductive compensation is needed for full cable compensation in PF4. However, bus voltage limit violations and overloading of cables and transformers in the system do not allow the load-flow algorithm to converge and reach a steady-state operation.

*b) OWF ACVC with  $V_{ref}=1p.u.$  at 345kV Offshore Busbar.*

In Full-Load cases examined in which the OWFs apply ACVC, no shunt reactors were needed, and cable reactive power compensation can be entirely dispensed among the LFAC side converters, except case PF4bh that requires using extra 150MVAR out of the 705MVAR installed for the No-Load PF4 case.

### 5.4.1 Overall Results Evaluation

For the PtP LFAC TS schemes, Table 5-2 presents the Total Power Losses, Reactive Power Compensation and Voltage Regulation of the examined Full-Load cases listed in Table 5-1. The results are reviewed graphically in Figure 5.8 and compared in the analysis that follows.

*Table 5-2: Evaluation Criteria for the PtP LFAC TS Cases (Dark Colouring for Higher Values).*

[%]	Total System Voltage Regulation				Total Power Losses				Total Reactive Power Compensation			
	RPC		ACVC		RPC		ACVC		RPC		ACVC	
	a	ah	b	bh	a	ah	b	bh	a	ah	b	bh
<b>PF1 - 100km</b>	10	12	4	6	5.7	6.0	5.7	5.9	48	88	27	67
<b>PF2 - 200km</b>	20	21	6	9	9.4	9.7	9.1	9.3	76	118	54	95
<b>PF3 - 300km</b>	29	31	9	11	13.9	14.1	12.6	12.9	109	150	83	123
<b>PF4 - 400km</b>	N/A	N/A	14	15	N/A	N/A	16.3	16.5	N/A	N/A	114	155

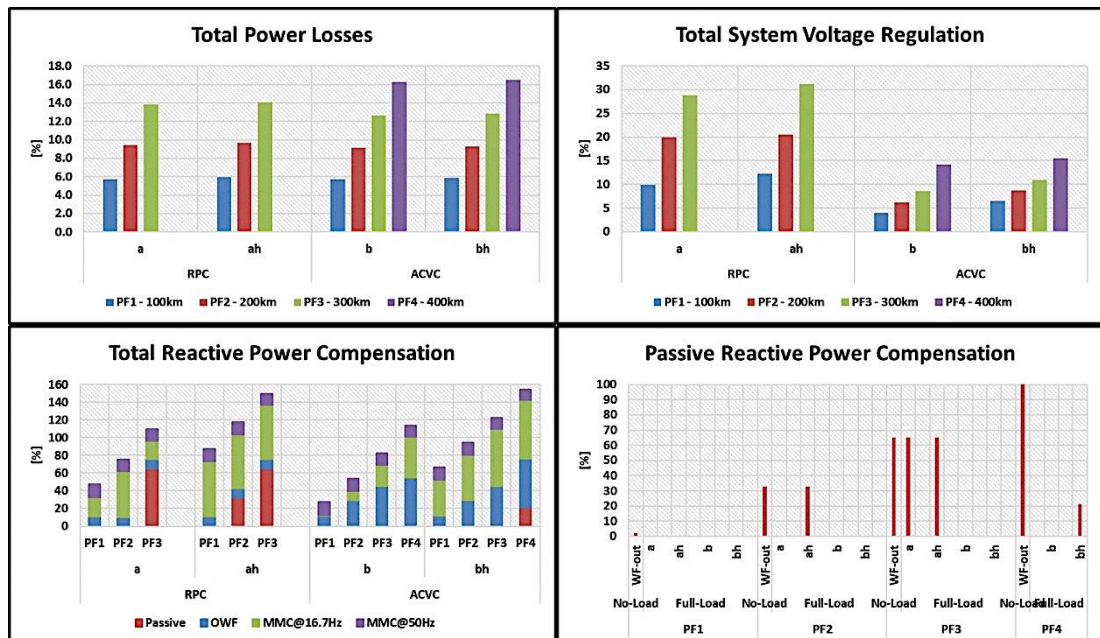


*Figure 5.8: Top Graphs: Total Power Losses and Voltage Regulation, Bottom Graphs: Total and Passive Reactive Compensation, for the PtP LFAC TS Cases.*

As expected, the most dominant factor that considerably increases the total power losses, voltage regulation and reactive power compensation of the system, is the length of the LFAC export cable. For the same cable lengths, the application of harmonic filters that attenuate the system resonances at the onshore 362kV GISs largely increases the onshore reactive compensation needed and to a smaller extent the power losses of the system. Moreover, the bottom graphs demonstrate that when the system employs passive harmonic filters (h-cases) in full-load operation, it is more probable to utilise (even partly) the shunt reactors that are installed for system compliance with the breaking charging current limit at no-load operation. In addition, when the OWFs apply RPC (a) instead of ACVC (b) the total voltage regulation of the scheme upsurges significantly, and more reactive compensation per case is needed to keep the system operation stable. Thus, passive shunt compensation is added to the cable at the onshore end, increasing further the total power losses for the respective cable lengths. Shunt reactors are also needed in (ah)-cases with added harmonic filtering, for cables longer than 150km while in (bh)-cases they may only be partly utilised for cables longer than 350km. Hence, from a system techno-economic feasibility perspective, the ACVC strategy shall be selected for operating the OWTGs, while the damping filters shall be avoided if possible.

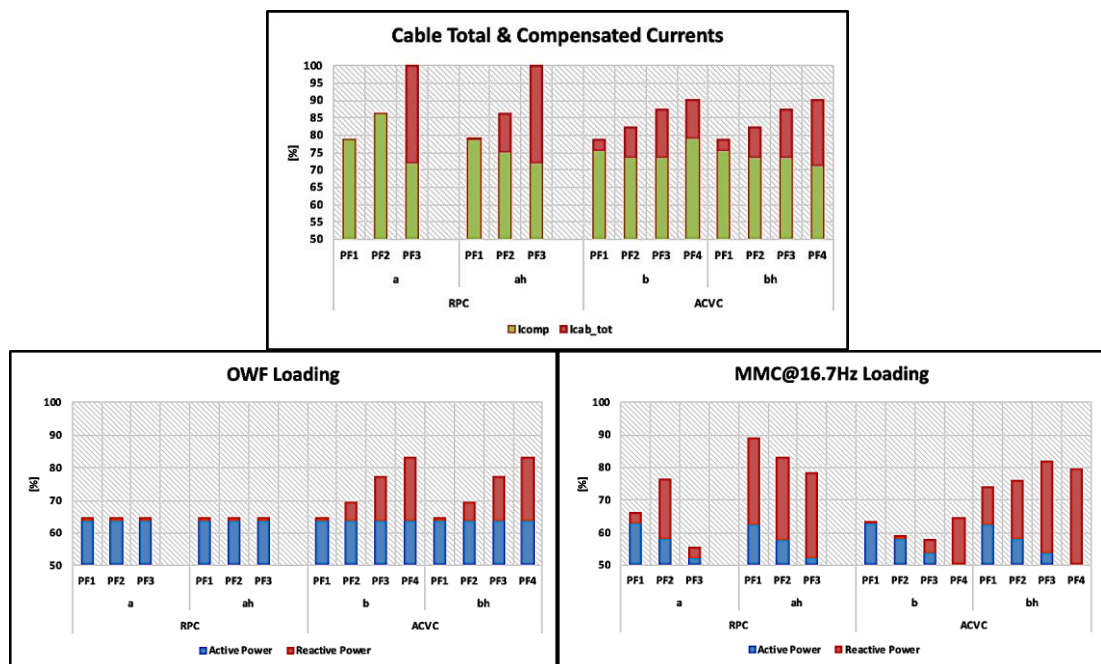


Figure 5.9: Top Graphs: Cable Total and Compensated Currents Loading, Bottom Graphs: OWF and MMC-T1 Loading, for the PtP LFAC TS Cases.

Apart from the overall system steady-state performance, there are some critical aspects regarding the operation of specific components such as the cables' charging currents, the loading of converters, etc. that should be kept within a specified range. The loading



percentages of the active and reactive power of the OWTGs and MMCs (in  $\%(P, Q/S)^2$ ), as well as the total current of the LFAC export cable and its current after compensation, are illustrated in the related graphs of Figure 5.9, for all the export cases.

It is obvious that the loading of the cable is significantly reduced in (b) cases that utilise the reactive power capability of the OWTGs, without the need for additional shunt compensation in most cases. The WTGs can provide the amount of compensation needed to adjust the voltage level offshore without reaching their reactive power capability limits. This facilitates the desired absence of shunt reactors at the offshore end of the cable. The onshore MMC-T1 reaches its reactive power capability limit in all the (ah) cases adopting harmonic filters or even in (a) cases for cables longer than 250km, while in (b) cases is reached only for cables longer than 350km that also adopt damping filters (PF4bh).

In particular, PF3a and PF3ah cases show that by using RPC arrangement in the OWF, the LFAC cable reaches its maximum loading before being compensated at its onshore receiving end. Thus, cables longer than 300km should not be used for such single-cable LFAC export schemes without utilising any offshore reactive power support either from the OWTGs or from any additional shunt reactors, as both-ends compensation should be applied.

Generally, exploiting the reactive power capability of the OWF means that almost 500MVar of dynamic reactive power compensation are available into the offshore side of the cable, minimising the need for placing additional passive shunt compensation in the offshore platform, regulating the system voltage profile adequately, reducing the power losses and charging current through the cable and improving the overall system stability. It also refines the onshore compensation management, as less reactive power is required by the onshore MMCs and no shunt reactor is needed in Full-Load operation, except for cases with LFAC cables longer than 350km. Then, part of the already installed reactors that are applied during the system energisation (No-Load) to mitigate the cable braking current shall be used.

Since the (b) set of cases with WTGs applying ACVC outperforms the (a) set in every operating aspect for the selected scenarios with only onshore shunt compensation, an overall optimised LFAC TS reactive power strategy shall include the offshore 345kV voltage support offered by the reactive power capability of the OWTGs. Therefore, the (b) cases for 100km-300km long LFAC cables that are also more practical in terms of power losses compared to longer cables are more thoroughly examined in section 5.4.2 and they are employed to form the meshed, Multi-Terminal LFAC arrangement that is assessed in section 5.5.

## 5.4.2 Feasible Point-to-Point Cases Examination

In this section, a detailed overview of the PtP LFAC TS (b) cases is presented for Full-Load operating conditions. Figure 5.10 shows the Power Losses, Voltage deviation and Reactive Power Compensation degree in each main busbar of the examined export cases utilising the OWTGs ACVC approach, for 100km-300km cable lengths.

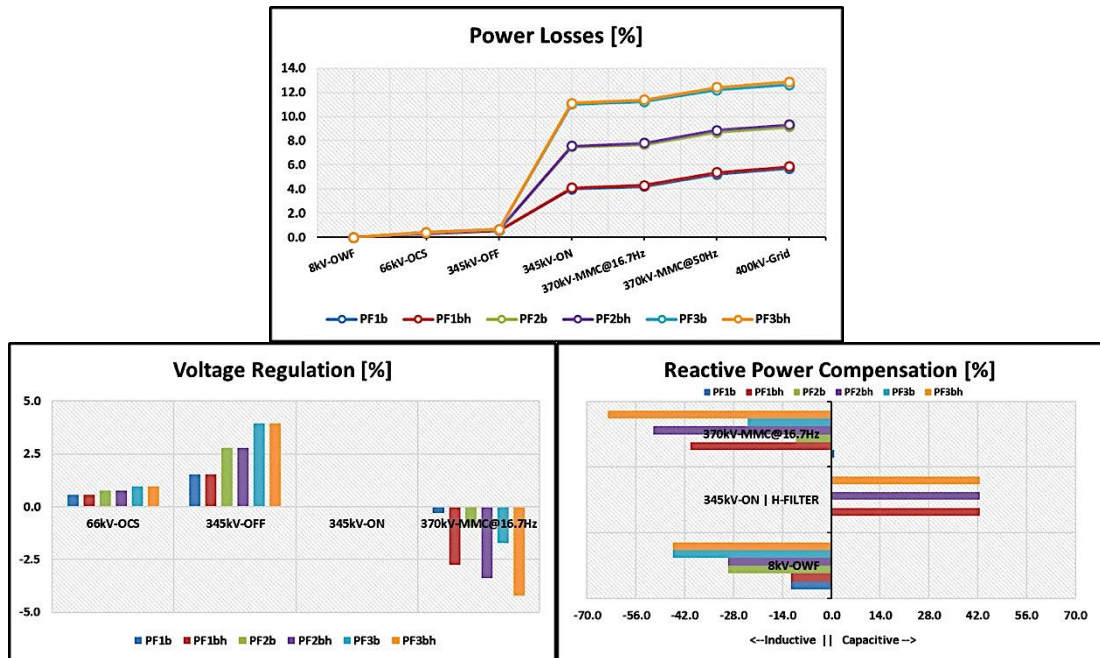


Figure 5.10: Power Losses, Voltage Regulation and Reactive Power Compensation, in each Main Busbar, for the Optimised PtP LFAC TS Cases.

It is evident that the main contributing factor to the power losses, voltage deviation and the amount of reactive power compensation in the scheme is the LFAC subsea cable. Depending on its length it can cause from 3.5% losses for 100km to 10.5% for 300km, while the onshore BtB MMC system with its converter transformers and other related equipment present almost fixed losses of ~2%. The biggest voltage deviation in each scenario appears in the offshore 345kV busbar that is droop controlled by the OWTGs absorbing the corresponding reactive power at the 8kV VSI output, without reaching their capability limits. Relatively high divergence can be also noticed in the 370kV MMC output voltage for cases in which harmonic filters are employed, as the MMC tries to maintain the onshore 345kV busbar voltage at 1p.u., absorbing reactive power that reaches its capability limits for 300km cable length.

Figure 5.11 shows the voltage and current distribution in the cable for these cases. The highest voltages and currents occur at the offshore cable end. Yet Again, the bigger the cable length, the higher the current and voltage values are at the offshore end of the cable as well as the power losses, and the bigger are the variations of both quantities within the cable. The



maximum loading of the cable, though, is less than 90% even for the 300km case and the maximum voltage difference between the two ends of the cable is 4%, respectively. Hence, no shunt reactive compensation is needed in any of the cable-ends for these cases.

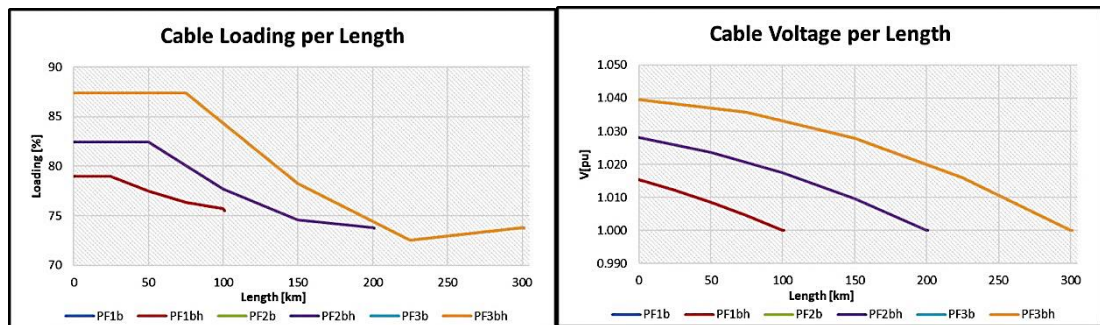


Figure 5.11: Current and Voltage Distribution in the Cable, for the Optimised PtP LFAC TS Cases.

Finally, Figure 5.12 shows a linear approximation of the LFAC cable current profile between its offshore and onshore ends plotted against its real and reactive current counterparts and its maximum current limit. In addition, the operating points of the 16.7Hz and 50Hz side MMCs are plotted in the active-reactive power domain against their desired capability limits.

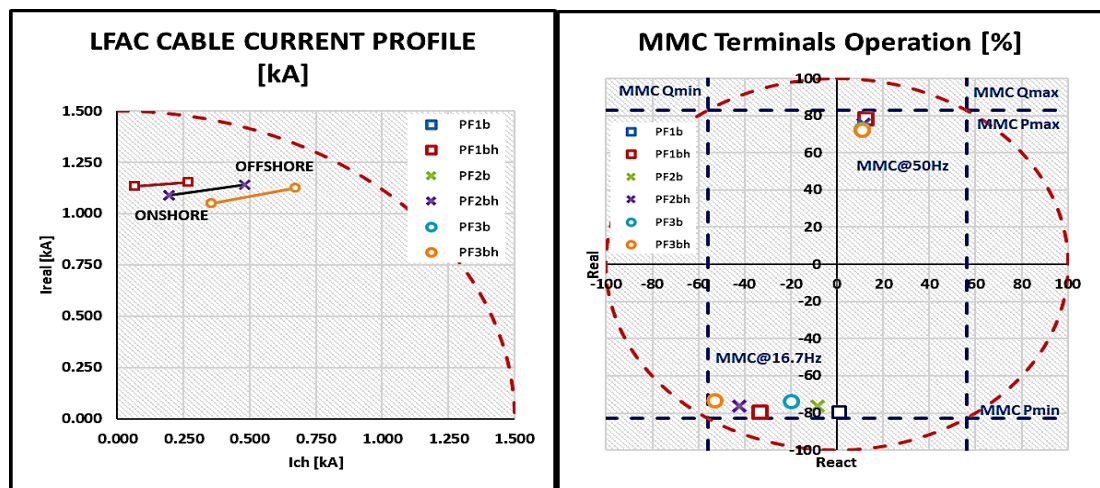


Figure 5.12: LFAC Cable Current Profile and Operating Points of the Frequency MMC against their Real and Reactive Counterparts, for the Optimised PtP LFAC TS Cases.

In these plots, the active current flowing through the cable decreases due to its resistance, while the reactive part due to the dynamic compensation offered by the VSCs in both ends of the cable, resulting in a total much lower current at the onshore 345kV end of the cable than its maximum current limit (1.5kA). Moreover, the grid-forming MMC facing the 16.7Hz network operates close to its specified maximum reactive power limit in case PF3bh. Hence, for schemes using cables longer than 300-350km, shunt compensation is needed. In general, as the LFAC cable length increases, more reactive power is needed by the VSCs to adjust the voltage level on the LFAC network, while there is no impact to the VSCs facing the 50Hz grid.

## 5.5 Multi-Terminal (Meshed) Offshore LFAC TS Schemes

Figure 5.13 shows a meshed-interconnected offshore LFAC TS approach that can be utilised to enable the exchange of power between different grids or different substations (points) of the same grid, as well as the power export of two interconnected offshore windfarms. For this scheme, two cables are utilised, and there are four transformer sets of three single-phase units each, placed in two distant platforms.

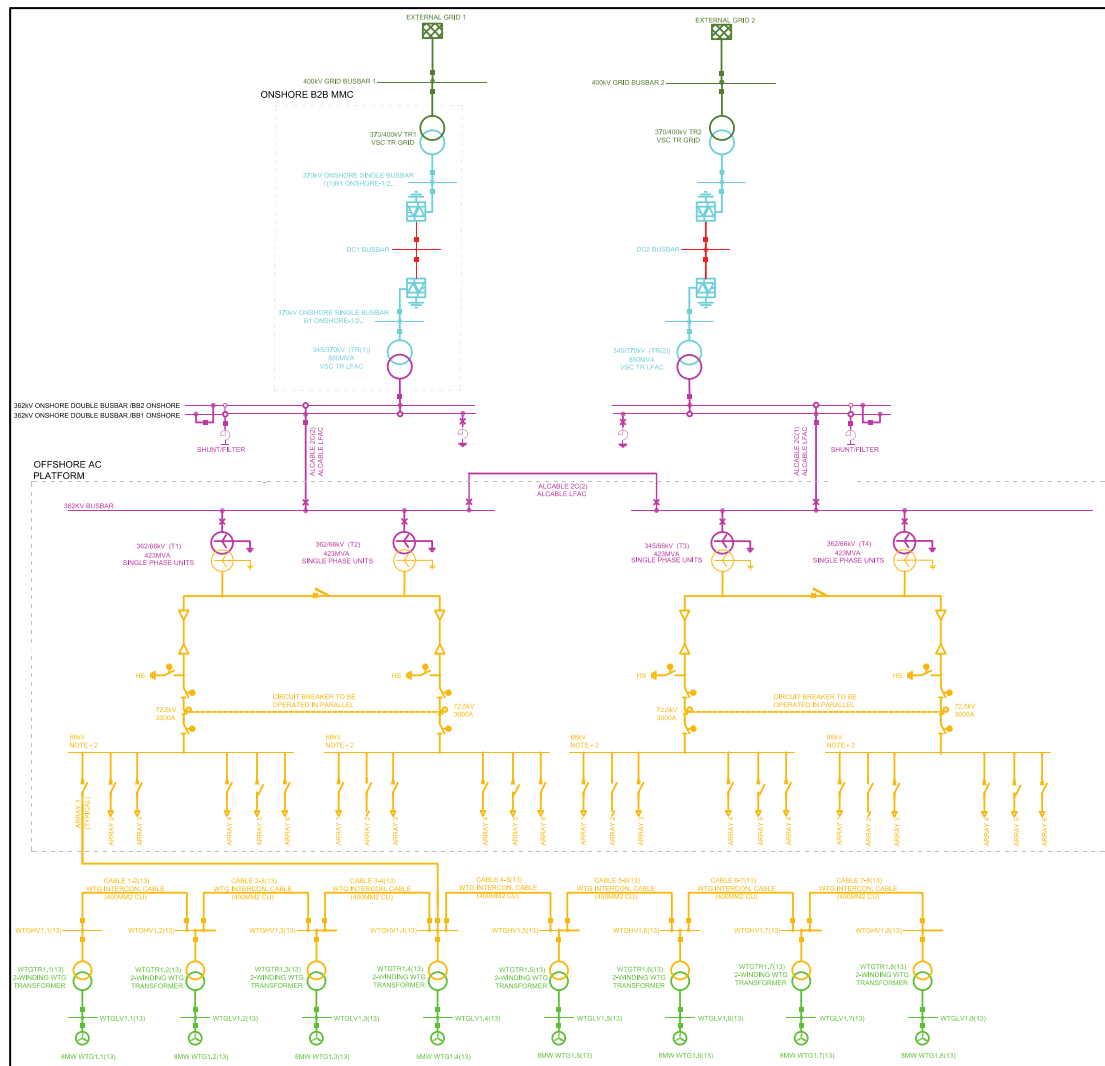


Figure 5.13: SLD of the MT-LFAC TS Configuration.

In the above arrangement, the shunt passive elements placed in the onshore 362kV busbars may be case-dependent, as it may even be possible to mitigate the effects of potential system resonances by applying suitable active control arrangements in the onshore MMC system. In addition, the compensating shunt reactors represent the additional reactive power that needs to be absorbed by the converter system in case it provides dynamic compensation.

### 5.5.1 Set-Up of Meshed LFAC TS Power Flow Cases

In this section, the steady-state performance of an offshore MT-LFAC TS scheme is assessed. This MT-LFAC system comprises of two equivalent PtP schemes, the Side 1 and Side 2 systems, each having a 704MW OWF, an offshore LFAC platform with two step-up transformers and a 200km subsea export cable that is integrated to a separate 50Hz grid through an onshore BtB MMC-HVDC system, with one of its terminals facing the 16.7Hz side (MMC-T1) and the other the 50Hz grid (MMC-T2). The systems are interconnected at their offshore 345kV high-voltage side through an identical 50km, 1400mm<sup>2</sup>Al-XLPE, LFAC subsea cable. The ACVC strategy for the OWTGs that results in a more efficient export system, as seen in section 5.4.2, is also applied here to establish a more feasible MT-LFAC TS, that could also support a practical standalone Side 1 and/or Side 2 OWF power export operation.

Power flow study PF5 (and PF5h - with harmonic filters) is set-up for five separate cases with different operating scenarios. These cases are listed in Table 5-3, and described below. The various scenarios are assessed to determine the maximum size of shunt reactors that would need to be installed at the onshore end of the 200km LFAC cables (315MVar without and 620MVar with H-Filters) regardless the specific amount of MVar needed for each operating scenario. In this work, only cases PF5d and PF5e are explicitly analysed in the next sections of this chapter and further investigated in EMT simulations of the MT-LFAC TS in Chapter 7.

Table 5-3: List of the Power-Flow Cases for the MT-LFAC TS.

List of Meshed Power Flow Cases								
PF	Cables & Control	Cases	Scenario	Power Transfer	Shunt Reactor [MVar]			
					PF5 - Side 1	PF5 - Side 2	PF5h - Side 1	PF5h - Side 2
PF5	2 x 200km + 1 x 50km with 2 x OWFs ACVC	a) LFAC TS ENERGISATION	2 x OWF OUT NO ACVC	No Load Side 2	315	315	315	315
			2 x OWF IN ACVC ONLY		315	315	315	315
		b) GRID INERCONNECTION POWER EXCHANGE ONLY	2 x OWF OUT NO ACVC	Max Load Side 2 ~380MW	315	0	620	0
			2 x OWF IN ACVC ONLY	Max Load Side 2 ~530MW	315	0	450	0
		c) 1 x OWF FULL EXPORT & GRID IC POWER EXCHANGE	2 x OWF IN 1 x FULL POWER 1 x ACVC	Half Load Side 1, 2	0	0	150	150
				Full Load Side 2 ~704MW	150	0	450	0
d) 2 x OWF EXPORT & GRID IC POWER EXCHANGE	2 x OWF IN 2/3 OF POWER	Full Load Side 2	120	0	420	0		
e) 2 x OWF FULL POWER EXPORT	2 x OWF IN FULL POWER	Full Load	0	0	0	0		

The listed cases in the above Table are described as follows:

- **Case-a:** examines the meshed LFAC TS energisation with Side 1 MMC-T1 (or MMC1-T1) forming the LFAC voltage in the system, without a load in Side 2. In the first scenario of case-a, both OWFs are disconnected from the scheme, while in the second scenario OWFs are connected to the system applying ACVC to their respective offshore 345kV busbars,

without supplying real power. In all energisation scenarios, 315MVAR of onshore cable shunt reactors can be adequate in both Side 1 and 2.

- **Case-b:** examines the meshed LFAC TS that interconnects the two 50Hz grids, with MMC1-T1 forming the LFAC voltage in the system and supplying the maximum possible load in Side 2. In the first scenario of case-b, both OWFs are disconnected from the scheme, and the maximum load that can be supplied in Side 2 is 380MW. In the second scenario, the OWFs are connected to the system, only applying ACVC, and then the maximum possible load that can be supplied in Side 2 becomes 530MW. Without employing harmonic filters, the application of 315MVAR of shunt reactors in Side 1 can be adequate for both scenarios, though, with 300MVAR of damping filters, the installation of up to 620MVAR of shunt reactors is required in Side 1 for scenario 2, utilising up to 450MVAR for scenario 1.
- **Case-c:** examines the meshed LFAC TS that interconnects the two 50Hz grids and exports full power from the OWF of Side 1 (or OWF1), while OWF2 applies ACVC to its respective offshore 345kV busbar and produces zero power. In the first scenario, each of the MMC1-T1 and MMC2-T1 absorb half the amount of power produced by OWF1, while in the second scenario, MMC2-T1 demands 704MW which is more than the OWF1 can supply considering the losses of the LFAC TS. Hence, MMC1-T1 supplies the rest of the demanded power to MMC2-T1, interconnecting the two grids. This operation needs adopting shunt reactors in Side 1 that can be up to 150MVAR or even 450MVAR with harmonic filters.
- **Case-d:** examines the meshed LFAC TS that interconnects the two 50Hz grids and exports power from both OWF1 and OWF2. Each OWF supplies 1/3 of the total power to MMC2-T1 and applies ACVC to its corresponding offshore 345kV busbar. In this scenario, MMC2-T1 constantly demands full power with both OWFs supplying 2/3 of it and MMC1-T1 supplying the rest 1/3 of the requested amount of power to Side 2 load, interconnecting the two grids. Only 120MVAR of onshore shunt reactors are needed in Side 1 to achieve this operation without harmonic filters and 420MVAR if damping filters are adopted.
- **Case-e:** examines the meshed LFAC TS for exporting full power from both OWF1 and OWF2 with MMC2-T1 demanding full power, and thus MMC1-T1 also receiving the full power output of OWF1. This case integrates the two different interconnected OWFs to different grids using separate LFAC export systems since almost no power is exchanged through the 50km interconnection cable. Hence, PF5e and PF5eh cases can be seen as an aggregation of two PF2b or PF2bh cases, respectively, having no need for shunt reactors.

### 5.5.2 Full Power Export of the Two OWFs – (PF5e)

The MT-LFAC TS Power-Flow case PF5e (and PF5eh) that uses 200km subsea cables to export the full power output of OWF1 and OWF2 is equivalent with two PF2b (and PF2bh) Full-Load export cases in which the offshore platforms are interconnected through a 50km subsea cable. The Power-Flow results obtained for this operating scenario show that the total system power losses are 9.5% and 9.7% for cases PF5e and PF5eh respectively, which is 0.4% higher than the equivalent export cases, due to the extra losses introduced by the 50km cable link. Moreover, their total voltage regulation is almost double compared to the PtP cases, as the meshed scheme comprises twice the number of buses, while the reactive compensation has increased by 15% to reach 110%, all supplied by the converters of the LFAC TS.

The highest system voltage (1.03p.u.) is noticed in the offshore 345kV busbars, while the lowest voltage (0.963p.u.) in the output of both the MMC1-T1 and MMC2-T1 370kV busbars of PF5eh, as the converter voltage response is reduced to compensate for the 300MVAR harmonic filters added to each of the onshore 345kV busbars if no MVARs from shunt reactors are utilised. The damping filters are also responsible for the increase in the output currents of the onshore 345kV busbars from 1.114kA to 1.321kA. Finally, as in most cases, the steady-state operation of MMC-T2 converters facing the two separate 50Hz grids of Side 1 and Side 2, remain relatively unaffected by the operating conditions of the 16.7Hz LFAC TS.

### 5.5.3 Partly OWFs Export & Grid Interconnection Power Exchange (PF5d)

In the MT-LFAC TS Power-Flow case PF5d (and PF5dh), the MMC2-T1 demands full power with both OWF1 and OWF2 generating 2/3 and MMC1-T1 supplying the rest 1/3 of the requested power. In these conditions, to supply MMC2-T1 with full power, 120MVAR of shunt compensation shall be applied at the onshore 16.7Hz Side 1, out of the 315MVAR installed for energisation. Though, if damping filters are employed, then 420MVAR out of the installed 620MVAR shall be used. For these cases, the total voltage regulation is much better than for cases PF5e and PF5eh (9.9% and 11.7% instead of 13.6% and 18.6 % respectively), but they employ almost the same amount of compensating MVARs to those utilised in the full-power (1408MW) meshed cases for nearly half of total generated power in the LFAC TS. Besides, the losses here (120MW and 122MW) are lower than in the cases PF5e and PF5eh (134MW and 137MW), although the percentage of total system losses corresponding to the power input to the LFAC scheme can be much higher 15.8% and 16.1% instead of 9.5% and 9.7%. The corresponding graphs of Figure 5.14 demonstrate the results in terms of power losses, reactive compensation and voltage regulation in the busbars of this scheme.



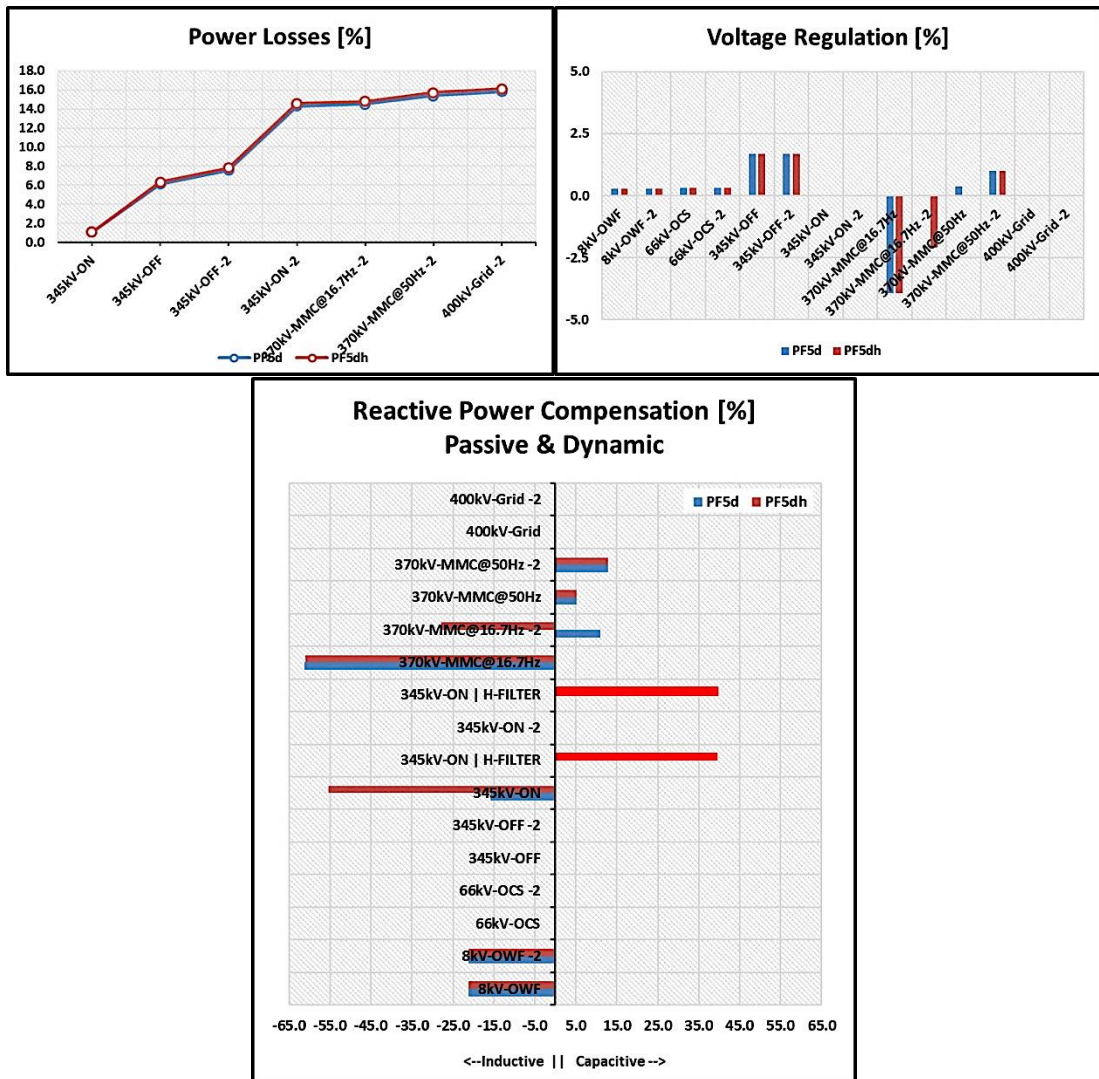


Figure 5.14: Power Losses, Voltage Regulation and Reactive Compensation in each Main Busbar of the MT-LFAC TS, for Cases PF5d and PF5dh.

As discussed, the losses in Side 2 are ~6.5% for the cable and ~2% for the BtB MMC-HVDC system, which is almost the same in MWs with the equivalent PF2b and PF2bh export cases. However, in cases PF5d and PF5dh, this percentage comes along with ~4.5% of additional losses in the 200km cable of Side 1 and ~1.5% in the 50km offshore interconnection cable. On top of these, there is an additional ~1.5% of losses in the OWFs and their VSCs, resulting in a total of ~16% losses, with respect to the total input power of 759MW to the MT-LFAC TS.

The lowest voltage drop is retrieved at the MMC1-T1 370kV level for both examined cases, as the MMC reduces its voltage output to keep the voltage level of the onshore 345kV busbar at 1p.u., by absorbing the reactive power coming from the LFAC cable system (and the harmonic filter for PF5dh). Even though additional shunt compensating reactors are applied utilised, the MMC1-T1 still operates near its reactive power limit, as shown in the 'Converter

Operation' graph of Figure 5.15. Furthermore, the highest current (1.364kA) is noticed at the offshore 345kV busbar of Side 1, while the lowest is in the onshore part of the corresponding cable, after the reactors. This occurs because power is induced to the system by the MMC1-T1 to supply the MMC2-T1 through an equivalent 450km subsea cable, while more active power is added at 200km and 250km respectively. The cable is compensated by the dynamic voltage support of MMC1, OWF1, OWF2 and MMC2 at 0, 200km, 250km and 450km of its length, with extra passive compensation at 0km. More details for the loading of the export cables in the scheme are shown in Figure 5.15.

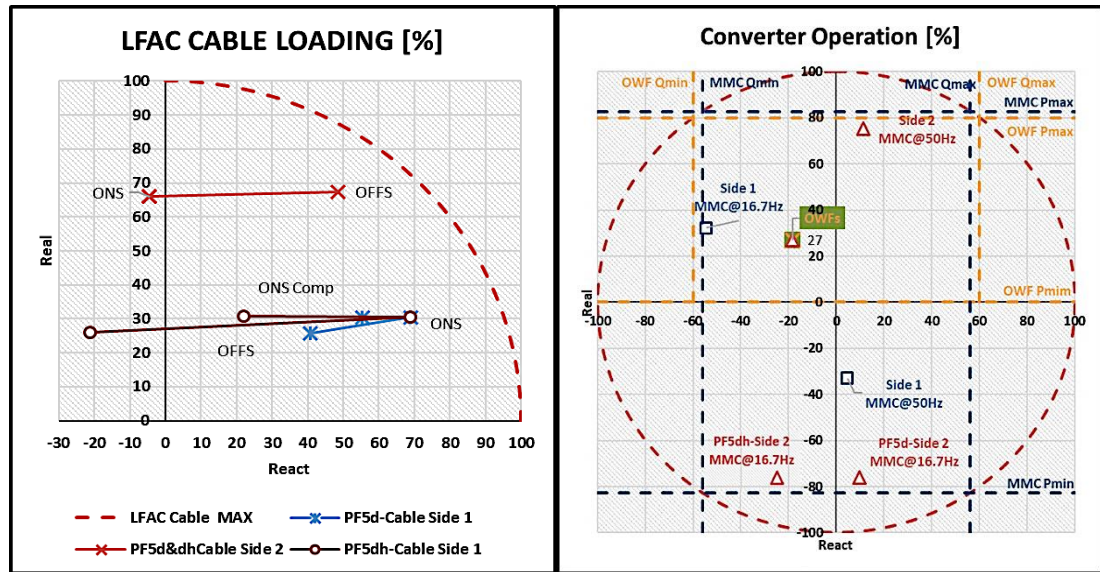


Figure 5.15: LFAC Cable Current Loading and Operation of the MMCs against their Real and Reactive Counterparts, for the MT-LFAC TS Cases PF5d and PF5dh.

The impact of the onshore compensation on the reactive current of the cable in Side 1 can be observed in the 'LFAC Cable Loading' graph of Figure 5.15. In case PF5dh the current becomes inductive on the offshore side of the 200km cable. However, the added 50km cable, in combination with the extra amount of power by OWF1 and OWF2 leads the cable to be further loaded and get closer to its maximum loading limit in offshore Side 2. The dynamic compensation offered by the OWF2 and the MMC2-T1 at the respective offshore and onshore sides of the cable leads to an inductive current at the onshore Side 2, which is useful especially if passive damping filters are present.

Overall, this case investigates an MT-LFAC TS that exports power from two OWFs and interconnects them, also enabling the power transfer between two different 50Hz grids. This MT-LFAC TS transfers power utilising only one subsea cable from each point of connection to the other over 450km without any passive shunt reactor installed in an offshore platform.

## 5.6 Summary and Conclusions

In this chapter, the LFAC TS steady-state performance is evaluated through a power-flow assessment. Steady-state models of the offshore PtP and MT-LFAC TS arrangements are produced for various export cable lengths, as designed and rated in Chapter 3. The LFAC TS main components are explicitly represented in these steady-state models that comprise the AC grids with their SCL and X/R characteristics, the LFAC export system with its LFAC submarine cables (distributed-constant parameter models), their shunt reactors (when needed), the LFAC step-up transformers and potential filtering equipment (as defined in Chapter 4), the OCS with its inter-array cables (pi-equivalent models), as well as the onshore BtB frequency MMC system and the OWTGs with their envisaged capability limits.

Power-flow studies of the PtP and MT-LFAC TS schemes are performed under Full-Load and No-Load operating conditions (LFAC TS energisation procedure) for various cable lengths with or without harmonic filtering application. Initially, a particular set of power-flow studies is designated for PtP LFAC TS arrangements to determine the most feasible schemes in terms of voltage regulation, total power losses, total reactive power compensation, the amount of the extra passive compensating equipment needed as well as the components loading. The produced PtP schemes are further assessed to evaluate the impact of cable length as well as the implemented mitigation measures on the system, and they are employed to establish and coordinate an efficient offshore MT-LFAC TS design that could be suitable for OWP export and grid interconnection.

Thus, optimised PtP and MT-LFAC TS schemes are produced in terms of minimum power losses and shunt compensation, placed only onshore. The efficient DCVC/ACVC OWTGs' inverter strategies are adopted while the reactive power capability of all the existing converters in the scheme is utilised, maximising the power transfer through the cables up to certain lengths in which the Ferranti effect or excessive losses would prevail. In addition, the LFAC TS compliance with operating standards is assured in terms of bus voltage levels, CBs' charging breaking currents, equipment loading and converter capability limits under various operating conditions for cases with and without passive harmonic filters.

Based on the optimised configurations produced in this Chapter, a comprehensive EMT analysis of the LFAC TS is performed in Chapter 7, while a quantitative LFAC TS availability assessment is presented in APPENDIX B. There, a comparative availability study is performed for the competitive offshore export technologies on a like-for-like basis.



## Chapter 6: System EMT Modelling and Controller Design

### 6.1 Introduction

In this chapter the detailed equivalent time-domain models are developed that are used in the EMT simulations of Chapter 7. EMT simulations are performed, as the phenomena involved in the dynamic performance of the offshore LFAC TS can be significantly outside the bandwidth of RMS simulations that use phasor equations to represent the positive-sequence phasor-time response of the electrical network. EMT analysis solve the system differential equations, as the models include the non-linear response of electrical devices (e.g. switching components, transformer saturation, surge arresters, etc.) and they are suitable for investigating dynamic performance, harmonic stability issues, resonant conditions, transient overvoltages and the control interactions among power electronic devices and the network.

The detailed modelling of each element of the system using manufacturer data could have been an ideal solution for accurately representing the dynamic response following events such as faults and evaluate the EMT stability. Though, as the number of nodes increases in the model, it becomes more challenging to model and computationally intensive to simulate the dynamic performance of a complex system. To achieve a reasonable balance between the accuracy and the computational burden involved in the time-domain simulations of such large-scale models, aggregation modelling techniques are employed with proper representation of the necessary functionalities for the specific EMT assessment [86].

To assess the dynamic performance of the optimised PtP and MT-LFAC TS configurations produced in Chapter 5, the cases with 200km submarine export cables and 50km OCS interconnection cables are further investigated. Each aggregate OWF module corresponds to several OWTGs and comprises a BtB VSC-HVDC system with two-level IGBT bridges. At the same time, the onshore frequency MMC terminals include several sub-modules that shall be aggregated without compromising the required accuracy. Moreover, as the transmission in the offshore LFAC networks occurs through long subsea cables, accurate representation using the frequency-dependent phase model described in Chapter 4 is essential, at least for those cable lengths that allow a travelling-wave within a reasonable simulation time step.

In the following sections, the time-domain modelling of the key LFAC TS components is described and evaluated in PSCAD EMTDC, while the related control systems' transfer function analysis is performed using MATLAB.

## 6.2 System EMT Modelling

### 6.2.1 AC Grid Representation

The 50Hz AC grid must be strong enough to exchange power with the LFAC TS, as this is interfaced to the grids through back-to-back frequency MMCs. The AC system should have certain Short-Circuit Capacity (SCC) and sufficient inertia to maintain the required voltage and frequency. The strength of the AC system at the PCC with an MMC can be characterised by the Short-Circuit Ratio (SCR) as defined by Equation (6.1), where  $V_t$  is the grid voltage at the PCC,  $P_{rat}$  is the rated power of the BtB frequency converter and  $Z_{mag}$  is the network impedance magnitude, with an angle  $Z_{ang}$  defined by its resistance  $R$  and reactance  $X$ .

$$SCR = \frac{SCC}{P_{rat}} = \frac{V_t^2 / Z_{mag}}{P_{rat}} \quad (6.1)$$

$$Z_{mag} = \sqrt{R^2 + jX^2} \quad \text{and} \quad Z_{ang} = \tan\left(\frac{X}{R}\right) \quad (6.2)$$

A system with SCR between 2 and 3 is considered weak, and if its SCR is greater than 3, it can be considered strong. As mentioned in the Load Flow studies of Chapter 5, the AC networks used in this work have an X/R of 20, while an SCC of 3400 has been assumed for the network in the point-to-point schemes corresponding to SCR of 4 and an SCC of 2550 for the second grid in an MT-LFAC configuration with an SCR of 3 respectively. A Thevenin equivalent circuit AC grid representation is adopted with a 50Hz-400kV voltage source connected to a parallel R-L branch in series with a resistor, as in Figure 6.1.

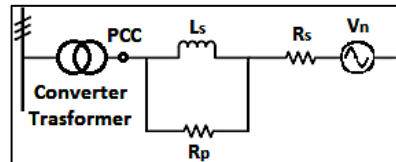


Figure 6.1: Equivalent Circuit for AC Grid Representation.

Table 6-1 presents the electrical parameters of the equivalent AC Grids used in this work.

Table 6-1: Equivalent AC Grid Parameters.

AC Grid System Characteristics			
Parameter	AC Grid1	AC Grid 2	unit
Vt	400	400	kV
fe	50	50	Hz
Pt	850	850	MVA
we	314.16	314.16	rad/s
SSC	3400	2550	MVA
SCR	4	3	
X/R	20	20	
Zsmag	47.06	62.75	Ohm
Zsang	87.14	87.14	Deg
Rp	6283	6283	Ohm
Ls	0.150	0.199	H
Rs	2.00	2.51	Ohm

### 6.2.2 Cable EMT Model and Energisation

The three-phase LFAC submarine XLPE-Al cable with a conductor cross-section area of  $1400\text{mm}^2$  is modelled in PSCAD EMTDC using the distributed parameter frequency-dependent phase model representation as described in Chapter 4. A trefoil configuration inside a pipe has been considered following the manufacturer's specifications and applying the required adjustments between the provided data and cable constants. Regarding the intra-array and array cables, only  $\pi$ -sections are used, as these cables are relatively short, not allowing a travelling-wave model with a  $50\mu\text{s}$  EMT simulation time step.

With a sharp voltage variation in a system, like a step or a pulse, most frequencies of the harmonic spectrum are excited. Thus, it is possible to assess the results in conjunction with their frequency responses. In the LFAC export system, cable energisation takes place only from the onshore end. Energization transients are simulated to examine any need for pre-insertion resistors, synchronized switching or line surge arresters or if the cable insulation is adequate. The cable models developed in the preceding sections are examined to characterize different frequency-dependent effects like EM propagation, damping due to skin effect and reflections, according to [95]. However, instead of a DC voltage step, an AC voltage step is used, i.e. an AC voltage source is suddenly connected to the cable. Therefore, the transient response of the designed cable model is obtained for a voltage step.

The LFAC cable is energised by a 345kV voltage source, as presented in Figure 6.2 and the results of the simulations carried out in PSCAD EMTDC are depicted in the following graphs of Figure 6.3. To carry out this analysis, a simulation of overvoltage and overcurrent during cable energisation is performed by closing the breaker in the worst-case scenario; when the LFAC voltage has the maximum value in phase-a at 0.0748s.

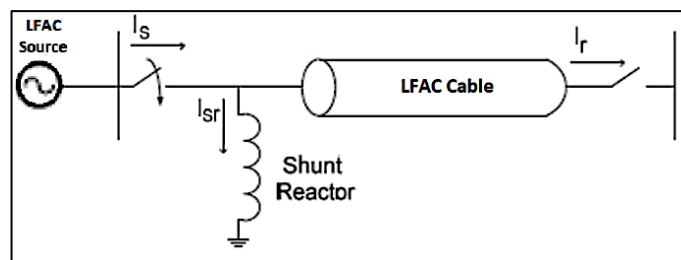
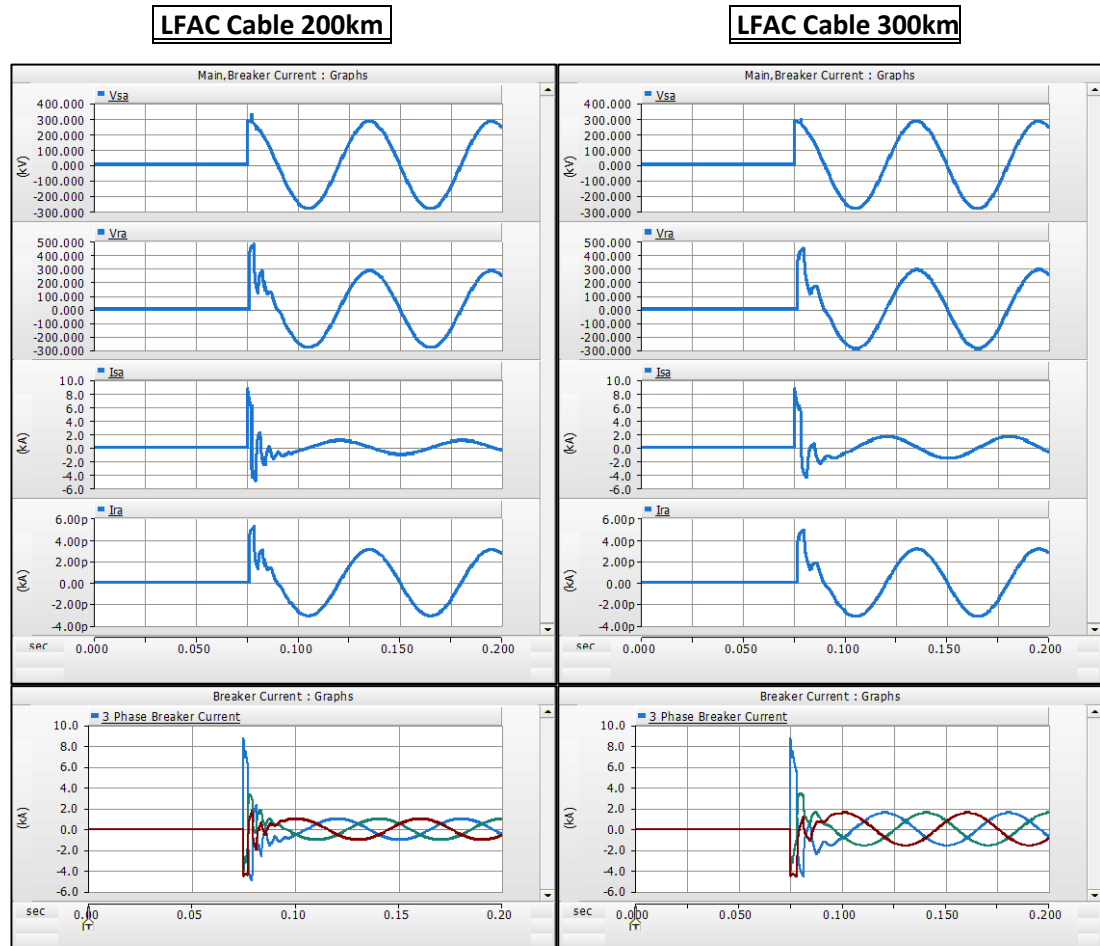


Figure 6.2: Equivalent Circuit for LFAC Cable Energisation Study.

Figure 6.3a,b, shows the graphs of the phase voltages and currents at the sending and receiving ends of 200km and 300km cables, during the energisation of each cable alone.

The symbols of the presented time responses in the graphs of Figure 6.3 are:

- **Vsa**: phase Voltage of the sending end [kV],
- **I<sub>sa</sub>**: current in the sending end [kA],
- **Vra**: phase Voltage of the receiving end [kV],
- **I<sub>ra</sub>**: current in the receiving end [kA].



**Figure 6.3:** Cable Energisation Graphs as they appear from Top to Bottom: Vsa, Vra, Isa, Ira and the Three-Phase Breaker Current, for a 200km (Left) and a 300km (Right) LFAC Subsea Cables.

The graphs show the phase voltages and currents at the sending and receiving ends of 200km and 300km cables when energising each cable alone (Figure 6.3), for the worst-case scenario; at the instant of phase A LFAC voltage peak. From these graphs, it can be inferred that the maximum overcurrent of  $\sim 8.8\text{kA}$  occurs in this phase for both cable lengths. However, the electromagnetic transients in the 200km system happen in higher frequency ( $\sim 210\text{Hz}$ ) than in 300km ( $\sim 130\text{Hz}$ ), which is an indication for the probable mitigation measures (e.g. for the insulation coordination). Finally, the reduced oscillations in the graphs of the 300km cable are mainly due to its increased damping offered by the increased cable resistance. This is also in accordance with the frequency scan studies in Chapter 4 for the respective cable lengths.

### 6.2.3 Onshore BtB MMC EMT Model

The representation of MMC VSC-HVDC systems in time domain presents challenges because of the large number of switches that can lead to computationally intensive EMT iterations. In this work, the onshore frequency MMCs operate with half-bridge sub-modules that are individually controlled. Due to the rated voltage of IGBTs and the associated sub-module capacitor ratings, the number of HBSMs per arm of each converter bridge is 128. Thus, the simulation of one or more full back-to-back MMC-HVDC systems can involve thousands of nodes, that can substantially reduce the simulation speed and become impractical.

The MMC modelling techniques range from very complex physics-based models with detailed semiconductor representation to simple voltage source equivalents. Very detailed models of these converters are very complex and impractical for EMT simulation studies due to the high number of switching operations performed by the MMC HBSMs, as every time a switch operates the whole network admittance matrix is inverted [86]. In contrast, Average Models (AVMs) compromise accuracy for computational efficiency and simulation speed.

There are three leading detailed modelling techniques which can simulate the HBSM capacitor voltages and the MMC arm currents that indicate whether the converter operates within its capacity limits during transient events. Those techniques are the Traditional Detailed Model (TDM), the Accelerated Model (AM) and the Detailed Equivalent Model (DEM). The DEM is used in this Thesis that has proven to be faster than the AM and the TDM while more accurate than the AM, offering a similar level of accuracy to the TDM [104].

In the DEM, each HBSM is replaced by an exact, but computationally simpler Thevenin equivalent circuit, as seen in Figure 6.4. The IGBTs and antiparallel diodes of each HBSM are patterned as a resistor ( $R_{HBSM}$ ) with two states (ON/OFF) with each state dependent on the arm current direction ( $I_{arm}$ ) and the IGBT firing pulse gate signal, while if the MMC is blocked the states of R1 and R2 only rely on the arm current direction [69]. The HBSM capacitance is assumed as an equivalent voltage source ( $V_{Cap_{eq}}$ ) connected in series with a resistor ( $R_{Cap}$ ).

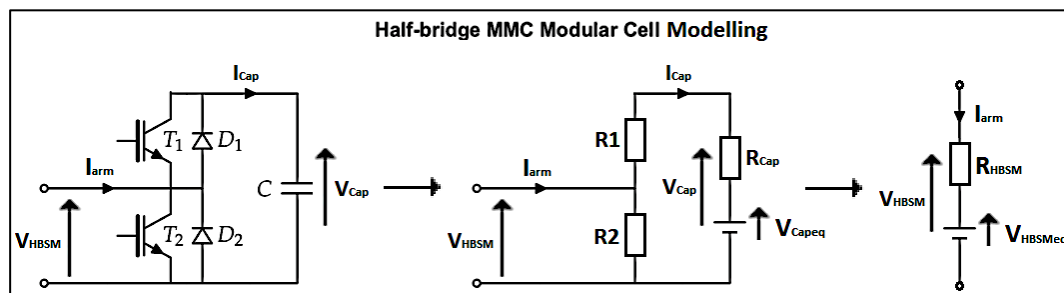


Figure 6.4: HBSM Switching Circuit (Left) to Thevenin Equivalent Circuit (Right) for MMC Cell Modelling.

The calculations require calculated as well as measured values from the current and the last time step by applying the trapezoidal integration method used in PSCAD EMTDC to solve the system's differential equations.

$$V_{Cap}(t) = V_{Capeq}(t - \Delta t) + R_{Cap}I_{Cap}(t) \quad (6.3)$$

Where:  $I_{Cap}(t) = C \frac{dV_{Cap}(t)}{dt}$  and  $R_{Cap} = \frac{\Delta t}{2C}$

The voltage at the terminals of the HBSM is given by

$$V_{HBSM}(t) = V_{HBSMeq}(t - \Delta t) + R_{HBSM}I_{arm}(t) \quad (6.4)$$

$$R_{HBSM} = R2 \cdot \left(1 - \frac{R2}{R1+R2+R_{Cap}}\right) \quad (6.5)$$

Solving Equation (6.4), using the trapezoidal integration method gives:

$$V_{HBSMeq}(t - \Delta t) = \left(\frac{R2}{R1+R2+R_{Cap}}\right)V_{Capeq}(t - \Delta t) \quad (6.6)$$

Since all the sub-modules in each converter arm are connected in series, a single Thevenin equivalent circuit can be calculated for each converter arm, with an equivalent voltage source ( $V_{armeq}$ ) and resistance ( $R_{armeq}$ ) and as shown in Equation (6.7), below:

$$R_{eq} = \sum_{i=1}^n (R_{HBSMi}) \quad \text{and} \quad R_{eq} = \sum_{i=1}^n (R_{HBSMeqi}) \quad (6.7)$$

The DEM version developed by PSCAD in Manitoba Hydro HVDC Research Centre team based on the work by Udana and Gole [127] is employed for modelling the MMC configurations in the course of this work. As explained above, the module significantly decreases the size of the admittance matrix for the EMT solver by representing the IGBTs and diodes with a two-state resistance improving the simulation speed and maintaining sufficient accuracy by calculating each HBSM capacitor voltages and currents separately [66].

Hence, the DEM model is suitable to perform EMT studies for LFAC and DC side dynamic performance analysis as well as for the design and tuning of both higher and lower level controllers such as the circulating current suppression controllers or the capacitor balancing algorithms. However, there are some general limitations associated with its use because the user cannot access individual HBSM components for studies that require internal converter access. Further details mentioned in the CIGRE TB 604 WG B4-57 "Guide for the development of models for HVDC converters in an HVDC grid" [86].

## 6.2.4 OWPP EMT Model

In contrast with MMC simulation models, the Two-Level VSCs have series connected IGBTs, and they need only two switches per phase and bridge, leading to a model with fewer nodes. Thus, a detailed representation of the power electronic switching elements can be utilized. As mentioned in Chapter 3, an aggregate 704MW back-to-back Two-Level VSC-HVDC full-switching model is developed for the time-domain representation of the total OWPP equivalent that includes 88 OWTGs.

The control strategy of the OWPP in the LFAC application remains the same in principle as in a conventional case shown in Figure 6.5, so the desired dynamic response could be achieved. The back-to-back equivalent system is composed of two identical VSCs and a DC-Link capacitor which is connected in between them and acts as a filter for the voltage variations or ripple produced by the VSCs. The DC-Link decouples the generator from the LFAC TS, and so the generator part can be simply represented as an AC voltage source connected to the rectifier terminal [82]. Thus, the wind turbine, drive train and generator side are not modelled in detail to avoid the slow dynamics of a detailed OWPP model, as the study focuses on the electromagnetic dynamics in the LFAC transmission system side [87]. The main electrical characteristic that could affect the active power control of the generator by the rectifier VSC is the DC-Link voltage which is controlled by the LFAC side inverter and is monitored throughout the EMT simulation studies [80] [84].

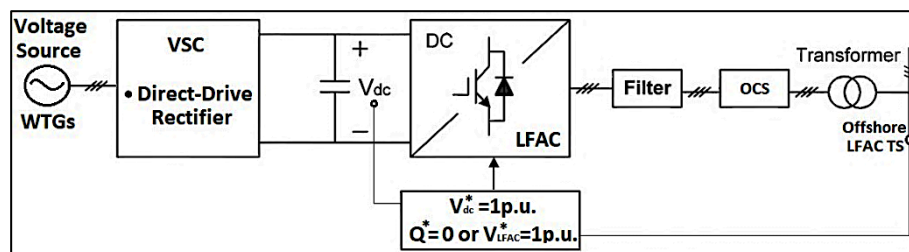


Figure 6.5: Layout of the Equivalent OWPP EMT Model.

The VSI is connected to the MV-66kV LFAC collection system through LFAC interface converter transformers and controls the DC-Link voltage and either the reactive power or LFAC voltage at the offshore 345kV busbar. Although the OWTGs VSI output is at the 66kV busbar and the 66 kV LFAC inter-array system with its associated equipment is retained in the model, the equivalent OWF output for the LFAC TS EMT studies can be considered at the offshore 345kV busbar after the 66/66kV and the 66/345kV LFAC transformers which are designed with 7% leakage reactance. No frequency control is needed by the OWF inverter as it is imposed by the corresponding LFAC side converter.

## 6.3 VSC Control System Structure and Design

### 6.3.1 VSC Models Control Hierarchy

The VSC HVDC converter controls are classified within two functional levels, namely the upper or high-level and lower-level controls, while their combination establishes the converter pole control. The high-level controls regulate the dispatch of the overall VSC regardless of the converter technology, while the lower-level controls, such as the converter PWM settings described in Chapter 3, correspond to a specific valve topology. This separation of the upper-level controls from the valves and their respective controls enables the usage of the same high-level control structure independent of the valve topology (e.g. two-level, modular multilevel, etc.) [86]. The control level hierarchy is shown in Figure 6.6.

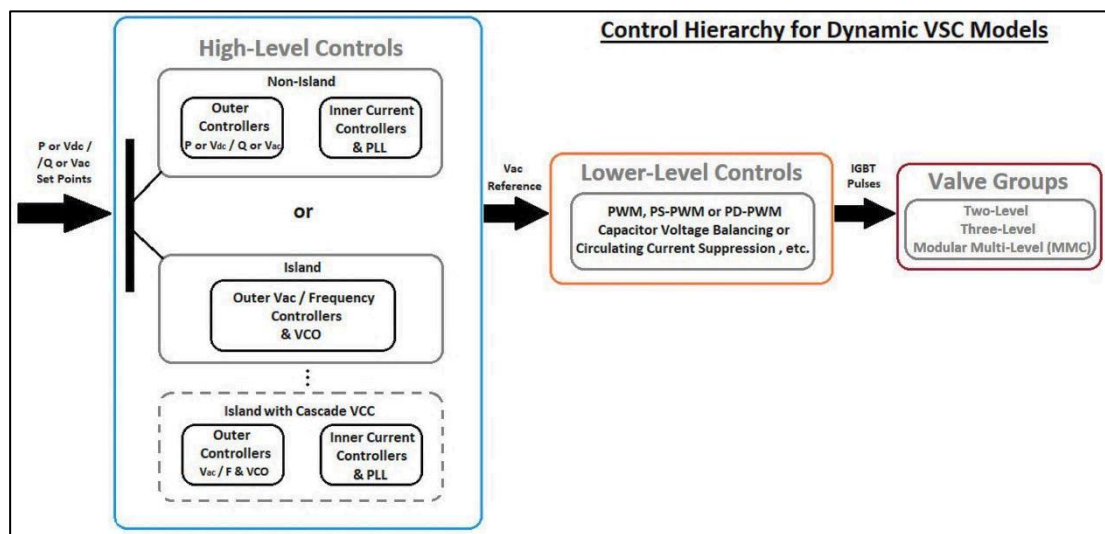


Figure 6.6: Control Hierarchy of the Dynamic VSC Models.

This approach provides a modular design of the VSC dynamic model that corresponds to most AC and DC side systems. The AC side system includes the converter transformers, phase reactors, filters (if utilised), current limiting resistors with bypass switches for start-up, etc. The DC side system comprises the DC capacitors, smoothing inductors, DC choppers, etc. Hence the primary control levels can be considered in a modular fashion as:

- The upper-level controls that have as input the dispatch setpoints directed by the operator or station control and the measured quantities from the AC and DC side systems and produce the three-phase voltage reference waveforms as output.
- The lower-level controls that take as input the three-phase voltage waveforms produced by the upper-level controls and output the suitable IGBT switching pulses for the respective VSC valve arrangements.



Hence, it is possible to substitute control schemes with others in each level without replacing the whole VSC model, provided that there is a consistent structure of the interfaces between the different levels, with the interface boundary between upper and lower-level controls being the three-phase voltage reference waveforms. Within the upper-level control, the correct configuration should be selected with regards to the system in which the VSC is connected. In a VSC connected to a passive AC system or an islanded AC network with partial or converter interfaced generation, the controller shall configure the AC voltage level and frequency. In the case of a non-islanded AC system that already has a reference voltage waveform, it may operate in a grid-following mode, adjusting either the real power or DC voltage level and the reactive power or AC voltage level of the system at the PCC.

### 6.3.2 VSC Synchronisation

The vector theory is the most widely used for the upper-level control of VSCs. The analysis of the VSC technology using VCC involves three-phase currents and voltages being expressed as vectors in the complex dq0 rotating reference frame through Park Transformation. This rotating coordinate system must be synchronised to the AC or LFAC grid so that the calculated voltages and currents occur as constant vectors during steady-state, producing static errors which can be eliminated by simple PI regulators in the control loops.

More specifically, the d-axis direction is aligned to the PCC voltage vector, while the q-axis voltage vector is assumed to be zero ( $V_q=0$ ), locking on the instantaneous phase angle  $\theta$  of the rotating AC voltage vector. This angle is vital for synchronising the output control quantities of the VSC with the system and achieve independent control of active and reactive power. The rotating angle reference is either calculated by a Phase Locked Loop (PLL- $\theta_{PLL}$ ) in a grid-following VSC mode or generated using an independent internal oscillator (VCO- $\theta_{VCO}$ ) in an islanded mode. Figure 6.7 shows a generic structure of the synchronisation techniques.

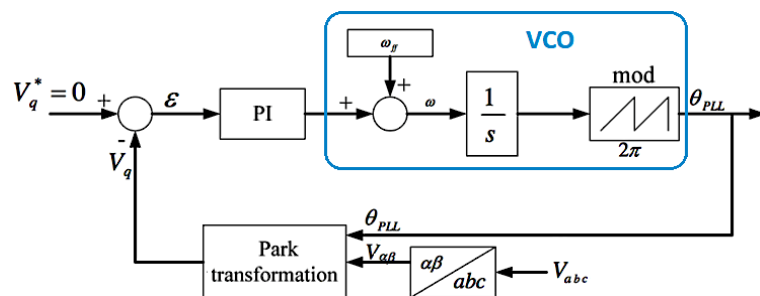


Figure 6.7: General Phase Lock Loop (PLL) and Voltage Controlled Oscillator (VCO) Structures.

The transformation from the three-phase abc stationary system to the dq0 synchronous rotating frame as well as the PLL and VSC functions are presented in APPENDIX C.

### 6.3.3 Generic VSC Control System

#### 6.3.3.1 The Upper-Level Control

The high-level control systems of the equivalent 704MW Type-4 OWF modules that comprise BtB VSCs and the onshore BtB frequency MMCs are based on the same VCC principles. All converters in the LFAC TS, apart from the onshore LFAC grid-forming MMC Terminal that forms the system voltage level and frequency, apply a classic cascade VCC structure with faster inner PI current controllers (ICC) and additional slower outer PI controllers (OC) as referred in Chapter 3. The types of outer controllers that calculate the reference values of the VSC current controller depend on the application.

Only one AC operating variable (either the AC/LFAC voltage or reactive power) and one DC operating variable (either the DC voltage or active power) can be controlled at each VSC when it functions at its grid-following operating mode. The outer control loops provide the reference values for the inner controllers in the dq domain. The inner current controllers regulate the converter AC voltage reference in the dq domain ( $v_{dq}^*$ ). Then, this signal is transformed into the three-phase coordinate system and subsequently provided as a modulation signal to the PWM algorithm, providing two degrees of freedom through the modulation index and phase angle. Thus, this technique provides decoupled real and reactive power control as well as fast dynamics. The control loops can be reviewed as follows:

➤ **Outer Controllers:**

- I. Active Power (APC) or DC Voltage Control (DCVC) provide d-axis current demand  $I_d^*$ .
- II. Reactive Power (RPC) or AC Voltage Control (ACVC) yield q-axis current demand  $I_q^*$ .

➤ **Inner Controllers:**

- I. D-axis, Active Current Control (ACC) provides d-axis voltage demand  $V_d^*$ .
- II. Q-axis, Reactive Current Control (RCC) provides q-axis current demand  $V_q^*$ .

However, one of the MMCs that interfaces the 16.7Hz LFAC side must impose the LFAC voltage magnitude and the frequency at its connection point (e.g. act as a slack bus) to form the LFAC voltage waveform, offer black-start capability and effectively energise the offshore LFAC TS. This MMC system shall operate in islanded control mode which does not typically include an ICC scheme [86], and the LFAC voltage can be directly controlled by varying the modulation index through an ACVC while the frequency can be imposed through an internal oscillator (Voltage Controlled Oscillator - VCO) that defines the valve firing-pulse sequence. In this work, an ICC scheme is also implemented, and its operation is contrasted with the typical islanded operation mode (Chapter 7) in order to enhance the functioning of the LFAC

TS and potentially improve rejection to current perturbations. Thus, the islanded control arrangements that could be applied in this MMC terminal can be:

- I. The Islanded LFAC Voltage and Frequency Control employed without ICC.
- II. The Islanded Cascade VCC with LFAC Voltage outer Control and Frequency Control.

It should be mentioned that if the onshore MMC terminal that imposes the LFAC TS voltage reference trips because of a contingency or disturbance in an OWF export system, then the LFAC voltage reference will be lost and no power can be transmitted, as in the case of the offshore converter in an HVDC export scheme. In a multi-terminal LFAC TS that also interconnects different grids, all the other onshore VSCs shall be synchronised on this LFAC voltage reference and operate in a grid-following mode as well; thus, no power balance can be achieved if such an event occurs. Hence, in an MT-LFAC TS, other onshore converters must have a backup island-control configuration, to re-synchronise the rest of offshore TS from another point of connection.

The upper-level operating VCC principles for the inner and outer control arrangements mentioned above can be applied to all grid-following converters of the LFAC TS. As a result, a parallel demonstration of their design, tuning and analysis is chosen that corresponds to both two-level VSC and MMC types. The only difference would be the supplementary lower-level circulating current suppression control (CCSC) regulators of the BtB frequency MMCs, which are used for circulating currents elimination and capacitor voltage balancing.

### 6.3.3.2 P.U. System for the Control Functions

Because of the number of VSCs that need to be tuned for the offshore LFAC system schemes, the analysis of their control systems should ensure that these models can easily be reset and re-used. Accordingly, their generic VCC structures are designed in p.u. basis with reference to the corresponding VSC ratings. The quantities that have been chosen as base values for the VSCs in this study are in accordance with the rating of each converter terminal as obtained in Chapter 3. These base quantities are presented in Table 6-2.

**Table 6-2: Base Parameters of the LFAC TS for p.u. Representation**

P.U. System Base Values for each Converter				
Base	WF VSI	MMCT1 / T2	Units	Where:
<b>S<sub>b</sub></b>	880	850	[MVA]	# <b>S<sub>b</sub></b> is the rated three-phase power of the AC or LFAC side converter transformer
<b>V<sub>b,p,ph</sub></b>	53.89	302.10	[kV]	# <b>V<sub>b</sub></b> is the nominal peak-phase voltage at the AC or LFAC side
<b>I<sub>b,p,ph</sub></b>	10.89	1.88	[kA]	# <b>I<sub>b</sub></b> is the nominal peak-phase current
<b>Z<sub>b</sub></b>	4.95	161.06	[ohm]	# <b>Z<sub>b</sub></b> is the base impedance calculated by V <sub>b</sub> /I <sub>b</sub>
<b>f<sub>e</sub></b>	16.7	16,7 / 50	[Hz]	# <b>f<sub>e</sub></b> is the corresponding AC or LFAC frequency
<b>ω<sub>b</sub></b>	104.93	104.93 / 314.16	[rad/s]	# <b>ω<sub>b</sub></b> is the corresponding AC or LFAC angular frequency
<b>V<sub>dcb</sub></b>	107.78	604.21	[kV]	# <b>V<sub>dcb</sub></b> is the minimum DC voltage level for a unity modulation index (m <sub>i</sub> =1)
<b>I<sub>dcb</sub></b>	8.16	1.41	[kA]	# <b>I<sub>dcb</sub></b> is the corresponding DC current for an invariant power transformation (i.e. 3/4I <sub>b</sub> )
<b>Z<sub>dcb</sub></b>	13.2	429.49	[ohm]	# <b>Z<sub>dcb</sub></b> is the base DC impedance calculated by V <sub>dcb</sub> /I <sub>dcb</sub>

### 6.3.3.3 PWM Converter

The high carrier frequency of the PWM pattern in a two-level VSC leads to a high switching frequency of the VSC, also resulting in a high resonant frequency of the low pass harmonic filter. Similarly, the high number of HBSMs in an MMC leads to a high effective switching frequency of the converter as described in Chapter 3, without any need for harmonic filters. Thus, the impact of a PWM-VSC in the VCC scheme can be considered as a delay, represented as a time delay block, before the voltage demand gets on to lines as shown in Figure 6.8 [88]. The lower the delay, the higher can be the ICC bandwidth that is crucial for LFAC TS.

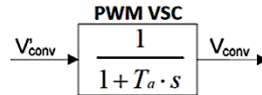


Figure 6.8: Equivalent PWM VSC Time-Delay Block Diagram.

The output voltage of the converter is assumed to follow a voltage reference signal with an average time delay ( $T_\alpha$ ) that equals half of a switching cycle ( $T_s/2$ ), due to VSC switches. The general PWM converter Transfer Function (TF) is:

$$TF_C = \frac{V_C}{V_C^*} = \frac{1}{1 + T_\alpha \cdot s} \quad (6.8)$$

The time constant of the two-level VSCs that interface the 704MW equivalent Full-Converter OWTG models with the LFAC system is  $T_{\alpha VSC} = 256 \mu s$ , while the corresponding time constant of the onshore back-to-back frequency MMCs is set at  $T_{\alpha MMC} = 323 \mu s$ .

### 6.3.4 Non-Island Control for Grid-Following Converters

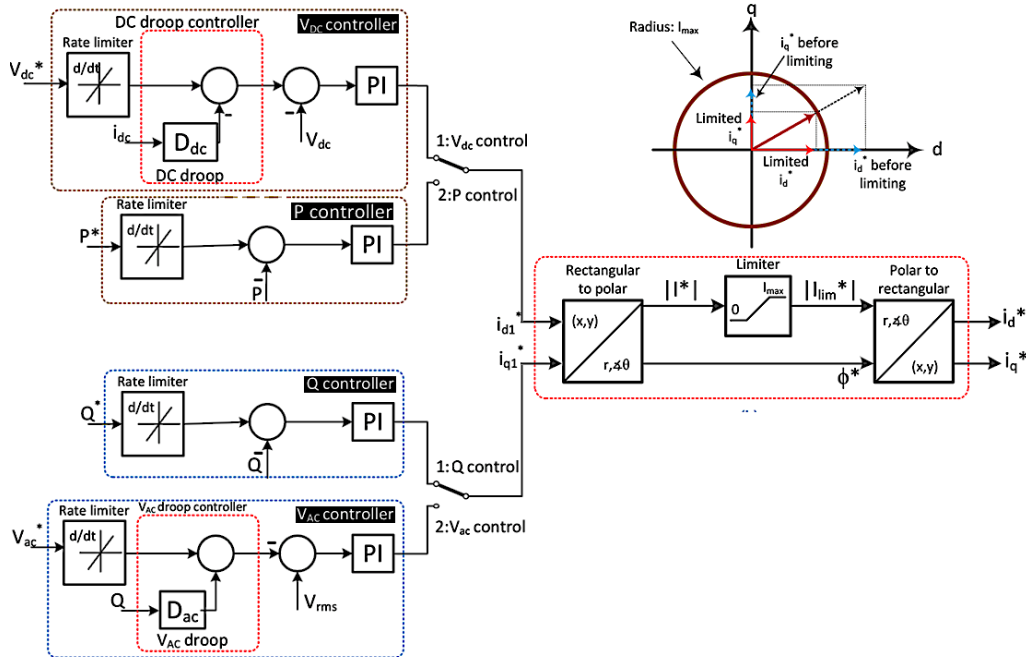


Figure 6.9: General VSC Outer Controller and Current Saturation Structure.

The cascade vector current control pattern for the grid-following VSCs connected to non-islanded and sufficiently strong systems is accomplished by outer controllers that provide the reference values for the inner controllers. In particular, the outer controllers of each VSC include a DCVC or an APC that derive the active current reference values for the d-axis ICC loop and an ACVC or an RPC that derive the reactive current reference values for the q-axis ICC loop as depicted in Figure 6.9, as mentioned in [86]. The output currents of this stage ( $i_{d1}^*$  and  $i_{q1}^*$ ) are then given to a current limiter block and the final references ( $i_d^*$  and  $i_q^*$ ) are led to the decoupled current-regulator loops.

The Proportional-Integral (PI) regulators of the outer controller loops that are applied in this work also employ output limiters and integrator anti-windup mechanisms. This strategy is implemented to turn off the integral part of the controller when the maximum set-limit of the controlled quantity is met. This helps the controlled quantity to recover faster in case of severe disturbances and avoid potential system instability.

#### *6.3.4.1 Current Saturation Scheme for Cascade VCC*

In Figure 6.9, a typical current limiting scheme is implemented between the inner and the outer control loops. It is technically a hard-limiter for the converter current level that saturates its magnitude to a maximum value depending on the VSC capability and device temperatures [86]. This current saturation scheme besides protecting the equipment during normal operation, e.g. after a module failure or during wind gusts, etc., it can also limit the VSC fault-current contribution to AC or LFAC system faults. However, during the current saturation mode, the ICC loop cannot effectively control the current, introducing an outer loop controller steady-state error. Thus, in order to prevent the outer loop output from continually rising and jeopardising system stability, an additional integrator anti-windup mechanism is employed that deactivates the outer control loop integrators whenever a difference between the input and output values of the current-limiter block is detected.

This setup applies to all the grid-following converters of this Thesis employing non-island control. The current limiting algorithm adopted by the VSIs of the equivalent OWF modules also prioritizes the d-axis current, at the expense of the q-axis vector counterpart. This can be more useful for the LFAC system's power balance, while the q-axis prioritization could benefit its fault recovery and post-fault voltage support. It should be mentioned, though, that all the above current restrictive approaches limit the total current vectors and do not act on the individual phase currents in the abc frame.

### 6.3.4.2 Droop Characteristics for Multi-Terminal LFAC TS

Standard droop controls need to be implemented in some of the outer controllers if an LFAC network is formed, allowing several converters to connect to the same system [86]. Particularly, onshore frequency converters can implement DC voltage droop characteristics in the DCVCs of their AC grid side MMCs, while the VSIs of the equivalent OWF modules can implement LFAC voltage droops in their ACVCs. This way, the LFAC voltage regulators can operate in conjunction with each other on the same LFAC system. The generic droop characteristics for the DC and LFAC voltage controller references are shown in Figure 6.10.

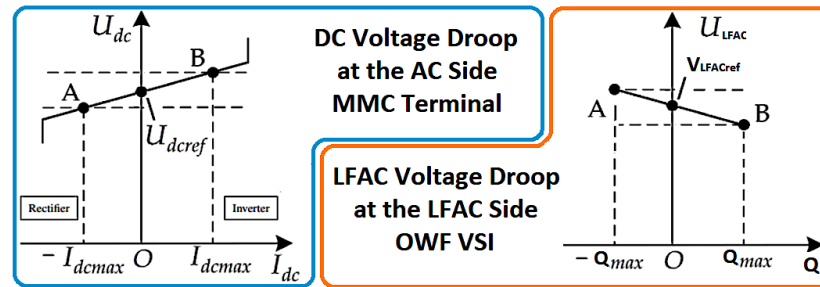


Figure 6.10: Generic Droop Characteristics for the DC and LFAC Voltage Controller References.

A DC current-based droop control that is integrated with the DC voltage control loop is intended to modify the DC voltage reference as well as to allocate unbalanced power in the multi-terminal LFAC network. The higher the droop coefficient ( $K_{DC}$ ) is, the lower the unbalanced power allocated to the MMC. This DC current-based droop control scheme benefits from its linear behaviour, as any DC current deviation will result in an equivalent DC voltage deviation as expressed in Equation (6.9). Since the back-to-back MMC-HVDC arrangements do not use any transmission mediums (e.g. Cable or TLs), they can tolerate high DC voltage variations, and the DC current-based droop control could be employed only to reduce the DC side current losses and smoothen the DC side dynamics.

$$K_{DC} = \frac{\Delta V_{DC}}{I_{DCn}} \quad (6.9)$$

Controlling the DC-Link voltage of the back-to-back frequency MMC-HVDC system that interfaces the offshore LFAC TS would only ensure that the energy output of the OWFs is transmitted to the AC grid according to predefined power dispatch criteria. However, in an MT-LFAC system, the use of DC voltage droop control can balance power, the same way it compensates power imbalances in an MTDC network. This can be assumed as equivalent to the frequency droop control that is typically used in AC systems; though since the LFAC system is formed only among converter terminals, it is preferred to keep the frequency constant and benefit the synchronisation of other power converters in the scheme.

Moreover, as seen in the steady-state assessment of Chapter 5, as the reactive power of the OWF VSCs in the offshore LFAC grid tries to adjust the voltage level of the buses to which they are connected, the voltage difference between these buses can produce additional reactive power flow. In the investigated MT-LFAC TS, the reactive power output of the OWTGs is managed by adopting LFAC voltage droop control at their VSIs, when operating in an ACVC mode. This is done by adjusting the LFAC voltage demand level at the offshore 345kV busbars with the reactive power output according to the gain ( $K_Q$ ) shown in Equation (6.10).

$$K_Q = \frac{\Delta V_{LFAC}}{2Q_n} \quad (6.10)$$

As it would be challenging to explicitly define a relationship between reactive power sharing and the voltage droop gains in such case of highly capacitive, islanded offshore network for each of the OWTGs, the high voltage droop gains shall be avoided because the controller interaction among the VSCs at the station controlled busbars may be significant.

### 6.3.4.3 Inner Current Controllers

The objectives of the inner current controllers are to determine the converter voltage output waveforms so that the desired AC/LFAC or DC voltage level and power flow characteristics are attained. They evaluate the necessary voltage drop over the series converter and transformer inductance to adjust the converter voltage output and send it to the lower-level controls. This voltage demand can develop the required AC current.

#### I. ICC Implementation Strategy and Plant Derivation

The implementation strategy of the ICC in a VSC/MMC system is shown in the block diagram of Figure 6.11. It comprises a dual-closed-loop design with decoupling and feed-forward voltage compensation terms for independent control of active and reactive power and faster dynamic response of the cascade control pattern, respectively [118].

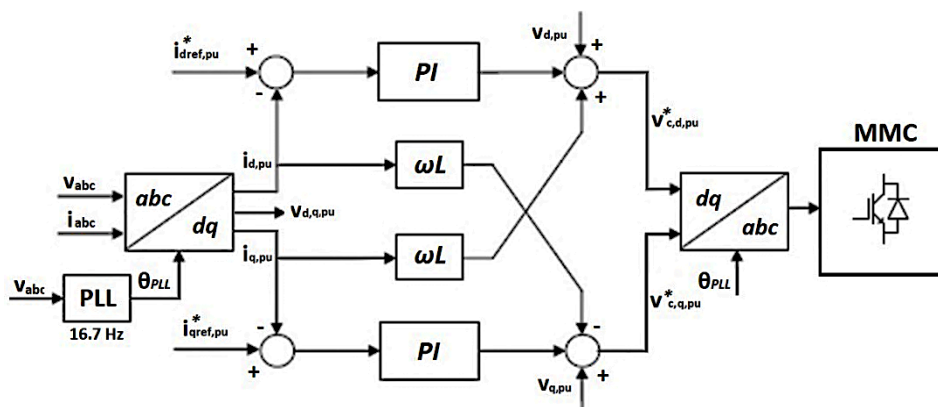


Figure 6.11: General ICC Block Diagram Implementation into a Grid Following VSC/MMC System.

The VSC output current and voltage vectors are measured, and the dq domain currents are compared with the corresponding reference signals. The yielded error signals are carried through the PI-controllers, which then provide the suitable converter voltage modulating signals after being compensated by the cross-coupling and feedforward terms. This way, the d and q-axis current controllers can operate independently. By defining the total equivalent resistance (R) and inductance (L) between the converter and the grid, a generic system for each converter up to its corresponding point of connection can be described as follows:

$$v_{dq,pu} - v_{c,dq,pu} = \frac{L_{pu}}{\omega_b} \cdot \frac{di_{dq,pu}}{dt} + R_{pu} \cdot i_{dq,pu} + L_{pu} \cdot i_{qd,pu} \quad (6.11)$$

From a control point of view, these cross-coupling terms can be considered as disturbances for each axis and a dual-closed-loop dq inner current controller with decoupled current compensation terms is required to obtain satisfactory control performance. Considering the above and by applying the Laplace transformation (LTF) on Equation (6.11), it is:

$$v_{c,dq,pu}(s) = \frac{L_{pu}}{\omega_b} \cdot s \cdot i_{dq,pu}(s) + R_{pu} \cdot i_{dq,pu}(s) \quad (6.12)$$

This equation relates the applied converter side voltage and the resulting current at the PCC for a purely inductive filter as in case of the onshore MMCs in the LFAC TS. From the transfer function of damped LCL filters with resistors ( $R_f$ ) installed in series with the capacitors ( $C_f$ ), key information can be extracted regarding the resonance of the filters applied to the OWF VSIs. Thus, appropriate resonance damping, and attenuation of their harmonic components can be assessed:

$$TF_{LCL} = \frac{i_{dq}(s)}{v_{c,dq}(s)} = \frac{C_f \cdot R_f \cdot s + 1}{L_1 \cdot L_2 \cdot C_f \cdot s^3 + C_f \cdot L \cdot R_f \cdot s^2 + L \cdot s} \quad (6.13)$$

However, in this case, a suitable resistor  $R_f$  is installed in series with the capacitance  $C_f$  so that the LCL filter resonance is well-damped, at the expense of increased losses, while its capacitance slightly affects the filter's impedance below its cutting frequency of ~880Hz, as explained in Chapter 3. Henceforth, an equivalent L-filter can be assumed for tuning the ICC, by neglecting its shunt capacitive branch, since the study does not focus on high order harmonics. The yielded TF for this AC branch, up to the point of connection, Equation (6.14), can be used as a generic Plant for the ICC loops and be accordingly adjusted for the equivalent OWF two-level VSC and the onshore frequency MMC modules.

$$TF_{AC-System} = \frac{i_{dq,pu}(s)}{v_{c,dq,pu}(s)} = \frac{1}{R_{pu} + L_{pu}/\omega_b \cdot s} \quad (6.14)$$



## II. ICC Design and Tuning

Based on the above, the ICC closed-loop block diagram can be derived by eliminating the cross-coupling and feed-forward elements, as shown in Figure 6.12.

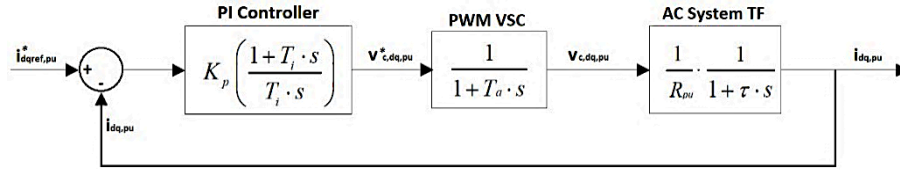


Figure 6.12: General ICC Closed-Loop Block Diagram.

The resulted Open Loop Transfer Function (OLTF) from the above block diagram is [88]:

$$OLTF_{ICC} = TF_{PI} \cdot TF_C \cdot TF_{AC-system} = K_p \cdot \left( \frac{1+T_i \cdot s}{T_i \cdot s} \right) \cdot \left( \frac{1}{1+T_\alpha \cdot s} \right) \cdot \left( \frac{1}{R_{pu}} \cdot \frac{1}{1+\tau \cdot s} \right) \quad (6.15)$$

Where:  $\tau = \frac{L_{pu}/\omega_b}{R_{pu}}$  is the AC line time constant, almost three times higher for an LFAC line.

The produced ICC generic equivalent plant, as seen in Figure 6.12 and described in Equation (6.15) is a second-order TF that only includes the PWM VSC and the respective AC/LFAC side TFs up to the point of connection disregarding the rest of the AC or LFAC parts. Having a dominant pole that corresponds to the AC or LFAC side time constant ( $\tau$ ) and a minor one that corresponds to the converter time constant ( $T_\alpha$ ), it could be adjusted accordingly to tune all the ICCs of the different converters in the scheme. Of course, to adopt a common tuning method for all ICCs, it shall also comply with some specific controller response requirements of each VSC at its point of connection.

In general, a fast and damped response is desired for an ICC loop. However, an explicit tuning requirement for each of the ICCs of the converters in the various LFAC TS arrangements described in Chapter 5, would be to mitigate the effect of the transmission system dynamic impedance as much as possible. To achieve this, the required bandwidth for each ICC of the scheme must be higher than the low-order resonant frequencies of the LFAC TS, as identified in the frequency assessment of Chapter 4. Thus, all the potential LFAC TS low-order resonances of the examined arrangement shall fall within the ICC bandwidth, so that the VSC controller can dominate the total system impedance characteristics and cancel their impact. Therefore, the ICC loops need to have higher bandwidths than the highest possible low-order resonant frequency in the scheme, which corresponds to the natural resonance frequency of the submarine export cable and could be excited during typical system energisation as in no-load cases studied in Chapter 4.

It is evident though that high PWM-VSC delay ( $T_\alpha$ ) can decrease the ICC bandwidth, so the VSCs that face the offshore LFAC TS shall have high switching frequency ( $f_{sw}$ ) even though the fundamental is reduced to 1/3, as described in Chapter 3. This occurs due to the controller requirement to dominate the low-order dynamic impedance of the specific offshore LFAC TS schemes and not because the system operates at the frequency of 16.7Hz. Though, LFAC may not lead to an inherent reduction of the VSC switching losses in this particular application.

In such control systems with low order plants (i.e. less than 3<sup>rd</sup> order) and no poles near or at the origin, the Modulus Optimum (MO) method can be used for tuning the PI regulators [100] [48]. This can be the common tuning method for all ICCs of the LFAC TS as it is simple and provides high-bandwidth-fast and non-oscillatory closed-loop tracking response. By applying the MO technique to the ICC, the following tuning criteria are adopted:

- I. Increase of the resulting cut-off frequency so that that faster response can be achieved. For this reason, the integral time constant ( $T_i$ ) that defines the controller zero can be chosen to eliminate the dominant pole of the ICC-OLTF, as follows:

$$T_l = \tau \quad (6.16)$$

- II. The closed-loop gain should be larger than unity for the highest frequencies possible, so that small overshoot and proper oscillations damping can be achieved [88]. Thus, the proportional gain of the PI controller becomes:

$$K_p = \frac{\tau \cdot R_{pu}}{2 \cdot T_\alpha} \quad (6.17)$$

Because of the zero-pole cancellation, both the ICC-OLTF and the CLTF result in second-order TFs with the ICC-CLTF being:

$$CLTF_{ICC} = \frac{OLTF_{ICC}}{1+OLTF_{ICC}} = \frac{1}{2T_\alpha^2 s^2 + 2T_\alpha s + 1} \quad (6.18)$$

From the CLTF, the damping factor  $\zeta$  and the natural frequency  $\omega_n$  are:

$$\zeta = \frac{1}{\sqrt{2}} \quad \text{and} \quad \omega_n = \frac{\zeta}{T_\alpha} \quad (6.19)$$

The above-mentioned ICC loop set-up is used for the current control tuning. Though, for further analysis of the outer control loops, the second-order ICC-CLTF can be approximated by a simplified equivalent first-order TF with a total equivalent time constant ( $T_{eq}$ ), as follows:

$$CLTF'_{ICC} = \frac{1}{2T_\alpha s + 1} = \frac{1}{T_{eq} s + 1} \quad (6.20)$$

This simplification is calculated by the respective error functions of the original second-order ICC-CLTF and the approximated first order CLTF in steady-state for a unit step input and is only used to simplify the OLTFS of the outer controller loops.

#### 6.3.4.4 Outer Controllers

Here, the outer controllers of the cascade control scheme and their tuning processes are described. For the control system analysis, the ICC loops can be approximated by equivalent time delays with respect to the outer control loops transfer functions, since the outer control loops are much slower.

##### I. DC Voltage Controller

The main objectives of the DCVC in every HVDC system are to establish the demanded DC voltage level and achieve active power balance. The DC side voltage must be maintained in steady-state but also during faults, severe disturbances and input or output power variations. This is the reason why one of the two HVDC converter terminals in any BtB VSC scheme in this Thesis must adopt DCVCs, including the inverter terminals of the BtB VSCs that represent the fully converted WTGs. Therefore, the power balance highly depends on the DC voltage measurement and can be attained by providing or absorbing sufficient charge to maintain the required voltage level across the DC capacitance. As mentioned in Chapter 3, the DC voltage level should be high enough, preventing saturation of current that cannot be controlled linearly when the AC voltage reference vector lies in the overmodulation region.

##### DCVC Implementation Strategy and Plant Derivation

The DC voltage outer controller utilises a PI regulator to eliminate the steady-state error between the measured and demanded quantities, adjust the DC-link voltage to the reference value and maintain it within limits. Its output is the d-axis current reference input ( $i_{d,pu}^*$ ) of the ICC, as shown in Figure 6.9.

To tune the DC voltage PI controller, the TF between the d-axis current reference value ( $i_{d,pu}$ ) and the DC-link voltage ( $v_{DC}$ ) shall be defined. However, the DC-Link system, as described by Equation (6.21) where  $C_{DC,eq}$  is the total DC capacitance, has a non-linear characteristic.

$$\frac{1}{\omega_b \cdot C_{DC,eq,pu}} \cdot \frac{dv_{dc}}{dt} = \frac{v_{d,pu}}{v_{DC,pu}} - i_{L,pu} \quad (6.21)$$

Thus, system linearisation around a steady-state reference point is performed, using Taylor series expansion [116] and the equation is further simplified by assuming that  $i_{L,pu}$  acts as a disturbance, while  $i_{d,pu}$  is the only system input. By applying LTF to the yielded reduced linear expression, the TF of the DC system, which is the Plant for the DCVC becomes:

$$TF_{DC-system} = \frac{\Delta v_{DC,pu}(s)}{\Delta i_{d,pu}(s)} = \frac{v_{d,pu}}{v_{DC,pu}} \cdot \frac{\omega_b \cdot C_{DC,eq,pu}}{s} \quad (6.22)$$

The DCVC closed-loop block diagram of Figure 6.13 the feed-forward terms are employed for faster dynamic response of the cascade control system and to enhance its stability.

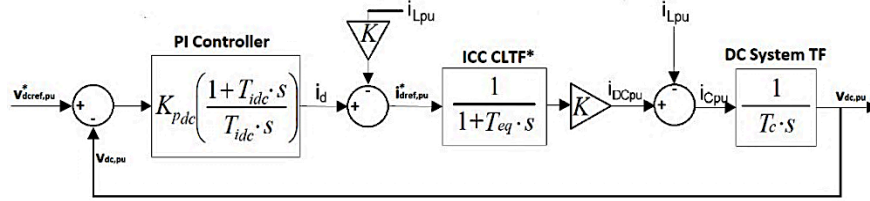


Figure 6.13: General DCVC Closed-Loop Block Diagram.

The resulted Open Loop Transfer Function (OLTF) from the above block diagram is:

$$OLTF_{DCVC} = TF_{PI} \cdot CLTF_{ICC} \cdot TF_{DC-system} = K_{pdc} \cdot \left( \frac{1+T_{idc} \cdot s}{T_{idc} \cdot s} \right) \cdot \left( \frac{1}{1+T_{eq} \cdot s} \right) \cdot \left( \frac{1}{T_c \cdot s} \right) \quad (6.23)$$

Where:  $K = \frac{v_{d,pu}}{v_{DC,pu}}$  and  $T_c = \frac{1}{\omega_b \cdot C_{DC,eq,pu}}$

The DCVC equivalent plant, as described by Equation (6.23) is a second-order TF that comprises the d-axis ICC CLTF and the DC system TF. The dominant pole here is at the origin. The other minor one corresponds to the ICC-CLTF total equivalent time constant ( $T_{eq}$ ). In control systems where the OLTFs have two poles at or near the origin, the Symmetrical Optimum (SO) method can be used for tuning the PI regulators. The SO method maximizes the phase margin for given frequencies providing disturbance rejection attributes to the system and hence, enhancing its stability [99]. Therefore, the SO tuning technique can specify the PI gains of the DCVC for maximum OLTF phase margin, as follows [88]:

- From the phase condition, the desired maximum phase margin occurs at the crossover frequency  $\omega_d$ , which is symmetric about the  $(1/T_{eq})$  and  $(1/T_{idc})$  and is expressed as:

$$\omega_d = \frac{1}{\sqrt{T_{idc} \cdot T_{eq}}} \rightarrow T_{idc} = \alpha^2 \cdot T_{eq} \quad (6.24)$$

Where  $\alpha > 1$  is the symmetrical distance between  $\omega_d$  and  $1/T_{eq}$  or  $1/T_{idc}$ , respectively.

- Then, the magnitude condition provides the proportional gain of the PI controller as:

$$K_{pdc} = \frac{T_c}{\alpha \cdot K \cdot T_{eq}} \quad (6.25)$$

The value of  $\alpha$  should be greater than unity, as for  $\alpha=1$  there is a real and a pair of complex conjugate roots on the imaginary axis of the CLTF. For  $\alpha=3$  the pair turns into real and equal root, while for further increase ( $\alpha>3$ ), the roots move become real and distinct. Thus, low  $\alpha$  values ( $1<\alpha<2$ ) result in more oscillatory system response with reduced stability phase margin, while  $\alpha$  values ( $\alpha>3$ ) lead to slower but more damped system response. Figure 6.14 shows a locus demonstrating the location of the roots in the complex plane with varying ' $\alpha$ '.

Therefore, the only tuning criterion of the SO method is the variable damping, once it results in the value of  $\alpha$  in an acceptable region that is defined by the desired phase margin. However, this method may produce large overshoot, and thus there is a small degree of freedom with a minimal range of variations in such a simplification.

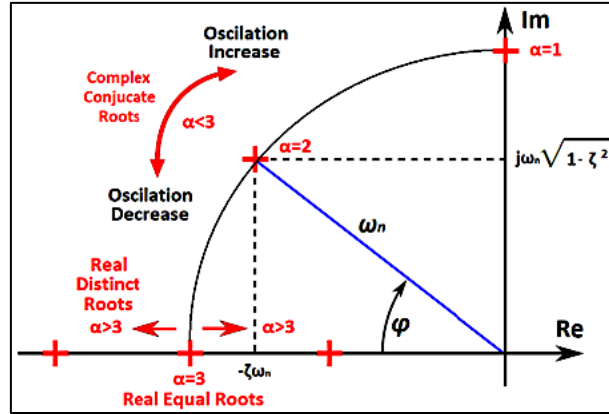


Figure 6.14: Locus demonstrating the Location of the Roots in the Complex Plane for Varying ' $\alpha$ '.

Instead of limiting the rate of change of DC voltage reference in case of such an overshoot, a particular case of SO method can be applied to closed-loop systems having complex poles ( $1 < \alpha < 3$ ) and tune the DCVC PI controller parameters by using pole placement. This technique assumes a second-order system by neglecting the real pole that is located far from the origin and extends the SO criteria so that the damping factor ( $\zeta$ ) can also be specified as part of the system's tuning procedure. The DCVC CLTF is then approximated by a second-order TF. As referred above for  $1 < \alpha < 3$ , the characteristic equation has a real  $s_1$  and a pair of complex conjugate roots  $s_{2,3}$ , which can be assumed as:

$$s_1 = \gamma \cdot \sigma \quad \text{and} \quad s_{2,3} = \sigma \pm j\omega \quad (6.26)$$

Where  $\gamma > 1$  is a constant showing the distance between the poles.

Then, the relation between the damping factor  $\zeta$  and the complex roots  $s_{2,3}$  is given by:

$$\omega^2 = \frac{1-\zeta^2}{\zeta^2} \cdot \sigma^2 \quad (6.27)$$

Hence, the PI controller parameters can be expressed in terms of  $\gamma$  and  $\zeta$ , which, as follows:

$$K_{pdc} = \frac{1+2\gamma\zeta^2}{\zeta^2 \cdot (\gamma+2)^2} \cdot \frac{T_c}{K \cdot T_{eq}} \quad \text{and} \quad T_{idc} = \frac{T_{eq} \cdot (\gamma+2) \cdot (1+2\gamma\zeta^2)}{\gamma} \quad (6.28)$$

Subsequently, there is a definite physical meaning in specifying the damping ratio  $\zeta$  for the controller gain calculation. With the above PI parameters, the DCVC CLTF becomes:

$$CLTF_{DCVC} = \frac{OLTF_{DCVC}}{1+OLTF_{DCVC}} = \frac{\gamma + (T_{eq} \cdot (\gamma+2) \cdot (1+2\gamma\zeta^2))}{(\gamma+2)^3 T_{eq}^3 \zeta^2 s^3 + (\gamma+2)^3 T_{eq}^2 \zeta^2 s^2 + (\gamma+2)(1+2\gamma\zeta^2) T_{eq} s + \gamma} \quad (6.29)$$

## II. AC Voltage Control

The ACVC regulates the AC or LFAC voltage at the points of connection to follow the voltage demand. By doing this, it adjusts the reactive power flow of the VSC to ensure that the measured voltage value follows the reference. The more significant the voltage difference, the more reactive power flow is needed to compensate for it. With ACVC mode, the VSC can assist voltage stability and also operate as a STATCOM, enhancing dynamic voltage support, diminishing voltage variations and helping the voltage recovery following a disturbance.

### ACVC Implementation Strategy and Design

The VSC's AC voltage is measured at the connection point and compared with the AC voltage reference to obtain the AC voltage error. A PI controller is utilised to eliminate the steady-state error and maintain the AC voltage within the required limits. Its output is directed to the q-axis ICC as a current reference input ( $i_{q,pu}^*$ ).

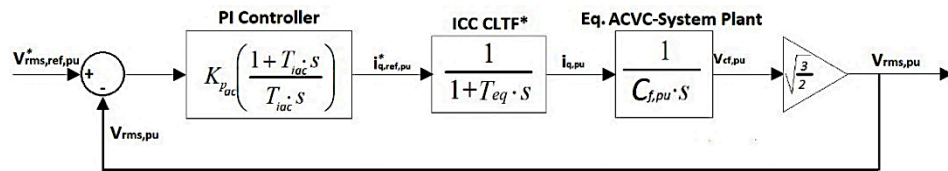


Figure 6.15: Generic ACVC Closed-Loop Block Diagram for the Equivalent OWF VSI.

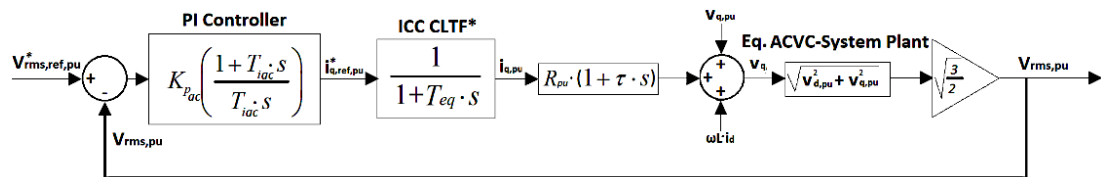


Figure 6.16: Generic ACVC Closed-Loop Block Diagram for the Grid-Following MMC facing the LFAC Side.

The ACVC plants for the equivalent two-level VSIs of the OWTGs and the onshore frequency MMCs can be fundamentally different, due to the presence of LCL-harmonic filtering in the former. The closed-loop block diagram for the OWTG-VSI systems can be seen in Figure 6.15 with  $C_f$  being the capacitance of the LCL filters, while for the MMCs in Figure 6.16. They both comprise a PI controller, the q-axis ICC loop and a block describing the respective electrical system up to the converter point of connection, disregarding the rest of the AC or LFAC parts.

The desired ACVC requirements comprise stable response, zero-steady state error and strong disturbance rejection. Because of the ACVC's lower bandwidth in comparison to the inner control loops, typical voltage perturbation may only produce negligible offset on the current references points which might only slightly affect the harmonic stability of the system. Theoretically, the ACVC loop is stable for any PI controller gains, if its bandwidth is kept low.

Since the offshore LFAC TS is formed only among static power electronic devices (only VSCs), the developed inertia-less system can also be relatively weak in terms of its available SCC. In such case, any fault, disturbance or sudden change that can create a power imbalance in the network may also directly impact the system voltages [89]. Although the ACVCs shall ensure network stability, its stable but slow response may not allow handling such transient events which may destabilise the VSC system, activate protection systems and jeopardise the stability of the whole LFAC TS.

### III. Active and Reactive Power Controls

The power control is accomplished by adjusting the phase angle of the converter AC voltage. The power flow in a grid-following BtB MMC arrangement is defined by one of the two converters while the other must establish the DC voltage control. On the contrary, the reactive power flow can be independently controlled in each converter station within the converter limits and according to each AC system requirements. This is achieved by modifying the amplitude of the converter output voltage waveform to regulate reactive power.

#### APC or RPC Implementation Strategy and Design

The VSC's active or reactive power is measured at the PCC and compared with the corresponding reference to obtain the P or Q error, respectively. In any case, a PI controller is utilised to eliminate the steady-state error and establish the specified set point. The controller output is directed as a current reference input to the corresponding ICC axis ( $i_{d,pu}^*$  or  $i_{q,pu}^*$ ), as shown in Figure 6.9, above.

The active power and reactive power are given in p.u. by Equation (6.30).

$$\begin{aligned} p_{pu} &= v_{d,pu} \cdot i_{d,pu} \\ q_{pu} &= -v_{d,pu} \cdot i_{q,pu} \end{aligned} \quad (6.30)$$

From the resemblance of the above active and reactive power equations, it can be inferred that the APC and RPC have the same structure and similar closed-loop transfer functions with the APC comprising the d-axis ICC loop, while the RPC the q-axis ICC loop. Their equivalent closed-loop block diagram is shown in Figure 6.17 and consists of a PI controller, the d or q axis current control loop, and a gain regulator as in Equations (6.33) above.

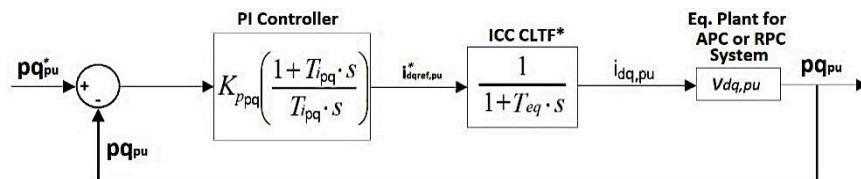


Figure 6.17: Generic APC and RPC Closed-Loop Block Diagrams.

### 6.3.5 Island Control of the Grid-Forming Converter

A passive system or one that has limited or only power converter-interfaced generation like the offshore LFAC network can be considered islanded. Although other WTG types can have mechanical inertia, the BtB VSC modules that interface the generators of the Type 4 OWTGs eliminate their inertial impact on the LFAC network [87], while the onshore BtB frequency converters decouple the grid generators from the LFAC network. Since the LFAC TS is an inertia-less network, its frequency can be subjected to severe perturbations, but the power injected to, or absorbed from the LFAC system may not necessarily alter the OWTGs power output or modify the LFAC system frequency. Thus, the grid-forming MMC terminal that establishes the voltage level of the LFAC TS shall impose a constant frequency of 16.7Hz on the offshore LFAC network and be able to absorb any abrupt power disturbances.

The LFAC side MMC terminal of the onshore frequency converter acts as a controlled LFAC voltage source, as it can energise the LFAC TS and impose its internal voltage and frequency reference, independently of the system size. To achieve this, the respective onshore 50Hz grid side MMC terminal must effectively control the HVDC voltage, so that the grid-forming MMC terminal can inherently absorb power variations of the network and embrace both the rectifying and inverting processes. The rectification occurs when the MMC exports power coming from the offshore LFAC TS to the main grid by absorbing the OWF generated power in a PtP arrangement or also the power that is not consumed by other terminals in an MT-LFAC TS. Inversion occurs when the MMC imports power coming from the main grid to the LFAC TS, either during the offshore system energisation or when the power demand of another MMC terminal cannot be covered only by the OWFs generation in an MT-LFAC TS.

In this Thesis, only one of the onshore MMC stations interfacing the LFAC side is allocated to establish the offshore LFAC network frequency at 16.7Hz and voltage at 345kV busbar, whilst balancing the transmitted active power in the offshore network. It employs an islanded control strategy, similar to the rectifiers in the HVDC connected OWPPs, regulating its output voltage magnitude and angle directly without any inner controller and utilising VCO algorithms to set the frequency. At the same time, the other VSCs of the LFAC network operates in a grid-following mode and synchronise their outputs to the system voltage through PLL devices. Nevertheless, an alternative islanded control strategy is also considered that implements an ICC loop based on the cascade VCC principle. This method still uses the VCO angle to impose the LFAC voltage waveform in the transmission system at the MMC's 370kV output and synchronises it according to the measured voltage at 345kV busbar.



### 6.3.5.1 Islanded Control System

The closed-loop offshore LFAC voltage control is performed through driving the d-axis value at its point of connection,  $v_d$ , providing that the q-axis voltage,  $v_q$ , equals to zero, as in Figure 6.18. The error signal between the dq voltage references and the measured voltage vector enters the PI controller blocks that regulate the voltage output signal of the MMC. Since the MMCs adopt the PS-PWM method, the LFAC voltage level can be directly adjusted through the modulation index of the reference signals. Hence, the point of connection is turned into a controlled voltage source adjusted by the immediate output of the converter terminal.

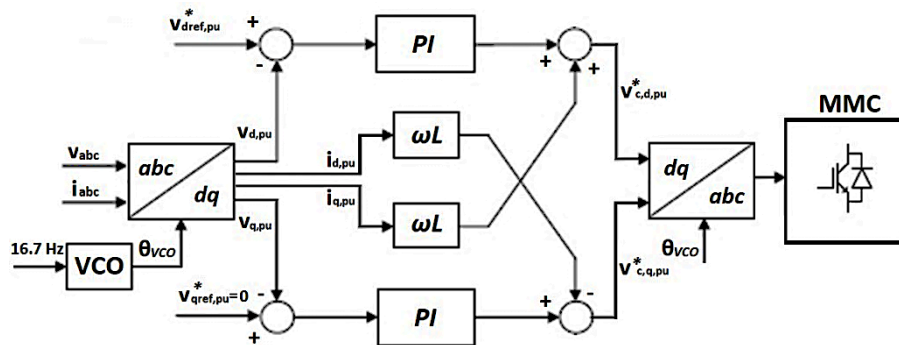


Figure 6.18: General Islanded Control Block Diagram Implementation into the Grid-Forming MMC System.

The inherent coupling between the d and q voltage vectors is avoided using the cross-coupling terms shown in Figure 6.18. These improve the transient response and diminish voltage oscillations. Also, a DC voltage feed-forward signal is inversely applied on the LFAC reference voltage waveforms when forming the modulation signals and before comparing them with the constant carrier waves of the PS-PWM method to prevent the DC side turbulences and harmonics from propagating into the LFAC side. The islanded LFAC voltage controllers are tuned using a recursive EMT simulation-based optimisation method that employs simplex algorithm to minimise the sum of the “Integral Time Absolute Error” (ITAE) of the LFAC voltage and obtain a suitable response. This technique is applied to the developed MMC models in PSCAD EMTDC and is described in APPENDIX D.

Since the LFAC voltage controller bandwidth is much lower than that of an equivalent current controller, its effect on the system impedance cannot be as dominant, and the current may be subject to severe perturbations following slighter LFAC system disturbances. Thus, due to the low-order resonances described in Chapter 4, the implementation of passive damping filters may be necessary, while due to the absence of ICC loops in this grid-forming MMC, there is no converter current saturation mechanism which may result in over-currents that may damage the equipment during faults, despite the LFAC CBs action to clear them.

### 6.3.5.2 Islanded Control System enhanced with ICC

As mentioned above, an inner current loop may need to be present in order to alleviate potential current perturbations and provide a faster response. These VSC control response characteristics can be accomplished as the ICC has inherently much higher bandwidth than a voltage controller, in which it dominates the LFAC TS impedance and cancels the impact of low-order resonances that fall within. One more benefit of implementing the cascaded vector current control structure is that the current reference for the fast inner current control loops can be saturated between the outer and inner controllers limiting the valve currents, as seen in 6.3.4.1. Thus, the islanded control structure with ICC may not only provide better and faster controller response but also protect sensitive equipment from over-currents, preventing converter failures and overloading of cables and converter inductors [106].

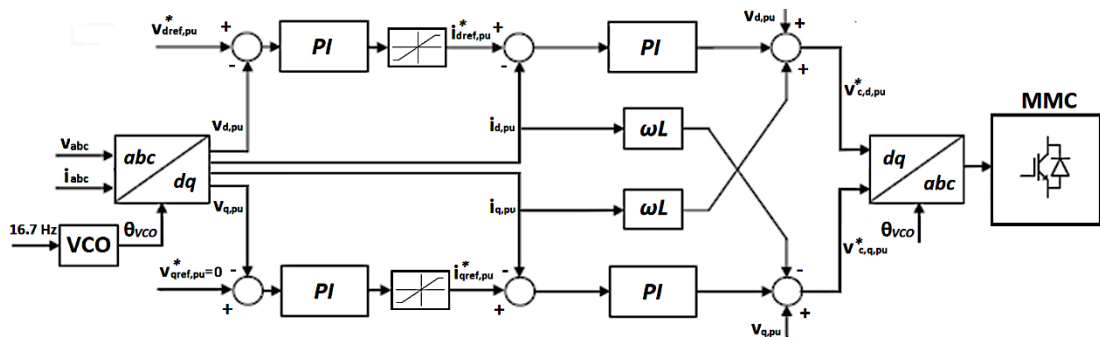


Figure 6.19: Enhanced Islanded Control with ICC Block Diagram Implementation into the Grid-Forming MMC.

This island cascade control system shown in Figure 6.19 is a combination of the typical islanded control system described in 6.3.5.1 and the non-island controller structure used by the grid-following VSCs, as seen in 6.3.4.3. More specifically, the above-mentioned island LFAC voltage control loops in both the d and q-axis are used here as outer controllers. The decoupled current control loops of the grid-forming converter have the same structure as the ICCs in the grid-following converters with a VCO providing the reference angle ( $\theta_{VCO}$ ) from the ordered frequency, instead of a PLL.

This ICC produces a reference voltage for the MMC based upon the current demand from the outer LFAC voltage controllers that determine the current needed to control the voltage at the PCC. The inner current loops use this as a reference to adjust the current flow through the equivalent converter inductor. In particular, they define the required converter output LFAC voltage for eliminating the voltage drop across the inductor, which can be substantial depending on the system condition and if the converter impedance is relatively large, as in the case of LFAC side inductor.

To attain the desired grid-forming MMC response, the regulator parameters for the implemented ICC also need to be specified. Its tuning requirements match those defined for the ICCs of the grid-following VSCs and the MO criterion described in 6.3.4.3 is adopted, with the controller's zero cancelling the time constant of the MMC impedance. Its outer LFAC voltage controllers are tuned using the ITAE optimisation method described in APPENDIX D.

### 6.3.6 Circulating Current Suppression Control (CCSC) in MMC Systems

In this work, the Circulating Current Suppression Controller (CCSC) based on the VCC theory is implemented to all the MMCs. According to Equation (6.31), the current that flows in each arm,  $i_z$ , comprises a part of the DC current ( $I_{dc}/3$ ) and the circulating current. The latter is a negative sequence (a-c-b) - second harmonic order current that depends on the difference between the sum of the arm voltages and the DC voltage [68].

$$I_{ua} = \frac{I_{dc}}{3} + \frac{I_a}{2} + I_{circ}, \quad I_{ia} = \frac{I_{dc}}{3} - \frac{I_a}{2} + I_{circ} \quad (6.31)$$

The CCSC (Figure 6.20) is synchronised to twice the line-frequency as tracked by either a PLL or a VCO and tuned using the MO method, with the Plant including only the arm inductor.

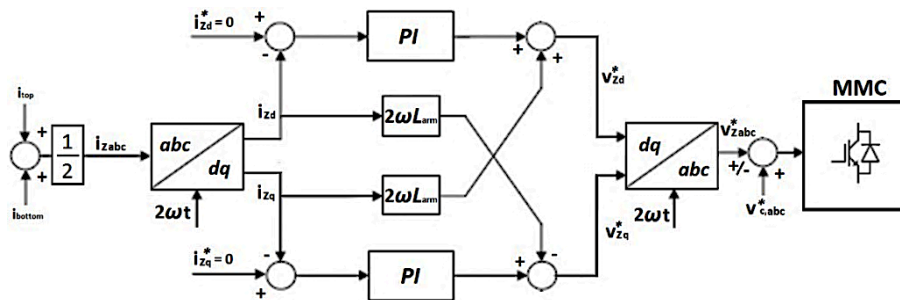


Figure 6.20: General CCSC Block Diagram Implementation into an MMC System.

## 6.4 Converter Control System Analysis

The VSC control system analysis is conducted to effectively tune the dynamic converter modules that are developed for the EMT models of the offshore PtP and MT-LFAC TS configurations, based on the generic optimisation methods analysed in the sections above. Here, the ICCs of all the VSCs, as well as the outer DCVCs and ACVCs of the grid-following VSCs in the LFAC TS are tuned by analysing their transfer functions. The calculated parameters are applied to the related VSC modules developed in PSCAD-EMTDC software, where by performing the recursive simulation-based optimisation procedure described in APPENDIX D, [76] for the OWF and the BtB MMC-HVDC modules separately, the rest of outer controllers are tuned and implemented in the total LFAC TS model for the EMT assessment.

The VSC modules that are analysed and tuned in this section correspond to the following offshore LFAC TS configurations:

- Point-to-Point LFAC TS scheme for grid integration of a 704MW OWF with a 200km export submarine LFAC cable.
- Multi-Terminal LFAC TS scheme that interconnects two of the above Point-to-Point LFAC TS schemes, offshore, through a 50km submarine cable, forming a meshed LFAC TS arrangement that connects to two different grids.

As explained in 6.3.4.3, the ICC loops in the onshore MMC terminals of the LFAC TS need to have high bandwidths regardless whether they are implemented in a grid-following (MT-LFAC arrangement) or the LFAC grid-forming MMC. Apart from the desired fast ICC response, high ICC bandwidth is required because if the potential low-order resonances of the corresponding LFAC TS configuration fall within the ICC bandwidth for any operating condition, then the VSCs “source” impedance dominates the total system impedance at this point and can effectively diminish the impact of the dynamic impedance of the passive LFAC TS to the LFAC network for normal operating conditions.

Depending on the operating mode of the PtP LFAC TS with 200km export cable, its low-order harmonic resonance at the onshore 345kV substation may range from  $\sim 55\text{Hz}$  to  $\sim 65\text{Hz}$  (3<sup>rd</sup> to 4<sup>th</sup> harmonic order), as seen in 4.2.5, while the highest resonant frequency of the system can be the natural resonance of the 200km cable at  $\sim 210\text{Hz}$ . In the MT-LFAC TS arrangement, the corresponding worst-case characteristic resonant frequency for tuning of the ICC bandwidth would also be the 210Hz for a 200km cable, while for a total cable length of 450km, this would lie at  $\sim 84\text{Hz}$ . Hence, the ICC regulator parameters that are selected for the PtP case can also be applied in the additional VSCs of the respective MT-LFAC TS arrangement without any potential adverse effect of the low-order dynamic impedance of the LFAC TS.

#### 6.4.1 Transfer Function Analysis

Transfer Function analysis is performed for the upper-level controllers of the equivalent OWF VSIs and both the LFAC and the AC grid side MMC terminals. The lower-level CCSC loops of the MMCs and all the ICCs are tuned for their desired characteristics, using the Modulus Optimum method described in 6.3.4.3. The outer DCVC gains are acquired by the pole placement technique discussed in 6.3.4.4 as a special case of the Symmetrical Optimum method for closed-loop systems that have complex poles.

#### 6.4.1.1 Time and Frequency Domain Analysis

The values of the PI compensators for the upper-level controllers are obtained by applying classic frequency and time response design techniques to the simplified linear models of the systems' Transfer Functions (TFs) in MATLAB. However, the simplified TFs only include the AC system up to the point of connection, while the linear analysis does not inform on the extent of the controller stability region, especially for the outer DCVC. Since the design of the controllers is based on linearizing the equations of the converter and neglecting the rest of the system, the stability of the controllers in the frequency domain analysis shall be considered only as "local" stability around the operating point.

With the OLTF of the systems calculated based on the above analysis, the Bode magnitude and phase are plotted while the phase and gain margins are identified by the stability criteria:

$$|G_{V,OLTF}(j\omega)| = 1, \text{ and } \angle G_{V,OLTF} = 180 + \Phi_M, \text{ where } \Phi_M \text{ is the phase margin.}$$

The related time-domain Transfer Function analysis of these systems is performed by exciting their total CLTFs through a unit-step function.

In this Thesis, all upper-level controllers tuned through the TF analysis have  $\zeta=0.707$ , while for the DCVCs tuning that the placement of the real pole and the damping of the complex pole can be specified, a distance of  $\gamma=10$  is assumed between the poles, according to [48].

#### 6.4.1.2 Tuning of Equivalent OWTGs VSI Modules

The PI regulator gains for the equivalent OWF VSI modules are presented in Table 6-3. The VSI ACVC gains are selected through MATLAB-SisoTool for fast, stable response, with adequate bandwidth, zero-steady state error and strong disturbance rejection.

*Table 6-3: Tuning Parameters of the Equivalent OWF VSI Modules.*

VSI Control System Tuning							
CS	Parameter	VSI	Unit	CS	Parameter	VSI	Unit
		fe	16.7		[Hz]		fe
I C C	$\tau$	0.8928	[s]	D C V C	Teq	0.00051	[s]
	$\zeta_{icc}$	0.707			Tc	0.0152	[s]
	$\omega_{nicc}$	2763.2	[rad/s]		K	0.8	
	Kp_icc	11.3620			$\zeta_{dcvc}$	0.707	
	Ti_icc	0.8928	[s]	$\gamma$	10		
ACVC	Kp_acvc	1.3773		Kp_dcvc	5.6898		
	Ti_acvc	0.0081	[s]	Ti_dcvc	0.0068	[s]	

In Figure 6.21, the Pole-Zero Maps of the ICC and DCVC of the yielded CLTFs are shown, after linearizing the systems TFs, while the Root-Loci of the OLTFs poles and zeros plot all the potential locations of the CLTF poles in the complex plane and demonstrate the "locally" stable behaviour of the CLTFs.

Table 6-4: Control System Response Characteristics of the Equivalent OWF VSI TFs.

VSI Control System Response											
CS	Parameter	VSI	Unit	CS	Parameter	VSI	Unit	CS	Parameter	VSI	Unit
		fe	16.7		[Hz]		fe		16.7	[Hz]	
I C C	RiseTime:	0.00078	[s]	D C V C	RiseTime:	0.0033	[s]	A C V C	RiseTime:	0.0022	[s]
	SettlingTime:	0.0022	[s]		SettlingTime:	0.0217	[s]		SettlingTime:	0.0210	[s]
	Peak:	1.043	[s]		Peak:	1.246	[s]		Peak:	1.246	[s]
	PeakTime:	0.0016	[s]		PeakTime:	0.0097	[s]		PeakTime:	0.0068	[s]
	GainMargin:	Inf	[dB]		GainMargin:	12.1	[dB]		GainMargin:	7.5	[dB]
	GMFrequency:	Inf	[rad/s]		GMFrequency:	2656.4	[rad/s]		GMFrequency:	2675.4	[rad/s]
	PhaseMargin:	65.53	[deg]		PhaseMargin:	56.027	[deg]		PhaseMargin:	61.45	[deg]
	PMFrequency:	1778.4	[rad/s]		PMFrequency:	327.5822	[rad/s]		PMFrequency:	502.4	[rad/s]

Also, the system response results in Table 6-4 show that fast regulation can be achieved with this high-bandwidth ICC loop,  $BW=2763\text{rad/sec}$  or  $\sim 440\text{Hz}$ ; much higher than the  $16.7\text{Hz}$  LFAC TS frequency. The fact that it is higher than even the natural resonance of the  $200\text{km}$  cable at  $\sim 210\text{Hz}$  can indicate that the dynamic impedance of the LFAC TS shall not cause any severe low-order harmonic stability issues to the LFAC network for normal operating conditions. Its time response in Figure 6.22 displays a stable and non-oscillatory closed-loop response, as through the MO method  $\zeta$  is defined and the controller zero (Ti) eliminates the dominant pole of the ICC-OLTF, as shown in the Pole-Zero Map.

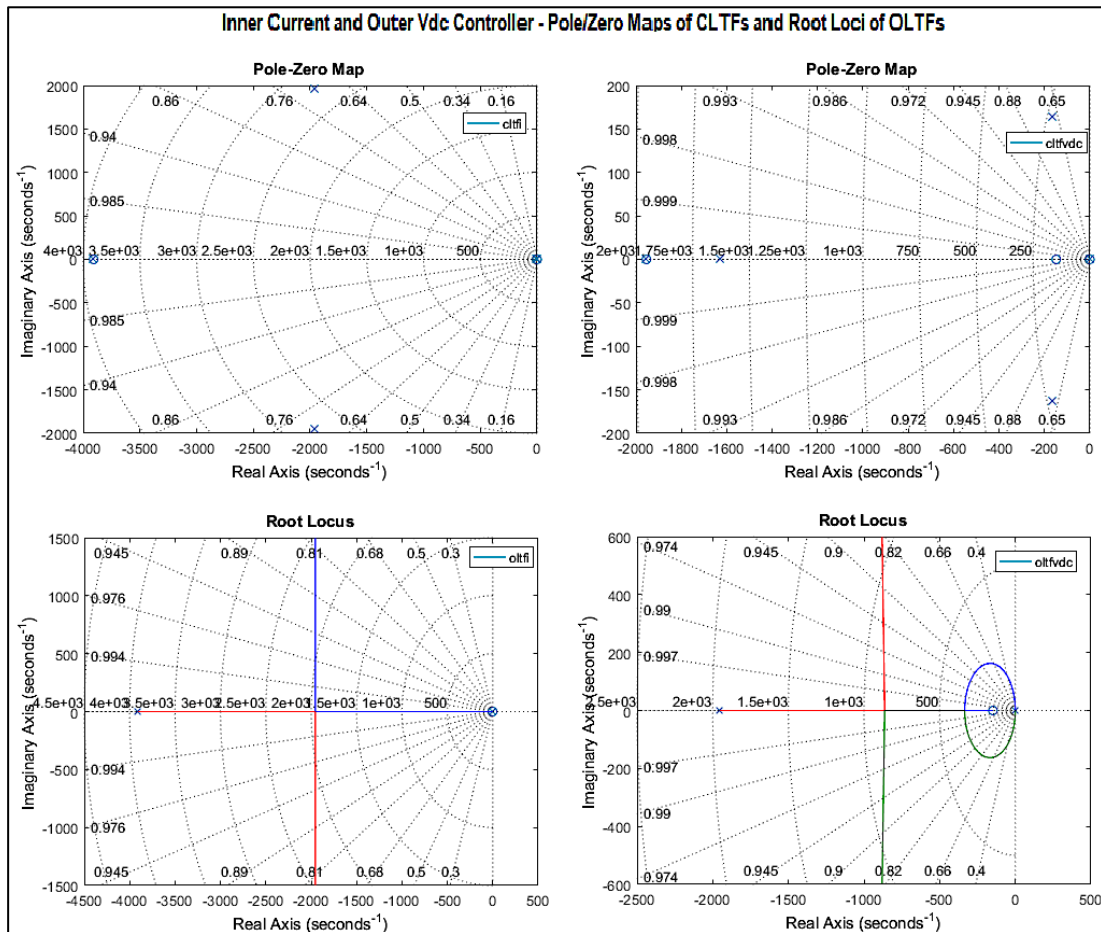


Figure 6.21: ICC (Left) and DCVC (Right) Pole-Zero Maps of CLTFs and Root Loci of OLTFS for the OWF VSI.

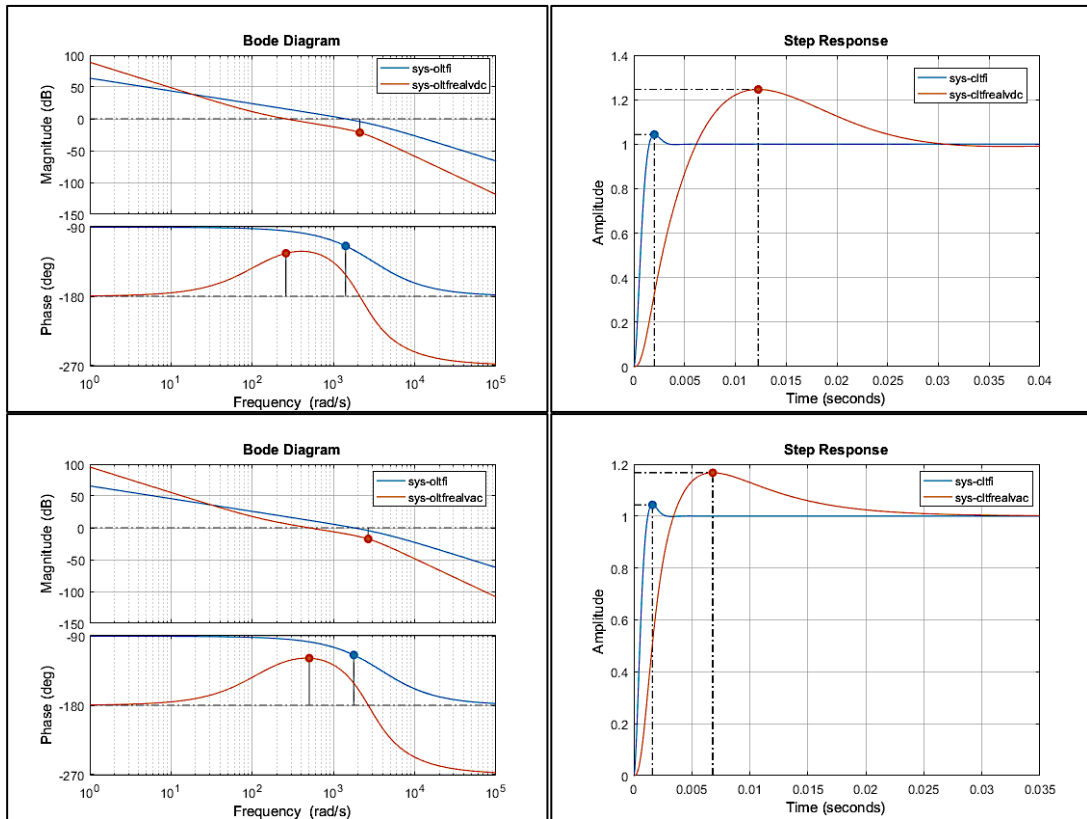


Figure 6.22: DCVC–ICC (Top) and LFACV–ICC (Bottom) Bode Diagrams and Step Responses for the OWF VSI.

The resulted DCVC may not have the largest possible phase-margin at  $56^\circ$ , but the desired closed-loop pole-zero configuration and system response is attained by specifying the damping factor ( $\zeta=0.707$ ; optimal damping) its complex poles, resulting in a bandwidth of 512rad/sec or 82Hz, while a slight decrease in overshoot but slower response would be achieved for higher values of  $\gamma$ .

Regarding the ACVC tuning, the phase-margin reaches its maximum value at  $61.45^\circ$  close to its crossover frequency, ensuring effective disturbance rejection and having a bandwidth of 840rad/sec. Generally, phase margins greater than  $45^\circ$  result in reasonably stable systems.

#### 6.4.1.3 Tuning of Frequency MMC-HVDC System

Here the ICCs for both the 16.7Hz LFAC and the 50Hz AC side MMCs are tuned according to the MO method for a bandwidth of 2192rad/sec and a damping factor of 0.707, presented in Table 6-5, which leads their corresponding controller zero eliminating their dominant poles of  $T_{i1}=0.2564\text{sec}$  and  $T_{i2}=0.0885\text{sec}$ , as plotted in Pole-Zero Maps of Figure 6.23 and Figure 6.24, respectively. This leads to the same frequency and time response characteristics, although the LFAC system operates with almost three times lower fundamental frequency. In the LFAC TS side, this ICC tuning corresponds to a bandwidth of  $\sim 350\text{Hz}$ , which is higher

than even the natural resonance of the 200km cable (~210Hz). This can indicate that the dynamic impedance of the LFAC TS shall not cause any severe low-order harmonic stability issues to the LFAC network for normal operating conditions. As expected, its bode plot in Figure 6.24 demonstrates stable response with infinite gain and phase margins.

*Table 6-5: Tuning Parameters of the Equivalent BtB MMC Modules*

MMC Control System Tuning				
CS	Parameter	MMC T1	MMC T2	Unit
	fe	16.7	50	[Hz]
C	tpuccsc	0.4547	0.1352	[s]
C	zccsc	0.707	0.707	
S	wnccsc	2192.0	2192.0	[rad/s]
C	Kp_ccsc	2.8005	0.8325	
C	Ti_ccsc	0.4547	0.1352	[s]
	τ	0.2564	0.0885	[s]
I	zicc	0.707	0.707	
C	wnicc	2192.0	2192.0	[rad/s]
C	Kp_icc	2.5113	1.2333	
C	Ti_icc	0.2564	0.0885	[s]
	Teq	0.00065	0.00065	[s]
D	Tc		0.0237	[s]
C	K		0.944	
V	zdcvc		0.707	
C	γ		10	
	Kp_dcvc		5.9336	
	Ti_dcvc		0.0085	[s]
RPC	Kp_rpc		1	
	Ti_rpc		0.0355	[s]
ACVC	Kp_acvc	1		
	Ti_acvc	0.0103		[s]

The DCVC of the 50Hz AC side MMC terminal is tuned by specifying its complex poles characteristics, as shown in Figure 6.25, leading to a closed-loop bandwidth of 407rad/sec or 65Hz, and a slightly smaller than maximum phase margin, shown in Figure 6.26, which would have been achieved by the classic SO tuning method, but here with lower overshoot at 25%.

Finally, the ACVC tuning can attain a stable response and strong disturbance rejection. As can be seen in Table 6-6, ACVC presents a phase-margin of 61.45° at its crossover frequency, and an adequate bandwidth of 659 rad/sec, zero-steady-state error and a settling time of 0.0265sec, that is almost ten times higher than the corresponding ICC.

*Table 6-6: Control System Response Characteristics of the Equivalent MMCs TFs.*

MMC Control System Response					
CST1	Parameter	MMC T1	MMC T2	Unit	CST2
	fe	16.7	50	[Hz]	
I C C	RiseTime:	0.00098	0.00098	[s]	I C C
	SettlingTime:	0.0027	0.0027	[s]	
	Peak:	1.043	1.043		
	PeakTime:	0.0020	0.0020	[s]	
	GainMargin:	Inf	Inf	[dB]	
	GMFrequency:	Inf	Inf	[rad/s]	
A C V C	PhaseMargin:	65.53	65.53	[deg]	D C V C
	PMFrequency:	1410.8	1410.8	[rad/s]	
	RiseTime:	0.0027	0.0044	[s]	
	SettlingTime:	0.0265	0.0274	[s]	
	Peak:	1.167	1.249		
	PeakTime:	0.0086	0.0123	[s]	
	GainMargin:	7.5	12.1	[dB]	
	GMFrequency:	2122.4	2107.0	[rad/s]	
	PhaseMargin:	61.45	56.03	[deg]	
	PMFrequency:	398.6	259.9	[rad/s]	



## 1) MMC-T1 Interfacing LFAC System with ICC

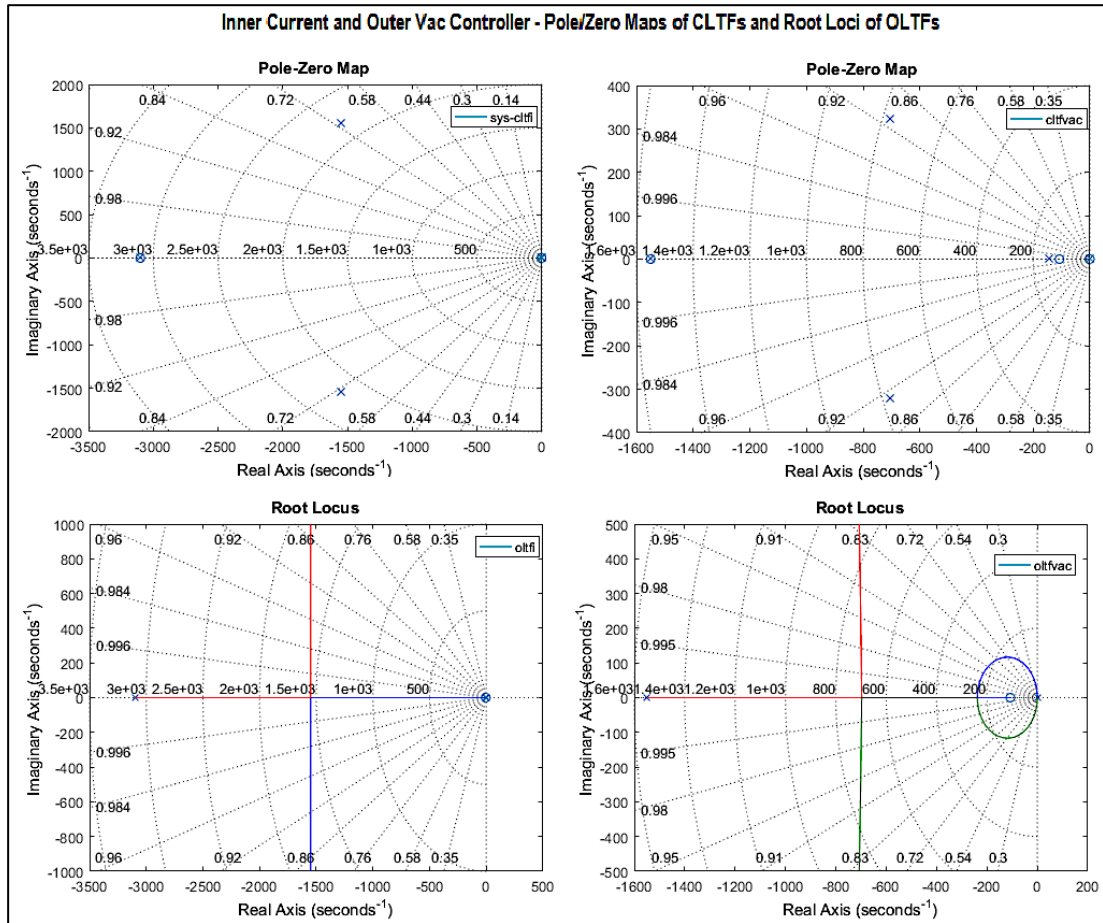


Figure 6.23: ICC (Left) and ACVC (Right) Pole-Zero Maps of CLTFs and RL of OLTFs for the MMC-T1 with ICC.

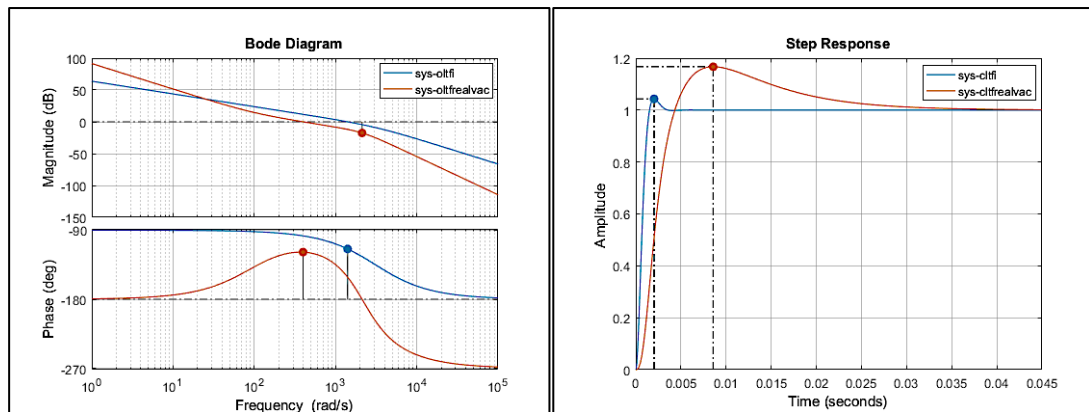


Figure 6.24: LFACVC – ICC Bode Diagram and Step Response for the MMC-T1 with ICC.

## 2) MMC-T2 Interfacing AC Grid

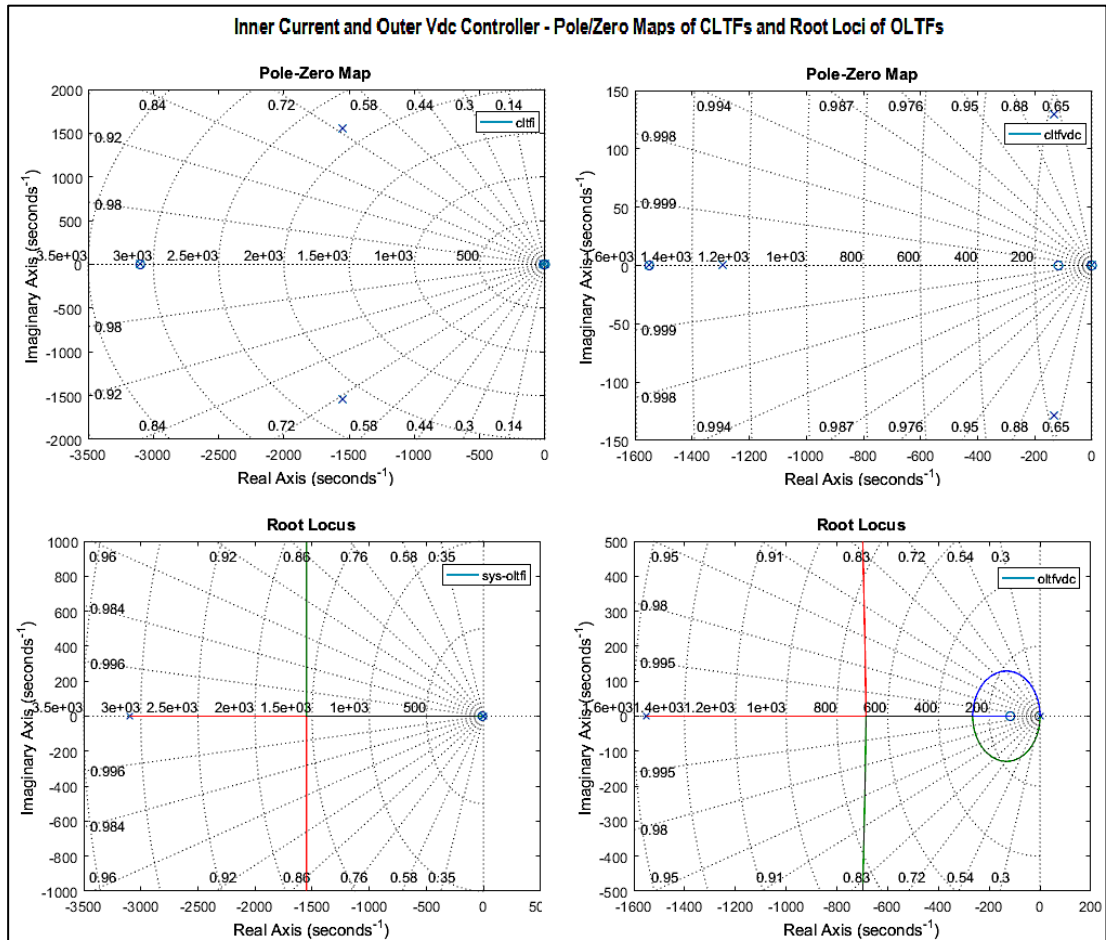


Figure 6.25: ICC (Left) and DCVC (Right) Pole-Zero Maps of CLTFs and Root Loci of OLTFs for the MMC-T2.

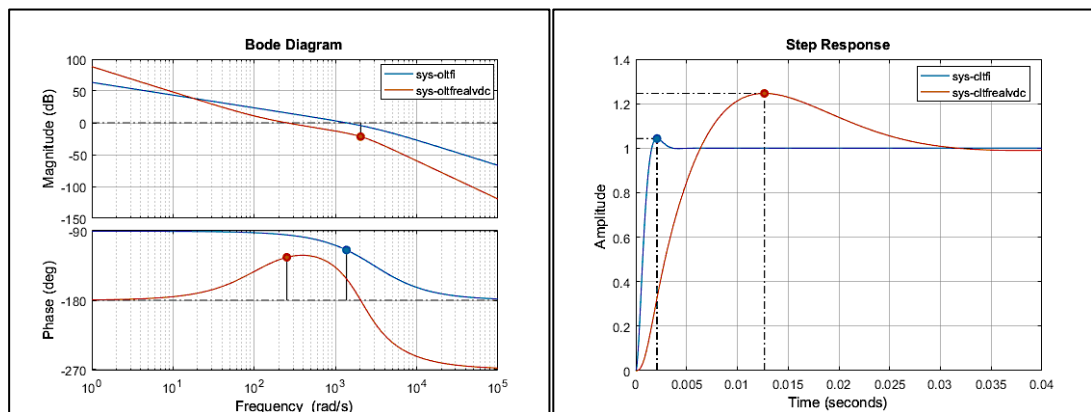


Figure 6.26: DCVC – ICC Bode Diagram and Step Response for the MMC-T2 with ICC.

## 6.4.2 OWF Module EMT Implementation

Based on the OWF VSI controller tuning in 6.4.1.2 and the recursive optimisation procedure described in APPENDIX D and [76], for the OWF rectifier APC, the OWF module dynamic performance is shown against APC demand variations in PSCAD EMTDC. The OWF is connected at 66kV to the OCS, the offshore 66/345kV step-up transformers and an ideal 16.7Hz voltage source at the 345kV connection point busbar.

Following the equivalent OWF module energisation procedure from the LFAC side at 3sec, the power ramps up to full within 1sec. Then, a power-step down to half occurs at 5sec and a power step-up at 6sec. The response of the rectifier's APC and the VSI's DCVC and ICC are presented in Figure 6.27, while the OWF response at 345kV busbar is shown in Figure 6.28.

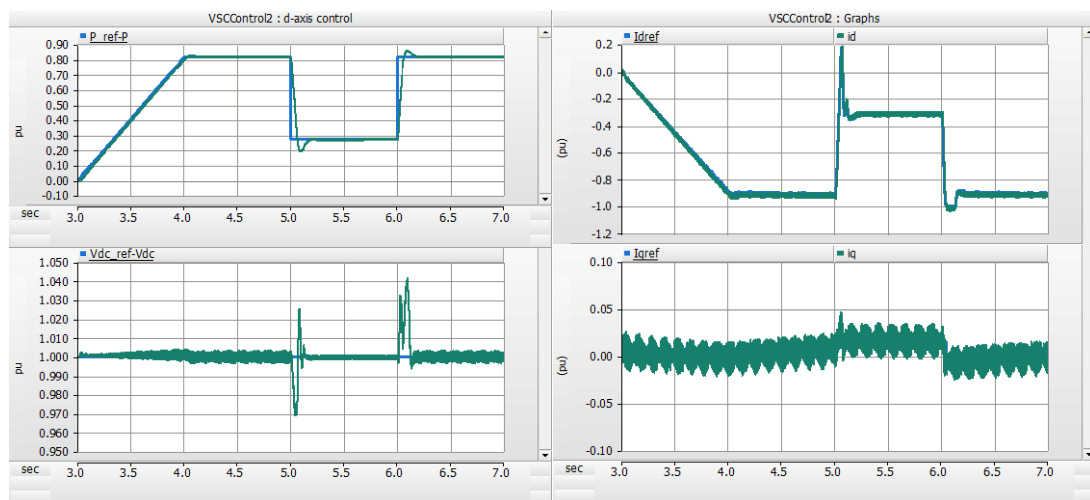


Figure 6.27: EMT Dynamic Response of the APC of OWF-VSC Rectifier and DCVC and ICC of OWF-VSI.

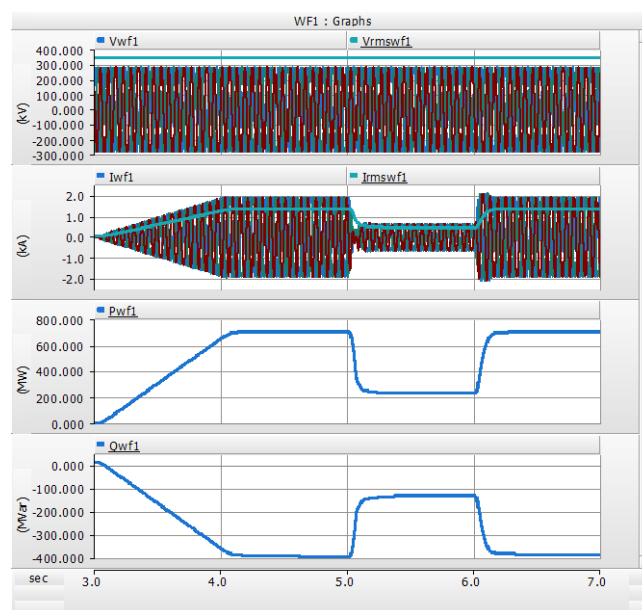


Figure 6.28: EMT Response of the OWF, showing the LFAC Voltage, Current, Active and Reactive Power.

## 6.5 Summary and Conclusions

In this chapter, the main LFAC TS components are modelled in time-domain, while the associated converter controllers are designed and tuned. The LFAC TS that is explicitly modelled for the EMT assessment of Chapter 7 comprises:

- The AC grids modelled as Thevenin equivalents based on their SCL and X/R characteristics.
- The LFAC subsea export cables which are modelled with frequency-dependent phase parameters (FDPM), as designed in Chapter 4.
- The OCS that is formed by its inter-array cables (pi-equivalent models) and the LFAC step-up transformers.
- The OWF module that aggregates 88 OWTGs modelled as an equivalent 704MW BtB VSC-HVDC system with two-level IGBT bridges, its LCL filters and 88 VSI transformers.
- The onshore BtB MMC-HVDC system, in which the HBSMs are represented by their Detailed Equivalent Model (DEM), for a reasonable trade-off between accuracy and simulation speed.

In addition, the control structures for the dynamic VSC and MMC models are introduced, and their upper-level control hierarchy is described. The generic VSC system Transfer Functions are presented for its AC and DC system sides up to the point of connection. The linearised TFs for the cascade VCC-based non-island control system of the grid-following converters and the island control system of the LFAC grid-forming converter are introduced. The desired VSCs' control system design and tuning requirements are assessed for the corresponding LFAC TS application, and suitable tuning methods are adopted.

More specifically, the cascade control systems adopt the MO method for tuning the inner PI controllers and a particular case of SO method for the outer DC voltage control loop. This can be considered an optimal combination for the offshore LFAC TS as the MO offers fast response and large ICC bandwidth, while the SO enhances system stability by improving its tolerance to disturbances. The upper-level controllers' tuning is evaluated through TF analysis in frequency and time domain. The outer APCs and RPCs of the grid-following converters, as well as the LFAC islanded voltage controller of the grid-forming MMC are tuned by employing a recursive simulation-based optimisation method that minimises the sum of the ITAE of the respective controlled quantities for the developed models in PSCAD EMTDC, as presented in APPENDIX D. Finally, the dynamic performance of the equivalent OWF module with its control system is examined for power output variations in PSCAD.

## Chapter 7: Dynamic Performance Time Domain Evaluation

### 7.1 Introduction

The previous chapters advocate that LFAC technology can be adopted for designing offshore transmission systems to integrate distant OWFs or even interconnect OWFs and grids with each other. However, the frequency scan studies in Chapter 4, as well as the power flow assessment in Chapter 5, demonstrate probable operating complications that may be surmounted by careful system design, effective harmonic filtering and proper VSC control arrangements. In prospective offshore developments using LFAC technology, long LFAC submarine cables would be associated with power converters on a much larger scale than the HVAC or HVDC OWFs. Accordingly, in these weak and inertia-less offshore LFAC systems, low-order harmonic resonances and control interactions can jeopardize the stable dynamic operation and economic feasibility of the systems.

In this section, the offshore LFAC transmission network is evaluated in time-domain, using EMT simulations. The EMT analysis of PtP and MT-LFAC TS arrangements is performed to produce technically feasible solutions that can assure stable operation in steady-state and dynamic conditions and comply with generic connection requirements for specific fault events and contingencies. The EMT studies assess the energisation procedures and evaluate the dynamic performance and fault handling ability of the LFAC TS arrangements following disturbances to the steady-state conditions. Such disturbances range from sudden OWF output power variations to onshore AC and offshore LFAC system faults in which the frequency converter station shall stay grid-connected for a predefined period of time, while the OWF converters shall stay connected to the LFAC TS, respectively.

Initially, PtP arrangements are assessed to discover any credible operating limitations, assess the different grid-forming converter control system configurations presented in Chapter 6 and evaluate potential passive mitigation measures (e.g. the harmonic filters designed in Chapter 4) that could improve the power quality and dynamic performance of the LFAC system. After a feasible PtP LFAC TS solution is established for the examined contingencies, the outcomes are adopted for the set-up of a multi-terminal connection that could potentially arise by merging multiple PtP systems or by expanding and interconnecting several LFAC terminals through submarine cables. The resulted cases can produce the foundations for practical meshed offshore LFAC TS arrangements and benefit the development of offshore LFAC grid systems.

### 7.1.1 LFAC TS Scheme Model for EMT Simulation Studies

The offshore LFAC TS design aims to achieve a technically feasible and straightforward solution, which would enable the power transfer among the interconnected OWFs and the respective grids as well as the exploration of its performance capabilities and thereof potential limitations. The focus is to study the transmission system dynamic stability and uncover potential interactions among its converter terminals and the rest of the system [96]. The PtP LFAC TS configuration under study is an OWF integration scheme using a 200km submarine cable export system, while the multi-terminal LFAC system comprises two similar OWF integration schemes (namely, Side-1 and Side-2) inter-connected with a 50km submarine cable linking the two different OCSs at the 345kV side. It is assumed that each OWF integration scheme connects to a different AC grid.

The LFAC TS configurations that are simulated here have been formerly reviewed in the steady-state assessment of Chapter 5, and the required conditions for the model set-up and initialisation in the EMT environment have been acquired. The converter control systems of the LFAC TS EMT models are developed using the standard control functions, and they are tuned using the general optimisation algorithms (e.g. MO, SO, ITAE), analysed in Chapter 6. The representation of the MMC systems is based on the DEM, while the Two-Level VSCs utilise an actual switching model with IGBTs, per the methods described in Chapters 3 and 6. In addition, each 704MW OWF is represented as one BtB VSC-HVDC model without being concerned with electromechanical transients related to the WT functioning or intra-WTG dynamics but reflecting the inter-array and OCS impedance characteristics of the OWPP configuration. Finally, the fidelity of subsea cable model is of particular importance for such offshore schemes and thus it is represented using the frequency-dependent phase model, which does also have an impact on the overall system response and simulation time.

The LFAC system EMT models need to produce a relatively accurate response for a range of studies, but the issue of accuracy against computational efficiency is of great concern for radial and meshed arrangements. The converter models are based on IGBTs that operate in microsecond scale, while their control systems cycles are in the order of 200-500 $\mu$ s, making them much faster and computationally intensive processes than those involved in classical transient stability analysis. Consequently, these timescales would have been too short for electro-mechanical phenomena or governor response effects on the LFAC TS and since the rotor-angle stability is not assessed here, the 50Hz AC grid systems can be represented by Thevenin equivalents, as presented in Chapter 6.

### 7.1.2 Offshore LFAC TS Energisation

As seen in Chapter 6, the energisation transient of the cable is similar to that of a capacitor bank, although the cable capacitance is distributed and surge propagation occurs along the cable, damping the transient. Since the cable's capacitance is in series with the transformer characteristic, isolating the LFAC transformer and cable can cause interactions between the capacitive cable component and transformer saturable iron-core inductive component due to the Ferro-Resonance of the system [110]. This may even result in sustained transient or temporary over-voltages with substantial time derivatives that can damage surge arresters and other equipment. In an equivalent HVAC system with long cables, the transformer-terminated switching energisation method [95] would be applied in which line is energised with an unloaded transformer already connected to the remote end.

However, when energising the cable or in a transformer-cable pair energisation process, the voltage can be gradually ramped up by the island-controller of the onshore frequency converter minimising the risk of high resonant over-voltages and high transient inrush currents in case of the energisation failure of un-loaded transformers. Thus, transient current and voltage stresses at the equipment can be avoided, and the restoration process can speed-up. Therefore, the MMC operation can present several advantages regarding black-start and energisation or restoration following blackouts in the LFAC grid. Naturally, during the energisation process, the LFAC system can be substantially disturbed, and thus a series of FFT measurements monitor the harmonic frequencies that are excited.

Another transient issue that can occur while energising cables using shunt reactors with a reactive power compensation ratio higher than 50%, that can be an LFAC TS case as seen in Chapter 5, is the zero-missing phenomenon [110]. During the energisation of a shunt compensated cable, the reactor current contains both an AC and a decaying DC component. The initial DC value reaches its peak if the terminal voltage value at the instant of energisation crosses zero, as the AC components of the cable capacitive and reactor inductive current are in phase opposition and partially cancel each other. Then, the breaker line current is dominated by the DC component and does not cross zero for several cycles, with the decay of the DC current depending on the cable and reactor resistance values. This DC component might also saturate nearby current transformers effectively “blinding” protection devices. Thus, for a fault during energisation, it may not be possible to open the CB's healthy-phase poles without damaging the breaker. Such breaker failures may be avoided if re-synchronised switching is applied where the three phases are connected at voltage zero crossing.



### 7.1.3 Offshore LFAC TS LVRT/FRT Requirements

As power converter interfaced systems are set to become key components of the power systems, their ability to ride-through AC system faults is of great importance. Depending on the grid strength at the PCC, a potential disconnection of a large OWF or interconnector (IC) that may occur during either an internal or a grid fault event can cause the voltage and frequency to drop further that may only disturb the grid, or even initiate cascade effects by triggering the disconnection of other devices and destabilise parts of the grid. Therefore, the grid code requires large OWFs and HVDC ICs to have certain LVRT and FRT capability [120].

A challenge when connecting OWFs via radial or multi-terminal LFAC TS to the host power systems can be to fulfil the related grid code requirements during power systems faults. It is essential to demonstrate that the OWFs and the rest of the LFAC TS can stay connected during AC grid fault conditions in order to meet the FRT requirements specified by grid codes. For faults in the offshore LFAC TS, a combination of suitable protection strategies and proper control system design for the various power converters of the scheme is required. The control shall ensure that the converters limit the fault current below the valve limits, but the output is enough for the system protection scheme to detect and isolate the fault. Once the offshore fault is cleared, the LFAC voltage and frequency of the offshore transmission system shall be imposed by the grid-forming converter that operates in islanded control mode, while the voltage levels to the various busbars of the system shall be promptly adjusted to their set points by all power converters, so that the stability of the offshore LFAC TS is maintained, and the power transfer is resumed. Depending on the control and protection strategy used, the FRT capability of the scheme can be further assisted by a DBR that absorbs excess power.

This Thesis solely focuses on the dynamic response of this converter dominated LFAC TS, on its inherent low-order harmonic issues as well as on its dynamic stability and FRT capability at the PCC with the AC grids. The system dynamic voltage stability is evaluated against typical requirements, though, no frequency or rotor-angle stability aspects are assessed. The developed LFAC TS models investigate the system's ability to meet grid code requirements for disturbances in the AC grid and the LFAC sides. The EMT simulation studies determine if the system is able to meet specific AC and potential LFAC FRT, voltage and reactive power requirements, and comply with related THD limits (e.g. the IEEE 519) in the tested cases. Furthermore, the system performance is reviewed for two control alternatives in the onshore grid-forming MMC and for applying of passive harmonic filters in the power export schemes. The most feasible approach is used for integrating a meshed MT-LFAC TS.



Consequently, the voltage-ride-through (VRT) capability for integrating OWPP to the grid system is essential for its stable operation. To evaluate the dynamic performance of the LFAC TS following a disturbance to a steady-state condition such as a sudden power variation or fault, the frequency converter station shall stay grid-connected for a predefined period of time, while the OWF converters shall stay connected to the LFAC TS, respectively. Typical grid connection requirements include a well-defined envelope of pre-fault, fault and post-fault voltage levels against time. Since the TSOs voltage profile requirements for SGs are usually different to 'Power Park Modules' or 'PPMs', the LFAC TS that is connected to the AC network through power electronic converters can be considered as a PPM. The plot in Figure 7.1 presents general voltage against time profile curves for PPMs proposed by ENTSO-E FRT Requirements for Generation (RfG) where the fault duration period shown can be defined by the specific critical clearing times of the respective power system [130].

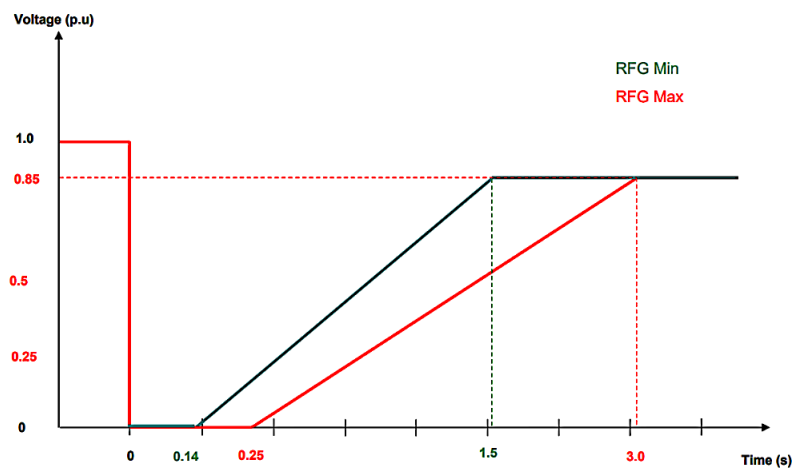


Figure 7.1: ENTSO-E RfG - Voltage Against Time Profile for PPM connected at or above 110kV.

In the horizontal-time-axis of Figure 7.1,  $T_{\text{fault}}=0\text{sec}$  is fault time,  $T_{\text{clearmin}}=0.14\text{sec}$  or  $T_{\text{clearmax}}=0.25\text{sec}$  are the minimum and maximum fault clearing times, and  $T_{\text{rec}}\sim 1.5\text{sec}$  to  $3\text{sec}$  is the recovery time, while their respective voltage points are marked in the vertical axis.

In the GB grid, generating units shall remain connected and transiently stable without tripping for a close-up solid three-phase short circuit fault or any unbalanced short-circuit fault on the transmission system operating at super grid voltages for a total fault clearance time of up to  $T_{\text{clear}}=140\text{msec}$  and for voltage dips bigger than 140msec in duration. The zero-voltage duration and the fault clearance time depends on local protection and circuit breaker operating times and is specified in an individual agreement between the TSO and the owner of the generation unit. Following fault clearance, recovery of the super grid voltage to 90% may take up to a certain period of time, even minutes [116].

## 7.2 EMT Studies Set-Up and Scenario Cases for LFAC TS Schemes

The EMT simulation studies are conducted using a 50µs time-step on a Dell Precision T7600 workstation including two Intel(R) Xeon(R) CPU at 3.10GHz, with a total of 16 Core(s) or 32 Logical Processor(s) and 32GB of RAM. The PSCAD X4.6.3 version with Parallel Network Interface (PNI) feature was utilised, splitting the model at each transmission cable segment so that each part of the system can be simulated separately by different dedicated cores. The EMT studies performed for the PtP LFAC TS as well as for the MT-LFAC TS are presented in Table 7-1 and Table 7-2. Each study comprises the following three different dynamic cases:

- a) System Energisation-to-Full Power
- b) System Response to OWF Power Output Variations
- c) FRT performance for solid three-phase to ground faults at the 50Hz AC grids as well as at the OCS of the 16.7Hz LFAC side of the transmission system.

Table 7-1: List of EMT Studies and Cases for PtP LFAC TS.

EMT Study	LFAC TS Dynamic Performance - Point-to-Point EMT Cases	
EMT 1	CASES	Point-to-Point LFAC TS with 704MW OWF and 1 x 200km Export Cable (ISLANDED - <i>NO ICC</i> )
	a	i) System Energisation-to-Full Power <i>Without H-Filter</i> , equivalent to PF2b study ii) System Energisation-to-Full Power <i>With H-Filter</i> , equivalent to PF2bh study
	b	Power Demand Variations
	c	i) FRT-1: 50 Hz Grid Side Fault at 400kV ii) FRT-2: 16.7 Hz OCS Side Fault at 345kV
EMT 2	CASES	Point-to-Point LFAC TS with 704MW OWF and 1 x 200km Export Cable (ISLANDED - <i>With ICC</i> )
	a	System Energisation-to-Full Power <i>Without H-Filter</i> , equivalent to PF2b study
	b	Power Demand Variations
	c	FRT: 50Hz Grid Side Fault at 400kV and 16.7Hz OCS Side Fault at 345kV

Table 7-2: List of EMT Studies and Cases for MT-LFAC TS.

EMT Study	LFAC TS Dynamic Performance - Meshed EMT Cases (MMC-1, ISLANDED - <i>WITH ICC</i> )	
EMT 3	CASES	Multi-Terminal Offshore LFAC TS Interconnecting 2 x 704MW OWFs and 2 Grids with a 50km and 2 x 200km Cables
	a	System Energisation-to-Full Power <i>Without H-Filters</i> , equivalent to PF5a and PF5e studies
	b	Power Demand Variations in Generation and Interconnection, equivalent to PF5d and PF5e studies
	c	FRT: 50Hz Grid Side 1 Fault at 400kV, 16.7Hz OCS Side Fault at 345kV and 50Hz Grid Side 2 Fault at 400kV

More specifically, for the PtP LFAC TS with 1x200km OWF export cable, two EMT scenarios are considered in terms of their dynamic performance. In **EMT 1** the frequency MMC Terminal facing the 16.7Hz side (*MMC-T1*) applies a typical island control to the LFAC system as presented in Chapter 6, without adopting an Inner Current Controller (*No ICC*). In this study, **case-a** also weighs the efficacy of Harmonic-Filters (H-Filters). In **EMT 2**, the MMC-T1 applies island control by engaging an Inner Current Controller scheme (*With ICC*), and the results between EMT1 and EMT 2 are compared. Finally, in **EMT 3** the LFAC grid-forming MMC Terminal facing the 16.7Hz system *Side-1* (*MMC1 T1*) employs the more suitable island control with ICC, while the MMC Terminal facing the 16.7Hz *Side-2* (*MMC2 T2*) applies classic

grid-following VCC using ACVC. All the above cases are set-up according to their corresponding Power-Flow studies of Chapter 5 with the OWF VSI employing ACVC and DCVC.

### 7.3 Point-to-Point LFAC TS Schemes for OWF Integration

The schematic of the EMT model for the PtP LFAC TS scheme is illustrated in Figure 7.2.

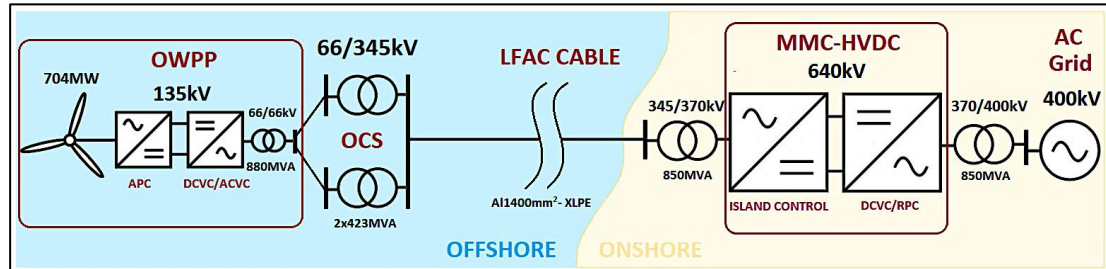


Figure 7.2: Schematic of the EMT model for OWPP Integration using the PtP LFAC Export System.

#### 7.3.1 EMT1: Island Control without ICC on the LFAC Side MMC-T1

The cases assessed in EMT1 study are specified in Table 7-3, and further explained below:

Table 7-3: List of Cases for EMT1 Study.

EMT Study	CASES	LFAC TS Dynamic Performance - Point-to-Point EMT Cases
EMT 1		Point-to-Point LFAC TS with 704MW OWF and 1 x 200km Export Cable (ISLANDED - NO ICC)
	a	i) System Energisation-to-Full Power Without H-Filter, equivalent to PF2b study ii) System Energisation-to-Full Power With H-Filter, equivalent to PF2bh study
	b	Power Demand Variations
	c	i) FRT-1: 50 Hz Grid Side Fault at 400kV ii) FRT-2: 16.7 Hz OCS Side Fault at 345kV

- **Cases EMT1ai** and **EMT1aii** demonstrate the energisation procedure of the LFAC export system and validate the effect of passive damping harmonic filters on the transmission system operation.
- **Case EMT1b** shows the dynamic performance of the LFAC export system and its associated control schemes on imposed power demand variations in the OWF.
- **Cases EMT1ci** and **EMT1cii** demonstrate the system's fault-ride-through (FRT) ability in case of a solid three-phase to ground faults at the 400kV busbars of the 50Hz grid as well as the offshore platform 345kV busbars of the 16.7Hz system.

#### a) LFAC TS Energisation-to-Full Power without and with Filtering

The timeline of system dynamic events for the LFAC TS energisation case EMT1a is shown in Table 7-4.

Table 7-4: Simulation Sequence for Case EMT1a.

EMT1		LFAC TS Dynamic Performance - Point-to-Point EMT Cases
Case a		Point-to-Point LFAC TS with 704MW OWF and 1 x 200km Export Cable (ISLANDED - NO ICC)
Time	[s]	LFAC System Energisation-to-Full Power: i) Without and ii) With H-Filter, equivalent to i) PF2b and ii) PF2bh studies
t0	0.0	Initialization: The 50Hz Grid-Side AC Voltage Source Ramps Up to 400kV within 0.05 [s]
t1	0.5	Grid Side MMC Terminal Deblocks: Imposes V <sub>dc</sub> and Q control at the 400kV PCC (v <sub>dc_ref</sub> =1pu, q <sub>ref</sub> =0)
t2	1.0	LFAC Side MMC Terminal Deblocks: Imposes V <sub>lfac</sub> and freq islanded control (v <sub>ac</sub> : 0-->1pu within 1[s], freq=16.7Hz)
t3	3.0	OWF Equivalent Back-to-Back VSC Module Connects
t4	3.5	OWF Inverter Deblocks: Imposes V <sub>dc</sub> and V <sub>lfac</sub> control (v <sub>dc_ref</sub> =1pu, v <sub>ac_ref</sub> =1pu with 0.0834 v <sub>ac</sub> /q droop)
t5	3.7	230MVar LFAC Cable Shunt Reactor Located Onshore Gradually Reduced to 0MVar within 1[s], according to Power Flow Studies i) PF2b and ii) PF2bh for No-Load and Full-Load Operation respectively
t6	4.0	OWF Rectifier Deblocks: Imposes P control (Pref=0)
t7	4.7	LFAC Cable's Shunt Compensator Circuit Breaker Opens, Disconnecting the Reactor
t8	5.0	OWF Active Power Ramps Up to Full Power with p <sub>ref</sub> : 0-->1pu within 1 [s]. Active power increase rate: 1pu/s
t9	8.0	End of Simulation

More explicitly, the simulation sequence of the LFAC export system Energisation-to-Full Power studies can be described as follows:

- t0: Initialization** - The 50Hz grid-side AC voltage source ramps up to 400kV within 0.05s, energizing the grid side MMC Terminal (MMC-T2) transformer. Although MMC-T2 is blocked at that moment, the DC voltage can never be zero as the modules used in the MMC converter are half-bridge (HBSMs) and not full bridge.
- t1: Grid Side MMC Terminal Deblocks** - Imposes  $V_{dc}$  and Q control at the 400kV PCC ( $v_{dc\_ref}=1pu$ ,  $q_{ref}=0$ ). The HBSM capacitors are being charged and DC voltage reaches the demand value. This causes a transient current surge at the PCC but damps out fast.
- t2: LFAC Side MMC Terminal Deblocks** - Imposes  $V_{LFAC}$  and freq islanded control without ICC scheme at the onshore 345kV LFAC busbar ( $v_{ac}$ : 0-->1pu within 1s, freq=16.7Hz), black-starting the 16.7Hz system with its H-Filters and energizing the LFAC submarine cable with its compensating reactors and the OCS transformers. LFAC voltage increase rate is 1pu/s. During this period, the system absorbs some active power from the 50Hz grid to feed the LFAC TS online equipment. The MMC-T1 absorbs a great amount of reactive power when the voltage reaches the demanded value, although the onshore 230MVar LFAC cable shunt reactor is connected.
- t3: OWF Equivalent Back-to-Back VSC Module Connects** - The Circuit Breaker that connects the 66kV inter-array cable system and the OWF Module closes.
- t4: OWF Inverter Deblocks** - Imposes  $V_{dc}$  and  $V_{LFAC}$  control at the offshore 345kV busbar ( $v_{dc\_ref}=1pu$ ,  $v_{ac\_ref}=1pu$  with  $v_{ac}/q=0.05/0.6=0.0834$  LFAC Voltage Droop). This can be considered analogous to t1 when the MMC-T2 de-blocks. However, the DC Voltage of the OWF BtB VSC system is already established by pre-charging the capacitors, and the ACVC adjusts the voltage level without causing a surge current in the LFAC system.

- **t5:** 230MVar LFAC cable shunt reactor located onshore gradually reduces to 0MVar within 1s, according to Power Flow studies PF2b PF2bh for No-Load and Full-Load operation respectively. This increases the reactive power that is absorbed by MMC-T1 and produced by the OWF.
- **t6: OWF Rectifier Deblocks** - Imposes P control ( $P_{ref}=0$ ).
- **t7:** LFAC cable's shunt compensator circuit breaker opens, disconnecting the reactor and avoiding the zero-missing phenomenon explained in 7.1.2.
- **t8: OWF Active Power Ramps Up to Full Power with  $p_{ref}: 0 \rightarrow 1pu$  within 1s** - Active power increase rate: 1pu/s. Thus, within 1s, the power output of the OWF reaches 704MW. As projected by the corresponding Power-Flow cases; the increase in the active current component of the system gradually increases the reactive current component in the offshore cable end while reducing it in the onshore cable end, resulting in a greater amount of total current.

i) Without Passive Filtering

The EMT1ai) study result graphs of Figure 7.3 display from top to bottom the Voltage, Current, Real Power, Reactive Power, and the bar charts of Voltage and Current THD, in the order that they appear, for the offshore (WF1 Graphs-Left) and onshore (T1-16.7Hz Graphs-Right) submarine LFAC cable sides.

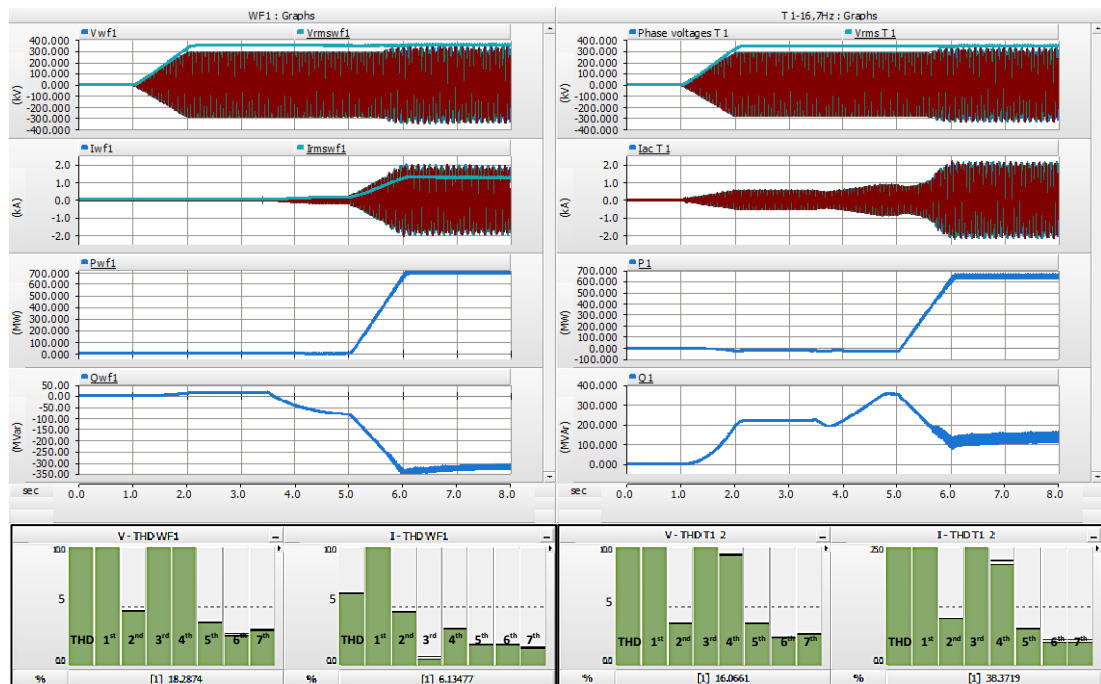


Figure 7.3: EMT1ai) Study Result Graphs at the Offshore (Left) and Onshore (Right) LFAC Cable Sides.

From the above graphs, it can be evident that during the energisation procedure of the export system, almost 29MW of real power are consumed by the subsea cable and the 230MVAR shunt reactor. Since there is no passive harmonic filter element installed in the onshore side of the subsea cable, the current measured at the 345kV busbar from 2sec to 3.5sec is the cable charging-breaking current after having been compensated by the shunt reactor which is less than 0.5kA peak phase current. This agrees with the PF2b No-Load case and the IEC preferred value of 0.355kA, although in PSCAD model, the step-up transformers are also included during energisation to accelerate the initialisation procedure. Besides, after 3.5sec, when the OWF BtB VSCs deblock applying ACVC without producing real power and the shunt reactors are gradually removed, the reactive power in the system is rearranged to support the corresponding voltages at each side of the cable. Thus, at the time that the OWF system generates full power, the reactive power value at the 345kV offshore cable side is close to -300MVAR and 115MVAR at the onshore that coincide with the PF2b Full-Load case.

In all the EMT cases studied in this Thesis, the sets of 8 harmonic bar-charts, as the one shown in the bottom of Figure 7.3, are drawn with a maximum displayed value of 10.0%, and as they appear from left-to-right, they present: the THD, the 1<sup>st</sup> or fundamental frequency, the 2<sup>nd</sup>, 3<sup>rd</sup>, 4<sup>th</sup>, 5<sup>th</sup> and 7<sup>th</sup> harmonic orders. Since no harmonic mitigation measures are applied in EMT1ai) and the LFAC grid-forming MMC does not control the current, the system resonance formed between the 3<sup>rd</sup> and 4<sup>th</sup> harmonic orders, as seen in Chapter 4, is not damped affecting the harmonic spectrum accordingly. This parallel resonance amplifies the harmonic currents and the harmonic voltages in the onshore LFAC side, as the “source” impedance of the islanded control system without an ICC does not dominate the LFAC TS impedance. As a consequence, these harmonics get more excited when the OWF output increases to full power as can be seen in Figure 7.4, where the current distortion (THDi~38%) is higher than the corresponding voltage THDv~16% at the onshore cable side.

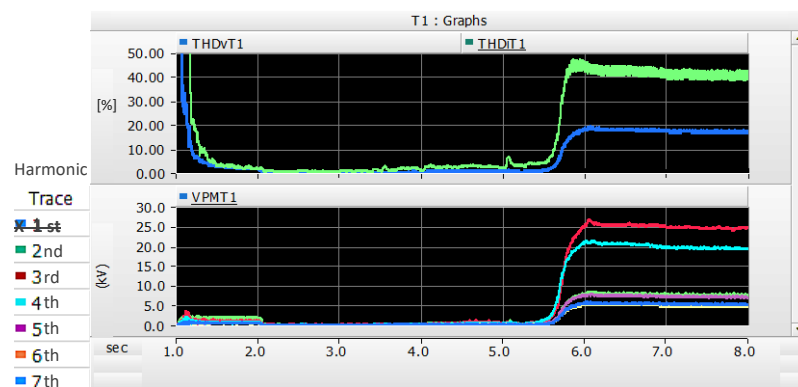


Figure 7.4: EMT1ai) Onshore 345kV-Top: THDv and THDi [%], Bottom: Voltage Harmonics [kV-Vllpeak] (1<sup>st</sup> out).

With the amplification caused by the dynamic impedance of the LFAC TS, a high voltage distortion appears mainly consisting of low order harmonics, despite the MMC converter being able to generate its own “timing voltage” and impose it upon the system. The harmonic distortion is also affected by the dq voltage controller, as shown in the plots of Figure 7.5. After 5.5sec, the controller’s attempt to adjust the severely distorted LFAC voltage waveform produces a disturbed converter output voltage in the absence of any ICC scheme, which leads to further amplification of current harmonics.

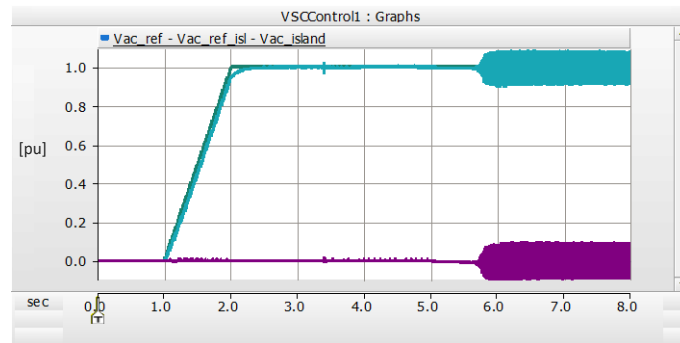


Figure 7.5: LFAC DQ-Voltage of the Islanded Controller in the MMC-T1 for EMT1ai), (d-green, q-purple).

Under the examined conditions, the LFAC system performance is unacceptable due to the THD produced by system resonance and uncontrolled system currents. As a first step, the impedance profile needs to be improved in order to sustain the operation of the BtB MMC system. If the system resonances remain undamped, they jeopardise low-order harmonic stability and may even create voltage stability issues during system disturbances. In Chapters 4 and 6, relevant mitigation measures are proposed that comprise either passive filtering with a proper compensation adjustment or ICC implementation on the LFAC side MMC controller or a combination of both.

Nevertheless, this harmonic distortion on the 16.7Hz side does not seem to affect the DC-Link voltage and current of the OWF equivalent module, but it has an impact on the DC side of the BtB frequency converter, increasing the DC-link current ripple to a level of 7% peak to peak. At the 50Hz AC side, an undistorted voltage (THD<sub>v</sub>=0.35%), and a relatively distorted 2<sup>nd</sup> harmonic order current (THD<sub>i2</sub>~1%) waveforms are noticed. From the rest of the graphs, during the energisation procedure of the LFAC export system, almost 36.5MW of real power need to be transferred from the 50Hz AC grid to the 16.7Hz LFAC system, while for full OWF power output, the system delivers to the grid 637MW which corresponds to ~9% of power losses, introducing 0.5% of harmonic losses. Finally, the MMC-T2 RPC always manages to maintain Q near zero at the 400kV PCC.

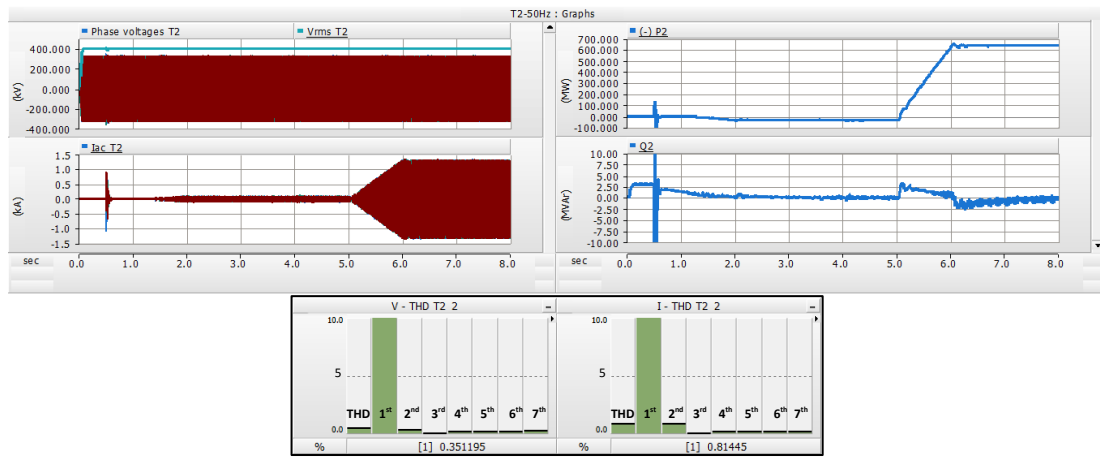


Figure 7.6: EMT1ai) Study Result Graphs at the PCC with the AC Grid.

Hence, the offshore LFAC export scheme with 200km long subsea cable that does not employ passive filtering equipment or other active mitigation measures should not utilise typical islanded control system without ICC in its onshore LFAC side frequency converter. Such an arrangement with its LFAC grid-forming MMC acting as a voltage source dependent only on the DC voltage condition without controlling the system current can be prone to low-order harmonic instability due to interactions with the system dynamic impedance that varies with its operating conditions.

ii) With Passive Filtering

In this case, 300MVar of harmonic filters are implemented in the onshore 345kV busbar to mitigate the system resonances for the most critical low order frequencies. More specifically, the LFAC export system with 200km long submarine cable is set-up according to power flow study PF2bh, utilising two c-type filters, a 200MVar tuned at 43Hz and a 100MVar tuned at 54Hz as designed in Chapter 4. The aim is to eliminate the harmonics excited in the energisation case EMT1ai and ensure the stable operation of the system without modifying the MMC-T1 control system. Figure 7.7 displays the related results in the offshore and onshore 345kV LFAC busbars, respectively.

Due to the presence of 300MVar passive damping filters installed in the onshore side of the subsea cable, the current measured at the 345kV busbar during energisation of the system is not the cable charging-breaking current. Thus, for full-power operation, the reactive power consumption by the onshore LFAC side MMC-T1 at the 345kV can be close to 415MVar, which matches the PF2bh results. Moreover, the harmonic bar-charts in Figure 7.7. confirm the effectiveness of the passive H-filters as both the offshore and onshore LFAC side voltage and current harmonics are diminished without amending the MMC-T1 control system.



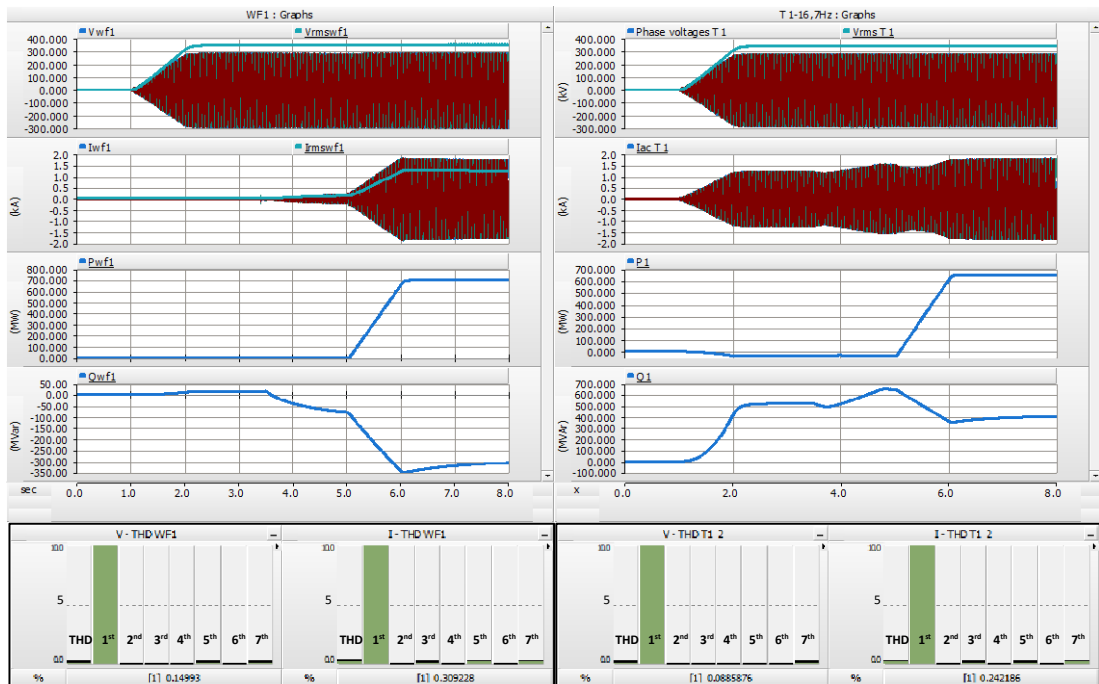


Figure 7.7: EMT1aii) Study Results at the Offshore (Left) and Onshore (Right) LFAC Cable Sides.

As can be seen in Figure 7.8., the  $THDi \sim 0.25\%$  and the  $THDv \sim 0.1\%$  at the onshore cable side are much lower than the specified IEEE-519, 2014 limits shown in Table presented in Chapter 4, so the harmonics neither affect the steady-state operation nor the transient stability of the scheme. Although in Figure 7.8, the THD values seem to get disturbed during transients, it can be contemplated as a harmonic measurement artefact, and the THD calculation should be considered valid only for the various steady-state conditions of each case.

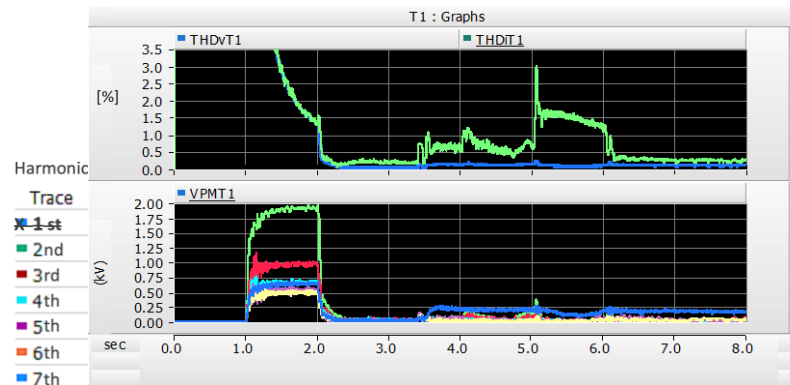


Figure 7.8: EMT1aii) Onshore 345kV-Top: THDv and THDi [%], Bottom: Voltage Harmonics [kV- $V_{llpeak}$ ] (1<sup>st</sup> out).

It is apparent that the LFAC system performs better in EMT1aii) than in the case without passive filtering, and apart from the additional filtering equipment losses ( $\sim 0.5\text{MW}$ ), no additional compensating reactors are employed which leads to only marginally higher system operating losses  $\sim 1\text{MW}$ , instead of almost  $3\text{MW}$  of harmonic losses in EMT1ai). In addition,

no voltage distortion appears in the islanded dq-voltage controllers shown in Figure 7.9, and the converter output voltage effectively follows the dq-domain references.

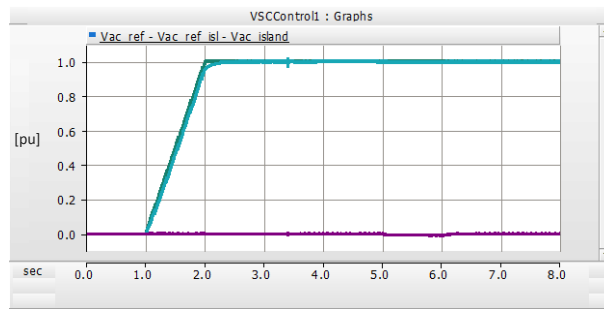


Figure 7.9: LFAC DQ-Voltage of the Islanded Controller in MMC-T1 for EMT1aii), (d-green, q-purple).

Hence, no related distortion is noticed either at the OWF or the MMC HVDC sides, while at the 50Hz AC side, the slightly excited second harmonic order current that is noticed in EMT1ai) does not appear in this case, as can be seen in Figure 7.10.

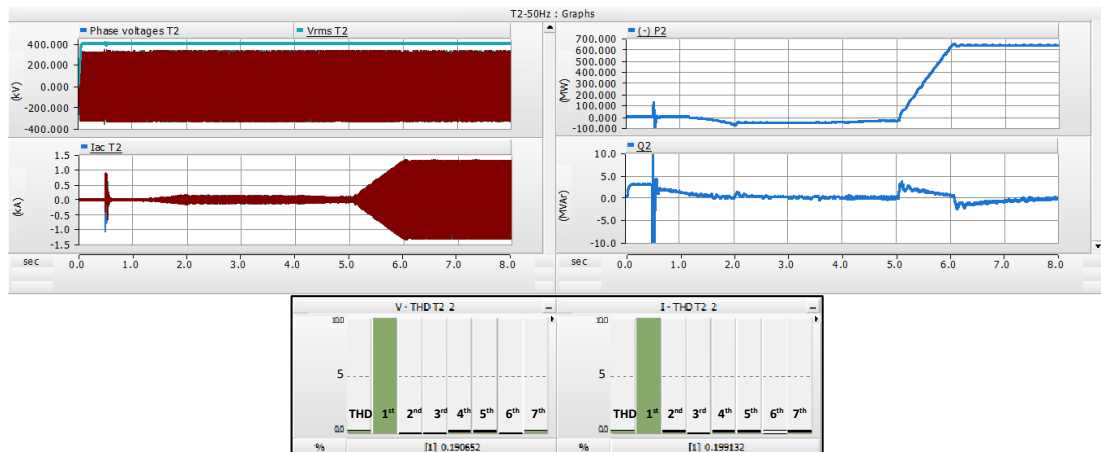


Figure 7.10: EMT1ai) Study Result Graphs at the PCC with the AC Grid.

This LFAC case resembles with offshore HVAC export schemes but having more extended potential submarine cable reach (e.g. up to 400km). In an equivalent HVAC export scheme, the grid could be considered as an independent 50Hz voltage source without a current control mechanism at the PCC, so a common approach to suppress system harmonics would also be to employ harmonic mitigation measures either in the form of passive damping filters or in the form of FACTS devices (e.g. STATCOMs, active filters, etc.). Similar harmonic mitigation measures might also be applied to the collector system at the offshore platform of an HVDC export scheme for much shorter AC cables and thus, for higher-order harmonics. Hence, the harmonic filtering equipment, as assessed in Chapter 4, can effectively be used to avoid harmonic instability on the 16.7Hz side of the LFAC TS as well.

b) Power Demand Variations with Filtering

The EMT1b case examines further the dynamic performance of the above point-to-point LFAC system arrangement for power demand variations in the equivalent OWF rectifier when employing passive damping filters in the onshore side. The timeline and sequence of simulation events for the LFAC export system dynamic response to OWF power demand variations in case EMT1b is demonstrated in Table 7-5.

Table 7-5: Simulation Sequence for Case EMT1b.

EMT1		LFAC TS Dynamic Performance - Point-to-Point EMT Cases
Case b		Point-to-Point LFAC TS with 704MW OWF and 1 x 200km Export Cable (ISLANDED - NO ICC)
Time	[s]	Power Demand Variations
t9	8.0	OWF Active Power Ramps Down to Half Power with p_ref: 1-->0.5pu in 0.5 [s]. Active power decrease rate: 1pu/s
t10	10.5	OWF Active Power Ramps Up to Full Power with p_ref: 0.5-->1pu within 0.5 [s]. Active power increase rate: 1pu/s
t11	13.0	End of Simulation

Figure 7.11 displays the relevant results in the onshore 16.7Hz/345kV LFAC busbar and the 50Hz/400kV AC grid busbar at the PCC, respectively.

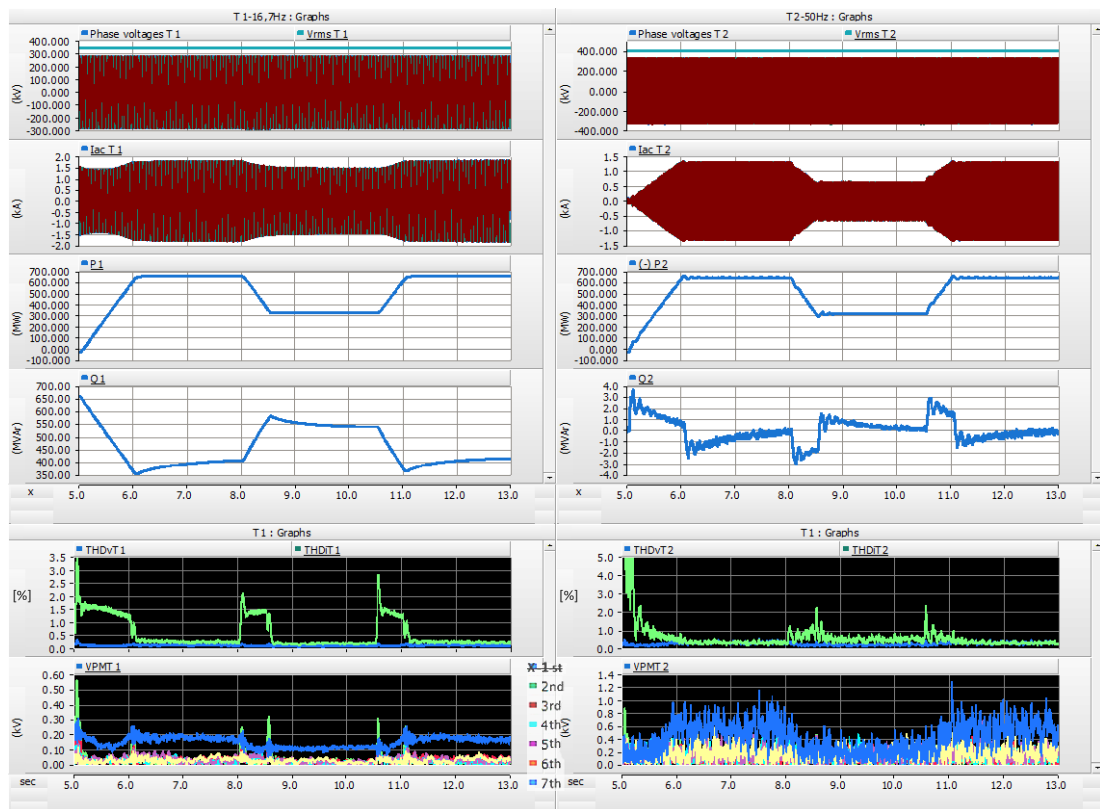


Figure 7.11: EMT1b Study Results at the Onshore LFAC Cable Side (Left) and the PCC with the AC Grid (Right).

The above graphs show that when the power output of the OWF reduces to 50%, generating 352MW, the MMC-T2 inverter delivers ~310MW to the 50Hz grid. During these active power variations, the AC grid side voltage remains unaffected, while the MMC-T2 RPC promptly responds by bringing reactive power to zero at the 400kV PCC. The MMC-T1 islanded

controller also manages to maintain the LFAC voltage seamlessly during the current and power variations. This is also verified by the dq islanded LFAC voltage controller shown in Figure 7.12, where the converter output voltage suitably follows the dq LFAC voltage demands without any apparent distortion. As the voltage and current harmonics in the system are not excited due to an interaction with its damped resonant impedance, the islanded LFAC voltage controller accurately adjusts the voltage level of the system regardless of the current variations. Thus, it acts as a low-frequency controlled voltage source that depends only on the HVDC voltage conditions, while the rest of the system with damped resonance determines the current.

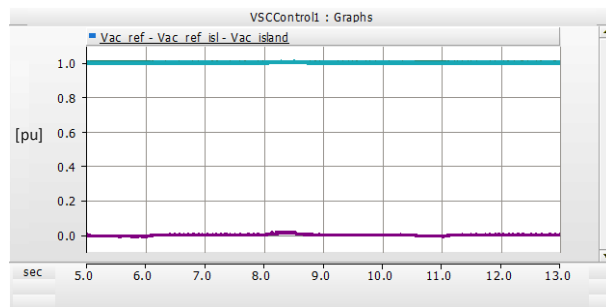


Figure 7.12: LFAC-DQ Voltage of the Islanded Controller in MMC-T1 for EMT1b, (d-green, q-purple).

The BtB frequency converter HVDC-Link voltages and currents from both the MMC-T1 and the MMC-T2 sides can be seen in Figure 7.13. The DCVC satisfactorily adjusts the DC voltage at 640kV, without being disturbed by the fixed DC current variations.

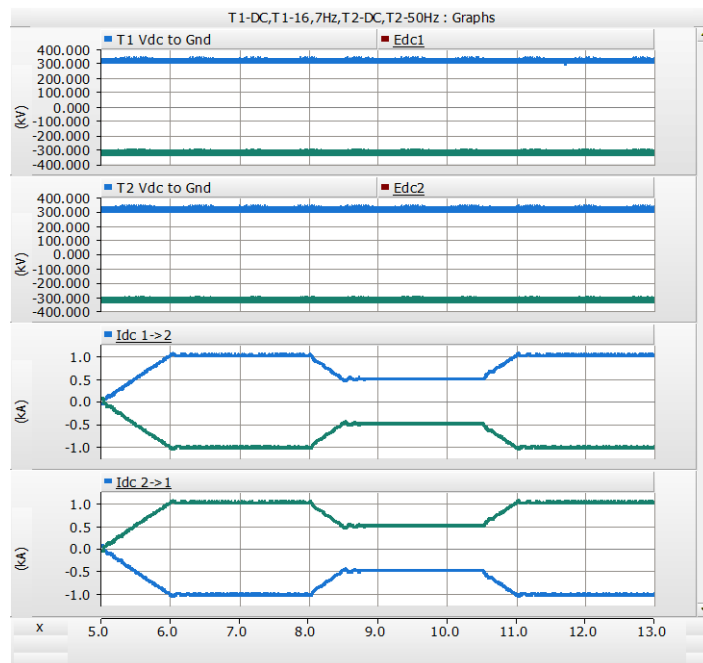


Figure 7.13: DC-Pole Voltages (Two-Top Graphs) and DC-Pole Currents (Two-Bottom Graphs), in MMC-T1 and MMC-T2 of the BtB Frequency MMC, Respectively, for EMT1b.

c) Solid Three-Phase to Ground Faults (FRT) with Filtering

The timeline and sequence of the simulation events for the LFAC export system FRT performance against solid three-phase to ground faults in case EMT1c is shown in Table 7-6.

Table 7-6: Simulation Sequence for Case EMT1c, i) and ii).

EMT1		LFAC TS Dynamic Performance - Point-to-Point EMT Cases
Case c	i)	Point-to-Point LFAC TS with 704MW OWF and 1 x 200km Export Cable (ISLANDED - NO ICC)
Time	[s]	50 Hz Grid Side Fault Ride Through
t9	8.0	Three Phase to Ground Fault applied at the 400kV, 50Hz AC Grid Side PCC, for 150ms
t10	8.15	Fault is Cleared
t11	11.0	End of simulation
Case c	ii)	16.7 Hz OCS Side Fault Ride Through
t9	8.0	Three Phase to Ground Fault applied at the offshore 345kV Busbar, 16.7Hz LFAC Export System Side, for 150ms
t10	8.15	Fault is Cleared
t11	11.0	End of simulation

In both simulation studies performed for case EMT1c, DBRs are adopted to protect the DC-link of the OWF BtB VSCs and the onshore BtB MMC-HVDC system from over-voltages. Each DBR is activated if the related DC-link voltage exceeds 1.15p.u., with a maximum operating point set to 1.2p.u., while it is deactivated once the DC voltage returns to its acceptable levels. These voltage thresholds define the operating region of the braking resistor, preventing it from interfering with the system under normal operating conditions.

i) FRT-1: 50 Hz Grid Side Fault at 400kV

In case EMT1ci, a 150ms solid three-phase to ground fault is applied at the 400kV PCC of the onshore MMC- HVDC system with the 50Hz AC grid, after 8 seconds of simulation. The sets of graphs in Figure 7.14 display the EMT3ci FRT study results in the onshore 16.7Hz/345kV LFAC busbar of MMC-T1 and the 50Hz/400kV AC grid busbar at the PCC of MMC-T2, respectively.

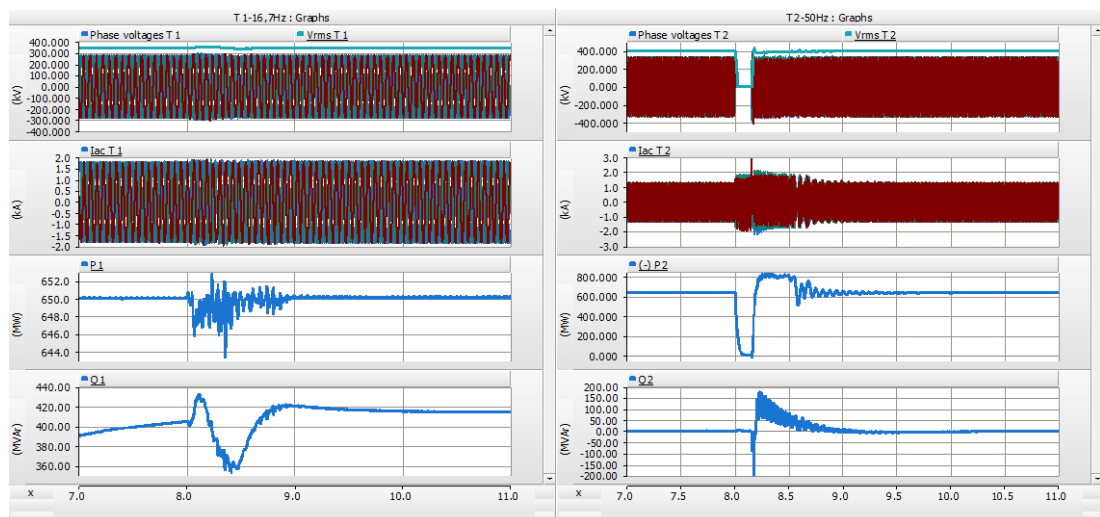


Figure 7.14: EMT1ci) Results at the Onshore LFAC Cable Side (Left) and the PCC with the AC Grid (Right).

During the 50Hz AC grid side fault applied at the 400kV busbar, no power is transferred at the PCC and the MMC-T2 limits the fault-current to 1p.u. Since the active power on the rectifier side is not reduced accordingly, there is an active power imbalance in the HVDC system, as the power injected into the HVDC link from the LFAC system is not fully transferred to the 50Hz grid. This leads to charging of the DC capacitance and, as a result, the DC voltage rises to a level that the DBR located in the HVDC side of the BtB frequency MMC is activated. The DBR temporarily absorbs the excess energy from the OWPP, which cannot be transmitted to the onshore grid. Thus, this large DC chopper rated (rated here for nearly the full power) is a robust and practical solution that “isolates” the disturbance in the onshore AC grid and prevents it from affecting the offshore LFAC TS, enhancing its stability.

The 16.7Hz LFAC TS perceives the fault as a minor disturbance and recovers within 1sec, as seen by the dq-voltage output graph of MMC-T1 in Figure 7.15. No severe over-voltage is noticed in the onshore 345kV busbar during the transient caused by the AC fault on the onshore grid thanks to the DC chopper as well as the LFAC voltage control function of MMC-T1, while the impact on the OWF collector system waveforms can be assumed negligible.

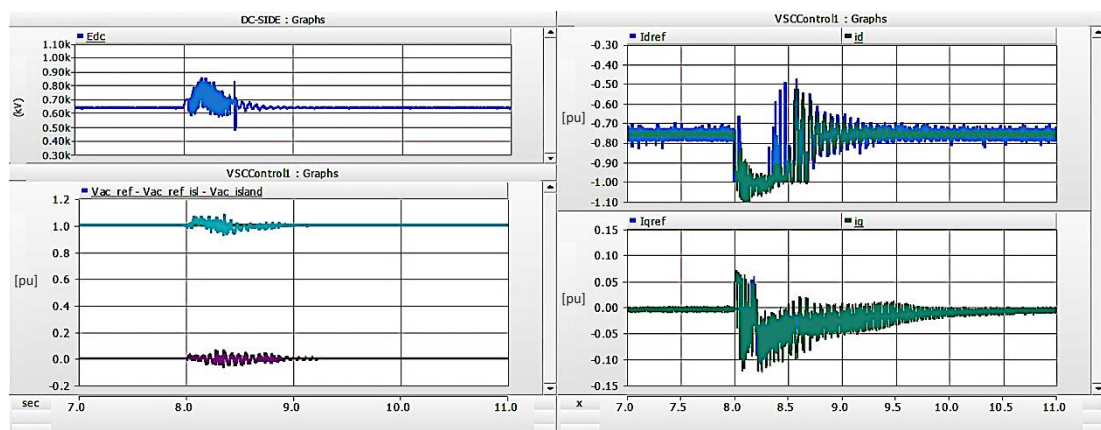


Figure 7.15: Left: DC-Voltage (Top), and DQ-Voltage (Bottom), Right: DQ-ICCs in the MMC-T1 for EMT1ci).

When the fault at the 400kV HV side transformer is cleared, the MMC-T2 responds by injecting higher active current ( $i_d$ ) into the system in order to balance the HVDC voltage and hence the active power flow, as presented in Figure 7.14. Since the voltage dip is large, the MMC-T2 current limiter restricts the further increase of  $i_d$  to 1 p.u. At the same time, the post fault recovery at the PCC is also handled by the RPC of MMC-T2, and hence the reactive current ( $i_q$ ) controller effectively adjusts its value to achieve zero reactive power ~1.5sec later. The post-fault oscillations seen in the reactive power graph at the PCC with the 50Hz grid in Figure 7.14 and the reactive current of Figure 7.15 are known as “Pseudo-inrush”

phenomenon, and they are related to the saturation of the MMC transformer that occurs due to the voltage recovery following the voltage sag caused by the fault [95]. Therefore, the LFAC TS with harmonic filtering equipment and typical islanded control on MMC-T1 successfully rides through this fault at the PCC.

ii) FRT-2: 16.7 Hz OCS Side Fault at 345kV

In case EMT1cii, a 150ms solid three-phase to ground fault is applied at the offshore 345kV LFAC busbar of the OWF, after 8 seconds of simulation. The sets of graphs in Figure 7.16 display the EMT1cii FRT study results in the offshore 16.7Hz/345kV LFAC busbar of the OWF collector system and the onshore 16.7Hz/345kV LFAC busbar of MMC-T1, respectively.

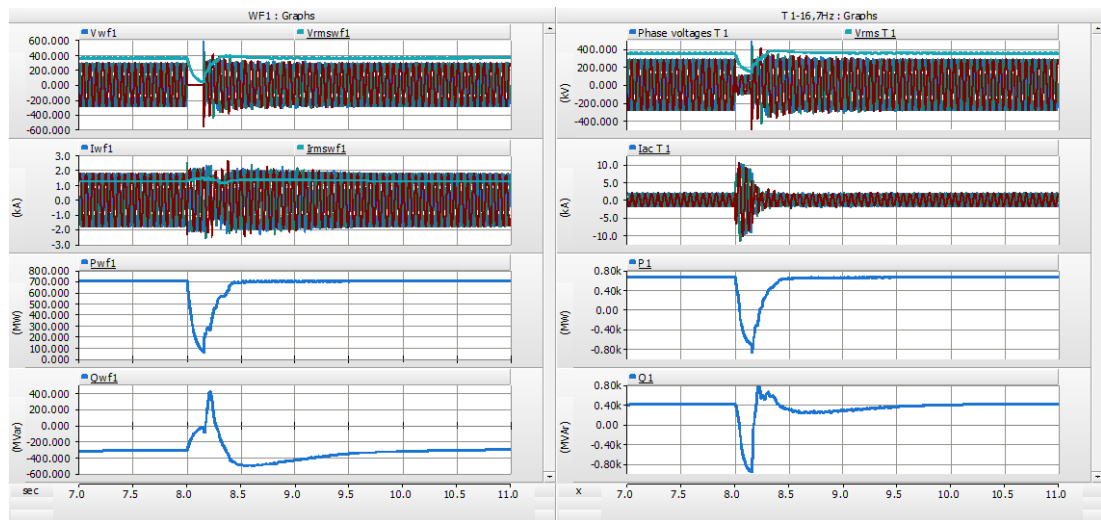


Figure 7.16: EMT1cii) Study Result Graphs at the Offshore (Left) and Onshore (Right) LFAC Cable Sides.

When the three-phase to ground fault occurs, the fault current is effectively controlled to 1p.u. on the OCS side by the OWF equivalent VSI, while when the fault is cleared, the reactive current is prioritised by the OWF-VSI and the current limiter slightly delays the active power flow by restricting any harsh increase of the active current. The DC voltage rise in the equivalent OWF BtB VSC module during the transient is handled by its DBR, as in Figure 7.17.

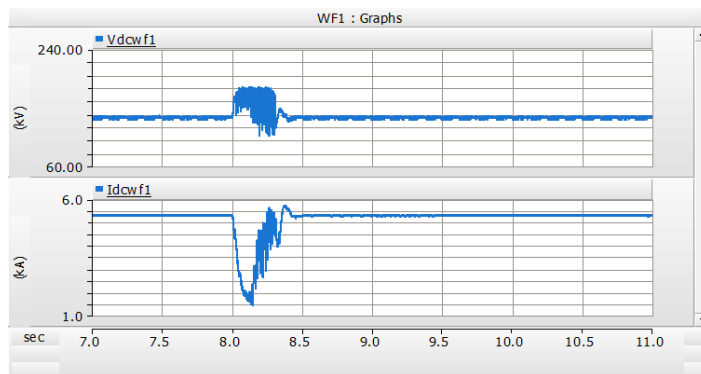


Figure 7.17: Equivalent DC-Voltage (Top), and DC-Current (Bottom) of the BtB VSCs in the OWF for EMT1cii).

Nonetheless, on the onshore 16.7Hz side, the current is uncontrollably increased to almost 4.5p.u. during the fault, and real as well as reactive power reverse the direction of their flow to feed the fault. This high current mainly appears because the typical islanded control system applied in the MMC-T1 cannot limit the current, e.g. through a current saturation technique, while the power reversal is also related with the contribution of passive damping filters to support the voltage at the onshore LFAC side. Power reversal in the 50Hz system does not only force current saturation on the MMC-T2 controller but also harshly increases the HVDC voltage, so the integrator anti-windup mechanism is energised which turns off the integral part of the DCVC when the maximum current limit is met to help the system recover. At the same time, the DC side DBR acts recurrently to restrain the voltage rise. Hence, this operation introduces unacceptable current spikes and a highly oscillatory response on the 50Hz AC grid side that damps out after 2 seconds. The sets of graphs in Figure 7.18 display the EMT1cii FRT study results in the 50Hz/400kV AC grid busbar at the PCC of MMC-T2.

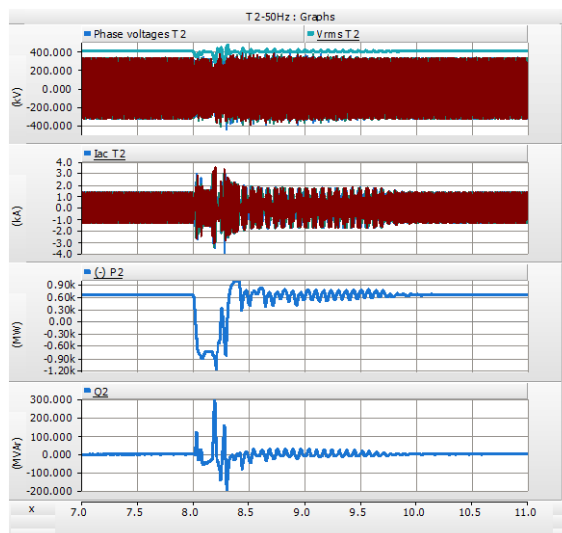


Figure 7.18: EMT1cii) Study Result Graphs at the PCC with the AC Grid.

The LFAC transmission system Fault Ride Through performance against a three-phase to ground fault on the OCS 345kV side is unacceptable, although it reaches a steady-state following the fault and can be detrimental for the operation of the scheme. Although this arrangement might be used for exports schemes with over-rated MMCs and proper operation and coordination of LFAC CBs isolating the faulty region, it would not be a suitable choice if a system expansion or if an LFAC meshed grid system would be considered, as equipment could be exposed to high fault currents during disturbances.

Consequently, the frequency converter system of this type together with other equipment elements of the scheme would need to be rated higher to provide additional fault current in



case of such onerous offshore system faults which could make the scheme impractical. It would be even more unreasonable to base a MT-LFAC TS design on this frequency converter arrangement, as the increased current from a potential LFAC system fault in the offshore region could damage the power converters, cables and other equipment of the scheme in case of a CB failure. Hence, there is a need to control the fault current in the whole LFAC TS, and thus the LFAC side MMC that forms the voltage waveform in the system should be enhanced with an ICC and a current saturation arrangement in its islanded control system.

### 7.3.2 EMT2: Island Control with ICC on the LFAC Side MMC-T1

The cases assessed in EMT2 study are specified in Table 7-7 and further explained below:

Table 7-7: List of Cases for EMT2 Study.

EMT Study	LFAC TS Dynamic Performance - Point-to-Point EMT Cases	
	CASES	Point-to-Point LFAC TS with 704MW OWF and 1 x 200km Export Cable (ISLANDED - With ICC)
EMT 2	a	System Energisation-to-Full Power Without H-Filter, equivalent to PF2b study
	b	Power Demand Variations
	c	FRT: 50Hz Grid Side Fault at 400kV and 16.7Hz OCS Side Fault at 345kV

➤ **Case EMT2a** simulated the energisation procedure of the LFAC export system when implementing an ICC with current saturation employed, as described in Chapter 6, to the onshore LFAC side MMC-T1 without passive damping harmonic filters applied during the transmission system operation. The simulation follows the sequence of case EMT1a), while its steady state response is in accordance with case PF2b with the same power losses measured on the 50Hz AC side.

In contrast to EMT1a), when the OWF generates full power, the system harmonics are not excited, leading to acceptable harmonic operation. Thus, by adding ICCs with a bandwidth of  $\sim 350\text{Hz}$ , as noted in Chapter 4, the steady-state voltage and current THD attains low values in both sides of the subsea cable, with  $\text{THD}_v \sim 0.09\%$ ,  $\text{THD}_i \sim 0.23\%$  at the offshore side and  $\text{THD}_v \sim 0.05\%$ ,  $\text{THD}_i \sim 0.13\%$  at the onshore side, respectively. These values are almost half compared to the distortion levels noticed in EMT1a) that employs harmonic filters without ICC in the LFAC side MMC, while their AC side THD levels are similar.

Finally, a minor harmonic current excitation at the very beginning of each transient during the energisation procedure fades out fast and is due to the fact that the resonance of the passive system is not inherently mitigated by filtering equipment, but it is actively dominated by the “source impedance” of the VSC due to its high ICC bandwidth. Hence, when transients are triggered, the controller acts to reject disturbances, but the harmonic impedance of the LFAC system may slightly interact with the system currents.

- **Case EMT2b** assesses the dynamic performance of the LFAC export system and its associated control schemes for imposed power demand variations in the OWF. The simulation sequence is the same as in case EMT1b), described in 7.3.1.

During these power variations, the AC grid side voltage remains unaffected, and the 50Hz side dynamics are almost identical to case EMT1b. In contrast to EMT1b, the dq LFAC voltage components that can be seen in Figure 7.19. appear to be somewhat sensitive to current variations. The converter output voltage appropriately follows the dq LFAC voltage demands with minor deviation during these transients. Due to the proper tuning of the MMC controllers as described in Chapter 6, the phenomena damp out relatively fast and in reasonable time. Figure 7.19, except for the MMC-T1 outer ACVC, also presents the dq current response of the supplementary ICC scheme that is added to the islanded control system. It is evident that the high bandwidth ICC of the LFAC grid-forming MMC responds fast and stable, without triggering any low-order harmonic issues in the system. Hence, the MMC-T1 acts as a low-frequency, “high impedance” controlled voltage source that needs an established DC-Voltage and it suitably controls the LFAC side currents.

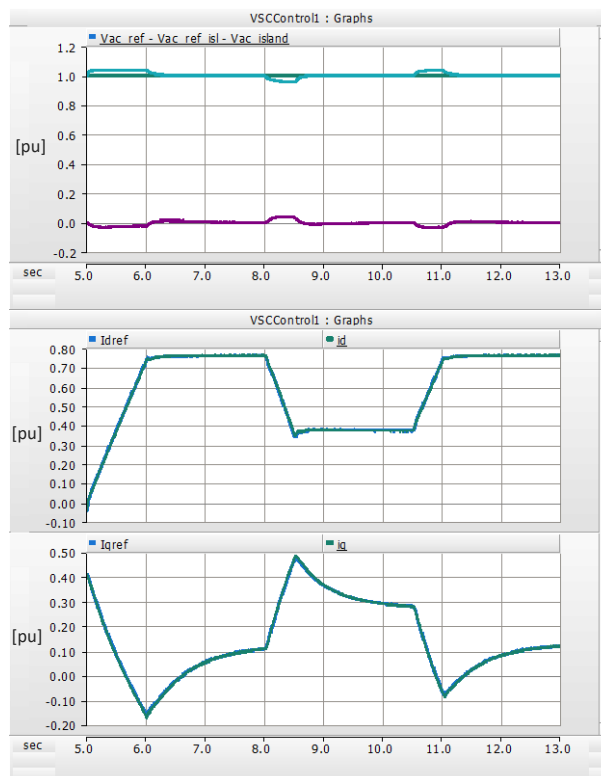


Figure 7.19: EMT2b) DQ-Voltage (Top), and DQ-ICCs (Bottom) of the Enhanced Islanded Control in MMC-T1.

- **Case EMT2c** demonstrates the system’s FRT ability in case of solid three-phase to ground faults at the 400kV AC busbars as well as the offshore 345kV busbars of the LFAC system.

c) Solid Three-Phase to Ground Faults at 400kV-50Hz Grid and 345kV-16.7Hz LFAC OCS

To investigate the fault current-limiting capability of the proposed control system, the EMT2c examines the LFAC export system FRT against 150ms solid three-phase to ground faults applied in the AC grid at 8.5sec and the LFAC TS at 10.5sec, in a single simulation study. The timeline and sequence of the events for the LFAC export system FRT are shown in Table 7-8.

Table 7-8: Simulation Sequence for Case EMT2c.

EMT2		LFAC TS Dynamic Performance - Point-to-Point EMT Cases
Case c		Point-to-Point LFAC TS with 704MW OWF and 1 x 200km Export Cable (ISLANDED - WITH ICC)
Time	[s]	FRT: 50Hz Grid Side Fault at 400kV and 16.7Hz OCS Side Fault at 345kV
t9	8.5	Three Phase to Ground Fault applied at the 400kV, 50Hz AC Grid Side PCC, for 150ms
t10	8.65	Fault is Cleared
t11	10.5	Three Phase to Ground Fault applied at the offshore 345kV Busbar, 16.7Hz LFAC Export System Side, for 150ms
t12	10.65	Fault is Cleared
t13	12.0	End of simulation

The graphs in Figure 7.20 display the EMT2c study results at the PCC with the AC grid (top), and the 16.7Hz/345kV LFAC busbar of the OCS with the onshore 345kV LFAC busbar (bottom).

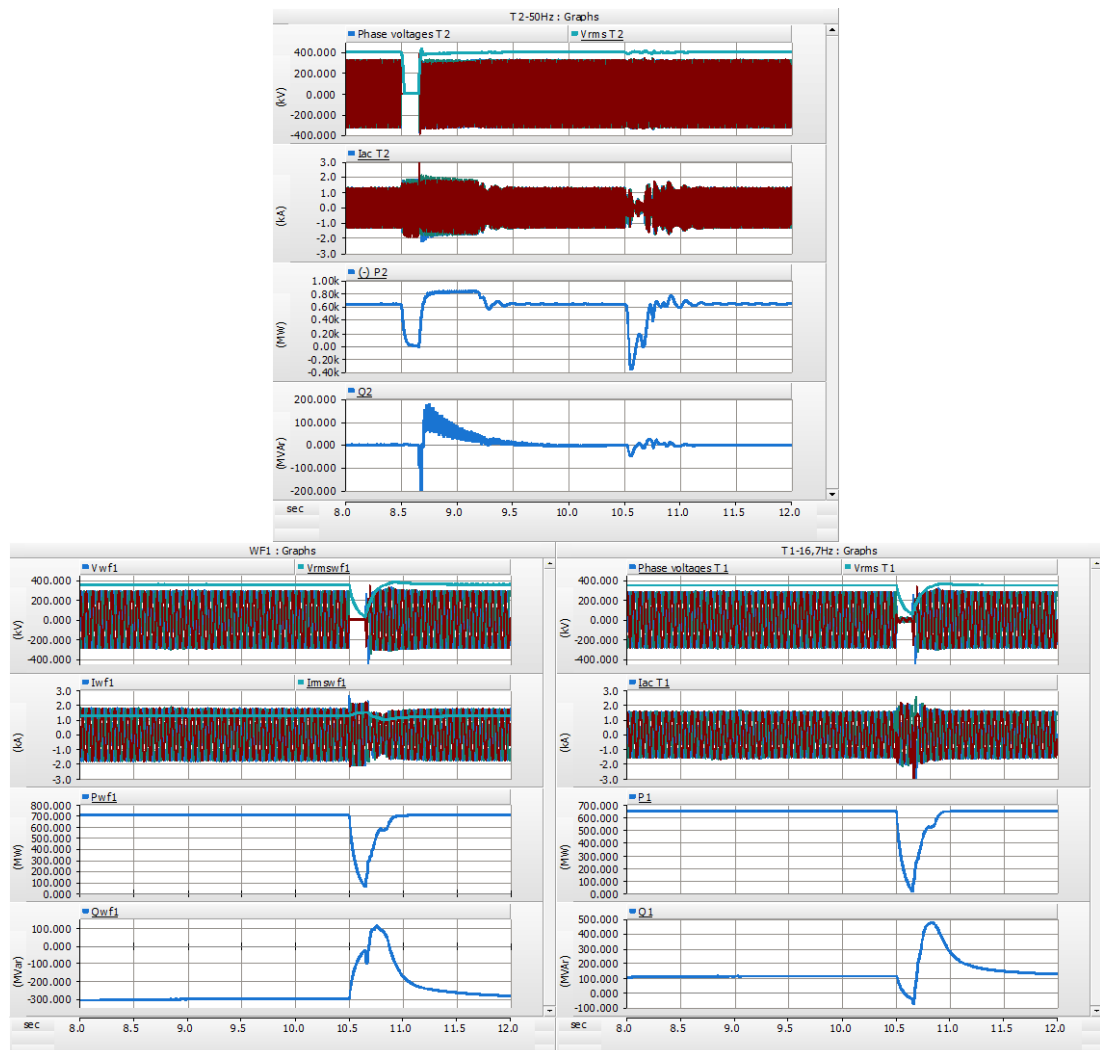
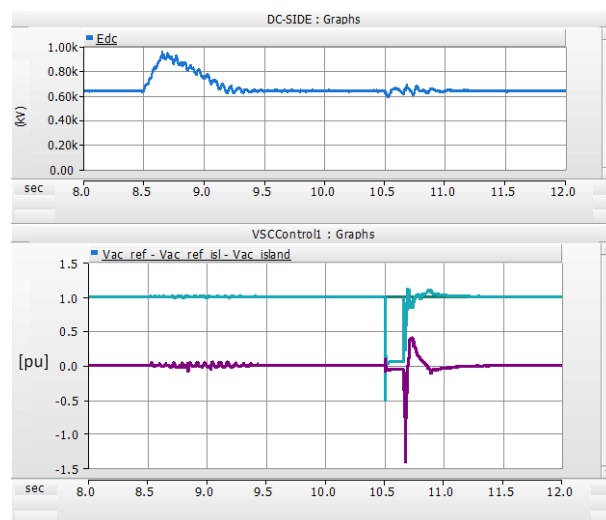


Figure 7.20: EMT2c Study Result at: Top - PCC at AC Grid, Bottom - OCS (Left) and Onshore (Right) LFAC Sides.

When a three-phase to ground fault is applied at the 400kV, 50Hz AC grid side PCC at 8.5sec, no power is transferred at the PCC, causing active power disparity and voltage rise in the HVDC system, and the LFAC transmission system response is almost the same as in case EMT1ci). Although both the MMC-T1 and the MMC-T2 ICCs control the current in this case, there is no significant change on the AC side response, as it is only the MMC-T2 current saturation mechanism that limits the fault current to 1p.u. Furthermore, neither a DBR nor an over-voltage protection scheme is adopted in the DC-Link of the frequency converter, allowing the HVDC voltage to reach up to 1.4p.u. and slightly delay recovery, as in Figure 7.21. Hence, if no DBR is installed in the HVDC side of the back-to-back MMC, there is a need for the converter valves to withstand up to  $\sim 1.4$ pu of DC voltage during an AC Grid fault.

After the fault clearance, the DC voltage is brought back to its pre-fault value by the MMC-T2 DC voltage controller (DCVC), and the active power transfer is resumed, driving its ICC to inject higher active current ( $i_d \sim 1$ p.u.) into the system. Concurrently, its RPC adjusts the reactive current controller value to achieve zero reactive power ( $i_q \sim 0$ ), while the current limiter restricts any further current increase, as presented in Figure 7.21. The post-fault oscillations noticed at the reactive power graph of the PCC in Figure 7.20 are because of the “Pseudo-inrush” phenomenon described in case EMT1ci).



*Figure 7.21: DC-Voltage (Top), and LFAC DQ-Voltage (Bottom) of the BtB Frequency MMCs for EMT2c.*

When a three-phase to ground fault occurs at the OCS 345kV busbar of the LFAC TS in 10.5sec, the equivalent OWF VSI effectively controls the fault current on the OCS side to 1p.u. The response of the equivalent OWF BtB-VSC module against this fault is very similar to case EMT1cii), though, with lower pre and post-fault reactive power contribution, as this case does not employ passive harmonic filters in the onshore 345kV busbar. The DBR that protects

the OWF BtB-VSCs DC-link from over-voltages is also utilised with the same min. and max. voltage thresholds at 1.15p.u. and 1.2p.u., respectively as in case EMT1cii).

The MMC-T1 current saturation mechanism manages to limit the fault current to 1p.u. at the onshore 345kV busbar, as seen in Figure 7.22 that demonstrates the ICCs' response, while its integrator anti-windup mechanism enables the LFAC voltage to recover. No power flow reversal is noticed on the LFAC side, although certain amount of power is reversed in the 50Hz AC side during the fault. However, they do not significantly contribute to the short circuit level (SCL) of the system, and during the fault, the voltage drop at the onshore LFAC 345kV busbar is deeper compared to case EMT1cii). Also, no DBR is adopted in the DC-Link of the onshore frequency converter, but the DC voltage rise during the LFAC side fault is lower, causing less disturbance to the AC network at the PCC, compared with case EMT1cii).

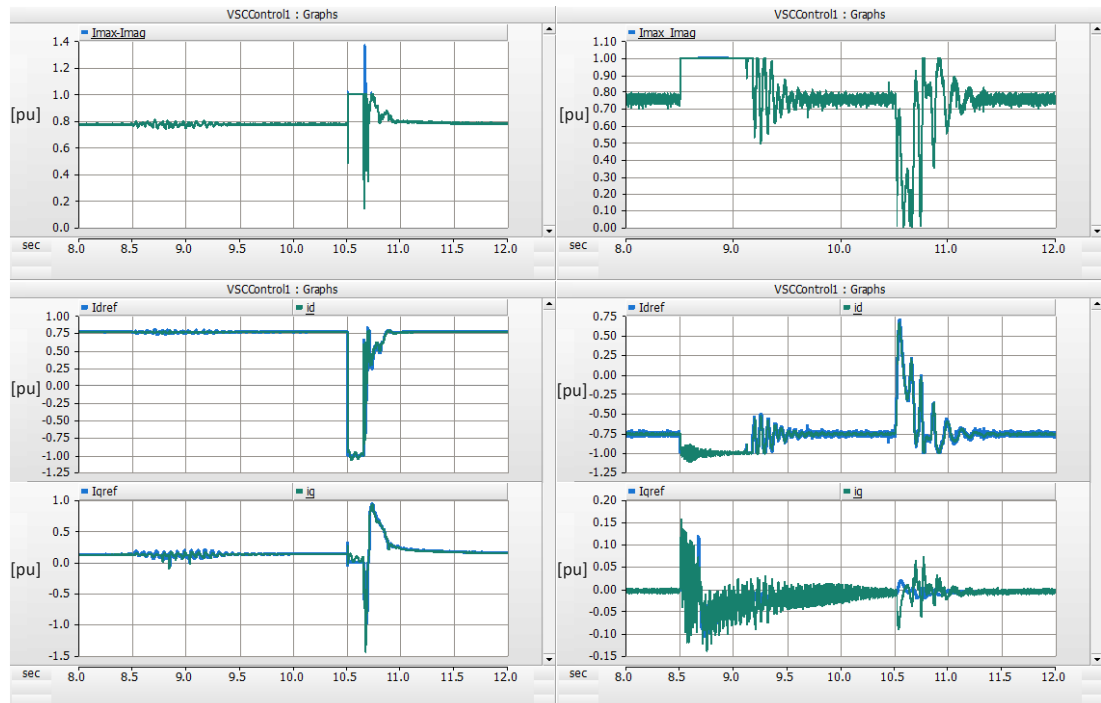


Figure 7.22: EMT2c) Total and Saturated Current (Top), and DQ-ICCs (Bottom) of the BtB Frequency MMCs.

The above results prove that the combination of Type-4 WTGs with VSI technology based on the VCC and this type of MMC islanded control system employing ICC can maintain the fault currents in the total LFAC export system. Therefore, the LFAC TS with an enhanced islanded control system employing an ICC in MMC-T1 but without implementing any harmonic filtering equipment or other mitigation measures can successfully ride through 150ms three-phase to ground faults in the AC and the LFAC systems and could potentially be used to establish an MT-LFAC system.

It is necessary that in offshore meshed or multi-terminal LFAC systems, the LFAC grid forming converter implements an islanded control enhanced with ICC and a current saturation scheme to impose the LFAC voltage waveform on the transmission system in order to avoid vast fault currents in case of CB failures and mitigate any high voltage and current harmonic excitation of the system. Thus, even in the case that further harmonic filtering might be needed for low or high-order system harmonics, it might be lower-rated and not necessitate installing more reactive power compensating equipment that could also increase power losses and affect the system economic feasibility.

### 7.3.3 Evaluation of the Point-to-Point LFAC TS Schemes

Table 7-9 summarises the EMT studies, showing their fundamental set-up configuration differences and the status (pass/fail) of each dynamic case examined that reflects the performance of the PtP LFAC TS schemes that integrate a 704MW OWF with a 200km export submarine LFAC cable. This status is classified according to the operation and recovery of the system following a fault, with fail (red) being due to high harmonic distortion, problematic fault response or post-fault recovery is observed.

*Table 7-9: Summary and Evaluation Table for the PtP LFAC TS EMT Cases.*

LFAC TS Dynamic Performance - Point-to-Point EMT Cases									
Grid Integration of 704MW OWF with 1 x 200km LFAC Export Cable									
Configuration Mode	Study	EMT1					EMT2		
	Case	ai	aii	b	ci	cii	a	b	c
MMC-T1 ICC							+	+	+
Onshore 345kV H-Filters			+	+	+	+			
MMC-HVDC DBR					+	+			
System Harmonic Distortion		✗	✓	✓	✓	✓	✓	✓	✓
System Stable Performance		✗	✓	✓	✓	✗	✓	✓	✓

Below, a summary of the examined export cases is presented. The results of the simulation studies are compared, to identify and evaluate potential key characteristics that could be utilised for implementation to the MT- LFAC TS arrangements and make them feasible. More specifically, the LFAC grid-forming MMC terminal that employs islanded-control system:

- Without inner current controller (ICC) – EMT1:
  - *The LFAC TS does not employ onshore passive filters for damping of system resonance:* It leads to high THD in the LFAC side and harmonic losses, especially as the OWF power output increases, it jeopardises harmonic stability. Interactions of the system voltages

and currents with its resonance are introduced that can vary with the system operating conditions and depend on the cable length, system topology and the specific rating of each component. The islanded controller, in its attempt to adjust the severely distorted LFAC voltage waveform, produces a converter output voltage that in the absence of a high-bandwidth ICC scheme can lead to further harmonic amplification.

- *The LFAC TS employs onshore passive c-type filters for damping of system resonance:* It leads to very low THD both in the AC and LFAC sides, as there is no interaction of the LFAC system voltages and currents with its damped passive resonance. The LFAC grid-forming converter accurately adjusts the voltage level of the system as its islanded controller output voltage suitably follows the dq voltage demands and remains unaffected by the power and current variations. Thus, it acts as a low-frequency controlled voltage source that depends only on the HVDC voltage conditions, while the rest of the system determines its current.

The FRT response of this PtP LFAC TS against a solid three-phase to ground fault:

- At the PCC with the 50Hz AC grid is acceptable.  
During the 50Hz AC grid side fault, the grid side MMC limits the fault-current to 1p.u and no power is transferred at the PCC, while post-fault it outputs full power until full DC voltage recovery. Post-Fault reactive power oscillations at the AC side are mainly due to the “Pseudo-inrush” phenomenon. The 16.7Hz LFAC transmission system perceives the fault as a minor disturbance. No over-voltage is noticed in the onshore 345kV busbar during this transient thanks to the DBR as well as the LFAC voltage control function of LFAC grid-forming MMC, while the impact on the OWF collector system waveforms is negligible. Therefore, the LFAC TS with harmonic filtering equipment and typical islanded control on the LFAC grid-forming MMC successfully rides through this fault at the PCC.
- At the OCS 345kV busbar is unacceptable.  
During this fault, although the OWF VSI effectively controls the fault-current on the OCS side to 1p.u., with a DBR protecting its DC-link from over-voltages, the onshore side equipment is exposed to very high fault-currents due to lack of a current saturation scheme in the LFAC grid-forming MMC terminal. This condition that can be detrimental for the operation of the system happens concurrently with massive power flow reversal on the LFAC side and AC system sides during the fault, although the system reaches a steady-state following the fault.

Hence, this arrangement might be barely adopted in Point-to-Point schemes. Only if the faulty region could be isolated with proper coordination and seamless operation of LFAC Circuit Breakers and protection devices, while the frequency converter together with other equipment elements of the scheme would be over-rated to provide and withstand very high fault current which most likely would make the scheme impractical. However, it would be unreasonable to base a Multi-Terminal LFAC TS design on this frequency converter arrangement, as the increased current in case of such onerous offshore system faults could damage the power converters, cables and other equipment of the scheme, especially in case of Circuit Breaker failure.

- With inner current controller (ICC) – EMT2:
  - *The LFAC TS does not employ onshore passive filters for damping of system resonance:*  
It leads to low THD in the AC and LFAC sides, and the LFAC TS low-order voltage and current harmonics vanish as the high bandwidth ICCs that are implemented in the LFAC grid-forming MMC terminal, dominate the system impedance at these frequencies without the need of passive filtering equipment. The MMC's output LFAC voltage accurately follows the dq voltage component demands, and the response of the inner current controllers is fast and stable. Nonetheless, the harmonic currents to a greater extent and the harmonic voltages to a lesser extent are somewhat excited at the beginning of any transient also due to instantaneous interaction with passive system resonance. Still, these transients fade out quickly due to the proper tuning and fast action of the decoupled current regulators. Moreover, the cascade controller operation introduces some minor voltage deviations during the current variations, e.g. when the OWF power ramps-up, which fade away quickly. Thus, the grid-forming MMC acts as a high-impedance and low-frequency controlled voltage source that needs an established DC-Voltage and suitably controls its LFAC side currents.

The FRT response of this PtP LFAC TS against a solid three-phase to ground fault:

- At the PCC with the 50Hz AC grid is acceptable.  
During and following the 50Hz AC grid side fault, the grid side MMC response is similar to the corresponding fault of case EMT1. Although in this case, the LFAC grid-forming MMC terminal current is controlled, it does not have a major impact on the overall system response. The BtB MMC-HVDC acts as a “firewall” preventing the disturbance from entering the offshore LFAC transmission system. Though if no



DBR is installed in the HVDC side, the valves shall be able to withstand up to  $\sim 1.4$ pu of DC voltage and the post fault system recovery can last slightly longer.

- At the OCS 345kV busbar is acceptable.

During this fault the power flow reversal level from the 50Hz AC network is not as eminent, the DC voltage is disturbed with no major increase and no power reversal is noticed in the LFAC side. The MMC terminal that employs islanded control system with ICC and current saturation mechanism limits the fault current to 1p.u. at the onshore 345kV busbar, whilst its integrator anti-windup mechanism enables the LFAC voltage to recover by disabling the outer voltage integrators. Since the equivalent OWF module effectively responds, limiting the fault-current on the OCS 345kV side to 1p.u. as in the previous equivalent case, the current in the LFAC export system is maintained, and the system successfully rides through this fault.

The above results prove that the combination of Type-4 WTGs with VSC technology and the BtB MMC frequency converter with an LFAC grid-forming MMC that employs islanded control enhanced with ICCs and appropriate current saturation, and integrator anti-windup mechanisms can maintain low THD levels without low-order harmonic issues under normal system operation. It can demonstrate satisfactory dynamic performance for OWF output power variations and effectively ride-through faults and limit fault-currents in the LFAC export system. Even if additional harmonic filtering strategies or other mitigation measures need to be applied, they may be less complex, or lower-rated without necessitating further reactive power compensating equipment that would also increase power losses and affect the system economic feasibility. However, the converters with such limited fault-current may not significantly contribute to the SCL and thus, the strength of the offshore LFAC TS.

Hence, to establish a feasible offshore Multi-Terminal LFAC TS, the LFAC grid-forming converter must implement in its islanded-control system:

- An ICC to control its output currents fast and dominate the system impedance at its bandwidth. Thus, a high ICC bandwidth is desired as noted in Chapter 6 so that all the potential resonant points of the LFAC system regardless of its operating condition lie within it, and no current and voltage interactions occur with the resonance of the passive LFAC network.
- A current saturation mechanism to limit the fault-currents which could severely damage the LFAC TS equipment and devices, especially in cases of LFAC CB failures.

- Integrator anti-windup mechanisms that temporarily disable the integral parts of the outer voltage controllers under current saturation conditions to support the voltage recovery and avoid potential control instability.

Besides, DBRs shall be applied in the DC sides of the OWTGs and the onshore BtB frequency converters to temporarily absorb the excess energy and mitigate DC over-voltages, if the converter valves cannot withstand high DC voltage levels.

In the PtP cases, the implementation of adequately tuned ICCs in the islanded-control system of the LFAC grid-forming MMC eliminates the need for harmonic filtering equipment. Since the MT-LFAC arrangement examined in this Thesis is actually the merging of two equivalent PtP LFAC export systems, the potential system resonances that are seen from the onshore MMCs' points of connection lie within lower frequencies than the equivalent PtP case, as explained in Chapter 4. Hence, according to the ICC controller analysis in Chapter 6, the same converter tuning could be utilised for the onshore converters of the MT-LFAC TS arrangement, upsurging the LFAC-TS techno-economic feasibility and improving its expandability, as more flexible meshed arrangements can be envisaged.

#### 7.4 Multi-Terminal (Meshed) Offshore LFAC TS Scheme

The schematic of the EMT model for the offshore LFAC network, integrating two OWTs and interconnecting them with two different AC grids through a meshed MT-LFAC TS arrangement is illustrated in Figure 7.23.

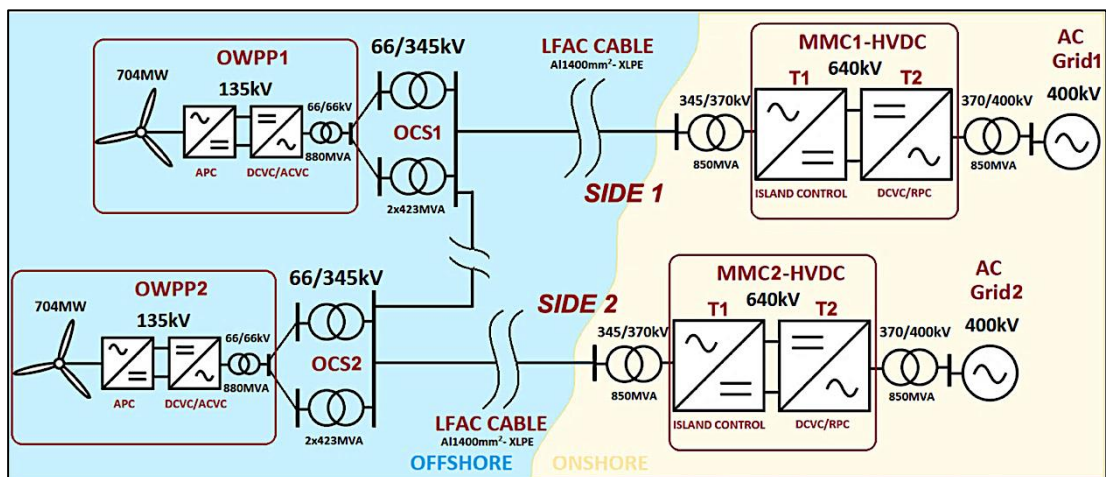


Figure 7.23: Schematic of the EMT model for OWPP Integration and Interconnection using the MT-LFAC TS.

### 7.4.1 EMT3: Island Control with ICC on the LFAC Side MMC1-T1

The cases assessed in EMT3 study are specified in Table 7-10, and further explained below:

Table 7-10: List of Cases for EMT3 Study.

EMT Study	LFAC TS Dynamic Performance - Meshed EMT Cases (MMC-1, ISLANDED - WITH ICC)	
EMT 3	CASES	Multi-Terminal Offshore LFAC TS Interconnecting 2 x 704MW OWFs and 2 Grids with a 50km and 2 x 200km Cables
	a	System Energisation-to-Full Power Without H-Filters, equivalent to PF5a and PF5e studies
	b	Power Demand Variations in Generation and Interconnection, equivalent to PF5d and PF5e studies
	c	FRT: 50Hz Grid Side 1 Fault at 400kV, 16.7Hz OCS Side Fault at 345kV and 50Hz Grid Side 2 Fault at 400kV

- **Case EM3a** shows the energisation procedure of the MT-LFAC TS when implementing an ICC with current saturation technique to the onshore LFAC side MMC1-T1 and the typical grid-following VCC with APCs and ACVC outer controllers to MMC2-T1, as designed in Chapter 6, without passive damping harmonic filters o the transmission system operation.
- **Case EMT3b** presents the dynamic performance of the meshed MT-LFAC TS and the associated control schemes when imposing power demand variations in OWF1 and OWF2.
- **Case EMT3c** demonstrates the MT-LFAC transmission system’s fault-ride-through (FRT) ability in the case of solid three-phase to ground faults at the 400kV busbars of the 50Hz AC grid as well as the 345kV busbars of the OWF2 collection platform of the 16.7Hz system.

#### a) LFAC TS Energisation-to-Full Power without Filtering

The timeline of system dynamic events for the MT-LFAC TS energisation case EMT3a is described in Table 7-11.

Table 7-11: Simulation Sequence for Case EMT3a.

EMT3	LFAC TS Dynamic Performance - Meshed EMT Cases (MMC-1, ISLANDED - WITH ICC)	
Case a	Multi-Terminal Offshore LFAC TS Interconnecting 2 x 704MW OWFs and 2 Grids with a 50km and 2 x 200km Cables	
Time	[s]	LFAC System Energisation-to-Full Power Without H-Filters, equivalent to PF5a, PF5d and PF5e studies
t0	0.0	Initialization: AC Voltage Sources Ramp Up to 400kV within 0.05 [s] in both 50Hz Grids 1 and 2
t1	0.5	Both 50Hz Grid Side MMC Terminals Deblock: Impose Vdc control to their respective HVDC terminals and Q control to their corresponding 400kV grid-side PCCs (vdc_ref=1pu with 0.2 vdc/idc droop, q_ref=0)
t2	1.0	LFAC Side MMC-1 Terminal Deblocks: Imposes Vlfac and freq islanded control (vac: 0-->1pu in 1[s], freq=16.7Hz)
t3	4.0	LFAC Side MMC-2 Terminal Deblocks: Imposes Vlfac and P control at its 345kV Onshore side (vac=1pu, p=0pu)
t4	5.0	Both OWF-1 and OWF-2 Equivalent Back-to-Back VSC Modules Connect
t5	5.5	Both OWF-1 and OWF-2 VSIs Deblock: Impose Vdc control to their respective DC Terminals and and Vlfac control to their corresponding offshore 345kV LFAC-side busbars (vdc_ref=1pu, vac_ref=1pu with 0.0834 vac/q droop)
t6	5.7	315MVar LFAC Cable Shunt Reactor Located at the Onshore MMC-1 Side Gradually Reduced to 120MVar in 0.65[s] for EMT3b Study according to PF5d or to 0MVar for EMT3c according to PF5e, respectively
t7	6.0	Both OWF-1 and OWF-2 Rectifiers Deblock: Impose P control (p_ref=0)
t8	6.35	LFAC Cable's Shunt Compensator Reaches the 120MVars
t9	7.0	Both OWF-1 and OWF-2 Active Power Demands Ramp Up to Full Power with p_ref: 0-->1pu within 1 [s]. Active power increase rate: 1pu/s
		LFAC Side MMC-2 Terminal Active Power Demand Ramps Up to Full Power with p_ref: 0-->1pu within 1 [s] as well.
t10	10.0	End of Simulation

The simulation sequence of the MT-LFAC TS with 2 x 200km and 1 x 50km submarine cables for the Energisation-to-Full Power study EMT3a can be considered as a dynamic path from power flow case PF5a to PF5e, without implementing any passive harmonic filters, since the MMC1-T1 employs island control with additional ICC and current limiting schemes according to case EMT2. In case PF5a, 315MVAR of shunt reactors are utilised for system initialisation in each of the onshore 345kV busbars of the LFAC system, to avoid the high cable charging-breaking currents and maintain the system voltages to an acceptable level, while for OWF1 and OWF2 full power export case PF5e, no shunt reactors need to be in operation. Hence, at 5.7sec each of the 315MVAR onshore shunt reactors gradually reduces to 0MVAR within 1s for the full OWF export case, increasing the amount of reactive power being produced by the OWFs and absorbed by the onshore back-to-back frequency converters.

Figure 7.24 displays the EMT3a study results corresponding to the Side-1 (left) and Side-2 (right) parts of the MT-LFAC TS. The top sets of graphs refer to the 400kV PCC1 and PCC2 at the respective 50Hz grid sides of the MMC1-T2 and MMC2-T2. The sets of graphs in the middle correspond to the onshore 345kV busbars at the 16.7Hz transmission system sides of the MMC1-T1 and MMC2-T1, while the final sets of graphs refer to the offshore 345kV busbars of the LFAC system that correlate with the output of OWF1 and OWF2, respectively. From these graphs, it can be evident that this study follows the two associated cases PF5a and PF5e, having the same active power losses (i.e. ~80MW at no-load and ~135MW at full-load), reactive power distribution and busbar voltage profiles in the MT-LFAC system.

When both OWFs generate electricity at full-power, a minimal amount of current is being transferred through the 50km interconnection cable, while when the generation is lower than nominal, MMC2-T1 APC-demand defines the amount of power that results to each terminal. Thus, proper coordination among the onshore MMC-HVDC controllers and the WF must be established to track the requirements of the operator. Furthermore, the compensated cable charging-breaking currents measured at each onshore 345kV busbar from 2sec to 5.5s are also in agreement with the IEC preferred value for No-Load operation, while the higher current and reactive power consumption noticed in MMC1-T1 between 2sec and 4sec is only because all the offshore step-up transformers were included during the energisation procedure in the PSCAD model to accelerate the system studies.

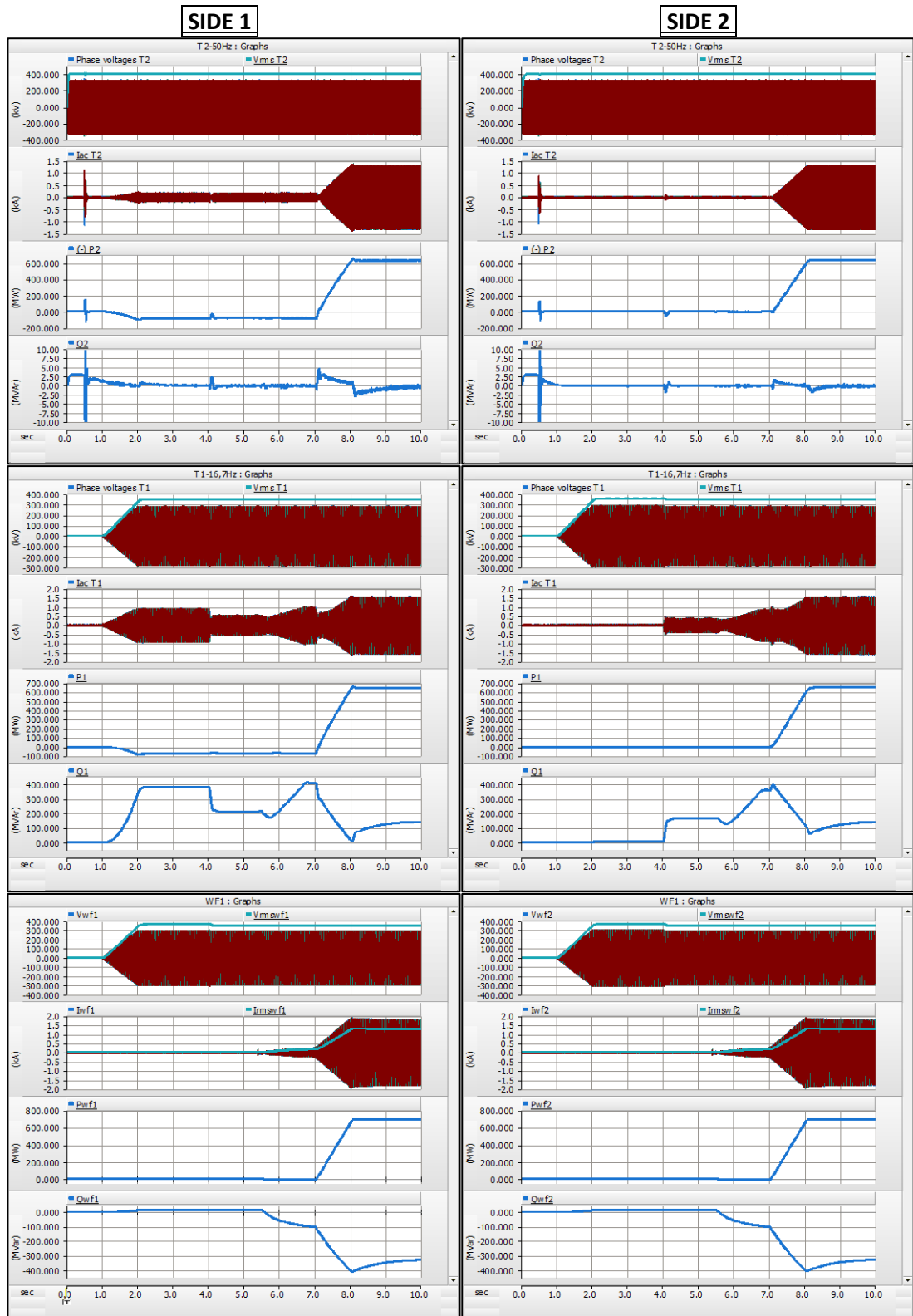


Figure 7.24: EMT3a Study Results at: → Top - PCC with the AC Grid, (MMC1-T2 and MMC2-T2)  
 → Middle - Onshore LFAC Cable Side (MMC1-T1 and MMC2-T1)  
 → Bottom - Offshore LFAC Cable Side (OWF1 and OWF2)

During the very early stages of the LFAC TS energisation procedure, particularly at the time when only the grid forming MMC operates in islanded mode and the LFAC voltage is building up with no wind power being generated as the OWF that is blocked, the system resonances may be poorly damped. At the time that the OWF system generates full power, the system harmonics are not excited, due to the high “source” impedance of the associated converters, leading to stable harmonic operation. The voltage and current THD under full-load conditions are kept at low values in all offshore and onshore system sides. In both offshore system 345kV sides the THDv is  $\sim 0.1\%$ , and the THDi is  $\sim 0.2\%$ , while in onshore 345kV sides that as can be seen in Figure 7.25, the THDv is  $\sim 0.05\%$ , and the THDi is  $\sim 0.15\%$ , respectively, which is very similar to the EMT2a case for a point-to-point LFAC export scheme.

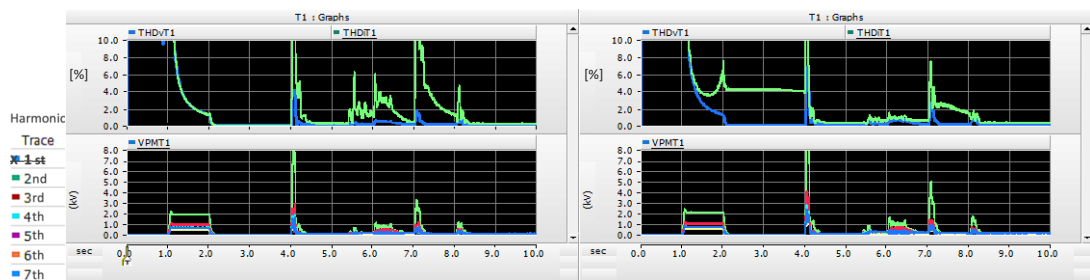


Figure 7.25: Onshore 345kV Left: MMC1-T1, Right: MMC2-T1 - THD (Top) and Voltage Harmonics (Bottom).

It can be inferred that from 2sec up to  $t_3=4$ sec, the THDi at the onshore LFAC Side of MMC2-T1 is  $\sim 4\%$ , while there is almost no THDi at MMC1-T1. After the MMC2-T1 is deblocked at  $t_3$  and its grid-following controllers are activated, applying ACVC and APC with ICCs, the current harmonic distortion significantly reduces. This also shows the benefit of implementing ICC to all converter terminals of the scheme but also verifies that the 16.7Hz part of the LFAC networks may be operated without extra low-order harmonic mitigation measures for relatively longer overall subsea cable systems in the region of up to 450km.

For meshed LFAC system applications, the implementation of Islanded Control with ICC in MMC1-T1 instead of passive filtering strategies can be beneficial. This can become evident if a potential offshore transmission system expansion leads to a dramatic alteration in its impedance profile. Then, H-Filters might be detuned, or necessitate enhancements that could also require additional shunt reactive compensation, resulting in increased power losses and affecting CAPEX, OPEX, reliability, etc.

#### *b) Power Demand Variations without Filtering*

The timeline and sequence of simulation events for the meshed MT-LFAC TS dynamic response to both OWFs power demand variations in case EMT3b is described in Table 7-12.

Table 7-12: Simulation Sequence for Case EMT3b.

EMT3		LFAC TS Dynamic Performance - Meshed EMT Cases (MMC-1, ISLANDED - WITH ICC)
Case b		Multi-Terminal Offshore LFAC TS Interconnecting 2 x 704MW OWFs and 2 Grids with a 50km and 2 x 200km Cables
Time	[s]	Power Demand Variations in Generation and Interconnection, equivalent to PF5d and PF5e studies
t10	10.0	Both OWF-1 and OWF-2 Active Power Demands Ramp Down to 1/3 of their Full Power with p_ref: 1-->0.34pu in 0.66[s]. Active power decrease rate: 1pu/s
		LFAC Side MMC-2 Terminal Active Power Demand Remains Unchanged at Full Power: Pref=650MW LFAC Side1 Back-to-Back Frequency Converter Must Deliver the Rest 1/3 of Power from Grid-1 to MMC-2: It automatically reverses its power output from ~+645MW to ~-275MW in 0.66 [s], according to PF5d
t11	13.0	Both OWF-1 and OWF-2 Active Power Demands Ramp Up again to Full Power with p_ref: 0.34-->1pu in 0.66 [s]. Active power increase rate: 1pu/s
		LFAC Side MMC-2 Terminal Active Power Demand Remains Unchanged at Full Power: Pref=650MW LFAC Side1 Frequency Converter Must Absorb the Rest of Generated Power from the LFAC System to Grid 1: It automatically reverses its power output from ~-275MW to ~+645MW in 0.66 [s].
t12	16.0	End of Simulation

This study can be perceived as a combination of power flow cases PF5e and PF5d, without harmonic filters, as MMC2-T1 demands full-power with both OWFs supplying approximately 2/3 of it and MMC1-T1 supplying the rest ~1/3 of the requested power to MMC2-T1, through the interconnection submarine cable. The MMC2-T1 APC-demand of 650MW remains constant during the course of this study. In case PF5d, 120MVAR of shunt reactors are utilised for voltage support only in the onshore 345kV LFAC busbar of MMC1-T1, while in the OWFs full power export case PF5e, the dynamic compensation from MMC-T1 can be adequate without utilising MVARs from shunt reactors. Still, the 120MVAR shunt reactors do remain connected during the whole simulation study, reducing the reactive loading of MMC-T1 during OWF full power export.

The sets of graphs in Figure 7.26 display the EMT3b study results corresponding to the Side-1 (left) and Side-2 (right) parts of the MT-LFAC TS in the same manner that Figure 7.24 does for EMT3a study. It is evident that this study follows the two associated cases PF5e and PF5d, having the same active power losses (i.e. ~135MW at OWF full-power export and ~120MW at the partly export and interconnection case), similar reactive power distribution and busbar voltage profiles in the MT-LFAC system. As happens in case PF5e, when both OWFs generate electricity at full-power, a minimal amount of ~3.5MW is being transferred through each side of the 50km interconnection cable, while when each OWF generates 1/3 of its nominal output and MMC1-T1 supplies the remaining power to MMC2-T1, almost 475MW are transferred through the 50km submarine cable, having ~10MW losses. Following the power reversal at 10.5s, the 50Hz AC grid Side-1 supplies ~280MW to the system, in order to meet the demanded power of MMC2-T1, which results in almost 640MW being delivered to the Side-2 grid system. In EMT3b no harmonic excitation and interactions with system impedance are apparent since the MT-LFAC TS resonance is more mitigated than in the export systems.



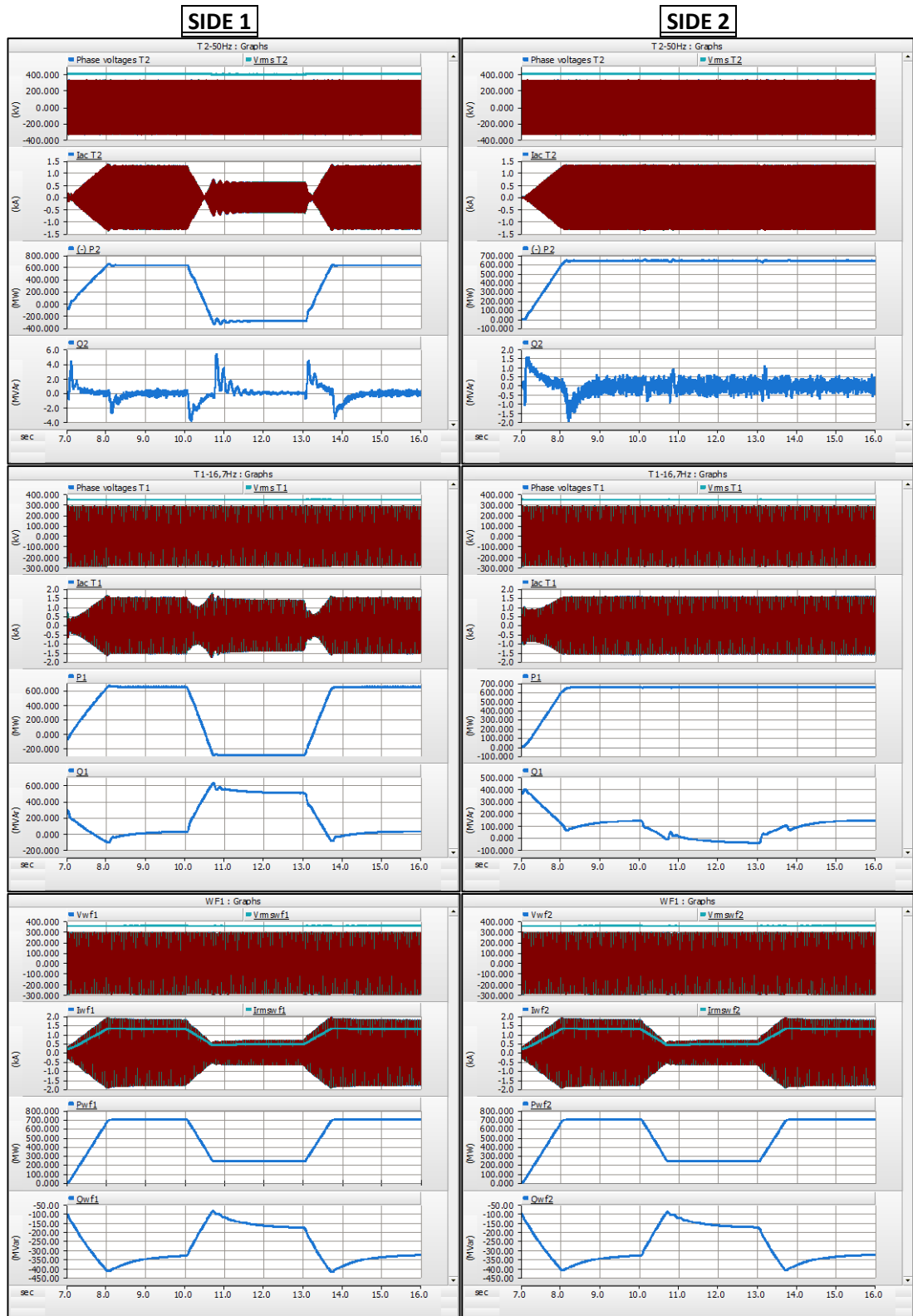
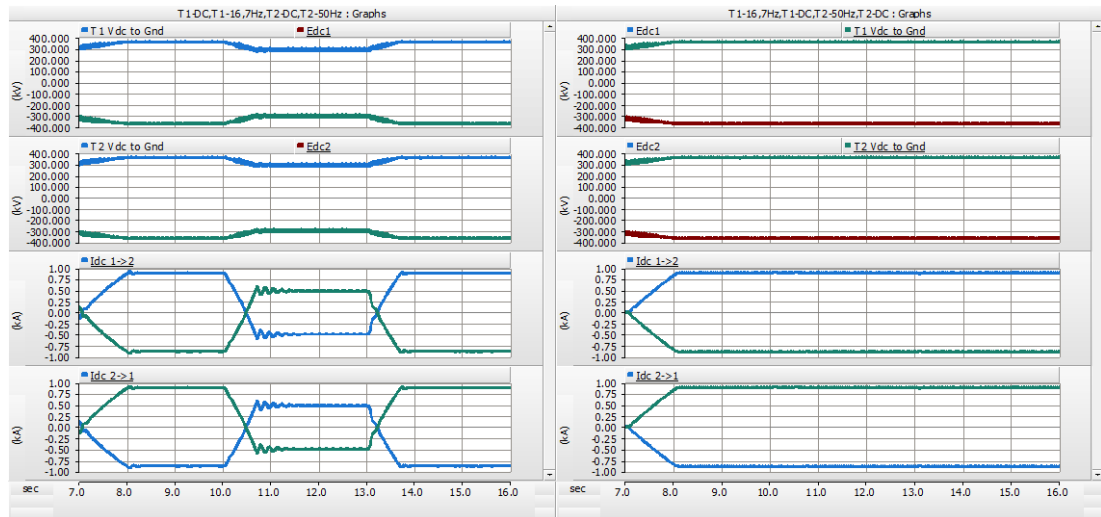


Figure 7.26: EMT3b Study Results at: → Top - PCC with the AC Grid, (MMC1-T2 and MMC2-T2)  
 → Middle - Onshore LFAC Cable Side (MMC1-T1 and MMC2-T1)  
 → Bottom - Offshore LFAC Cable Side (OWF1 and OWF2)



During the dynamic power changes in the system, both the 400kV AC grid voltages remain unaffected. Power variations cause only consequent reactive power changes at the onshore 345kV busbar in the Side-2 part of the LFAC TS. At the same time, they do not affect the DC-Link of BtB MMC2-HVDC shown in Figure 7.27, or the Side-2 50Hz AC grid system response.



**Figure 7.27: DC-Pole Voltages (Two-Top Graphs) and DC-Pole Currents (Two-Bottom Graphs), in MMC1 (Left) and MMC2 (Right) BtB Frequency Converters, Respectively, for EMT3b.**

On the contrary, they introduce slight and damped current oscillations in the Side-1 50Hz AC grid system response at the time that power is reversed which are eliminated 1sec later, and they can be spotted on the matching active and reactive power graphs. These oscillations are apparent in the DC-current of the BtB MMC1-HVDC as seen in Figure 7.28.

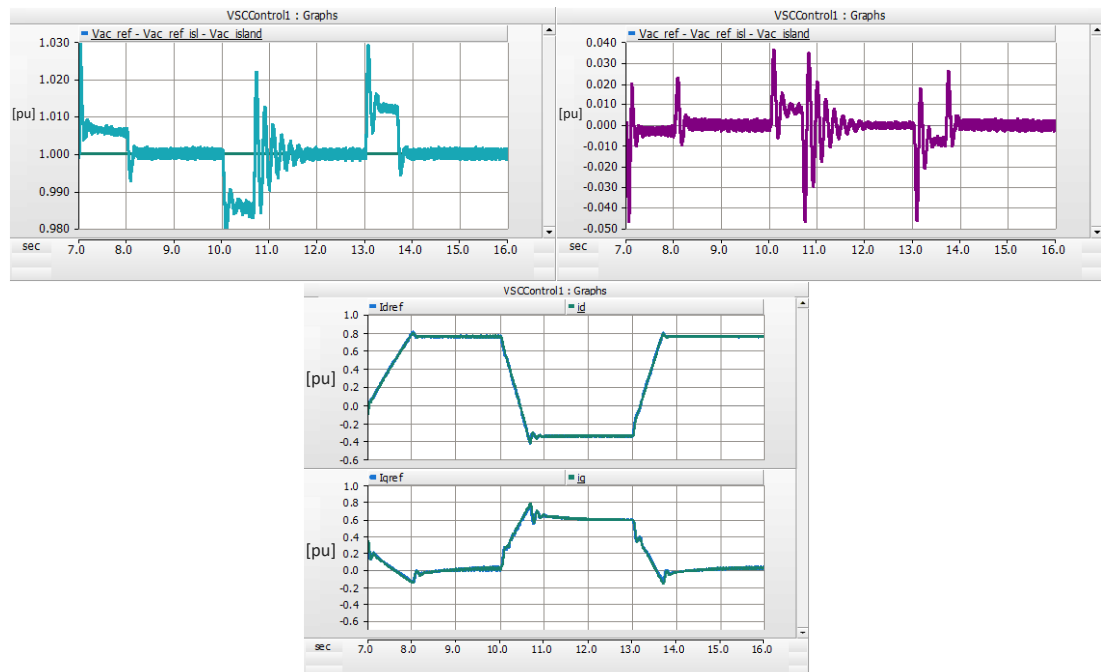


**Figure 7.28: EMT3b) DQ-Voltage (Top), and DQ-ICCs (Bottom) of the Enhanced Island Controller in MMC1-T1.**

Although the oscillations that are noticed in the onshore MMC1-T1 345kV busbar are mitigated, the MMC1-T1 LFAC output voltage dq components shown in Figure 7.28. appear to be sensitive to these variations, slightly deviating from the dq LFAC voltage demands during transients but with a damped oscillatory response and adequate settling time. The dq currents of the ICC configuration follow their references very fast resulting in damped converter output currents.

*c) Solid Three-Phase to Ground Faults at 400kV-50Hz Grids 1&2 and 345kV LFAC OCS2*

The EMT2c examines the FRT of an MT-LFAC TS arrangement against 150ms solid three-phase to ground faults applied in the AC grid Side-1 PCC at 10.25sec, in the LFAC Side-2 OCS at 13.75sec, and in the AC grid Side-2 PCC at 17sec, respectively, in the same simulation study. The timeline and sequence of the simulation events for the LFAC meshed system FRT performance study case EMT3c is defined in Table 7-13.

*Table 7-13: Simulation Sequence for Case EMT3c.*

EMT3		LFAC TS Dynamic Performance - Meshed EMT Cases (MMC-1, ISLANDED - WITH ICC)
Case c		Multi-Terminal Offshore LFAC TS Interconnecting 2 x 704MW OWFs and 2 Grids with a 50km and 2 x 200km Cables
Time	[s]	FRT: 50Hz Grid Side 1 Fault at 400kV, 16.7Hz OCS Side Fault at 345kV and 50Hz Grid Side 2 Fault at 400kV
t10	10.25	Three Phase to Ground Fault applied at the 400kV, 50Hz AC Grid Side 1 PCC, for 150ms
t11	10.40	Fault is Cleared
t12	13.75	Three Phase to Ground Fault applied at the offshore 345kV Busbar, 16.7Hz LFAC Side2 OCS, for 150ms
t13	13.90	Fault is Cleared
t14	17.00	Three Phase to Ground Fault applied at the 400kV, 50Hz AC Grid Side 2 PCC, for 150ms
t15	17.15	Fault is Cleared
t16	20.00	End of simulation

This simulation study follows case PF5e having the same active power losses, reactive power distribution and busbar voltage profiles in steady-state operation without implementing any harmonic filters or shunt reactors. Furthermore, neither a DBR nor an over-voltage protection scheme is adopted in the DC-Link of MMC1-HVDC scheme, while a DC-chopper is employed on the frequency converter of Side-2 (MMC2-HVDC) with a DC voltage operating region for the braking resistor between 1.2p.u. and 1.3p.u, because of the applied DC-Voltage droop characteristic as described in Chapter 6 for the MT-LFAC arrangements, on the frequency converters. Finally, both of the equivalent OWF modules also utilise a DC-link DBR for over-voltage protection with minimum and maximum voltage thresholds of 1.15p.u. and 1.2p.u., as applied in EMT1cii) and EMT2c).

The sets of graphs in Figure 7.29 display the EMT3c study results corresponding to the Side-1 (left) and Side-2 (right) parts of the MT-LFAC TS at the 50Hz/400kV PCC with the AC grids (top), the onshore 16.7Hz/345kV LFAC busbar (middle) and the 16.7Hz/345kV LFAC busbars of the OCS (bottom), respectively.

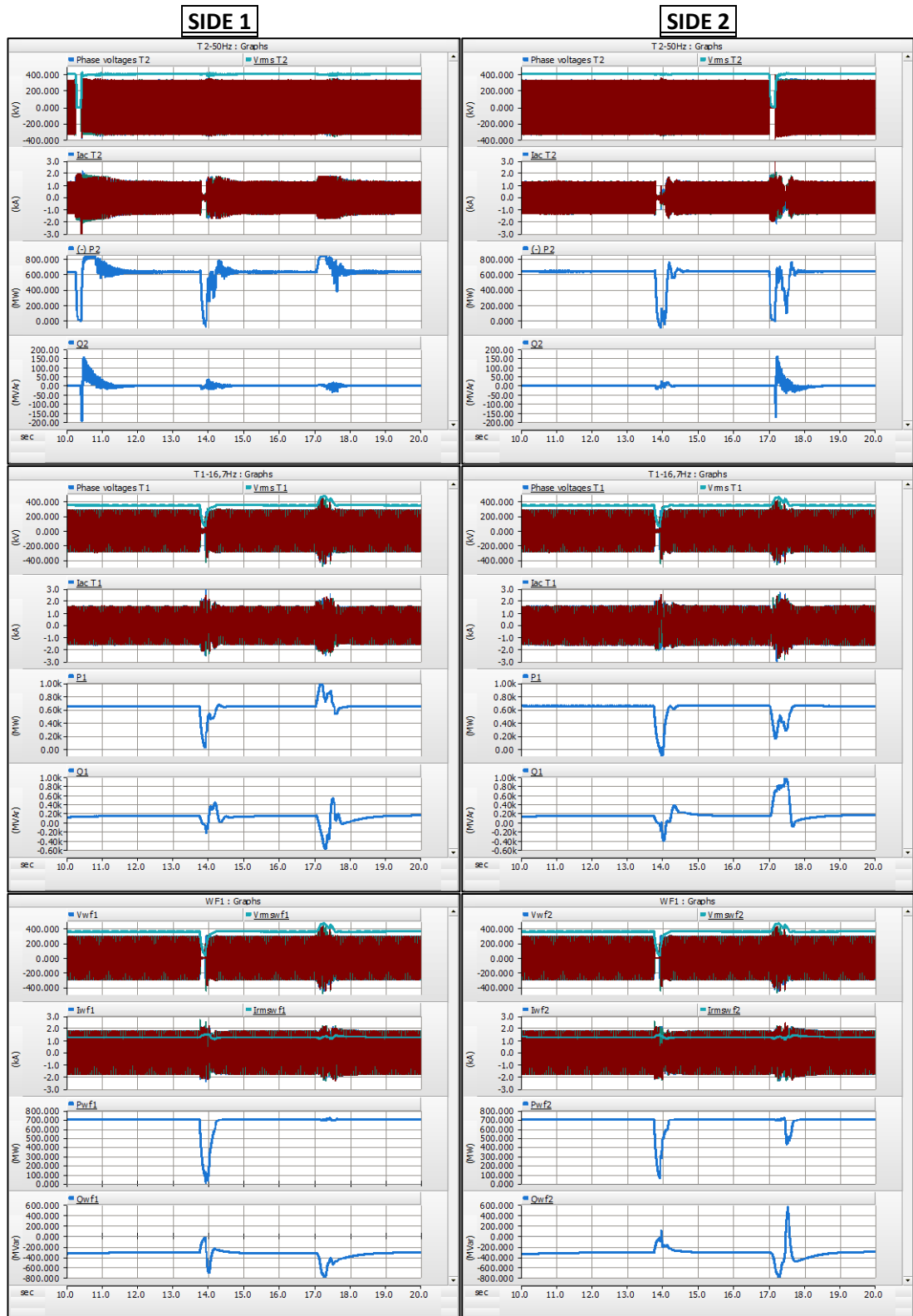
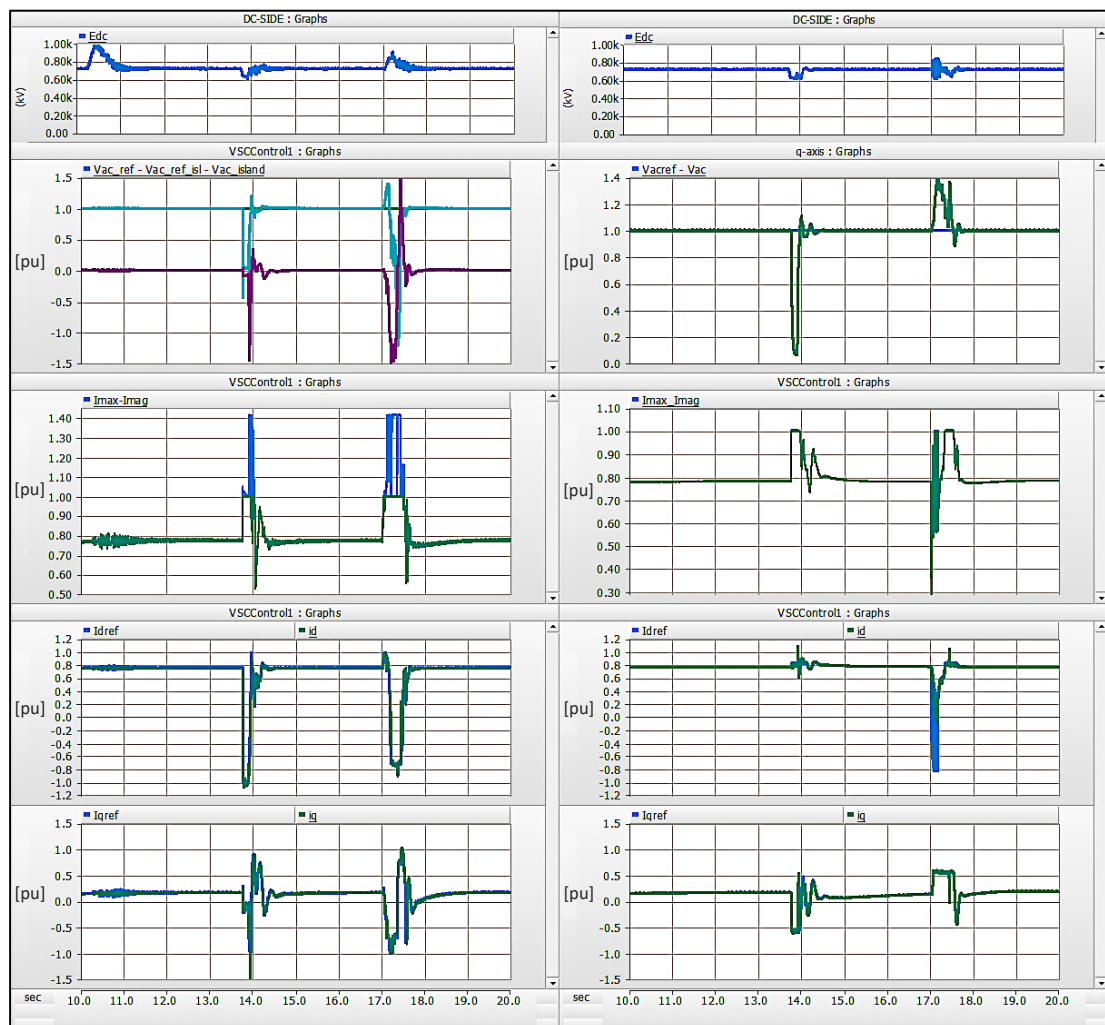


Figure 7.29: EMT3c Study Results at: → Top - PCC with the AC Grid, (MMC1-T2 and MMC2-T2)  
 → Middle - Onshore LFAC Cable Side (MMC1-T1 and MMC2-T1)  
 → Bottom - Offshore LFAC Cable Side (OWF1 and OWF2)

Regarding the three-phase to ground fault imposed on the AC grid Side-1 PCC at 10.25sec, the frequency converter (MMC1-HVDC) that forms the LFAC voltage waveform in the meshed LFAC scheme responds as in LFAC export case EMT2c). During the fault, the MMC1-T2 current saturation mechanism limits the fault current to 1p.u, while no power is transferred at the PCC due to the collapsed AC voltage and DC-voltage rises in the BtB-HVDC system up to 1.4p.u., as no DBR is adopted. Post-fault, the DCVC of the MMC1-T2 restores the DC voltage to its pre-fault value by injecting high active current ( $i_d \sim 1p.u.$ ) at full power output, and the RPC adjusts the reactive current controller value to attain zero reactive power ( $i_q \sim 0$ ), as presented in Figure 7.30. The post-fault oscillations on the Side-1 AC grid response are mainly due to the MMC1-T2 transformer saturation or “Pseudo-Inrush” phenomenon that occurs during the AC voltage recovery following the voltage sag. The effect of this fault to the rest of the MT-LFAC system or the Side-2 AC grid dynamic performance is insignificant.



**Figure 7.30: Onshore LFAC 345kV Left: MMC1-T1, Right: MMC2-T1 - EMT3c Results in the order they appear: DC-Voltage (Top), LFAC DQ-Voltage (Left) and ACVC (Right), Total and Saturated Currents, DQ-ICCs (Bottom).**

Likewise, in the three-phase to ground fault that occurs at the Side-2 OCS 345kV busbar at 13.75sec, the LFAC TS responds very similar to the LFAC export system in case EMT2c), with both the equivalent OWF1 and OWF2 BtB-VSC modules controlling effectively the fault current on their corresponding OCS to 1p.u., and their DBRs protecting their DC-links from over-voltages. Moreover, the MMC1-T1 islanded control system with its ICC, and the MMC2-T1 with its typical grid-following VCC strategy manage to limit their output fault currents to the maximum of 1p.u. To achieve this, their integrator anti-windup mechanisms turn off the integral parts of their outer controllers to support the system recovery and avoid the loss of control, under current saturation conditions. Since the converters manage to control and limit their current during this disturbance, their SCC contribution to the LFAC system is relatively small, and the voltage at the onshore LFAC 345kV busbar is very low (almost collapsed especially since no passive harmonic filters utilised here), forcing the power flow of the LFAC side to reach almost zero but without being reversed. However, power is slightly reversed in both the Side-1 and Side-2 AC systems during the LFAC side fault, the DC-Link voltages decrease but without seriously disturbing the 50Hz AC network voltages and the reactive power at the corresponding PCCs.

Finally, in the three-phase to ground fault imposed on the AC grid Side-2 PCC at 17sec, the MMC2-T2 responds in a very similar manner to MMC1-T2 against the equivalent three-phase to ground fault imposed on the AC grid Side-1 PCC at 10.25sec. Thus, during the fault, it limits the fault current to 1p.u, while the post-fault oscillations on the MMC2-T2 reactive power response are also due to the MMC2-T2 transformer saturation or “Pseudo-Inrush” phenomenon that occurs during the AC voltage recovery following the sudden voltage drop because of the fault. Nonetheless, as the MMC2-T1 power demand remains unchanged, it causes  $\sim 1.25$ p.u. HVDC over-voltage that activates the DBR and an LFAC over-voltage that instantaneously reaches up to 1.4p.u. at the onshore 345kV busbar. This increases the ICC q-reference rapidly as the converter that needs to absorb instantly the maximum amount of reactive power, which is set at 0.56p.u. of reactive current ( $i_q$ ), both during and after the fault. Though current saturation occurs, and the integrator anti-windup mechanism is energised that turns off the integral parts of the outer controllers. This action somewhat delays the active power restoration in the converter LFAC terminal, but it enables the LFAC system voltage recovery to avoid potential system instability.

Through this onerous fault, the LFAC over-voltage and the active power delayed response, without the simultaneous coordination of the OWPP modules disturbs the LFAC TS. More

specifically, the 345kV over-voltage is propagated to the MT-LFAC TS busbars leading all the converters of the scheme to respond close to their reactive power limit. At the same time, since the amount of real power produced by the OWF2 cannot be absorbed by MMC2-T1 due to its APC integral part disengagement, the generated power is redirected to flow through the 50km submarine interconnection cable towards the MMC1-T1 that acts as a “power-sink” for the system, absorbing part of the excess current, as long as it is within its current limit of 1 p.u. This active power growth also gives rise to its HVDC-Link voltage, since no DBR is applied and passes to the AC grid Side-1 through the LFAC-grid-forming frequency converter, whilst no significant disturbance is observed at the AC side voltages except for certain harmonic excitation during the transient. In the meanwhile, the DC voltage of the OWF2 equivalent module rises over 1.15p.u., triggering its DBR and temporarily reducing its active power output. These power variations can be easily addressed in the LFAC TS graphs of Figure 7.29, and they can be noticed in both AC grid Sides 1&2 as two consecutive power drops in AC grid Side-2 and as increased power consumption in the AC grid Side-1.

Although there are no related standards for high voltage LFAC systems that mention any limits for the change in the rms value of the Temporary Over-voltage (TOV) and its duration, a point could be made if the National Grid Technical Guidance Note (TGN(E) 288 – Issue 1 – May 2016) “Limits for AC-RMS Value of TOVs in England and Wales Network” is assessed, as shown in Figure 7.31 [120]. In this plot, the p.u. values are on the base of system continuous voltage of 420kV and 300kV rms for phase to phase nominal system voltages of 400kV and 275kV respectively. For the needs of the examined LFAC-TS, a phase to phase nominal system voltages of 345kV would correspond to a base of 362kV.

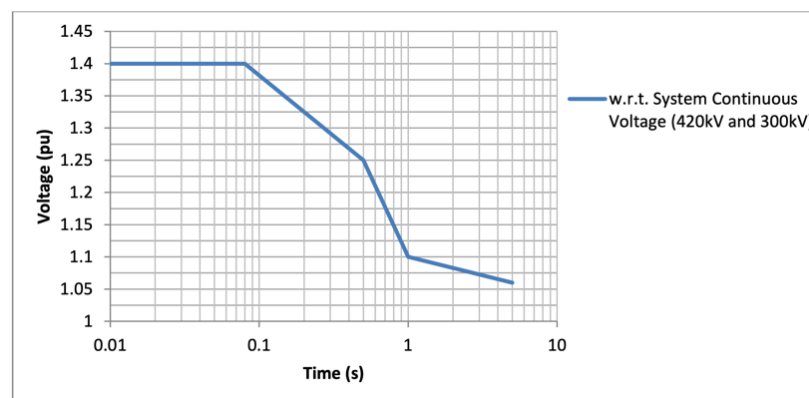


Figure 7.31: Limits for RMS Value of TOVs for 400kV and 275 kV in GB Network.

The maximum value of 1.4p.u. would then match an equivalent of ~507kV in the examined system, which together with the requirements of 7.1.3 could substantiate an overall

acceptable MT-LFAC FRT response for the tested cases. Therefore, an MT-LFAC system utilising only offshore submarine cables can have a satisfactory dynamic response on transient events and ride through faults that occur either in AC grid systems or in the offshore LFAC TS. DBRs in the DC sided of the OWTGs as well as the onshore frequency converters are essential, except if the valves could withstand specific HVDC instantaneous voltage rise. Considering a certain degree of technology readiness for High-Voltage LFAC circuit breaker and protection devices, it could be inferred that forming offshore meshed LFAC transmission systems for exporting power from OWFs and interconnecting different grids can be technically feasible for certain distances without implementing offshore passive compensation and harmonic filters.

#### 7.4.2 Performance Evaluation of the Feasible LFAC TS Cases

In these feasible cases, a properly tuned ICC is implemented in the islanded-control system of the LFAC grid-forming MMC. The resulted configurations are effectively energised, as demonstrated in cases EMT2a) and EMT3a), by ramping-up the voltage of the onshore grid-forming frequency converter, avoiding high cable charging-breaking currents and maintaining the system voltages to an acceptable level. This way, the risk of transient voltage and current stresses at the equipment is minimised, and the black-start or restoration processes following system black-outs can be accelerated.

The dynamic response of these arrangements to OWFs output power variations, as examined in EMT2b) and EMT3b), is satisfactory as all converter-controllers suitably follow their reference values and their response in the LFAC, as well as the AC side, is within their capacity limits. In some cases, the output dq-voltage of the grid-forming MMC can be sensitive to power variations when the ICC is employed, slightly deviating from the demanded values during transients but with damped oscillatory response and reasonable settling time.

Finally, the Fault-Ride-Through capability of the resulted LFAC TS arrangements is investigated in cases EMT2c) and EMT3c) and discussed below:

- **A solid three-phase to ground fault is imposed at the high-voltage side of the LFAC offshore collector system.** During this fault, the OWTG VSI modules and the onshore frequency MMCs ICCS and current saturation mechanisms effectively feed the fault and limit the fault-currents on their corresponding LFAC busbars to 1p.u., whilst the WTGs DBRs protect their DC-links from over-voltages the integrator anti-windup mechanisms enable the LFAC voltage to recover by disabling the outer voltage integrators. The power



flow in all parts of the LFAC TS drops to zero, and a certain amount of power is instantaneously reversed in all the 50Hz AC networks. This amount depends on the electrical proximity of the AC network to the fault and the number of the interconnected AC networks and flows to the corresponding HVDC sides, while the frequency converters DC-Link voltages reduce. Thus, the harsh AC side current decrease slightly disturbs the 50Hz AC network voltages and the RPC response at the corresponding PCCs. Although the system rides through this fault, the limited VSCs fault-current contribution may result in a relatively weak LFAC transmission system with low SCL, if it is not adequately meshed.

- **During a solid three-phase to ground fault occurring in any of the connected 50Hz AC grids**, no power is transferred at that PCC, and the operation of the respective grid side MMC terminal is essentially the same, as it limits its fault-current to 1p.u., while post-fault, 1p.u. of active current is injected until the full DC voltage recovery and the rather oscillatory RPC response is mainly due to the “Pseudo-Inrush” phenomenon. However, the effect that an AC grid side fault has on the 16.7Hz LFAC side, or even on other LFAC-Interconnected AC grid systems in case of an MT-LFAC TS, depends on the control system adopted by the MMC facing the 16.7Hz LFAC TS side. Hence, regarding the LFAC TS response against a three-phase to ground fault imposed on:
  - *The PCC with the 50Hz AC grid that interfaces the frequency converter operating in grid-forming control mode:* This fault is independent of the LFAC TS arrangement type as all the PtP, and the MT arrangements engage a grid-forming MMC. Moreover, all systems demonstrate very similar response on this fault, since the LFAC side perceives the fault as a trivial disturbance, while the effect it has on the dynamic performance of another interconnected AC grid can be negligible. This happens because the LFAC grid-forming BtB MMC-HVDC acts as a “firewall” preventing the disturbance from entering into the offshore LFAC transmission system, but if no DBR is installed in its DC side, the valves shall be able to withstand up to a specific DC over-voltage.
  - *The PCC with a 50Hz AC grid that interfaces a frequency converter operating in grid-following control mode:* This onerous fault occurs only in MT-LFAC TS arrangements that interconnect different AC grids or grid points, and so they can have grid-following MMCs in the LFAC side. Since these MMCs employ APCs, if their power demands remain constant during such an AC fault, the generated excess power that cannot be handled by the corresponding frequency converter’s DBR is redirected to flow through the submarine interconnection cable towards the grid-forming frequency converter.



Hence, the grid-forming MMC acts as a “power-sink” for the system, absorbing part of the excess current, as long as it is within its current limit of 1 p.u. rapidly increasing its AC grid system currents and slightly disturbing the AC system’s voltage.

However, if there is more excess power in the system, it can cause further rise to the HVDC voltages of the frequency-converters which together with the simultaneous power flow redirection inside the LFAC TS can develop over-voltages in the LFAC side. The LFAC over-voltages can be propagated to multiple LFAC TS busbars and prompt the respective converters to respond close to their reactive power capability limits. This may not only disturb the dynamic response of the LFAC TS, but also cause cascade effects by triggering control and protection measures of the related parts, creating more implications in the active power flow of the system which can be reflected to the power output of the AC grids. Still, the system may ride through the fault successfully and comply with equivalent AC overvoltage regulations in case EMT3c). Nevertheless, it is clear that for such fault conditions in meshed or MT schemes, proper coordination among the OWTGs and the APC demands of the grid-following MMCs shall be attained.

## 7.5 Summary and Conclusions

In this chapter, the LFAC TS dynamic performance is evaluated through time-domain EMT assessment. The representative offshore PtP and MT-LFAC TS arrangements with 200km export cable lengths are modelled in time-domain adopting the design principles and operating features defined in Chapters 3,4,5 and 6, and a set of EMT studies is introduced to estimate the system’s technical performance. The EMT studies comprise the offshore LFAC system energisation, power output variations for OWF power export and grid interconnection scenarios as well as three-phase to ground faults in the AC and LFAC sides. Through these studies, the characteristic offshore LFAC TS schemes are suitably configured in terms of VSC control system functions, low-order harmonic filtering and reactive compensation needs, while appropriate coordination of the VSC control modes and protection strategies is attempted.

More specifically, the EMT assessment of the PtP LFAC TS arrangements demonstrated stable steady-state and dynamic response as well as compliance with typical grid code requirements for specific fault events and contingencies. The typical islanded control mode without ICCs and the enhanced islanded control with ICCs, appropriate current saturation, and integrator

anti-windup mechanisms were compared. If the typical islanded control mode is employed, it shall be implemented with passive harmonic filtering to avoid excessive voltage and current THD and low order harmonic stability issues caused by the system resonance. However, an uncontrolled and excessive fault-current can be produced in case of an offshore LFAC side fault, which may severely damage the power converters, cables and other equipment of the scheme, especially in case of a CB failure.

If the enhanced islanded control mode with ICCs is employed for the PtP arrangement, then no passive harmonic filtering for damping low-order resonances may be needed as long as the ICCs are tuned to attain a suitable bandwidth and dominate the system impedance at the potential low-order resonant point. This way, low THD levels can be achieved without low-order harmonic issues under normal operation while the scheme can effectively ride-through AC and LFAC side faults by limiting the fault-currents in the LFAC export system, utilising a typical current saturation technique. Consequently, this control configuration shall be considered for the grid forming converters in MT-LFAC TS designs.

It can be inferred that forming an offshore meshed MT-LFAC TS can be technically feasible, even without passive, shunt compensation placed offshore if the reactive power capability of the converters is utilised, and without employing harmonic filters if the islanded-controller of the grid-forming MMC implements:

- ICCs to regulate the output currents with a desired high bandwidth to dominate the system impedance.
- Current saturation mechanism to limit the fault-currents that could damage the MMC valves and other LFAC system devices.
- Integrator anti-windup mechanisms that temporarily disable the integral parts of the outer voltage controllers under current saturation conditions.

In addition, DBRs shall be applied in the DC sides of the OWTGs and the onshore BtB frequency converters to mitigate DC over-voltages, by absorbing the excess energy temporarily.

Thus, coordinated control and protection strategy shall be applied to support the voltage recovery and avoid potential control instability in PtP and MT-LFAC TS schemes. Therefore, technically feasible offshore PtP and MT-LFAC TS arrangements are produced that can assure stable steady-state and dynamic operating response and comply with generic connection and grid code requirements for specific faults and contingencies.

## Chapter 8: Conclusion and Future Work

### 8.1 Summary and Discussion

The main goals of the current industrial research were to define and investigate robust and feasible LFAC TS schemes for offshore applications that could be materialised by the industry in a quite ordinary fashion and achieve straightforward and compliant offshore system solutions to effectively transfer the rated capacity of bulk OWPPs to the grid. This was attempted through the examination of PtP and multi-terminal, meshed network schemes that could interconnect different OWFs to each other and different grids. Also, the designated transmission equipment design and rating were appropriately adapted for High Voltage LFAC operation based on standard industry practices and the literature.

Another aim of this study has been to determine the respective LFAC TS operating aspects (e.g. control arrangements, potential compensation and mitigation measures, etc.) that would enable the designed schemes to be technically and economically competitive over a certain distance range to the already established HVAC and HVDC alternative technologies for OWPP integration. Accordingly, the power transfer capacity of a single LFAC export cable was optimised to transfer the full power output of each OWPP, while any necessary passive mitigation and compensating equipment was placed in the onshore frequency converter substations. This way the minimum number of cables is utilised for power transmission and the installation of additional components on the offshore LFAC platforms that could further increase the size, footprint and cost of the schemes is avoided.

With respect to the research aims, the main LFAC equipment parameters have been obtained, and the designated LFAC TS arrangements have been optimised. The technical feasibility of LFAC TS was assessed for different subsea cable lengths and network arrangements, through engineering studies in order to explore the system's performance capabilities, potential limitations and compliance issues. Detailed system models were set-up in DigSilent PowerFactory and PSCAD-EMTDC to conduct steady-state, frequency and time-domain dynamic simulation studies of several LFAC TS configurations under various operating conditions and for different transient and fault events.

High-fidelity EMT models were developed even for the complex MT-LFAC TS scheme for the dynamic performance assessment. They comprise the onshore BtB frequency MMCs with DEM employed for its HBSMs and switching aggregates for the OWF BtB VSCs. Optimum control strategies were obtained by steady-state analysis and controllers were generically tuned through TF analysis. Finally, FDPM is used for the export cables, suitable transformer and filter parameters are included, while the AC grids are modelled as Thevenin equivalents.

## 8.2 Conclusions and Recommendations

Summarising, some of the most significant concluding points and findings to emerge from this study are discussed below:

- I. Subsea cable parameters explicitly adapted for LFAC TS purposes were obtained by a cable manufacturer (NEXANS). The LFAC operation of the adjusted cables presents:
  - Benefits in power losses, reactive current, compensation, loading conditions, and power transfer capability for extended cable lengths.
  - Benefits if operating at higher voltage levels as the power transfer capability significantly increases but for relatively reduced cable lengths.
- II. LFAC and AC power transformer designs were estimated for various impedance levels based on transport limitations, according to standard industrial design methods and assumptions [128]. The corresponding Site Weights that primarily define the LFAC platform weight and the Total Power Losses were yielded and compared. Results showed that the estimated LFAC transformers could be 2-2.15 times bigger in terms of size and weight and consume 1.45-1.65 times more power than their 50Hz equivalents for the same p.u. impedance. Hence, for the appropriate transformer impedance selection, there is a trade-off between transformer weight and losses, although in an offshore transmission system application both the losses and weight of the transformers shall be reduced as much as possible.
- III. In case of equally rated converters having the same configuration and equal number of modules and switching elements, the passive equipment components of a converter facing a 16.7Hz LFAC network need to be rated almost three times higher than those of an equivalent converter interfacing a 50Hz grid. This is considered based on typical calculations performed for the rating of DC capacitors and arm or converter reactors.
- IV. PtP and MT-LFAC TS resonance responses were evaluated, and the impact of the LFAC cable length and the LFAC transformer leakage reactance to the system dynamic impedance frequency and amplitude were investigated. At the offshore side, the resonance has a relatively higher magnitude than at the onshore busbar, while the lowest resonance levels are noticed at the OWTGs, compared in a per-unit scale. Accordingly, with an increasing submarine cable length, the resonant frequencies decrease due to the higher cable capacitance and inductance, but as cable ohmic

resistance increases, it produces natural damping, and lower magnitudes are noted. Furthermore, the lower the transformers relative leakage inductance in p.u., the higher the system's resonant frequency and the lower its magnitude, whilst the fundamental 16.7Hz frequency impedance magnitude affecting the system losses is reduced.

- V. Suitable C-Type harmonic filter combinations were introduced to mitigate the LFAC TS resonances for various cable lengths and reduction of the filtering losses was attained compared to former studies where single-damped filters introduced excessive losses [7].
- VI. In the MT-LFAC TS schemes, the resonance magnitude and frequency are reduced compared to the corresponding PtP base cases, mainly due to the natural damping introduced by the parallel cable paths and the characteristics of the added cables. Thus, the harmonic filters designed for the PtP schemes can be effective for MT systems as well, also supporting the standalone radial operation of these schemes. However, to efficiently accommodate the MT operation, switching steps may be introduced to the filters to reduce their MVar and losses and avoid any additional compensation needs.
- VII. The correlation between the operating frequency and the dynamic impedance of an offshore system is discussed, through the investigation of simplified subsea cable-transformer pairs that were found to dominate the system resonance characteristics. It is estimated that in a radial offshore arrangement, the harmonic order of the resonant point and the resonance magnitude can be higher for lower operating frequencies.
- VIII. Optimised PtP and MT-LFAC TS arrangements were yielded by steady-state analysis in terms of minimum active power losses and shunt compensation, only at the onshore side. The power-flow studies resulted in efficient DCVC/ACVC strategies for the inverters of the OWTGs while the reactive power capability of all the available converters was utilised for maximising the power transfer through the cables up to a length that the Ferranti Effect or excessive losses would prevail. At the same time, the LFAC TS compliance with operating standards is assured in terms of bus voltage levels, charging breaking currents in the CBs, equipment loading and converter capability limits under various operating conditions for cases with and without passive harmonic filters.
- IX. Higher PtP LFAC TS availability was attained based on the optimised steady state export cases compared to corresponding HVAC and HVDC systems over the cable length, while the superior availability of a potential meshed MT-LFAC was showcased. This is a strong indication of the system's reliability and economic feasibility, as seen in APPENDIX B

X. The EMT assessment of the optimised PtP LFAC TS arrangements revealed that they could be technically feasible. Stable steady-state and dynamic operating response was demonstrated, and compliance with typical connection and grid code requirements for specific fault events and contingencies was attained. In a PtP LFAC TS, the LFAC grid-forming MMC of the onshore BtB frequency converter can employ:

- *The typical islanded control mode without Inner Current Controllers (ICCs):*

It should always be implemented with passive harmonic filtering to avoid excessive voltage and current THD and low order harmonic stability issues caused by the system resonance. This option combined with suitable C-Type filters demonstrated acceptable dynamic performance during energisation and for OWF output power variations as well as sufficient FRT capability against a 150ms solid three-phase-to-ground fault at the PCC with the 50Hz AC grid. However, an uncontrolled and excessive fault-current was produced in case of an offshore LFAC side fault, which could have severely damaged the power converters, cables and other equipment of the scheme, especially in case of Circuit Breaker failure. Hence, these settings could be barely applied only in a PtP scheme by over-rating the frequency converter modules and with proper coordination and seamless operation of LFAC CBs and protection devices, but they should not be considered for any MT-LFAC TS design.

- *The enhanced islanded control mode with ICCs, appropriate current saturation, and integrator anti-windup mechanisms:*

If the ICC could be tuned to attain a suitable bandwidth in order to dominate the system impedance at the potential low-order resonant points, then no passive harmonic filtering for damping the low-order resonance would be needed, as low THD levels could be maintained without low-order harmonic issues under normal operation. In this study, the system demonstrated adequate dynamic performance for OWF output power variations; it effectively rode-through AC and LFAC side faults and limited the fault-currents in the LFAC export system. Even if additional harmonic filtering strategies or other mitigation measures need to be applied, they may be less complex, or lower-rated without necessitating further reactive power compensating equipment that would also increase power losses the system overall costs.

XI. To establish a feasible offshore MT-LFAC TS, coordinated control and protection should be applied. Thus, the islanded-controller of the grid-forming MMC should implement:

- ICCs to regulate the output currents with a desired high bandwidth to dominate the system impedance. As explained in Chapter 6, most low-order resonant frequencies of the LFAC system regardless of its operating condition should lie within it, so that no current and voltage interactions occur with the passive system resonance.
- Current saturation mechanisms to limit the fault-currents that could damage the MMC valves and other LFAC system devices, especially in cases of LFAC CB failures.
- Integrator anti-windup mechanisms that temporarily disable the integral parts of the outer voltage controllers under current saturation conditions to support the voltage recovery and avoid potential control instability.

Besides, DBRs shall be applied in the DC sides of the OWTGs and the onshore BtB frequency converters to temporarily absorb the excess energy and mitigate DC over-voltages, if the converter valves cannot withstand high DC voltage levels.

- XII. The EMT simulations of the MT-LFAC TS demonstrated satisfactory dynamic response, as all the converter-controllers suitably followed their reference values and their outputs in the LFAC, and AC sides were within their capability limits. The fault response was similar to the corresponding PtP cases for faults imposed at the LFAC side and the PCC with the 50Hz AC grid of the grid-forming frequency MMCs side. However, a fault at the PCC with the AC grid system of the grid-following frequency converter side caused severe over-voltages in the LFAC system that were propagated to multiple LFAC network busbars. This condition could prompt the respective converters to respond close to their reactive power capability limits, depending on specific system settings. Such event could potentially disturb the dynamic response of the total LFAC TS and even cause cascade effects by triggering control and protection measures of the related parts, creating more implications in the active power flow of the system which would be reflected to its power output to the AC grid. Still, the examined system managed to ride through this onerous fault successfully and comply with the respective AC overvoltage limits.

In general, the combination of Type-4 OWTGs and onshore BtB MMC frequency converters with one LFAC-grid-forming MMC employing islanded control enhanced with ICCs, appropriate current saturation, and integrator anti-windup mechanisms can be a feasible and straightforward solution for the formation of an efficient and compliant offshore LFAC TS. This LFAC TS set-up can benefit from low THD levels without low-order harmonic issues under normal system operation, while it can demonstrate satisfactory dynamic performance for OWF power output variations and effectively ride-through faults and disturbances.

The investigation of LFAC technology has shown that the design, engineering and production of the main LFAC power transmission components would not be a major technical challenge, considering the minor technical differences with the components for 50Hz AC systems. Moreover, there is a prior operational experience in the area, as many parts of the single-phase version of LFAC are entirely developed by rail track electrification system. The fact that most of this LFAC experience can be found concentrated in some of the most reputable T&D vendors advocates that they may be able to combine the knowledge of the rail industry with that of power T&D, regulating solutions with the least amount of development burdens.

Nevertheless, LFAC in the proposed form and size is a new technology with no prior design or operating experience and development can be expected. The practical implementation may come across some unforeseen difficulties, and it may still be necessary to undertake efforts in order to optimise the equipment for low frequency operation such as new type testing, certification, etc. The time until components become physically available may also depend on the certification period, especially regarding WTGs, cables, transformers, CBs and switchgears. Finally, it needs to be considered whether there can be a standardisation of the LFAC grid solution in order to rely on suppliers' components as is the case for conventional AC systems or will there be a need for a design authority to study the system as a whole and then specify and integrate each of the components in a functional or optimised system.

### 8.3 Thesis Contributing Points

As mentioned in section 1.4, the findings and conclusions of this Industrial PhD Thesis contribute to the state-of-the-art and provide a path to accelerate the industrial exploitation of the offshore LFAC TS technology, by introducing:

❖ **Explicit adaptations in the design and rating of key transmission components for LFAC operation, based on industry practices.** Parameters were obtained for the main transmission equipment:

- 1) The LFAC submarine export cable parameters acquired by a cable manufacturer.
- 2) The LFAC power transformer parameters were estimated based on industry methods and assumptions (aspects like transport size and weight restrictions for various impedance levels were considered).
- 3) The BtB frequency MMCs with HBSM capacitors sizing and WTG VSCs rating for interfacing a 16.7Hz system.



❖ **Accurate investigation for the passive resonance of the isolated LFAC TS in the frequency domain with FDP subsea cable representation.**

A low-order resonance in the LFAC network could produce sustained overvoltages during transformer energisation or at fault-clearing which may even damage the equipment. By knowing the frequency response for the offshore LFAC TS, wider harmonic propagation problems can also be avoided that can create potential system performance or harmonic stability issues. In this Thesis, the impact of the cable length to the total LFAC TS impedance profile is evaluated, while the effect of adding branches to form Multi-Terminal LFAC schemes is addressed. Also, the implementation of passive harmonic filtering equipment to mitigate the system low-order resonances is assessed.

❖ **Optimised offshore PtP and MT-LFAC TS layouts for minimum power losses and minimum shunt compensation are placed only at the onshore side, through Steady-State analysis.** Thus, the fundamental conditions to achieve the Thesis' objectives are established that include using only one-single LFAC export cable to maximise its power transfer capability and installing only onshore any passive mitigation and compensating equipment needed, where possible. This assessment results in:

- 1) Efficient operation by implementing the appropriate control strategies for the OWTG inverters (ACVC/DCVC mode), and the added grid-following MMC terminals (APC/ACVC) in the MT arrangement, within their capability limits.
- 2) Conforming operation to the equipment steady-state loading limits (i.e. avoiding overloading) and typical network operating standards, e.g. voltage regulation to  $\pm 5\%$ . Moreover, the edge that the LFAC technology can have over the HVAC and HVDC for certain offshore TS is indicated through an availability assessment in APPENDIX B.

❖ **Effective tuning of the LFAC TS designated control strategies, in coordination with appropriate mitigation measures and system enhancements in EMT domain, so as to comply with typical grid code requirements and equipment capability limits for transient conditions (e.g. ENTSO-E LVRT Requirements -for minimum and maximum fault clearing and recovery times as well as the GB Network TOV Limits).** This coordination is considered both for PtP and MT-LFAC TS schemes in order to achieve:

- 1) Elimination of the low-order resonance impact on the THD and the harmonic stability of the system. The resonance effect can be mitigated by the proper islanded control type selection on the onshore grid forming MMC with a high bandwidth ICC or by applying passive damping filtering equipment, or a combination of both.

2) Improvement of the FRT capability of the system to contain the fault currents within limits, support voltage recovery and ensure appropriate system response in the LFAC, the DC and AC sides. The FRT of the feasible LFAC TS schemes is examined against faults in the offshore LFAC, and the AC grids and appropriate enhancements are adopted. Hence, by combining some operating principles from the analysed PtP cases and by appropriately coordinating converter control schemes with protection mechanisms, technically feasible offshore MT-LFAC TS arrangements are designed that demonstrate stable dynamic operating response.

#### **8.4 Limitations and Future Work**

LFAC technology can provide an attractive transmission solution for exporting power from large and remote offshore wind power plants (OWPPs) within a specific distance range of e.g. 80-300km. As seen, it can be realised as an equivalent offshore HVAC TS combined with an onshore BtB MMC-HVDC, with long HVAC sea and land cables operated at lower frequencies. Thus, it can eliminate capacitive currents, reactive compensation and losses compared to HVAC, while at the same time, offering a potentially more cost-efficient and reliable approach, especially for MT arrangements in comparison to HVDC.

However, there can be certain limitations towards the commercial exploitation of the LFAC TS. Currently, the only real-time applications of LFAC system involve the supply of passive LFAC load networks in the Rail and Oil & Gas industries. Thus, there has been no prior operational experience of LFAC in other applications that would correspond to a similar-scale of power exchange between the LFAC and AC systems or fulfil analogous requirements to an offshore TS. From the T&D equipment vendors' perspective, the LFAC technology for offshore transmission could be considered as "new", because there is a shortage in testing standards and prior LFAC equipment manufacturing experience of the expected size and ratings, even for key system components such as the power transformers, inductors, CBs, etc.

Consequently, among the various project investors and stakeholders, uncertainty can be precipitated regarding the LFAC technology readiness level for transmission purposes. Even if an economic feasibility evaluation of the LFAC TS scheme assures its efficiency in theory, it may be argued that certain implications could emerge upon operation that would render its practical implementation difficult. Hence, this ambiguity that the LFAC TS may encounter some unforeseen pitfalls jeopardising its technical feasibility and compliance with the

demanding modern grid codes shall be tackled through further research and development.

Hence, additional research should be undertaken to explore more operating aspects of the LFAC technology for offshore power transmission and to suggest a clear path towards industrial development. The fact that practical LFAC TS arrangements may be “isolated” from the grid, and only formed among power electronic converters presents a challenging task for analysis. The dynamic nature of the systems’ impedance profiles implies that the related converters’ control system regulation, their bandwidth requirements and the coordinated response would highly vary with the specific conditions of each project. Thus, for potential system planning or insulation coordination purposes and in order to achieve adequate system performance, accurate EMT simulations would be required with project-specific data and the full-knowledge of the detailed control schemes, component parameters and proprietary information from cable and transformer manufacturers and vendors of the WTGs, the frequency converters, etc.

Recommendations for further work may involve:

- The stability assessment of individual OWTGs for different OWF layouts operating in LFAC and the detailed investigation of interactions among the OWTGs and the onshore MMCs, to calibrate the offshore system control and protection. Related aspects regarding wind power fluctuations, aerodynamics and electro-mechanical dynamics may be considered.
- The analysis of the impact that PLL has on the dynamic response and stability of the isolated and converter dominated LFAC TS.
- Fault assessment considering asymmetric faults at the onshore AC and offshore LFAC networks and respective negative sequence controllers to evaluate the system response.
- Larger OWPPs or more OWF connections integrated to various grids through multiple onshore frequency MMC Terminals for which further control adjustments might be required, e.g. alternative synchronisation control, decentralised power-sharing control, extra DC and LFAC voltage droop regulation schemes.
- Detailed and optimised designs for essential transmission equipment, in order to attain accurate dimensions and weights and for estimating the corresponding offshore LFAC topside characteristics for the economic evaluation of the scheme.
- If the LFAC TS proves itself worthy of development, different topologies might be developed as well in the future, and innovative frequency converter solutions designed explicitly for LFAC (e.g. hexverter and matrix converter) might be further improved to comply with grid code requirements and move towards industrial development.

## References

- [1] X. Wang, X. Wei and Y. Meng, "Experiment on Grid-Connection Process of Wind Turbines in Fractional Frequency Wind Power System," *IEEE Transactions on Energy Conversion*, vol. 30, no. 1, pp. 22-31, March 2015.
- [2] A. Canelhas, S. Karamitsos, U. Axelsson and E. Olsen, "A Low Frequency Power Collector Alternative System for Long Cable Offshore Wind Generation," *IET*, ACDC 2015, Birmingham, February 2015.
- [3] I. Erlich, F. Shewarega, H. Wrede and W. Fischer, "Low Frequency AC for Offshore Wind Power Transmission – Prospects and Challenges," *IET*, ACDC 2015, Birmingham, February 2015.
- [4] Y. Tang, P. Wyllie, J. Yu, X. Wang, L. Ran and O. Alatise, "Offshore Low Frequency AC Transmission with Back-to-Back Modular Multilevel Converter (MMC)," *IET*, ACDC 2015, Birmingham, February 2015.
- [5] P. Wyllie, Peter, Y. Tang, L. Ran, T. Yang, J. Yu, "Low Frequency AC Transmission - Elements of a Design for Wind Farm Connection". *IET Seminar Digest*, 2015. pp. 1-5.'
- [6] V. Illa and A. Rajagopal, "Solar Wind Hybrid System On Offshore With Low Frequency Power Transmission," *SPRJ*, vol. 2, no. 21, 2014.
- [7] E. Olsen, U. Axelsson, A. Canelhas and S. Karamitsos, "Low Frequency AC Transmission on Large Scale Offshore Wind Power Plants. Achieving the best from two worlds?," in *13th Wind Integration Workshop*, Berlin, November 2014.
- [8] A. Ram, R. Nethra and M. Reddy, "Power Transmission from Offshore Wind Energy for Low-Frequency," *IJATES*, vol. 02, no. 11, pp. 401-411, 2014.
- [9] W. Xifan, W. Xiaohui, N. Lianhui and W. Xiuli, "Integration Techniques and Transmission Schemes for Off-shore Wind Farms," *Proceedings of the CSEE*, vol.34, no.31, [Chinese], November 2014.
- [10] V. Prasuna, K. Mohiuddin and P. Kumar, "Power Transmission of Low Frequency Wind Firms," *IJCSMC*, vol. 3, no. 10, pp.419-423, 2014.
- [11] M. Manaswi and K. Kumar, "Low Frequency HVAC Transmission System for Wind Power Systems," *IJRAET*, vol. 2, no. 1, pp. 16-22, 2014.
- [12] B. Kannan, G. Rao and Yo.Puvvadi, "A Grid Interfaced Low Frequency Offshore Wind Power," *IJARSE*, vol. 3, no.9, pp. 338-343, 2014.
- [13] M. Adelian, N. Maher and F. Soorani, "Remote Power Generating Systems WHIT Using Low Frequency Transmission," *IJERGS*, vol. 2, no. 5, pp. 159-167, 2014.
- [14] M. Manohara and S. Sonia, "Design of Low-Frequency AC Transmission System for Offshore Wind Farms," *IJETAE*, vol. 4, no. 8, pp. 111-121, 2014.
- [15] P. Chennaiah, S. Anupama and N. Thulasi, "AC Transmission with Low Frequency for Renewable Energy Sources in Offshore Location," *IJCSIS*, vol. 12, no. 2, pp. 27-32, 2014.
- [16] G. Reddy and K. Sagar, "Low Frequency AC Transmission System for Grid Connection of Offshore Wind Farm," *IJRSAE*, vol. 2, no. 7, pp. 128-135, 2014.
- [17] M. Pasha and S. Khamuruddin, "PV Connected Low-Frequency AC Transmission System," *IJPRES*, vol.3, no. 1, pp. 71-78, 2014.

- [18] M. Manohara and S. Sonia, "Low-Frequency AC Transmission System for Offshore Wind Farms," *IJERM*, vol. 1, no. 4, pp. 157-162, 2014.
- [19] C. Jambotkar and U. Satpute, "Simulation of Dc-Link Power Converter for Integrating Offshore Wind Turbine Generator to Grid," *IJSETR*, vol. 3, no. 7, pp. 1940-1945, 2014.
- [20] Cigre Working Group B4.39, "Integration of Large-Scale Wind Generation using HVDC and Power Electronics," *Cigre*, ISBN: 978-2-85873-057-5, Doc. 370, February 2009.
- [21] R. Meere, J. Ruddy, T. O'Donnell, "Variable Frequency Operation for Future Offshore Wind Farm Design: A Comparison with Conventional Wind Turbines," *Energy Procedia*, vol. 53, pp. 280-289, 2014.
- [22] P. Achara and T. Ise, "Operating Phase and Frequency Selection of Low Frequency AC Transmission System Using Cyclo-converters," in *IEEE The 2014 International Power Electronics Conference*, pp. 3687-3694, 2014.
- [23] H. Chen, M. Johnson and D. Aliprantis, "Low-Frequency AC Transmission for Offshore Wind Power," *IEEE Transactions on Power Delivery*, vol. 28, no. 4, pp. 2236-2244, 2013.
- [24] X. Wu, X. Yang, H. Shen and Q. Zhou, "Research on the Long-distance Transmission," *SciRes*, pp. 1293-1297, 2013, doi:10.4236/epe.2013.54B245, <http://www.scirp.org/journal/epe>.
- [25] Y. Miura, T. Mizutani, M. Ito and T. Ise, "Modular Multilevel Matrix Converter for Low Frequency AC Transmission," pp. 1079-1084, 2013.
- [26] R. Barrera-Cardenas and M. Molinasa, "Multi-objective Design of a Modular Power Converter Based on Medium Frequency AC-Link for Offshore DC Wind Park," *Energy Procedia*, vol. 35, pp. 265-273, 2013.
- [27] D. Zhao, S. Meliopoulos, R. Fan, Z. Tan and Y. Cho, "Reliability Evaluation with Cost Analysis of Alternate Wind Energy Farms and Interconnections," *IEEE*, 2013, <http://energy.ece.illinois.edu/>.
- [28] C. Nguyen Mau, K. Rudion, A. Orths, P. Eriksen, H. Abildgaard and Z. A. Styczynski, "Grid Connection of Offshore Wind Farm based DFIG with Low Frequency AC Transmission System," *IEEE*, vol. 1, pp. 1-7, 2012.
- [29] R. Vaid, "Low Frequency AC (LFAC) Transmission for Long Distance Power Transmission and Offshore Interconnection," *GradCon*, Winnipeg, MB, Canada, October 2012.
- [30] W. Fischer, R. Braun and I. Erlich, "Low Frequency High Voltage Offshore Grid for Transmission of Renewable Power," *3rd IEEE PES Innovative Smart Grid Technologies Europe (ISGT Europe)*, Berlin, 2012.
- [31] V. Gevorgian, M. Singh, and E. Muljadi, "Variable Frequency Operations of an Offshore Wind Power Plant with HVDC-VSC," in *IEEE Power and Energy Society General Meeting/NREL*, CP-5500-53464, July 2012.
- [32] D. Wang, C. Mao, J. Lu and H. Lou, "General Aspects and Fundament of Variable Frequency Electric Power Transmission," *Electrical Review*, ISSN 0033-2097, R. 88 NR 8/2012 pp. 255-259, 2012.
- [33] W. Xifan, W. Xiuli and T. Yufei, "Fractional Frequency Transmission System and Its Applications," *Proceedings of the CSEE*, vol.32, no.13, May 2012.

- [34] Z. Song, X. Wang, Y.Teng, L. Ning and Y. Meng, "Optimal Control Study for Fractional Frequency Wind Power System," *IEEE Power and Energy Engineering Conference (APPEEC)*, Shanghai, Asia-Pacific, pp. 1-5, March 2012
- [35] Y. Cho, G. Cokkinides and A. Meliopoulos, "Advanced Time Domain Method for Remote Wind Farms with LFAC Transmission Systems: Power Transfer and Harmonics," *IEEE*, pp. 978-984, 2012.
- [36] Y.Cho, G. Cokkinides, A. Meliopoulos, "LFAC-Transmission Systems for Remote Wind Farms Using a Three-phase, Six-pulse Cyclo-converter," *IEEE*, pp. 1-7, 2012.
- [37] T. Yufei, W. Xifan, N. Lianhui, M. Yongqing and S. Zhuoyan, "Unified Iterative Method to calculate Power Flow of the Interconnected System with Fractional Frequency Transmission System," in *IEEE 4th International Conference on Electric Utility Deregulation and Restructuring and Power Technologies (DRPT)*, pp. 438-443, July 2011.
- [38] N. Lianhui, W. Xifan and T. Yufei, "Experiment on Wind Power Integration Grid via Fractional Frequency Transmission System: Realization of the Variable-Speed Variable-Frequency Power Wind," in *IEEE 4th International Conference on Electric Utility Deregulation and Restructuring and Power Technologies (DRPT)*, pp. 444-449, July 2011.
- [39] G. Stamatiou, K. Srivastava, M. Reza and P. Zanchetta, "Economics of DC Wind Collection Grid as affected by Cost of Key Components," *WREC/WE*, Linkoping, Sweden, pp. 4177-4184, May 2011.
- [40] U. Satpute., S. Jangamshetti, D. Joshi, "Feasibility Study of Fractional Frequency Transmission System," in *IEEE Joint International Conference on Power Electronics, Drives and Energy Systems (PEDES)*, New Delhi, India, pp. 1-6, December 2010.
- [41] Y. Quan-xin, W. Wei, X. Li-jie, N. Ping-hao, Xi.Ming-chao, W.Lin and L. Heng-lin, "Research on Wind Power Connected to Power Grid by Fractional Frequency Transmission System," in *IEEE Power and Energy Engineering Conference (APPEEC)*, 2010 Asia-Pacific, Chengdu, pp. 1-4, May 2010.
- [42] M. Rao and A. Pradesh, "Integration of Low Frequency Alternator to Utility Grid via Fractional Frequency Transmission System," *IEEE*, 2010.
- [43] A. Kumaran, "Power Transmission through Fractional Frequency System," September 2009, [cktana.co.uk/education](http://cktana.co.uk/education).
- [44] X. Wang, X. Wang and Z. Bie, "Integrating Wind Farm into Grid via Fractional Frequency Transmission System, Future Energy - Bornholm," <http://www.futureenergy.dk>, September 2009.
- [45] N. Qin, S. You, Z. Xu and V. Akhmatov, "Offshore Wind Farm Connection with Low Frequency AC Transmission Technology," *IEEE PES '09*, pp. 1-8, July 2009.
- [46] A.Nakata, A.Torii, A.Ueda, "Inverter Frequency and Transformer for Low Frequency Power Transmission," *SIST: Shizuoka Institute of Science and Technology*, Seattle, WA, March 2009.
- [47] T. Yufei and W.Xifan, "Three-Phase Short-Circuit Fault on the Lower Frequency Bus of Cyclo-converter in FFTS," *IEEE/PES, Power Systems Conference and Exposition PSCE '09*, pp. 1-5, March 2009.
- [48] C. Bajracharya, M. Molinas, J. Suul and T. Undeland, "Understanding of Tuning Techniques of Converter Controllers for VSC-HVDC," in *Nordic Workshop on Power and Industrial Electronics*, June 9-11, 2008.

- [49] W. Xifan, C. Chengjun and Z. Zhichao, "Experiment on Fractional Frequency Transmission System," *IEEE Transactions on Power Systems*, vol. 21, no. 1, pp. 372-377, 2006.
- [50] R. Bhat, M. Bhattacharya, S. Goyal, S. Abhang, "Fractional Frequency Transmission System," Fr C Rodrigues Institute of Technology, 2004.
- [51] S. Meier, S. Norrga and H. Nee, "New Topology for more Efficient AC/DC Converters for Future Offshore Wind Farms," in *Proceedings of the 11th International Power Electronics and Motion Control Conference, EPE-PEMC '04*, Riga, Latvia, September 2004.
- [52] R. Nakagawa, T. Funaki and K. Matsuura, "Installation and Control of Cyclo-converter to Low Frequency AC Power Cable Transmission," *IEEE PCC-Osaka 2002*, pp. 1417-1422, September 2002.
- [53] T. Funaki and K. Matsuura, "Feasibility of the low frequency AC transmission," *IEEE, Power Engineering Society Winter Meeting*, vol.4, pp. 2693-2698, January 2000.
- [54] X. Wang and X. Wang, "Feasibility Study of Fractional Frequency Transmission System," *IEEE Transactions on Power Systems*, vol. 11, no. 2, pp. 962-967, 1996.
- [55] W. Musial et al, U.S. Department of Energy (DOE), "2018 Offshore Wind Technologies Market Report," U.S. Department of Commerce National Technical Information Service, 2018.
- [56] M. Safder, S. Rizvi, Y. Meng, M. Javed, M. Jaffery and M. Hassan, "Low-Frequency AC Power Transmission and Distribution for Subsea Application using Hexverter," *Electronics 2020*, vol. 9, no. 61, December 2019.
- [57] T. Ngo, Q. Nguyen, and S. Santoso, "Voltage stability of low frequency ac transmission systems," *2016 IEEE/PES Transmission and Distribution Conference and Exposition (T D)*, pp. 1-5, May 2016.
- [58] J. Li and X. Zhang, "Small signal stability of fractional frequency transmission system with offshore wind farms," *IEEE Transactions on Sustainable Energy*, vol. 7, no. 4, pp. 1538-1546, 2016.
- [59] H. Waje-Andreassen, "Low Frequency AC Transmission Investigating the Dynamics of an Export Cable for Offshore Wind Power Applications," Master of Energy and Environmental Engineering, Norwegian University of Science and Technology, 2016.
- [60] J. Ruddy, R. Meere and T. O'Donnell, "Low Frequency AC transmission as an alternative to VSC-HVDC for grid interconnection of offshore wind," *2015 IEEE Eindhoven PowerTech*, Eindhoven, pp. 1-6, 2015.
- [61] J. Ruddy, R. Meere and T. O'Donnell, "Low Frequency AC transmission for offshore wind power: A review," *Renewable and Sustainable Energy Reviews, Elsevier*, vol. 56, pp. 75-86, 2016.
- [62] J. Ruddy, "Low Frequency AC Transmission for offshore wind," PhD thesis, University College Dublin, September 2017.
- [63] J. Ruddy, R. Meere, C. O'Loughlin and T. O'Donnell, "Scaled hardware verification of low frequency AC transmission system for interconnection of offshore wind," *5th IET International Conference on Renewable Power Generation (RPG) 2016*, London, pp. 1-6., 2016.
- [64] J. Ruddy, R. Meere, C. O'Loughlin and T. O'Donnell, "Design of VSC Connected Low Frequency AC Offshore Transmission With Long HVAC Cables," in *IEEE Transactions on Power Delivery*, vol. 33, no. 2, pp. 960-970, 2018.



- [65] E. Abildgaard and M. Molinas, "Modelling and Control of the Modular Multilevel Converter (MMC)," *Energy Procedia*, vol. 20, pp. 227-236, 2012.
- [66] S. Khan and E. Tedeschi, "Modeling of MMC for Fast and Accurate Simulation of Electromagnetic Transients: A Review," *Energies*, vol. 10, no. 1161, pp. 1-32, 2017.
- [67] F. Martinez-Rodrigo, D. Ramirez, A. Rey-Boue, S. de Pablo and L. Herrero-de Lucas, "Modular Multilevel Converters: Control and Applications," *Energies*, vol. 10, no. 11, p. 1709, 2017.
- [68] Q. Tu, Z. Xu and L. Xu, "Reduced Switching-Frequency Modulation and Circulating Current Suppression for Modular Multilevel Converters," *IEEE Transactions on Power Delivery*, vol. 26, no. 3, pp. 2009-2017, 2011.
- [69] A. Beddard and M. Barnes, "Modelling of MMC-HVDC Systems – An Overview," *Energy Procedia*, vol. 80, pp. 201-212, 2015.
- [70] ABB, "Static Converters Dynamic Performance," ABB review 2|10, 2010
- [71] M. Said-Romdhane, M. Naouar, I. Belkhouja and E. Monmasson, "An Improved LCL Filter Design in Order to Ensure Stability without Damping and Despite Large Grid Impedance Variations," *Energies*, vol. 10, no. 336, pp. 1-19, 2017.
- [72] H. Brantsæter, Ł. Kocewiak, A. Årdal and E. Tedeschi, "Passive Filter Design and Offshore Wind Turbine Modelling for System Level Harmonic Studies," *Energy Procedia*, vol. 80, pp. 401-410, 2015.
- [73] B. Li, R. Yang, D. Xu, G. Wang, W. Wang and D. Xu, "Analysis of the Phase-Shifted Carrier Modulation for Modular Multilevel Converters," *IEEE Transactions on Power Electronics*, vol. 30, no. 1, pp. 297-310, 2015.
- [74] T. Normann, "Ultra-Long Subsea Power Transmission Using Frequency Step-Up Equipment," MCE Deepwater Development 2014, Madrid, Spain, 9 April 2014.
- [75] A. Kadir, A. Mohamed, H. Shareef and M. Wanik, "Impact of Multiple Inverter Based Distributed Generation Units on Harmonic Resonance," *Renewable Energy and Power Quality*, vol. 1, no. 10, pp. 225-230, 2012. DOI: 10.24084/repqj10.280.
- [76] A. Rasool, M. Jamil, H. Rasool, M. Asif, M. Numan and I. Ahmad, "Improvement in Stability of HVDC System by Optimizing PI Control Parameters in PSCAD," *Indian Journal of Science and Technology*, vol. 9, no. 21, pp. 1-6, 2016.
- [77] J. Ruddy, R. Meere and T. O'Donnell, "A Comparison of VSC-HVDC with Low Frequency AC for Offshore Wind Farm Design and Interconnection," *Energy Procedia*, vol. 80, pp. 185-192, 2015.
- [78] M Transmission Code 2007. Networks and System Rules of the German Transmission System operators, VDN-e.v. beim VDEW, August 2007.
- [79] W. Cao, Y. Xie and Z. Tan, "Wind Turbine Generator Technologies," in *Advances in Wind Power*, 2012, pp. 177-204.
- [80] Manitoba Hydro International Ltd., "Type-4 Wind Turbine Model," Winnipeg Manitoba, 2018, pp. 1-34.
- [81] R. Boinne, "Stability Studies of an Offshore Wind Farms Cluster Connected with VSCHVDC Transmission to the NORDEL Grid," Master of Science, Norwegian University of Science and Technology, 2009.



- [82] C. Sourkounis and P. Tourou, "Grid Code Requirements for Wind Power Integration in Europe," in *HINDAWI Conference Papers in Energy*, Limassol, Cyprus, 2013, pp. 1-11.
- [83] M. Singh and S. Santoso, "Dynamic Models for Wind Turbines and Wind Power Plants," National Renewable Energy Laboratory (NREL), Texas, 2011.
- [84] S. Uski-Joutsenvuo and S. Niskanen, "Wind turbine models - Model development and verification measurements," *VTT*, Finland, 2013.
- [85] Chan Shan, "Harmonic analysis of collection grid in offshore wind installations," Master's Thesis, NTNU-TU Delft, 2017.
- [86] Cigré 604, "Guide for the Development of Models for HVDC Converters in a HVDC Grid," *CIGRÉ Working Group Session B4.57*. Paris-France, pp.1-221, 2014.
- [87] Cigré 727, "Modelling of Inverter-based Generation for Power System Dynamic Studies," *CIGRÉ Joint Working Group Session C4/C6.35/CIREC*. Paris-France, pp.1-293, 2018.
- [88] T. Kalitjuka, "Control of Voltage Source Converters for Power System Applications," Master of Science, Norwegian University of Science and Technology, 2011.
- [89] Z. Zhou, "Co-ordination of Converter Controls and an Analysis of Converter Operating Limits in VSC-HVdc Grids," Doctor of Philosophy, The University of Manitoba, 2013.
- [90] Yalong Li, "Arm Inductance and Sub-module Capacitance Selection in Modular Multilevel Converter," Master's Thesis, The University of Tennessee, 2013.
- [91] Tamiru Woldeyesus Shire, "VSC-HVDC based Network Reinforcement," M. Sc. Thesis Electrical Power Engineering, TU Delft, 2009.
- [92] Electric Systems Consulting ABB Inc., "System Frequency Scans for Underground Transmission Options using HVDC Light," Raleigh, 2004.
- [93] L. Lazaridis, "Economic Comparison of HVAC and HVDC Solutions for Large Offshore Wind Farms under Special Consideration of Reliability," Master's Thesis, Royal Institute of Technology Stockholm, 2005.
- [94] B. Jacobson, P. Karlsson, G. Asplund, L. Harnefors and Tomas Jonsson, "VSC-HVDC Transmission with Cascaded Two-Level Converters," in *Cigré Conference Technical Committee B4-110*, 2010.
- [95] Cigré 568, "Transformer Energization in Power Systems: A Study Guide," *CIGRÉ TECHNICAL BROCHURES WG C4.307*. Paris-France, pp.1-126, 2014.
- [96] E. Malz and S. Laza, "Controller Interaction Assessment between a Full-scale Converter Wind Turbine and a MMC-HVDC Transmission System," Master Thesis, Aalborg University, 2020.
- [97] R. Meere, J. Ruddy and T. O'Donnell, "Variable Frequency Operation for Future Offshore Wind Farm Design: A Comparison with Conventional Wind Turbines," *EERA Deep Wind*, 2014.
- [98] M. Mirabile, V. Marchal and R. Baron, "Technical note on estimates of infrastructure investment needs," in the OECD report *Investing in Climate, Investing in Growth*, OECD, 2017
- [99] S. Sanchez, G. Bergna and E. Tedeschi, "Tuning of control loops for grid-connected Modular Multilevel Converters under a simplified port representation for large system studies," 2017 Twelfth International Conference on Ecological Vehicles and Renewable Energies (EVER), Monte Carlo, 2017, pp. 1-8.
- [100] A. Giles, L. Reguera and A. Roscoe, "Optimal Controller Gains for Inner Current Controllers in VSC Inverters," in *IET International Conference on Renewable Power Generation*, 2015.

- [101] Edvard Csanyi, "Analysing the costs of High Voltage Direct Current (HVDC) transmission," in EEP - Electrical Engineering Portal, 2017
- [102] M. Zubiaga, G. Abad, J. Barrena, S. Aurtenetxea and A. Cárcar, "Energy Transmission and Grid Integration of AC Offshore Wind Farms," Chapter 4, IntechOpen, 2014
- [103] M. Zubiaga, G. Abad, J. Barrena, S. Aurtenetxea and A. Cárcar, "Evaluation of the Frequency Response of AC Transmission Based Offshore Wind Farms," Wind Farm - Impact in Power System and Alternatives to Improve the Integration, ISBN: 978-953-307-467-2, InTech, 2011.
- [104] Antony Beddard, Mike Barnes and Robin Preece, "Comparison of Detailed Modelling Techniques for MMC Employed on VSC-HVDC Schemes," IEEE Transactions on Power Delivery, Vol. 30, No. 2, April 2015.
- [105] R. Marquardt, "Modular Multilevel Converters," IEEE Power Electronics Magazine, pp. 24-31, 2018.
- [106] H. Terry and C. Young, "AC Voltage Control of a Future Large Offshore Wind Farm Network Connected by HVDC," PhD, Durham University, 2016.
- [107] T. Yuan, "Modular Multilevel Converter: Submodule Dimensioning, Testing Method, and Topology Innovation," Doctor of Philosophy, University of Warwick, 2015.
- [108] Cigré TB 269, "VSC TRANSMISSION," CIGRÉ Joint Working Group Session B4.37. Paris-France, 2005.
- [109] Cigré TB 713, "Designing HVDC Grids for Optimal Reliability and Availability Performance," in CIGRÉ Joint Working Group Session B4.60. Paris-France, pp.1-134, 2017.
- [110] Cigré TB 556, "Power System Technical Performance Issues Related to the Application of Long HVAC Cables," in CIGRÉ Joint Working Group Session C4.502. Paris-France, pp.1-119, 2013.
- [111] M. Zubiaga, "Evaluation of Harmonic Risk in Offshore Wind Farms," Energy Transmission and Grid Integration of AC Offshore Wind Farms, MSc Markel Zubiaga (Ed.), ISBN: 978-953-51-0368-4, InTechopen, 2012.
- [112] R. Abdikarimuly, A. Ruderman and B. Reznikov, "Calculation of current total harmonic distortion for a three-phase two-level inverter with LCL-filter," in 2017 IEEE Dubrovnik 19th International Conference on Electrical Drives and Power Electronics (EDPE), pp. 1-7, 2017.
- [113] T. Vrana, O. Mo, "Optimal Operation Voltage for Maximal Power Transfer Capability on Very Long HVAC Cables," in Norway 2016 Deep Sea Offshore Wind R&D Conference EERA DeepWind'2016, Procedia, vol. 94, pp. 99 – 408, 2016.
- [114] C. Maclver, "A Reliability Evaluation of Offshore HVDC Transmission Network Options," Doctor of Philosophy, University of Strathclyde Glasgow, 2015.
- [115] S. Chaudhary, R. Teodorescu, P. Rodríguez and P. Kjar, (2009). "Chopper controlled resistors in VSC-HVDC transmission for WPP with full-scale converters". IEEE PES/IAS Conference on Sustainable Alternative Energy (SAE), 2009, pp. 1-8.
- [116] "Implementation guidelines for the network code requirements for generators-Recommendations from the European wind industry," in Wind Europe Task Force on Grid Connection Requirements, 2016.
- [117] C. Bajracharya, "Control of VSC-HVDC for wind power," Master of Science, Norwegian University of Science and Technology Department of Electrical Power Engineering, 2008.

- [118] S. Cunningham, "Theory, Simulation, and implementation of grid connected back to back converters utilizing voltage-oriented control," Master of Science in Engineering, The University of Wisconsin-Milwaukee, 2017.
- [119] N. Negra, "Offshore Wind Power: Grid Connection and Reliability," in partial fulfilment of the requirements for the degree of Doctor of Philosophy in Electrical Engineering, Faculty of Engineering, Science and Medicine at Aalborg University, 2008.
- [120] National Grid ESO, "The Grid Code," Issue 5 Revision 22, Tech. Rep. National Grid, May 2018.
- [121] DNV GL, "Power Frequency Optimisation for OWF," EWEA Offshore 2015, Copenhagen, March 2015.
- [122] WindEurope, "Implementation-Guidelines-for-the-NC-RfG", windeurope.org, July 2016.
- [123] Uwe Behmann, Thorsten Schütte, "niederfrequenz – nicht nur für Bahnen," Elektrische Bahnen, Technologie Stromübertragung, Bulletin 4/2015.
- [124] M. Bradt, B. Badrzadeh, E. Camm, D. Mueller, J. Schoene, T. Siebert, T. Smith. M. Starke and R. Walling, "Harmonics and resonance issues in wind power plants," *PES T&D 2012*, Orlando, FL, pp. 1-8, 2012.
- [125] L. Brand, R. I de Silva, E. Bebbington and K. Chilukuri, "Grid West Project HVDC Technology Review," *PDC*, 2014.
- [126] ECOFYS Report, "OWA HVAC Optimisation Study-Low Frequency AC," POWUK14331, Chap. 4-5, pp. 26-63, 2014.
- [127] U. Gnanarathna, A. Gole and S. Chaudhary, "Multilevel Modular Converter for VSC-HVDC Transmission Applications: Control and Operational Aspects," *Computer Science*, pp. 1-6, 2010.
- [128] Areva T&D, "Power Transformers Expertise," Areva T&D, vol.2, August 2008
- [129] O. Anaya-Lara, D. Campos-Gaona, E. Moreno-Goytia and G. Adam, *Offshore Wind Energy Generation: Control, Protection, and Integration to Electrical Systems*, 1st ed. Chichester: John Wiley & Sons, Ltd., 2020, pp. 223-269.
- [130] COMMISSION REGULATION (EU) 2016/631, "Establishing a Network Code on Requirements For Grid Connection Of Generators," Official Journal of the European Union, L 112/1, 2016.
- [131] A. Beddard, "Factors Affecting the Reliability of VSC-HVDC for the Connection of Offshore Windfarms," Doctor of Philosophy, University of Manchester School of Electrical and Electronic Engineering, 2014.
- [132] ERA Technology Limited, "Economic Analysis of Large Submarine Cables," *Edif ERA*, 2016.
- [133] Igor SowaabJosé, Luis Domínguez-García, Oriol Gomis-Bellmunt, "Impedance-based analysis of harmonic resonances in HVDC connected offshore wind power plants," *Electric Power Systems Research*, Volume 166, January 2019, Pages 61-72.
- [134] Jakob Bærholm Glasdam, "*Harmonics in Offshore Wind Power Plants: Application of Power Electronic Devices in Transmission Systems*," Springer Theses, 2015.
- [135] M. Zygmanski, B. Grzesik and R. Nalepa, "Capacitance and inductance selection of the modular multilevel converter," in *15th European Conference on Power Electronics and Applications (EPE)*, Lille, pp. 1-10, 2013.
- [136] Ofgem Systems and Networks Team, "9 August power outage, Ofgem," [www.ofgem.gov.uk](http://www.ofgem.gov.uk), 2019.

- [137] Othmane El Mountassir, "HVDC transmission cables in the offshore wind industry: reliability and condition monitoring," ORE Catapult, December 2015.
- [138] C. Buchhagen, C. Rauscher, A. Menze, J. Jung, "BorWin1-First Experiences with harmonic interactions in converter dominated grids," International ETG Congress 2015, Bonn, Germany, November 2015.
- [139] Y. Zhang, C. Klabunde and M. Wolter, "Harmonic Filtering in DFIG-based Offshore Wind Farm through Resonance Damping," 2019 IEEE PES Innovative Smart Grid Technologies Europe (ISGT-Europe), Bucharest, Romania, 2019, pp. 1-5, doi: 10.1109/ISGTEurope.2019.8905699.
- [140] X. Xiang, M. M. C. Merlin and T. C. Green, "Cost analysis and comparison of HVAC, LFAC and HVDC for offshore wind power connection," 12th IET International Conference on AC and DC Power Transmission (ACDC 2016), Beijing, 2016, pp. 1-6, doi: 10.1049/cp.2016.0386.
- [141] S. V. Kulkarni, S. A. Khaparde, "Transformer Engineering: Design, technology, and diagnostics," 2nd Ed., CRC Press, Boca Raton, Fla. 2012. ISBN: 978-1-4398-5377- 1, DOI: 10.1201/b13011.
- [142] BHEL (Bharat Heavy Electricals Limited), "Transformers," Second Edition, McGraw Hill Education (India) Private Limited, 2003.
- [143] Martin J. Heathcote, "The J & P Transformer Book, a Practical Technology of the Power Transformer," Twelfth edition Reed Educational and Professional Publishing Ltd, 1998.
- [144] IRENA (2019), "Future of wind: Deployment, investment, technology, grid integration and socio-economic aspects (A Global Energy Transformation paper)," International Renewable Energy Agency, Abu Dhabi.

## APPENDIX A

### FDPM Subsea Cable Parameters Adjustment

The PSCAD Model for the frequency scan studies of the MT-LFAC TS is depicted in Figure 1.

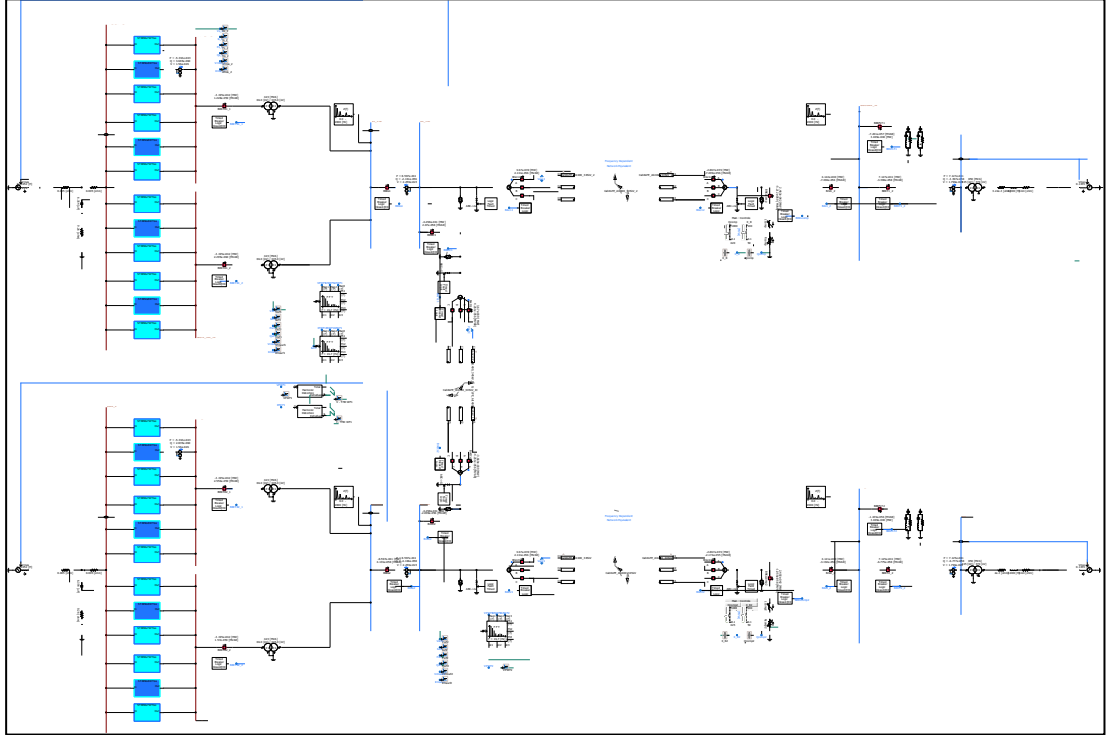


**Figure 1: MT-LFAC TS Model in Frequency Domain.**

The calculated output phase model parameters represent the input parameters but may not reflect the actual cable electrical characteristics. To explicitly represent a subsea cable in PSCAD, some input parameters of the default template need to be corrected before. The purpose of this correction is to match the cable electrical parameter values calculated by PSCAD with those measured by the cable manufacturer (NEXANS), as described in Chapter 2 and 3. Therefore, some parameters of the conductor, shield and insulation of the LFAC cable and the sea (burial) depth below the ground surface can be adapted for PSCAD Modelling.

As the cable conductor is considered as solid-core, circular and homogenous according to the PSCAD template then its actual  $A_r$  and its effective cross-section area  $A_c$  will be different. These cable geometrical characteristics affect its resistive component [102]. Thus, in the conductor PSCAD input data, the resistivity value of the conductor material ( $\rho_{c\_PSCAD}$ ) is changed to maintain the same absolute resistance of the conductor as follows:

$$\rho_{c\_PSCAD} = \rho_s \cdot \frac{A_r}{A_c} \quad (\text{A.0.1})$$

Where:  $\rho_{c\_PSCAD}$ , is the PSCAD input equivalent conductor resistivity value, [Ohm/km].

$A_c$ , is the effective cross-section area of the conductor (1400 mm<sup>2</sup>).

$A_r = \pi \cdot r_c^2$ , would be the real cross-section area for a circular conductor [mm<sup>2</sup>].

$\rho_s = R_{DC20} \cdot A_r$ , is the conductor specific resistivity at 20°C, [Ohm/km].

In addition, since the cable insulation or shield may have more complex forms, some adjustments shall apply to the shield dimensions to fill in the PSCAD template. These will alter the insulation layer input dimensions which affect the capacitance of the cable as well. Then, according to Equation (A.2), the equivalent relative permittivity ( $\epsilon_{r\_PSCAD}$ ) of the insulation needs to change in PSCAD input data to represent the capacitive component of the subsea cable correctly.

$$\epsilon_{r\_PSCAD} = C_{cab} \cdot \frac{\ln\left(\frac{r_{sh\_in}}{r_c}\right)}{2\pi \cdot \epsilon_0} \quad (A.2)$$

Where:  $\epsilon_{r\_PSCAD}$ , is the PSCAD input equivalent relative permittivity value.

$\epsilon_0$ , is the relative permittivity (vacuum).

$C_{cab}$ , is the characteristic capacitive component given by the manufacturer, [F/m].

$r_c$ , is the conductor radius and  $r_{sh\_in}$ , is the inner radius of the shield conductor, [mm].

According to the above correction procedure, the LFAC cable manufacturer (NEXANS) geometrical and physical data as presented in Table 3 of Section 2.2.1.3 and Table 16 of Section 3.2.2.2 are adjusted for modelling in PSCAD as shown in the Table below.

CALCULATIONS FOR PSCAD ADJUSTMENT			
GEOMETRICAL CHARACTERISTICS - DIMENSIONS			
Radius of the Conductor	r_c	23.2	[mm]
Outer Radius of Shield Conductor	rsh_out	50.7	[mm]
Inner Radius of Shield Conductor	rsh_in	50.12	[mm]
Distance Between Conductor Axes - Trefoil	s	147.05	[mm]
PHYSICAL CHARACTERISTICS - ASSUMPTIONS			
Initial Cond. Specific Resistivity@20 C	ρs	2.968E-08	[ohm/km]
Equiv.Cond. Resistivity@20 C PSCAD	pc_pscad	3.585E-08	[ohm/km]
Absolute Permittivity	ε	2.214E-11	
Equiv. Relative Permittivity PSCAD (Insulation)	εr_pscad	2.395E+00	

As a result, the Table below shows that the positive-sequence cable electrical parameters supplied by the manufacturer are the same as those calculated by PSCAD Line Constants Program (LCP)

CABLE ELECTRICAL RESPONSE-PSCAD			
Insulation Capacitance per km	Ccab*	1.73E-07	[F/km]
Meas.Cable Inductance per km	Lcab*	4.19E-04	[H/km]
Meas. Cable Resistance per km	Rcab*	3.07E-02	[ohm/km]

## APPENDIX B

### Availability Estimation of Offshore Transmission Technologies

Scheduled and forced outages on transmission assets connecting OWFs to the onshore transmission network restrict the exported power, which leads to loss of revenue. Reliability studies are performed for power grids and transmission systems to analyse the probability that the system can deliver a specific amount of power to the grid at the PCC, under defined conditions for a specified period. The availability for the offshore export system can be considered as the probability of all individual transmission assets being in an operational state but can also be used as a reference to the overall systems ability to transmit power. Each component is assigned an estimated downtime in case of failure and a failure frequency rate. The availability of the system's transmission components indicates its reliability and estimates the potential short and long-term financial impact of these outages.

The availability of individual components can be determined by two separate parameters, namely the Mean Time to Repair (MTTR, or the component Downtime) which is the time required to repair a failed module and the Mean Time to Failure (MTTF, or the component Uptime), which is the meantime expected until the failure of the quoted equipment [119].

The availability (A) and unavailability (U) of a component are probabilistic measures:

$$A = \frac{UPTIME}{UPTIME+DOWNTIME} = \frac{MTTF}{MTTF+MTTR} \quad (B.1)$$

$$U = \frac{MTTR}{MTTF+MTTR} = 1 - A \quad (B.2)$$

Where the sum MTTF+MTTR in the denominator can be defined as the reciprocal of a component's failure rate ( $\lambda$ ):

$$MTTF + MTTR = \frac{1}{\lambda} \quad (B.3)$$

The availability with regards to an offshore export system can be assessed by specifying the related conditions such as the electrical system topology, operating state, availability of components within the system and the duration required to maintain and repair apparatus or plant. Since there is a shortage of reliability assessments and standard definitions for LFAC systems, a high-level availability investigation is performed, comparing the existing transmission technologies and LFAC TS. Conditions related to any power quality issues that would typically require detailed dynamic system analysis are not covered here as generic system designs are assumed. An availability estimation for the offshore MT-LFAC TS is also endeavoured only for the full power export case, as the detailed calculation for other operating states should also account that are out of the scope of this Thesis.

## 1. Assumptions

Failure rates used in the availability calculation of the main components are reflective of the relevant values as given in the literature [109]. MTTR and MTTF data for the calculations have been sourced by the relevant CIGRE working group information papers, published reports, as referenced in the availability assumptions Table 1.

*Table 1: Availability Parameter Assumptions.*

Availability Assumptions	Failure Rate/ Annum $\lambda$	MTTR (hours)	MTTF (hours)	Reference
Onshore Converter	0.499	24	17532	[31]
Offshore Converter	0.4949	168	17532	[31]
Onshore Transformer	0.02	1440	436560	CIGRE 2017
Offshore Transformer	0.04	2160	216840	CIGRE 2017
DC Transmission Cable	0.0007/km	1440	12512846	[31]
AC Transmission Cable	0.0007/km	1440	12512846	[31]
Bay	0.007	24	1250690	
Harmonic Filters	0.313	10.9	27976	ABB data
Onshore Reactor	0.1428	24	61320	[31]
Offshore Reactor	0.1424	192	61320	[31]

Assessing the MTTR for submarine cables and other offshore assets depends on many factors, some of which may be controllable, but others may not. For example, an important consideration would be the ability to obtain suitable vessels in combination with the appropriate weather windows. In general, MTTR for assets placed offshore is higher than for those placed on the shore particularly for major plant components such as transformers, cables or switchgears, e.g. repairing a defective submarine cable involves undertaking a major engineering operation. Though, it is possible to considerably reduce repair time with proper planning procedures that include, among others:

- Ease of fault finding
- Spares and repair facilities, such as cable repair vessels
- Accurate records of the as-laid cable's position
- Standardisation and inter-changeability of cables and accessories

Nowadays, subsea cables are identified as key components affecting the availability of export schemes regardless of the utilised transmission technology, i.e. HVAC, HVDC, or LFAC.



According to CIGRE, the annual failure rate of a DC submarine cable is estimated to be 0.07 failures per 100km based on the distance between the converter stations and not the installed length of cable, while the average repair time for submarine cables is approximately 60 days [109]. Up to a certain extent, submarine cable failure rates are somewhat subjective because of the scarcity of reported failures and as they are heavily influenced by factors such as the mechanical protection provided, shipping and fishing activity around cable routes, anchor drags, seabed hardness and water depth. Since most subsea cable failures occur due to external damage, their failure rate is directly proportional to the length of the cable, regardless of its type or voltage rating.

Other fundamental components of the export systems are considered including converters, transformers, reactors, harmonic filters, etc. As expected, although the MTTF levels of an equivalent onshore and offshore (considered only for HVDC) converter can be the same, the MTTR is almost 7 times higher when the converter is placed offshore. Likewise, an MTTF value of 50 years is assumed for an onshore placed grid type transformer, while for an offshore converter transformer 25 years, with a failure rate of 0.02 (onshore) and 0.04 (offshore) per year respectively.

Except for the bulk components of the export systems mentioned above, control and protection (C&P) equipment with bigger MTTF and smaller failure rates, circuit breakers (CBs) and switches should also be included and referred as “bay” elements in Table 1, to compensate for data-scarcity regarding less basic equipment of such schemes. Further availability data regarding auxiliary system failures that may have an impact on primary equipment downtime or their redundancy characteristics that act to prevent system outages may be reflected in the main components availability values.

## 2. Availability Network Models.

Once the availability of each component has been determined regarding the operational framework, a wider availability assessment for the corresponding offshore export system can be performed by combining the availability records of the individual components. The utilised method is based on the average interruption rate, providing an estimate of continuity rather than service quality.

Each PtP offshore system comprises components connected in series and parallel configurations. These set-ups can be represented either with Fault-Tree or with Availability Block Diagrams that map a process from start to finish. In this study, component failures are

assumed to be independent, and a probability of simultaneous failure is not considered. Thus, if a subsystem is not operating, the system is down regardless of the status of another subsystem. Therefore, system components only operate in two states: available or unavailable. The availability rate of a component is represented as “*a*”, while the probability of it being unavailable is given by its outage rate “*u*”. It is always:

$$a + u = 100\% \quad (\text{B.4})$$

➤ **Series Connections**

In a serial process, all components must be available for power to flow to the receiving point, creating an “OR-Gate” connection of events. A series network is shown in Figure 1, where several components of the system are represented by availability blocks connected in series.

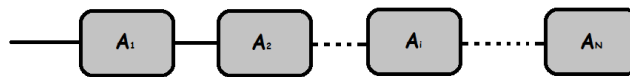


*Figure 1: Series Connection Network.*

The availability of the series connection is a multiplication of the estimated availability of each individual, repairable component:

$$A_s = \prod_{i=1}^N (A_i) = A_1 \cdot A_2 \cdot \dots \cdot A_i \cdot \dots \cdot A_N \quad (\text{B.5})$$

Where:  $A_s$  = Availability of the series connection

-  $N$  = Number of components in the series connection

-  $A_i$  = Availability of component number  $i$

➤ **Parallel Connections**

In parallel processes of offshore export systems, all components must be unavailable for no power to flow into the receiving point, like “AND-Gate” connections. A parallel network is shown in Figure 2, where several components of the system are represented by availability blocks connected in parallel.

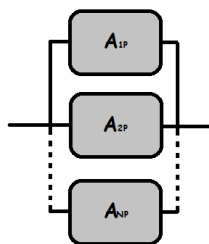


*Figure 2: Parallel Connections Network.*

The availability of the connection depends on the number of components required for a specific type of operation, which may be either the normal nominal or lower power flow operation:

- *One out of NP*

In a system with parallel-connected components, all of them must fail before no power flows into the receiving end, so the system availability is significantly improved. The system requires at least one out of the total number of components connected in parallel NP to be available so that the connection can be operational even at a minimum power flow level. The unavailability of this parallel connection is a multiplication of the estimated unavailability of each individual, repairable component:

$$U_P = \prod_{i=1}^{NP} (U_i) = \prod_{i=1}^{NP} (1 - A_i) \quad (\text{B.6})$$

Hence, the minimum level availability of the scheme for repairable components is given:

$$A_{Pmin} = 1 - U_P = 1 - \prod_{i=1}^{NP} (1 - A_i) = 1 - [(1 - A_{1P}) \cdot \dots \cdot (1 - A_i) \cdot \dots \cdot (1 - A_{NP})] \quad (\text{B.7})$$

Where:  $U_p$  = Unavailability of the parallel connection

- $A_{pmin}$  = Availability of the parallel connection for a minimum power flow level
- NP = Number of components in the parallel connection
- $U_i$  = Unavailability of component number  $i$
- $A_i$  = Availability of component number  $i$

- *kp out of NP:*

In a system with NP parallel-connected components, at least kp need to operate under certain conditions. For repairable components that have the same individual availability ( $A_r$ ), the availability of the parallel network for specific conditions can be calculated as follows:

$$A_{Psc} = \sum_{i=kp}^{NP} \binom{NP}{i} (A_r)^i \cdot (1 - A_r)^{NP-i} \quad (\text{B.8})$$

Where:  $A_{psc}$  = Availability of the parallel connection for specific power flow level

- *NP out of NP:*

This system requires all NP components connected in parallel to be available so that the connection can operate at the rated standards. In such a system, even though all components are connected in parallel, if one component fails, not all the required power

flows into the receiving end, and thus the system availability for full or maximum power operation is significantly reduced. Hence, the series connection approach can be used to estimate the availability of such active parallel networks, as the product of the estimated availability values of each individual, repairable component:

$$A_{Pmax} = \prod_{i=1}^{NP} (A_i) = A_1 \cdot A_2 \cdot \dots \cdot A_i \cdot \dots \cdot A_{NP} \quad (\text{B.9})$$

Where:  $A_{Pmax}$  = Availability of the parallel connection for a maximum power flow level

### ➤ Combined Series and Parallel Connections

Many pragmatic systems, including the offshore export transmission systems, are combinations of series and parallel components, as shown in the Availability Block Diagram of Figure 4.

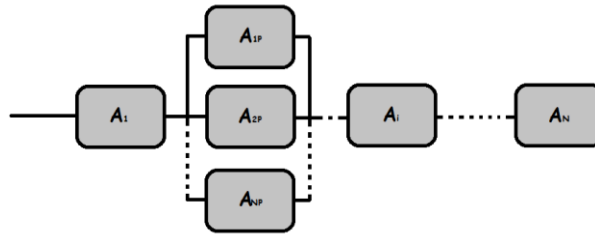


*Figure 3: Combined Series and Parallel Connections Network.*

To solve this network, the above-mentioned series and parallel formulas are applied to decompose and recombine the network step by step. Detailed system SLDs are needed to identify the key segments and yield the respective relationships between the components.

### 3. Availability Assessment

The overall system performance can be projected by identifying the fundamental elements in the main segments of the SLDs and their system dependency [119]. The block diagrams have been proved to be an effective method to assess the availability of such export systems. Figure 4 shows the availability block diagram of the examined 700MW LFAC radial system and a potential 1400MW meshed LFAC arrangement formed by connecting two separate point-to-point systems with equal export cable lengths, through a 50km submarine cable.

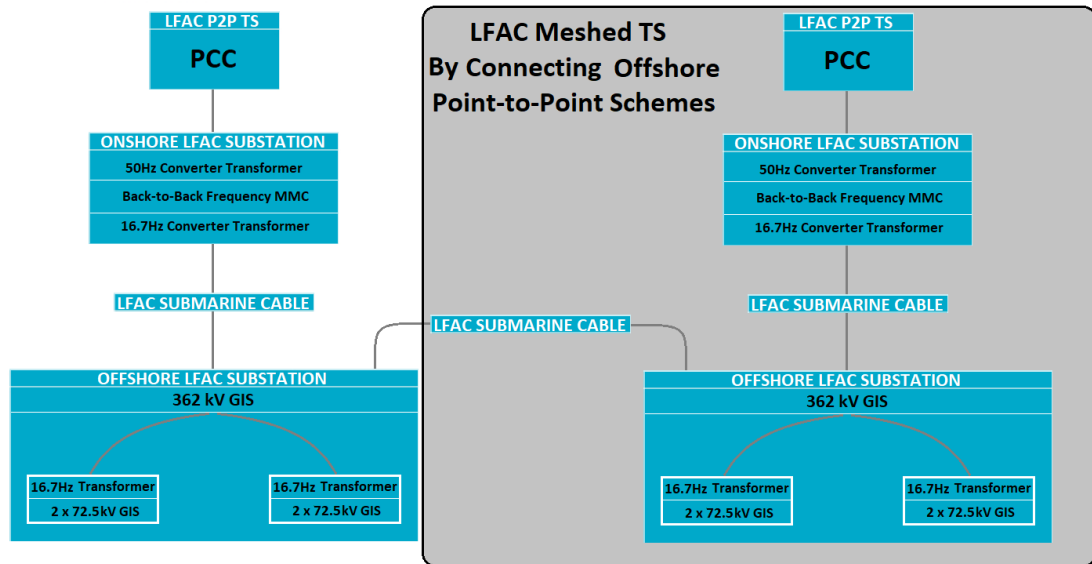


**Figure 4: Availability Block Diagrams of the PtP and MT-LFAC TS Configurations.**

The components of the transmission topologies that are not explicitly modelled are assumed to have almost 100% availability record, i.e. unavailability of 0%. Since this work studies only the transmission segments, the unavailability indices of inter-array components, array cable circuits and the related WTGs are not considered, i.e. assumed 100% available.

The scenario cases are compiled based on the estimated component failure rates and repair times, as referenced in the assumptions section above. Three availability indices are yielded for each studied topology, namely:

- The availability of a connection for the maximum power flow level of 700MW ( $A_{P_{max}}=A_{700}$ ). It gives the probability that the full OWF output power can be available at the onshore connection point. Thus, “NP out of NP” availability calculation is considered for the export system.
- The availability of a connection for a minimum power flow level, the value of which depends on the number of parallel branches of the examined topology (e.g.  $A_{P_{min}}=A_{350}$  for LFAC and HVDC,  $A_{P_{min}}=A_{233}$  for HVAC). This means that the “one out of NP” availability calculation is considered for all parallel connections of the export system.
- The percentage of energy availability of the scheme ( $A_E$ ). This is yielded by the energy unavailability ( $U_E$ ) of the system that is calculated by summing the potential energy loss per year ( $E_{Loss}$ ) because of each of the components failure rate in the scheme. The energy loss because of each component in [MWh/Year] is given by:

$$E_{Loss} = \lambda \cdot MTTR \cdot P_U \quad (B.10)$$

Where:  $P_U$  is the power loss in the scheme if the component is unavailable, [MW].

The percentage of energy availability of the scheme is then:

$$A_E = 1 - U_E = 1 - \frac{\sum_{i=1}^{NP} E_{iLoss}}{8760 \cdot P_{rat}} \cdot (1 - p_{Loss}) \quad (B.11)$$

Where:  $P_{rat}$  is the rated power of the scheme, [MW] and  $p_{Loss}$  is the power losses [p.u.].

The  $A_{Pmin}$  and  $A_{Pmax}$  indices for the PtP LFAC export system, as appears in the availability block diagram of Figure 4 are shown in Figure 5 from 100km to 400km cable lengths.

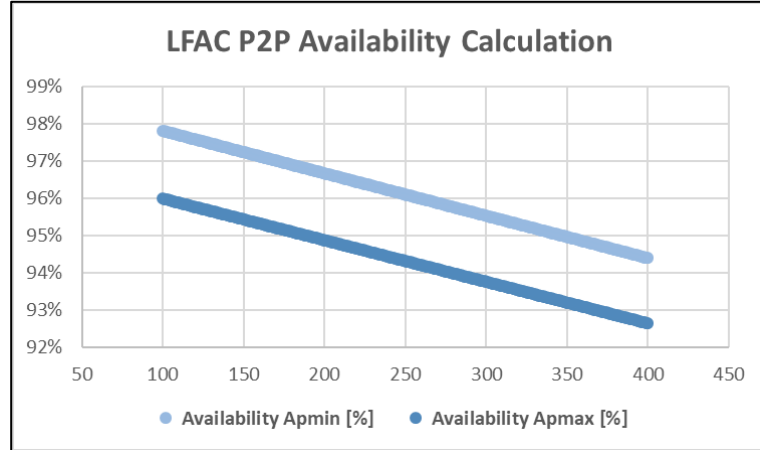


**Figure 5: Minimum and Maximum Availability Indices for PtP LFAC TS Configuration.**

The availability of the PtP LFAC connection for the maximum power export level of 700MW is around 1.8% lower than for the 350MW for almost the entire 300km range, due to the different parallel power flow paths that the lower power can take when two LFAC transformers and four GISs operate in the offshore platform. In addition, there is a difference of 3.3% between the 100km and the 400km availability values, mainly because of the failure rate ( $\lambda$ ) dependency on increasing cable length. This availability range or “window” between the minimum and maximum power export is useful for assessing the reliability of the scheme.

Nevertheless, this information should be evaluated in conjunction with the competitive OWF integration technologies for equally rated configurations, corresponding to the power that could be transferred using a single LFAC cable. Below, Figure 6a) and b) depicts the availability block diagrams of the corresponding offshore HVAC and HVDC transmission systems respectively, for exporting 700MW [114].

From these block diagrams, it is obvious that the HVAC system is actually configured as three identical PtP schemes, which can be the case for 700MW capacity and distances over 50km, with its minimum power level availability ( $A_{Pmin}$ ) corresponding to ~233 MW (700/3 MW), in contrast to the 350MW of the HVDC and LFAC systems.

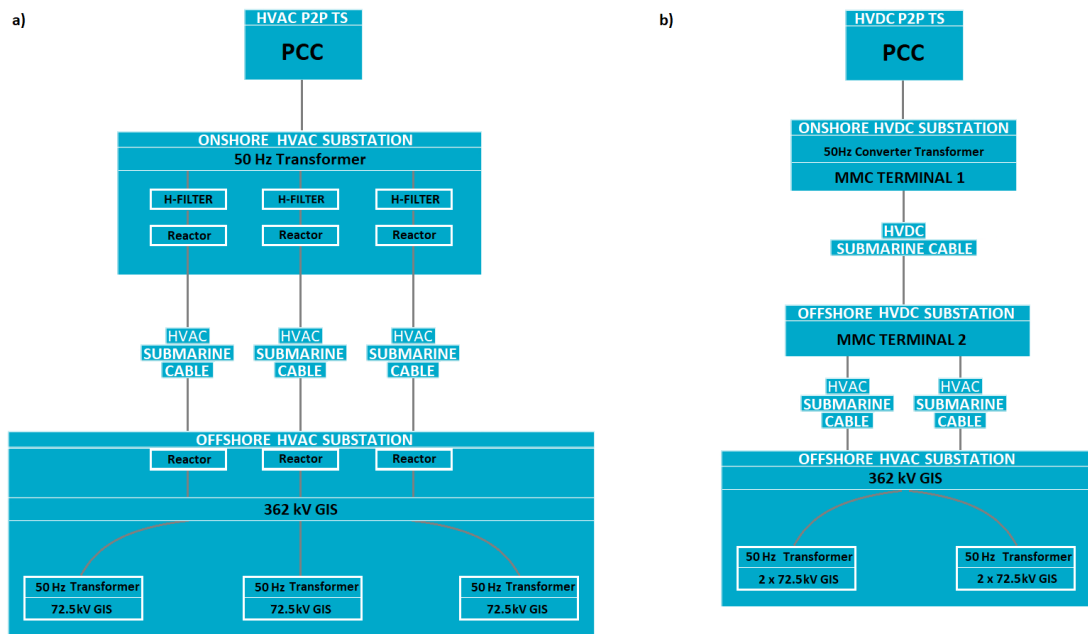


Figure 6: Availability Block Diagrams of the: a) HVAC, and b) HVDC TS Configurations.

Figure 7 shows the availability indices of the three competitive transmission solutions for the offshore PtP schemes as well as for the LFAC meshed system arrangement, for various cable lengths that can be considered feasible for each technology.

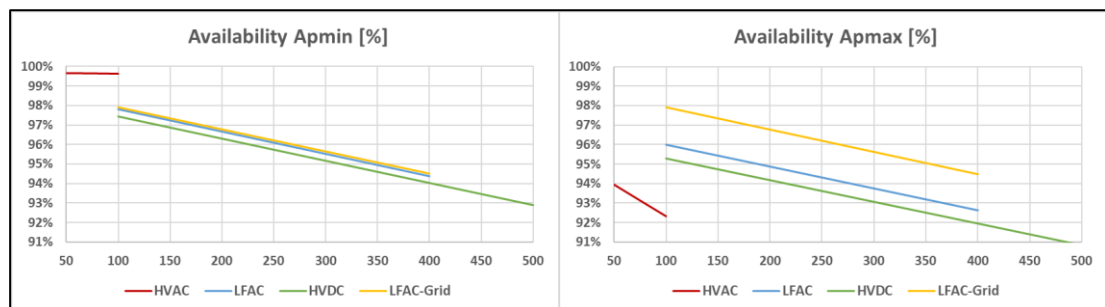


Figure 7: Minimum and Maximum Availability Indices for HVAC, HVDC, PtP and MT-LFAC TS Schemes.

The multiple parallel paths of the potential HVAC topology lead the HVAC system to present the highest  $A_{Pmin}$  for 233MW, where its value is almost constant at 99.6% for the whole 50km of its range, while its 700MW availability reaches as low as 92.3% for 100km HVAC cables, as the increased amount of components, increases the probability of at least one failure. By ignoring the related power losses, the LFAC TS has steadily higher availability rate than HVDC for cable lengths between 100 and 400km, mainly due to the added offshore infrastructure and the related equipment O&M hurdles. For the same range, the HVDC and LFAC technologies have a similar availability “windows” ( $A_{Pmax}-A_{Pmin}$ ), with the MT-LFAC technology having the smallest, as its  $A_{Pmax}$  is almost equal to its minimum availability index  $A_{Pmin}$ . Due to

its meshed arrangement, the MT-LFAC TS also has the highest maximum power availability,  $A_{Pmax}$ , which is equal to the minimum availability of the PtP LFAC configuration, as expected. This verifies that utilising the increased LFAC transmission range to form offshore LFAC grids can lead to much higher reliability levels for offshore transmission systems.

The percentage of energy availability for each scheme ( $A_E$ ) is shown in Figure 8, disregarding the power losses of the systems. Based on these results, it is clarified that the PtP LFAC TS linearly extends the energy availability characteristic of the HVAC system and can enable more distant connections. Moreover, it can supply more energy to the grid than HVDC system over time, especially if meshed offshore LFAC connections are designed.

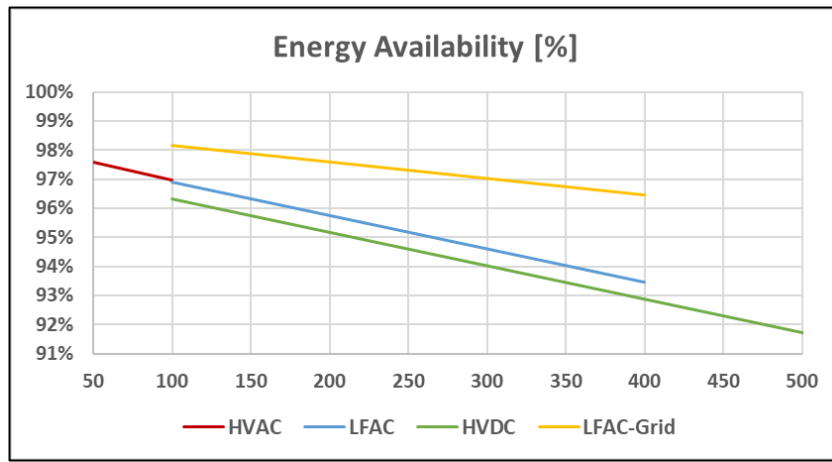


Figure 8: Energy Availability Comparison among the HVAC, HVDC, PtP and MT-LFAC TS Configurations.

The above analysis does not assess power losses in the cables and the related infrastructure. If the corresponding the LFAC TS losses are considered from the power flow cases, then the percentage of the expected available energy at the PCC can be seen in Figure 9.

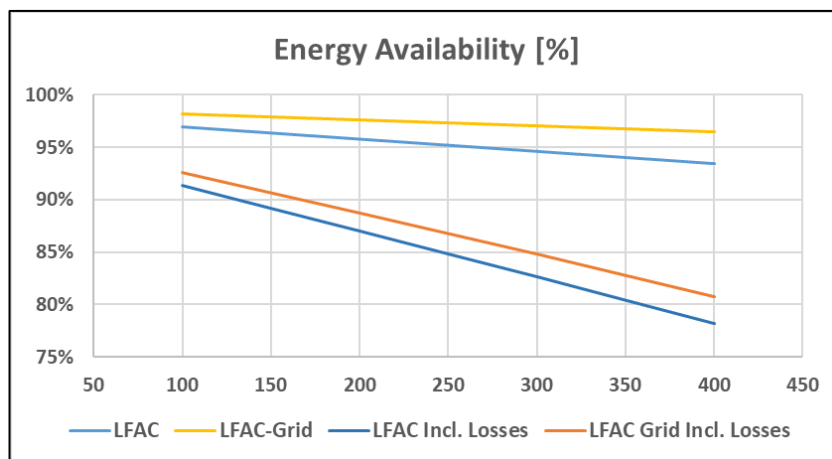


Figure 9: Energy Availability Comparison between PtP and MT-LFAC TS with and without Losses.



## APPENDIX C

### Transformation to dq(0) Domain

The analysis of the VSC technology using vector control involves three-phase currents and voltages being described as vectors in the complex (dq0) rotating reference frame. Zero declares that the zero-sequence components for unbalanced three-phase modelling could be taken into account. This rotating coordinate system must be synchronized to an AC/LFAC system so that the calculated voltages and currents occur as constant vectors during steady state. This way, the fundamental current and voltage components become DC variables and produce static errors in the control system, which can be eliminated by simple PI control structures that offer great controlling possibilities.

The transformation from the three-phase abc stationary coordinate system to the dq synchronous rotating frame is shown in Figure 1 and involves two steps:

- 1) The transformation from abc to the  $\alpha\beta$  stationary reference frame using Clark-equations.
- 2) The transformation from the  $\alpha\beta$  stationary to the dq rotating frame using Park-equations.

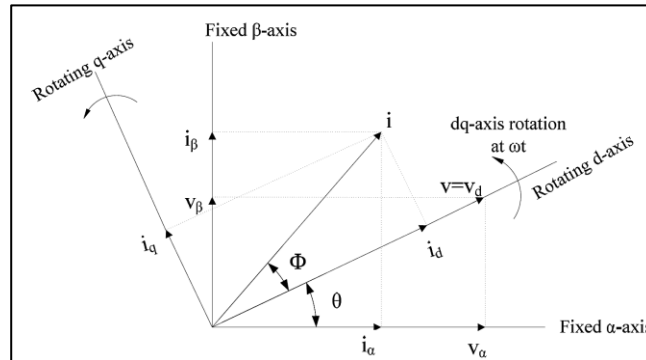


Figure 1: Direct-Quadrature Rotating Reference Frame Transformation

The stationary  $\alpha$ -axis is aligned with the a-axis for simplicity. The dq reference frame rotates at synchronous speed  $\omega_e$  [rad/sec] with respect to the  $\alpha\beta$  frame, and the position of d-axis with reference to  $\alpha$ -axis is given by  $\theta(t)=\omega_e t$ , at any instant. The following abc to dq0 and its inverse transformation (IT) return the dq0-axis quantities in a rotating reference frame from the three-phase sinusoids and vice-versa [129]. The same also apply for three-phase currents.

$$\begin{array}{l}
 V_d = \frac{2}{3}(V_a \sin(\omega t) + V_b \sin(\omega t - 2\pi / 3) + V_c \sin(\omega t + 2\pi / 3)) \\
 V_q = \frac{2}{3}(V_a \cos(\omega t) + V_b \cos(\omega t - 2\pi / 3) + V_c \cos(\omega t + 2\pi / 3)) \\
 V_0 = \frac{1}{3}(V_a + V_b + V_c),
 \end{array}
 \begin{array}{l}
 \Leftrightarrow \\
 V_a = V_d \sin(\omega t) + V_q \cos(\omega t) + V_0 \\
 V_b = V_d \sin(\omega t - 2\pi / 3) + V_q \cos(\omega t - 2\pi / 3) + V_0 \\
 V_c = V_d \sin(\omega t + 2\pi / 3) + V_q \cos(\omega t + 2\pi / 3) + V_0
 \end{array}
 \quad (C.1)$$

The peak-convention is adopted by the above transformation equations. If  $x$  stands for either voltage or current vector, then the peak-convention can be demonstrated as:

$$x_{dq} = \sqrt{x_d^2 + x_q^2} = \sqrt{2} \cdot X_{ph} \quad (C.2)$$

The active and reactive power are:

$$P = \frac{3}{2} \cdot (V_d \cdot I_d + V_q \cdot I_q) \xrightarrow{V_q=0} P = \frac{3}{2} \cdot (V_d \cdot I_d) \quad (C.3)$$

$$Q = \frac{3}{2} \cdot (V_d \cdot I_q + V_q \cdot I_d) \xrightarrow{V_q=0} Q = \frac{3}{2} \cdot (V_d \cdot I_q)$$

Also, the DC current can be calculated as:

$$I_{DC} = \frac{3}{4} \cdot M_i \cdot i_d = \frac{3}{2} \cdot \frac{V_d}{V_{DC}} \quad (C.4)$$

Since the PCC voltage vector is aligned with the d-axis direction, the q-axis voltage vector is assumed to be zero ( $V_q=0$ ) in the equations above. The angle between the  $\alpha$ -axis of the  $\alpha\beta$ -frame and d-axis of the dq-frame is used for transformation between the  $\alpha\beta$  and dq coordinates. The information on this instantaneous phase angle of each AC network voltage is vital for synchronizing the output control quantities with the system and achieve independent control of active and reactive power. The value of the angle  $\theta$  is calculated by using a synchronization technique called Phase Lock Loop (PLL).

## PLL and VCO - Setting the LFAC Offshore System Frequency

One of the main differences between the non-island and the island control systems is the origin of the rotating angle reference, which in the former comes from the phase locked loop (PLL- $\theta_{PLL}$ ), shown in Figure 2. In this PLL module, the q-axis reference signal is always set to zero resulting in the lock of its output on the phase angle of the measured AC voltage vector.

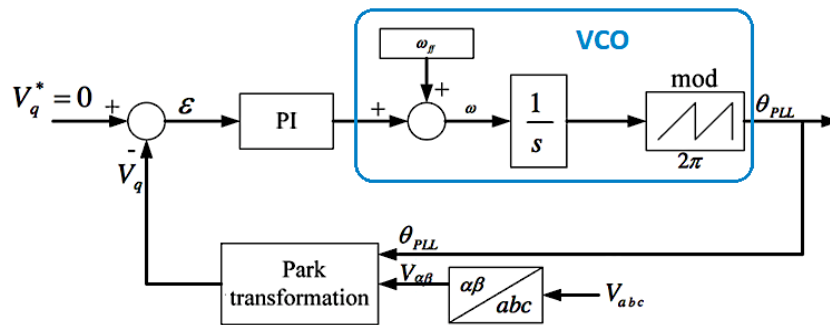


Figure 2: General Phase Lock Loop (PLL) and Voltage Controlled Oscillator (VCO) Structures.

In the islanded operation mode, the grid-forming MMC terminal employs an independent internal oscillator (VCO, Figure 2) with constant frequency demand that generates a

reference angle ( $\theta_{VCO}$ ) to transform the modulating signals for the PS-PWM that determines the valve pulse firing sequence. Since only one grid-forming MMC terminal may impose the constant frequency of 16.7Hz even to a meshed offshore MT-LFAC networks with multiple converters, all other VSCs shall synchronise their current outputs to the LFAC voltage reference at their connection points using PLLs to avoid undesirable power oscillations.

The VCO produces the rotating angle reference output  $\theta_{VCO}$  by integrating the demanded 16.7Hz frequency, as shown in Equation (C.5) and resetting at every  $2\pi$  rads, to avoid continuous ramping to infinity. The resulted output signal is a sawtooth waveform in the time domain. Thus, all the offshore system voltages and currents synchronise at 16.7Hz as well.

$$\theta(s) = \frac{2\pi}{s} f(s) \quad (C.5)$$

Thus, the island control structure can produce a set of three-phase voltages at the frequency of 16.7Hz, imposing the LFAC system frequency in an open-loop manner so no PLL related delays or de-synchronisation issues are assessed in the system analysis. The default PLL module of the PSCAD EMTDC library that uses an automatic gain PI controller to eliminate the q-axis component is employed for the grid-following converters of this Thesis.

## APPENDIX D

### PI Controllers Design and Tuning Methods

The Proportional-Integral (PI) regulator is used in all VCC loops. In Equation (C.1), a PI controller is expressed in Laplace transform form as a function of its design parameters  $K_p$  and  $T_i$ .

$$TF_{PI} = K_p \cdot \frac{1+T_i s}{T_i s} \quad (C.1)$$

Where:  $K_p$  is the proportional gain and  $T_i$  the integral time constant.

The outer APCs and RPCs of the grid-following converters, as well as the LFAC islanded voltage controller of the grid-forming MMC terminal, are tuned by employing an optimisation method based on the simplex algorithm to obtain suitable performance. The simplex algorithm is a classic iterative process that is used to solve the optimisation problem of linear programming (LP), which is to maximize a linear objective function (O.F.). Thus, the selection of an appropriate objective function is vital. Simplex starts from the origin of the n-parameter vector space that may range from 2 to 20. For any number of variables in this range, it can be faster compared to other optimisation techniques making it an ideal choice for the VSC-HVDC outer PI controller tuning. It goes through a sequence of vertices that form a geometric polytope object comparing the values of the objective function, each time, discarding the worst case to eventually reach the optimal vertex for which the function is maximized.

The adopted recursive simulation-based optimisation method minimizes the sum of the “Integral Time Absolute Error” (ITAE) of the available AC voltage, active and reactive power outer controllers in the respective converters. The ITAE is an error-integral index that can be used to evaluate the dynamic response of a control system [76] and is expressed as follows:

$$J_{ITAE} = \int_0^T t \cdot |e(t)| dt \quad (C.2)$$

Where:  $t$  can be the time after the disturbance is applied,

$|e(t)|$  is the absolute value of the respective control system error and

$T$  is chosen to allow the system to reach a steady-state (i.e. end of simulation time).

The objective function minimizes the sum of ITAE indices ( $i$ ) of each control system is:

$$O.F._{ITAE} = \sum_i J_{ITAE} = \sum_i \int_0^T t \cdot |e_i(t)| dt \quad (C.3)$$

The optimisation process is based on a recursive procedure, as shown in Figure 1, that is applied to the developed electromagnetic transient (EMT) models of the OWF VSC and BtB

MMC systems in PSCAD EMTDC software. To obtain optimised PI compensator parameters, these models are tested against various disturbances, such as step and ramp changes in power order as well as a solid three-phase-to-ground fault, while facing a relatively weak system with a Short Circuit Ratio (SCR) of 2.5 and an X/R ratio of 20. The system variable values are taken straight from the simulation results as can be seen in Figure 1, where the flow chart of the adopted optimisation procedure is depicted. This method can be very convenient and efficient, especially when considering extensive and complex networks [76]. The system time domain response to these disturbances is evaluated to achieve specific control system design requirements in terms of rising and settling times, overshoot, etc.

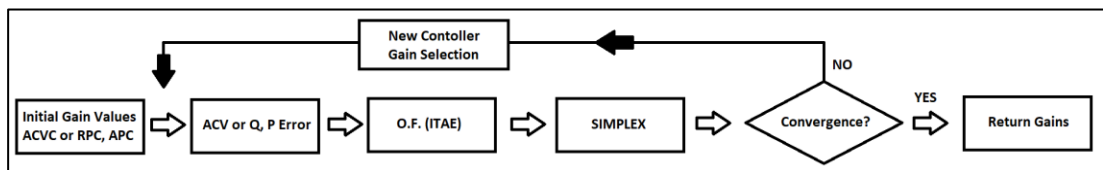


*Figure 1: Recursive Simulation-Based Optimisation Process for Controllers Tuning using PSCAD EMTDC.*